Optical control and measurement of metabotropic glutamate receptors and K_{2P} potassium channels

By
Joshua Levitz

A dissertation submitted in partial satisfaction of the requirements for the degree of

Doctor of Philosophy

in

Biophysics

in the Graduate Division of the University of California, Berkeley

Committee in charge:
Professor Ehud Isacoff, chair
Professor Mu-ming Poo
Professor Richard Kramer
Professor Diana Bautista

Spring 2014

Abstract:

Optical control and measurement of metabotropic glutamate receptors and K_{2P} potassium channels

Doctor of Philosophy in Biophysics
University of California, Berkeley
Professor Ehud Y. Isacoff, Chair

G protein-coupled receptors (GPCRs) are an extremely important class of membrane receptors that convert extracellular stimuli into intracellular signals through interaction with G proteins. These receptors are intimately involved in most physiological processes and for this reason are the largest drug targets in biology. In the nervous system a wide range of GPCRs function in nearly all subcellular locations, including the synapse, where they modulate cellular excitability, neurotransmission, synaptic plasticity, and behavior. An ultimate goal for the understanding of GPCR neurophysiology is to reconstruct a functional map of when and where GPCRs are activated and how this activation affects larger scale network outputs like behavior. However, due to the limitations of classical techniques, such as pharmacology and transgenic approaches, it has been difficult to decipher the role of individual GPCRs in specific cell types with temporal precision.

In order to gain a foothold toward understanding the contribution of different GPCRs in physiological functions, I developed a means of optically controlling individual GPCRs. This work focused on the metabotropic glutamate receptors (mGluRs) which are crucial neuronal GPCRs that respond to the major excitatory neurotransmitter, glutamate. There are eight different subtypes of mGluRs that have unique, but overlapping expression profiles and distinct G protein coupling and regulatory properties. Since pharmacological agents often can't distinguish between subtypes, can only be poorly targeted spatially, and are slow to apply and remove, we used a chemical optogenetic approach to individually agonize or antagonize mGluRs with light. This approach was based on a previous body of work from the Isacoff lab and is the basis of chapters 2 and 3. I show the molecular engineering and characterization of these tools, their initial characterization as tools for optical control of neuronal activatity, and validate their *in vivo* function in zebrafish and mice. Light-activated mGluRs, or "LimGluRs", are both a useful tool that are applicable in many contexts, but also an important test case that should serve as a model for the development of optical control over other GPCRs.

Structurally, GPCRs share a common 7 transmembrane domain structure but show divergence in extracellular N-terminal domains and intracellular C-terminal domains. Recent breakthroughs in X-ray crystallography have led to a greater structural understanding of how GPCRs bind ligands, activate, interact with G proteins, and oligomerize. However, functional experiments, which are required to gain a more complete understanding, have been hampered by the lack of high resolution techniques to probe these same processes. mGluRs are particulary interesting in this biophysical context because of their dimeric arrangement and large extracellular ligand binding domains (LBDs) that indirectly couple glutamate binding to G protein activation. In chapters 4 and 5, I use a combination of optical techniques including LimGluRs to measure oligomerization, structural dynamics, and function of mGluRs. While

Förster resonance energy transfer (FRET) is an established technique for probing of protein structure, it has recently been greatly enhanced in power by its application at the single molecule level. Single molecule FRET (smFRET) allows for individual receptors to be measured which allows for the observation of distinct states and their transitions, without the obscuring effects of averaging. Using intersubunit smFRET experiments on the extracellular ligand binding domains of mGluRs I found that these receptors visit three distinct conformations that have dynamics which determine receptor activation properties. Using another single molecule fluorescence technique based on counting fluorophore bleaching steps, I was able to show that mGluRs form homo- and heterodimers in living cell membranes. Furthermore, using a variety of perturbations I found that mGluRs have a covalent and non-covalent dimer interface within their LBDs that is complemented by a weak interface at the trans-membrane domains. Using LimGluRs, which allow for individual subunits within a dimer to be liganded, I demonstrate cooperativity that is dependent on receptor subtype and dynamics. All of these studies have given insight into the molecular biophysics of mGluRs and should serve as the basis for future studies on other GPCRs.

A final goal of the study of GPCRs is to understand the responses of their downstream signaling targets, including ion channels. One ion channel subfamily of particular interest for this objective are the K_{2P} potassium channels which classically function as leak channels to maintain cellular resting potential. K_{2P} channels have been shown to be highly regulated by different extracellular and intracellular signals, including GPCR activation. Despite the extreme regulation of these channels by a variety of signals, it has been difficult to determine which forms of regulation happen endogenously on individual channel subtypes. This is especially complicated by the fact that there is very limited pharmacology to individually block K_{2P} channels. To overcome this, I developed, using a similar design to LimGluRs, a means of optically blocking the K_{2P} channel, TREK1. Using a conditional expression system, native TREK1 channels were manipulated in hippocampal neurons where it was shown that they are non-canonical targets of $GABA_B$ receptor activation. This work is reported in Chapter 6 and provides the basis for future understanding of the physiological contribution of individual K2P channels. Finally, in Chapter 7 using a variety of approaches I show that TREK channels are specifically regulated by the enzyme phospholipase D through direct interaction. Using the photoswitchable conditional subunit system, this regulation was shown to occur in hippocampal neurons where it may explain some of the long term effects of alcohol exposure.

This work is dedicated to my entire family and, especially, my wife Jessica for her unwavering support and belief in me.

Table of Contents

Acknowledgements:

The work presented in this thesis has been a major collaborative effort that has given me the opportunity to work with a number of great people. Most importantly, I would like to thank my thesis advisor Ehud Isacoff for his initial support which helped get me to Berkeley and his continued support which was foundational in my development as a scientist. His inquisitiveness, fearlessness to tackle new subjects, trust in others, and persistence has given me an inspiring model for how to become a great scientist. Within the Isacoff lab the help I've received has been spread out over nearly everyone but there are a few key people without whom I could not have accomplished any of the work enclosed in this thesis.

Andreas Reiner and Guillaume Sandoz both started in the lab at the same time as me and have been the most influential on my understanding and approach to science throughout the last 5 years. Andreas has been a constant sounding board for ideas and an extremely principled and critical voice that has resonated throughout all of my work. His deep insights into various aspects of molecular biophysics and photochemistry have greatly expanded my understanding of these fields which form the core of my work. Guillaume has also been a constant supporter since I started in the lab. His enthusiasm is contagious and he has shown me how to tackle problems with clear ideas and experiments. Through our ongoing collaboration I have been introduced into the rich world of K2P potassium channels which has broadened my view of molecular neurobiology. Guillaume and his family hosted my wife, Jess, and I when I visited his lab in France which was one of the highlights of my time as a graduate student. The confidence that Andreas and Guillaume showed in me, from the beginning, has been crucial in my ability to propose and execute experiments.

Carlos Pantoja has been another major influence on me over my time in the Isacoff lab. Carlos truly fulfills the scholar-scientist model and provides refreshing perspective when, as can happen so easily, I get bogged down in the minutiae of science. His work in zebrafish has also greatly inspired me to move toward behavioral neuroscience to work toward gaining an understanding of how the molecular and cellular organization of the brain produces behavior and behavioral variability. His friendship has been a great support over the last five years.

Without the ongoing work of Zhu Fu nearly everything presented in this thesis would not exist. She has tirelessly worked on the molecular cloning, neuron and slice preparation, mouse breeding, and anything else I needed help with that she inevitably is an expert in. Zhu is not only a masterful technician but truly a collaborator in every sense. Her questions are always deceptively challenging and have lead to greatly improved experimental design or data presentation. In addition to Zhu, I have had excellent assistance from a slew of technicians in the Isacoff lab, including most notably Hitomi Okada.

Both Reza Vafabakhsh and Shashank Bharill have been crucial to the molecular biophysics work presented in this thesis. Reza arrived a year ago and brought amazing skill in the single molecule FRET approach that has become a very exciting project. His molecular insight and collaborative approach has, I believe, led to us making a major contribution to the understanding of GPCRs. Shashank Bharill has been a great, ongoing collaborator on the assembly of mGluRs. As the project has ebbed and flowed he has stayed committed and offered great insight into the mechanism of protein assembly in addition to his technical expertise.

In addition to the aforementioned people, there are more people from the Isacoff lab that deserve special praise. Harald Janovjak was my initial rotation advisor and was instrumental in getting the LimGluR project off of the ground. Benji Gaub also greatly contributed to the early

work on LimGluRs. Michael Kienzler, as well as chemists from the lab of Dirk Trauner, put in the hard work to synthesize the chemicals on which I rely for my experiments. Shai Berlin and Thomas Berger have also provided great insight along the way into various aspects of working with neurons, brain slices, and mice. The rest of the Isacoff lab, in addition to many other people at UC Berkeley, have created a wonderful atmosphere to do science and has made my time as a graduate student a very special one.

Chapter I: Introduction

G protein-coupled receptors and their roles in the nervous system

G protein-coupled receptors (GPCRs) are among the most widely studied families of proteins in all of biology. They are the largest class of membrane receptors and constitute ~1% of the genes in the human genome[1,2]. The GPCR family is extremely diverse and, due to their roles in nearly every described physiological process and disease pathology, GPCRs account for >60% of all current drug targets[3]. The ~1,000 human GPCRs are grouped into 6 classes (A through F) [4]. Classes A, B, and C have been the most studied and represent the majority of characterized GPCRs. Despite the lack of sequence homology between classes, all GPCRs share the topology of a seven transmembrane helix domain. On the extracellular side there is more divergence where most class A GPCRs, such as rhodopsin or adrenergic receptors, have very limited extracellular domains, while class B and C GPCRs are characterized by their large, multi-domain extracellular composition.

Generally, GPCRs convert a variety of extracellular signals, such as hormones, neurotransmitters, ions, light, peptides, and voltage, into intracellular signals via the activation of heterotrimeric G proteins. Over the last five years, a number of technological advances have lead to an explosion in the number of crystal structures available of GPCRs[5-8]. These structures have shown the conservation of the general 7-TM fold and given atomically-detailed insight into the diverse ways that ligands interact with GPCRs. Furthermore, crystal structures have given clues into the alterations in receptor tertiary structure that lead to G protein activation. One exceptionally beautiful crystallographic study has given a snapshot of a GPCR in complex with a G protein heterotrimer[9]. However, crystal structure analysis must be complemented by a variety of functional studies to gain a full picture of the dynamic process of GPCR signaling.

The signaling mechanism of GPCRs have been extensively studied which has led to a canonical model of G protein activation and signaling. In this model GPCRs are activated by their ligand which induces a conformational change which, in turn, leads to binding of a G protein heterotrimer. This GPCR-G protein interaction induces a conformational change in the Gα subunit which promotes GDP exchange for GTP and subsequent dissociation of the $G_{\beta\gamma}$ subunits. Activated G_{α} and $G_{\beta\gamma}$ then activate effectors, such as enzymes or ion channels, which initiate a number of divergent downstream pathways. Finally, signaling is terminated by either GTPase activity of Gα or regulator molecules, such as G protein receptor kinases (GRKs), which can phosphorylate GPCRs and recruit an array of desensitization machinery including arrestins. Despite the strong evidence for these basic ideas, the textbook model is becoming increasingly challenged and complicated by a wealth of studies that have expanded the potential mechanisms involved in GPCR signaling. These unresolved and controversial questions include the existence and associated consequences of GPCR oligomerization[10], the potential preassembly of multiple proteins within the signaling pathway[11], biased signaling of ligands to produce different signaling outputs through the same GPCR[12], G-protein independent signaling via non-canonical effectors[13], and GPCR signaling in intracellular compartments[14]. These questions have been approached in a number of ways but have been challenging to fully answer until recently due to the shortcomings of classical techniques for measurement and manipulation of GPCRs with high precision.

Despite the molecular diversity of GPCRs and their associated ligands, all GPCRs signal through the same 4 classes of G proteins as defined by the identity of the Gα protein: G_s, $G_{i/o}$, G_t, or G_q. However, the uniqueness of each GPCR is mediated by promiscuous coupling to multiple G proteins, divergent expression pattern, subcellular targeting, regulation, kinetics, crosstalk or co-assembly with other GPCRs, basal activity, and other properties[15,16]. This complexity in the various receptor-specific properties is especially important in the nervous system where many GPCRs can respond to the same neurotransmitter or neuromodulator but produce different cellular and network responses based on targeting and accessory proteins[17].

In the nervous system, in general, GPCRs play key roles in the processes of synaptic plasticity and neuromodulation. GPCRs at a variety of synapses respond to neurotransmitters and control, over a range of time scales, synaptic strength by activating downstream pathways that modulate electrical, biochemical, or structural properties of either the pre or post synaptic side of the synapse[18-20]. Many of the well-characterized forms of GPCR-dependent synaptic plasticity involve either metabotropic glutamate receptors (mGluRs) or $GABA_B$ receptors, which respond to the primary excitatory and inhibitory neurotransmitters, respectively. Neuromodulation, which is the major means by which neuronal activity is regulated by multiple signaling molecules other than glutamate and GABA, in almost all cases is mediated by GPCRs[21]. The primary response to the neuromodulators acetylcholine, dopamine, serotonin, endocannabinoids, ATP, and various neuropeptides and hormones are mediated by GPCRs which, unlike ionotropic neurotransmitter receptors, can induce slow, long-lasting control over large brain regions and modify global brain state[22]. Furthermore, orphan GPCRs, which have unidentified native ligands, have been key in the identification of new neuromodulators[23].

The major questions about GPCR signaling in the brain revolve around the desire to construct a spatial and temporal map of the activation properties of each receptor subtype and downstream pathway. These questions aim to ultimately understand how different receptors in different cell types can dynamically modulate excitability, synaptic strength, network oscillations, and behavior. By determining such a complete picture of the individual GPCRs and G protein pathways involved in given processes a rigorous determination of the ideal drug targets will emerge for different disorders. The classical means of probing such questions has revolved around targeting of receptors with drugs that either positively (i.e. agonists, positive allosteric modulators) or negatively (i.e. antagonists, inverse agonists) influence receptor activation. While powerful and simple, this approach has an inherent limitation in the ability to spatially and temporally control application, especially in living organisms. Furthermore, drugs are unable to distinguish between receptor subtypes within many GPCR subfamilies and in all cases cannot be targeted to specific cell types. Genetic experiments, while also very useful, are inherently limited temporally and are subject to confounding factors including developmental effects. The inherent limitations of these techniques underscores the need for new methods to control G protein signaling with high spatial and temporal precision. Recently, optogenetics has revolutionized neuroscience by allowing for the orthogonal control of electrical signaling in specific neurons *in vivo* with light. The spatiotemporal precision, and genetic control afforded by optogenetics has allowed for mapping of synaptic connectivity and probing of the cellular basis for a wide variety of behaviors and disorders[24]. Despite the extreme prevalence of GPCRs in the nervous system, the effort to similarly control metabotropic signaling has been less widespread due to its inherent complexity. In the next section I will outline the currently existing means of orthogonally manipulating GPCR signaling in the nervous system.

Methods for orthogonal control of GPCRs

Designer GPCRs. Classically GPCRs have been manipulated by the application of exogenous synthetic ligands that target a subset of receptors. These agonist, antagonists, and modulators have been useful for probing the general roles of different receptors in physiological processes and have established some receptors as valuable drug targets. However, these ligands, as discussed above, lack subtype specificity and have poor spatial control which hampers their effectiveness in identifying the role of individual brain regions or cell types in a neurological function or behavior. To overcome this, the concept of designer GPCRs which would respond to a synthetic ligand, but not native ligands, was first introduced in the early 1990s and subsequently optimized[25,26]. An early breakthrough in this approach came in 1998 when Coward et al[27] mutated the human κ opioid receptor to reduce its affinity for its native ligand, dynorphin A, while maintaining high affinity for small molecule synthetic agonists. This RASSL, or "receptor activated solely by synthetic ligands", paved the way for further engineering of a variety of GPCRs with weak affinity for native ligands that could still be manipulated by synthetic drugs. RASSLs were applied *in vivo* were they were, most notably, used to control $G_{i/o}$ signaling in the heart of transgenic mice that expressed the Ro1 RASSL[28]. While RASSLs were useful, they were limited in the nervous system by the fact that the synthetic drugs used maintained affinity for native receptors and were, thus, not always orthogonal. The breakthrough that paved the way for potential widespread use of designer GPCRs came from the laboratory of Bryan Roth which used directed molecular evolution to produce DREADDs, or "designer receptors exclusively activated by designer drug" for G_q, G_s, and $G_{i/o}$ pathways[29,30]. These tools, which are based on muscarinic receptors, respond to the synthetic drug CNO, which is bioavailable and pharmacologically inert. The hM3Dq DREADD was successfully applied *in vivo* in mice using transgenic mice that were able to respond behaviorally to CNO injection with an onset of minutes and offset of hours[31]. DREADDs have subsequently been used in a number of studies to produce orthogonal effects on neuronal activity in genetically defined neurons to probe neurological phenomena such as learning and memory[32] and addiction[33,34]. Notably, RASSLs and DREADDs maintain much of the native GPCR on which they are built and may maintain some of the unique properties of these receptors, although this has not been rigorously tested. In addition, these receptors may be engineered based on the body of knowledge that exists on the GPCRs on which they are based. For example, Nakajima et al[35] mutated the M3-based DREADD hM3Dq so that CNO activation would favor arrestin activation rather than G protein activation to develop a tool for studying G protein-independent signaling. Compared to the optically controllable GPCRs described below, designer GPCRs offer the great advantage of relative ease of application that does not require targeted illumination or, for *in vivo* application, implantation of optical fibers. However, spatial and temporal control is severely limited by drug application, especially *in vivo* where the only level of targeting is genetic. Due to these shortcomings, interest has remained in developing optically controllable GPCRs for heterologous use.

ChARGe. The first attempt to optically control a GPCR heterologously in the nervous system, and the first published optogenetic control of neuronal activity, was based on the

naturally photosensitive rhodopsin[36]. This original tool, termed "chARGe" consisted of a multigene system that was based on the Drosophila rhodopsin as a light sensor. The invertebrate rhodopsin was chosen because, unlike vertebrate rhodopsins that couple to G_t or $G_{i/o}$, it activates G_q proteins and would, thus, be more likely to induce neuronal firing. However, the Drosophila rhodopsin required the expression of up to 9 other Drosophila genes in order to reconstitute the signaling pathway including the opsin itself, G proteins, arrestin, phospholipase C, trafficking and folding cofactors, and ion channels. This version of chARGe was shown to work heterologously in Xenopus oocytes and a minimal version containing just rhodopsin, arrestin-2, and Gα was able to induce neuronal firing in cultured rat hippocampal neurons in response to white light. This result was a major breakthrough for the orthogonal control of GPCR signaling and for optogenetics in general. However, the slow kinetics, indirect mechanism, and especially the need for multiple genes to be co-expressed limited the utility of chARGe, which was quickly surpassed by channelrhodospin as the optimal means of optical excitation of neurons.

Vertebrate Rhodopsin. Following the successful proof-of-principle of chARGe, the group of Stefan Herlitze turned to the vertebrate rhodopsin as a means of optically controlling GPCR activity heterelogously. It had previously been shown that verterbrate rhodopsin, which natively couples to the transducin (G_t) G protein, can effectively couple to the related $G_{i/o}$ family of G proteins. Li et al[37] showed that heterologously-expressed rat rhodopsin RO4, without the need to co-express anyother proteins, can activate GIRK channels or inhibit voltage gated calcium channels via the endogenous $G_{i/o}$ pathway in both HEK cells and rat hippocampal neurons. Rhodopsin activation was used to inhibit neuronal firing and to presynaptically inhibit neurotransmitter release in culture and tissue. However, rhodopsin suffered from relatively slow OFF kinetics which due to receptor desensitization limited the repeatability of activation[38]. It is important to note that rhodopsin, which is not natively expressed outside of photoreceptors in the retina, is only able to reconstitute the general activation of a G protein pathway but lacks the ability to specifically replicate the complexity of GPCRs that are natively expressed in neurons. Despite these limitations rhodopsin was virally expressed in the cerebellum of mice and manipulated *in vivo* to modulate motor behavior[39].

Rhodopsin chimeras. The heterologous expression of rhodopsin in neurons paved the way for the application of photoactivatable G protein signaling. However, given the inability of rhodopsin to recapitulate the signaling complexitiy of specific receptors and the limitation to the $G_{i/o}$ pathway, the potential applications were limited. To expand the toolset, chimeras between rhodopsin and other GPCRs were developed. These chimeras were developed first to expand rhodopsin-based optical control to the Gq and Gs pathways and to move closer to manipulation of specific receptors. Airan et al[40] developed the "OptoXRs" which were based on previous constructs [41] that combined the transmembrane helices of rhodopsin with the intracellular loops and C-terminal domain of either the β_2 or α_1 adrenergic receptors. These tools, dubbed "opto-β_2AR" and "opto-α_1AR" were able to optically activate the G_s and G_q pathways, respectively. These optoXRs were successfully applied *in vivo* where they were used to drive conditioned place preference via the nucleus accumbens of virally-infected mice. Despite containing the intracellular domains of adrenergic receptors, limited characterization of the optoXRs has been performed to determine if any of the non-canonical properties, such as desensitization, arrestin signaling, or subcellular targeting of specific receptors had been maintained. Using a somewhat similar strategy, Oh et al[42] added the C-terminal tail of the 5-HT_{1A} receptor to rhodopsin to

produce a light activated GPCR that retains some aspects of the 5-HT_{1A} receptor. This receptor maintained $G_{i/o}$-coupling and light-induced neuronal inhibition while showing some aspects of the subcellular targeting of 5-HT_{1A} receptors to the distal dendrites of hippocampal neurons. This Rh-$CT_{5\text{-}HT1A}$ construct was transfected into the dorsal raphe nuclei of 5-HT_{1A} knockout mice where they were able to introduce light-induced inhibition of firing. While more characterization was performed than the optoXRs, there was still limited evidence indicating that this chimera actually mimics any of the unique properties of the 5-HT_{1A} receptor rather than simply improving membrane expression relative to rhodopsin. While useful for expanding the toolbox of photoactivatable GPCRs, rhodopsin chimeras have yet to be convincingly demonstrated to maintain properties of the receptors on which they are modeled and are still limited by the slow kinetics and limited repeatability of rhodopsin.

Non-rhodopsin opsins. While rhodopsin is the most characterized of the vertebrate opsins, a number of other opsins are present which function as GPCRs in various cell types within the retina. In recent years, in part to overcome the shortcomings of rhodopsin, non-rhodopsin opsins have been applied for the optical control of G protein signaling, including in the nervous system. These studies have been based on either the G_q-coupled melanopsin[43,44] or the G_t and $G_{i/o}$-coupled cone opsins. Karunarathne et al[45] used a number of opsin variants to optically control $G_{i/o}$, G_q, or G_s signaling in cultured cells with subcellular precision. $G_{i/o}$ signaling was controlled by a number of cone opsins that respond to blue, green, or red light while G_q signaling was induced via melanopsin activation. Finally, for optical G_s signaling they developed a chimera between a blue cone opsin and a previously described jellyfish opsin[46]. In an accompanying paper, the same group used a blue cone opsin to optically manipulate immune cell migration by targeting light subcellularly[47]. In parallel, the Herlitze group used both the cone opsins[48] and melanopsin[49] to manipulate neuronal GPCR signaling. In HEK293 cells and brain slices, Masseck et al[48] showed that both long wavelength ("vLWO") and short wavelength ("vSWO") cone opsins show faster activation and deactivation kinetics compared to rhodopsin which facilitated improved repeatability. Furthermore, they produced more 5-HT_{1a} receptor chimeras with cone opsins that were used to manipulate firing in dorsal raphe nucleus (DRN) and ultimately, to manipulate anxiety behavior. Spoida et al[49]used chimeras between melanopsin and the C-terminus of the 5-HT_{2C} receptor to manipulate G_q signaling in GABAergic neurons of the DRN to optically relieve anxiety. In addition, light-activation of both cone opsins and melanopsin have been demonstrated *in vivo* in *C. elegans* to manipulate locomotion[50]. Overall, these new tools have greatly improved the applicability of opsin-based GPCR manipulation but issues remain unresolved about the ability to truly manipulate individual GPCRs.

Caged compounds. While all of the previously reported means of manipulation of GPCRs has been based on heterologous expression, caged compounds have been of increasing use in the study of GPCR signaling. Caged compounds are based on characterized pharmacological ligands that are linked to a group that can be rapidly photolyzed to release a compound which can agonize or antagonize a specific receptor[51]. These tools have the advantage of targeting natively-expressed receptors and offering, in theory, a range of types of ligands that can agonize, antagonize, or allosterically modulate a GPCR. While classically these tools have found the most success targeting ion channels, such as ionotropic glutamate receptors with caged glutamate[52], recently specific caged GPCR ligands have been developed. Banghart et al[53,54] developed photoactivatable peptides that could target specific opioid receptors, which they used

to probe the subcellular properties of opioid signaling in locus coeruleus in slice. Using a slightly different chemistry, a photoswitchable agonist was also recently developed that could reversibly activate μ-opioid receptors[55]. While soluble chemical photoswitches are potentially very powerful in their ability to target native receptors with high precision, they are subject to many of the limits of traditional pharmacology including the incomplete ability to target specific subtypes, limited spatial control due to diffusion, and slow off kinetics due to irreversibility.

LimGluRs. In chapters 2 and 3 I report the development and initial application of optically agonized and antagonized versions of the metabotropic glutamate receptors mGluR1, 2, 3, 6, and 7 which couple to either $G_{i/o}$ or G_q pathways. These receptors, generally termed LimGluRs, are based on the entire full-length sequence of different mGluRs and contain a single cysteine substitution to allow for the covalent conjugation of a chemical photoswitch that contains the native ligand, glutamate. This approach, while complicated by the requirement of a synthetic photoswitch rather than retinal, offers a number of advantages compared to opsin-based tools. The full-length receptor is maintained which allows for the complete recapitulation of all of the unique signaling properties of the native receptor, including the ability to respond to the native ligand glutamate. This property allowed for the development of optically agonized and antagonized versions of mGluRs that produce a means of manipulation that mimics the versatility of pharmacology while providing the spatiotemporal control of light. Furthermore, the azobenzene moiety on which the chemical photoswitch is based allows for extremely fast photoswitching (<1 ms) that is repeatable and spectrally tune-able. In many cases the azobenzene photoswitches are bistable,which allows for brief pulses of light to be used to turn the receptor on and off which may limit phototoxicity in tissue and allow easy complexing with optical sensors. In chapters 2 and 3 I demonstrate the development and use of photo-activatable mGluRs *in vivo* in zebra fish and mice, indicating that these tools provide the ability to probe the roles of specific mGluRs, and G protein signaling in general, in the nervous system. Finally, in chapter 5 I show experiments attesting to the power of the tethered photoswitch approach for probing the biophysical mechanism of coupling ligand binding to receptor activation in GPCRs. Most importantly, this is a general approach that was originally applied to ion channels[56,57] and may ultimately be applied to any type of membrane receptor.

Overall, great strides have been made on a number of fronts in recent years to expand the means of manipulating GPCRs in order to understand their biophysical and physiological properties. All of the aforementioned techniques have their advantages or were instrumental in the further development of a successful approach. Depending on the application, either designer GPCRs, opsins, caged compounds, or tethered photoswitches will be valuable tools for understanding GPCRs at the molecular, cellular, network, and behavioral level with a precision that was previously impossible.

Metabotropic glutamate receptors: a model GPCR for biophysical studies

Metabotropic glutamate receptors (mGluRs) are a unique family of GPCRs that are especially important in the nervous system where they serve as modulators at excitatory and inhibitory synapses[58]. Their intricate roles in the nervous system make mGluRs excellent targets for development of optogenetic tools, which was the basis of the design of the aforementioned LimGluRs. However, in addition to the importance in understanding their physiological

functions with high precision, mGluRs are ideal model GPCRs for the study of the structural and biophysical properties of GPCRs. mGluRs are members of the class C GPCR family which also includes $GABA_B$ receptors, the Ca^{2+}-sensing receptor, taste receptors, and a number of orphan receptors. Class C GPCRs are distinguished by their dimeric assembly and large, bi-lobed extracellular ligand binding domains. This dimeric assembly has raised a number of questions about how subunits within a GPCR can communicate to modulate G protein activation and potentially produce cooperativity. Furthermore, the large separation between extracellular ligand binding domains and the transmembrane domains in mGluRs raises the question of how glutamate binding can induce G protein activation. These have been well-studied questions but complete, consistent biophysical mechanisms have been elusive due to the limitations in the ability to measure and manipulate mGluRs with classical methods. Classical methods of manipulation often rely on soluble ligands which are hard to unambiguously target to individual subunits within an oligomer while classical methods of measurement are often indirect, slow, and rely on ensemble techniques that can obscure the inherent stochasticity of proteins. After characterizing and applying the aforementioned LimGluRs in neurobiological contexts in Chapters 2 and 3, I will report work in chapters 4 and 5 that use single molecule fluorescence techniques in concert with photoswitchable ligands to gain insight into the biophysical properties of mGluRs. In chapter 4, smFRET experiments between the extracellular domains of mGluR2 and 3 are used to show that mGluRs visit three distinct conformational states that show prominent dynamics that are different between subtypes. In chapter 5, I use single molecule subunit counting to define the dimer interfaces and heterodimer propensities of mGluR2. I then use the targeting of tethered photoswitches to one or both subunits within an mGluR dimer to determine the functional cooperativity of mGluR2 and mGluR2/3 heterodimers. This work is ultimately synthesized in the discussion of chapter 5 into a structural and functional model of how ligand binding couples to receptor activation.

K2P Channels: a potential hub for neuromodulatory pathways

One of the key means used by GPCRs for regulation of neuronal activity is the modulation of ion channels. A complex population of ion channels control neuronal resting potential, excitability, synaptic transmission, and induction of synaptic plasticity. Due to their extreme diversity, potassium channels are particularly common targets of GPCR regulation [59]. One class of channels of special interest are the relatively recently identified K_{2P} channels which form a diverse subfamilies of neuronal potassium channels that are highly regulated by GPCRs [60,61]. They serve as a hub for the generation and regulation of a negative resting membrane potential and thus, cellular excitability. In addition to background roles as leak channels, K_{2P} channels also play roles in the dynamic response of cells to extracellular and intracellular signals as diverse as GPCR signaling, pH, and membrane stretch[62]. TREK1, a particularly well studied K_{2P} channel, has been found to be involved in many physiological processes such as neuroprotection against ischemia [63], pain perception and depression [64]. Consistent with a proposed role for TREK1 in depression, TREK1 is inhibited by therapeutic doses of selective serotonin reuptake inhibitors (SSRIs) such as fluoxetine (Prozac) [64,65] and spadin, a sortilin-derived peptide that also has antidepressive effects [66]. However, despite the large interest in understanding the properties of K_{2P} channels and how their regulation by GPCRs mediates physiological phenomena such as depression, it has been difficult to decipher the precise roles of individual subtypes. In chapter 6, I report the development of a means of optical control of

TREK1 using a similar tethered photoswitch approach used for LimGluRs. Using a conditional photoswitch approach, native TREK1 channels were optically blocked which allowed for their identification as non-canonical targets of $GABA_B$ receptor activation in the hippocampus. In chapter 7, I report a study that analyzed the regulation of K_{2P} channels by the enzyme phospholipase D. Using a combination of techniques, including photoswitchable TREK1 channels, I propose a novel mechanism for regulation of an ion channel by an enzyme that produces a local second messenger gradient. Finally, these findings may explain some of the effects of alcohol on neurons via indirect effects on membrane composition.

References:

1 Pierce, K. L., Premont, R. T. & Lefkowitz, R. J. Seven-transmembrane receptors. *Nat Rev Mol Cell Biol* **3**, 639-650, doi:10.1038/nrm90nrm908 [pii] (2002).

2 Lefkowitz, R. J. A brief history of G-protein coupled receptors (Nobel Lecture). *Angew Chem Int Ed Engl* **52**, 6366-6378, doi:10.1002/anie.201301924 (2013).

3 Lagerstrom, M. C. & Schioth, H. B. Structural diversity of G protein-coupled receptors and significance for drug discovery. *Nat Rev Drug Discov* **7**, 339-357, doi:10.1038/nrd2518nrd2518 [pii] (2008).

4 Fredriksson, R. & Schioth, H. B. The repertoire of G-protein-coupled receptors in fully sequenced genomes. *Mol Pharmacol* **67**, 1414-1425, doi:mol.104.009001 [pii]10.1124/mol.104.009001 (2005).

5 Katritch, V., Cherezov, V. & Stevens, R. C. Structure-function of the G protein-coupled receptor superfamily. *Annu Rev Pharmacol Toxicol* **53**, 531-556, doi:10.1146/annurev-pharmtox-032112-135923 (2013).

6 Audet, M. & Bouvier, M. Restructuring G-protein- coupled receptor activation. *Cell* **151**, 14-23, doi:10.1016/j.cell.2012.09.003S0092-8674(12)01068-9 [pii] (2012).

7 Lebon, G., Warne, T. & Tate, C. G. Agonist-bound structures of G protein-coupled receptors. *Curr Opin Struct Biol* **22**, 482-490, doi:10.1016/j.sbi.2012.03.007S0959-440X(12)00043-7 [pii] (2012).

8 Venkatakrishnan, A. J. *et al.* Molecular signatures of G-protein-coupled receptors. *Nature* **494**, 185-194, doi:10.1038/nature11896nature11896 [pii] (2013).

9 Rasmussen, S. G. *et al.* Crystal structure of the beta2 adrenergic receptor-Gs protein complex. *Nature* **477**, 549-555, doi:10.1038/nature10361nature10361 [pii] (2011).

10 Ferre, S. *et al.* G protein-coupled receptor oligomerization revisited: functional and pharmacological perspectives. *Pharmacol Rev* **66**, 413-434, doi:10.1124/pr.113.00805266/2/413 [pii] (2014).

11 Lohse, M. J., Nuber, S. & Hoffmann, C. Fluorescence/bioluminescence resonance energy transfer techniques to study G-protein-coupled receptor activation and signaling. *Pharmacol Rev* **64**, 299-336, doi:10.1124/pr.110.004309pr.110.004309 [pii] (2012).

12 Reiter, E., Ahn, S., Shukla, A. K. & Lefkowitz, R. J. Molecular mechanism of beta-arrestin-biased agonism at seven-transmembrane receptors. *Annu Rev Pharmacol Toxicol* **52**, 179-197, doi:10.1146/annurev.pharmtox.010909.105800 (2012).

13 Heuss, C. & Gerber, U. G-protein-independent signaling by G-protein-coupled receptors. *Trends Neurosci* **23**, 469-475, doi:S0166-2236(00)01643-X [pii] (2000).

14 Irannejad, R. & von Zastrow, M. GPCR signaling along the endocytic pathway. *Curr Opin Cell Biol* **27**, 109-116, doi:10.1016/j.ceb.2013.10.003S0955-0674(13)00156-7 [pii] (2014).

15 Gainetdinov, R. R., Premont, R. T., Bohn, L. M., Lefkowitz, R. J. & Caron, M. G. Desensitization of G protein-coupled receptors and neuronal functions. *Annu Rev Neurosci* **27**, 107-144, doi:10.1146/annurev.neuro.27.070203.144206 (2004).

16 Ritter, S. L. & Hall, R. A. Fine-tuning of GPCR activity by receptor-interacting proteins. *Nat Rev Mol Cell Biol* **10**, 819-830, doi:10.1038/nrm2803nrm2803 [pii] (2009).

17 Bockaert, J., Perroy, J., Becamel, C., Marin, P. & Fagni, L. GPCR interacting proteins (GIPs) in the nervous system: Roles in physiology and pathologies. *Annu Rev Pharmacol Toxicol* **50**, 89-109, doi:10.1146/annurev.pharmtox.010909.105705 (2010).

18 de Jong, A. P. & Verhage, M. Presynaptic signal transduction pathways that modulate synaptic transmission. *Curr Opin Neurobiol* **19**, 245-253, doi:10.1016/j.conb.2009.06.005S0959-4388(09)00062-2 [pii] (2009).

19 Betke, K. M., Wells, C. A. & Hamm, H. E. GPCR mediated regulation of synaptic transmission. *Prog Neurobiol* **96**, 304-321, doi:10.1016/j.pneurobio.2012.01.009S0301-0082(12)00010-X [pii] (2012).

20 Lohse, M. J., Maiellaro, I. & Calebiro, D. Kinetics and mechanism of G protein-coupled receptor activation. *Curr Opin Cell Biol* **27**, 87-93, doi:10.1016/j.ceb.2013.11.009S0955-0674(13)00185-3 [pii] (2014).

21 Marder, E. Neuromodulation of neuronal circuits: back to the future. *Neuron* **76**, 1-11, doi:10.1016/j.neuron.2012.09.010S0896-6273(12)00817-3 [pii] (2012).

22 Lee, S. H. & Dan, Y. Neuromodulation of brain states. *Neuron* **76**, 209-222, doi:10.1016/j.neuron.2012.09.012S0896-6273(12)00820-3 [pii] (2012).
23 Civelli, O. Orphan GPCRs and neuromodulation. *Neuron* **76**, 12-21, doi:10.1016/j.neuron.2012.09.009 S0896-6273(12)00816-1 [pii] (2012).
24 Tye, K. M. & Deisseroth, K. Optogenetic investigation of neural circuits underlying brain disease in animal models. *Nat Rev Neurosci* **13**, 251-266, doi:10.1038/nrn3171nrn3171 [pii] (2012).
25 Strader, C. D. *et al.* Allele-specific activation of genetically engineered receptors. *J Biol Chem* **266**, 5-8 (1991).
26 Giguere, P. M., Kroeze, W. K. & Roth, B. L. Tuning up the right signal: chemical and genetic approaches to study GPCR functions. *Curr Opin Cell Biol* **27**, 51-55, doi:10.1016/j.ceb.2013.11.006 S0955-0674(13)00182-8 [pii] (2014).
27 Coward, P. *et al.* Controlling signaling with a specifically designed Gi-coupled receptor. *Proc Natl Acad Sci U S A* **95**, 352-357 (1998).
28 Redfern, C. H. *et al.* Conditional expression and signaling of a specifically designed Gi-coupled receptor in transgenic mice. *Nat Biotechnol* **17**, 165-169, doi:10.1038/6165 (1999).
29 Armbruster, B. N., Li, X., Pausch, M. H., Herlitze, S. & Roth, B. L. Evolving the lock to fit the key to create a family of G protein-coupled receptors potently activated by an inert ligand. *Proc Natl Acad Sci U S A* **104**, 5163-5168, doi:0700293104 [pii]10.1073/pnas.0700293104 (2007).
30 Conklin, B. R. *et al.* Engineering GPCR signaling pathways with RASSLs. *Nat Methods* **5**, 673-678, doi:10.1038/nmeth.1232nmeth.1232 [pii] (2008).
31 Alexander, G. M. *et al.* Remote control of neuronal activity in transgenic mice expressing evolved G protein-coupled receptors. *Neuron* **63**, 27-39, doi:10.1016/j.neuron.2009.06.014 S0896-6273(09)00467-X [pii] (2009).
32 Garner, A. R. *et al.* Generation of a synthetic memory trace. *Science* **335**, 1513-1516, doi:10.1126/science.1214985335/6075/1513 [pii] (2012).
33 Ferguson, S. M. *et al.* Transient neuronal inhibition reveals opposing roles of indirect and direct pathways in sensitization. *Nat Neurosci* **14**, 22-24, doi:10.1038/nn.2703nn.2703 [pii] (2011).
34 Mahler, S. V. *et al.* Designer receptors show role for ventral pallidum input to ventral tegmental area in cocaine seeking. *Nat Neurosci* **17**, 577-585, doi:10.1038/nn.3664nn.3664 [pii] (2014).
35 Nakajima, K. & Wess, J. Design and functional characterization of a novel, arrestin-biased designer G protein-coupled receptor. *Mol Pharmacol* **82**, 575-582, doi:mol.112.080358 [pii]10.1124/mol.112.080358 (2012).
36 Zemelman, B. V., Lee, G. A., Ng, M. & Miesenbock, G. Selective photostimulation of genetically chARGed neurons. *Neuron* **33**, 15-22, doi:S0896627301005748 [pii] (2002).
37 Li, X. *et al.* Fast noninvasive activation and inhibition of neural and network activity by vertebrate rhodopsin and green algae channelrhodopsin. *Proc Natl Acad Sci U S A* **102**, 17816-17821, doi:0509030102 [pii]10.1073/pnas.0509030102 (2005).
38 Levitz, J. *et al.* Optical control of metabotropic glutamate receptors. *Nat Neurosci* **16**, 507-516, doi:10.1038/nn.3346nn.3346 [pii] (2013).
39 Gutierrez, D. V. *et al.* Optogenetic control of motor coordination by Gi/o protein-coupled vertebrate rhodopsin in cerebellar Purkinje cells. *J Biol Chem* **286**, 25848-25858, doi:10.1074/jbc.M111.253674 M111.253674 [pii] (2011).
40 Airan, R. D., Thompson, K. R., Fenno, L. E., Bernstein, H. & Deisseroth, K. Temporally precise in vivo control of intracellular signalling. *Nature* **458**, 1025-1029, doi:10.1038/nature07926nature07926 [pii] (2009).
41 Kim, J. M. *et al.* Light-driven activation of beta 2-adrenergic receptor signaling by a chimeric rhodopsin containing the beta 2-adrenergic receptor cytoplasmic loops. *Biochemistry* **44**, 2284-2292, doi:10.1021/bi048328i (2005).
42 Oh, E., Maejima, T., Liu, C., Deneris, E. & Herlitze, S. Substitution of 5-HT1A receptor signaling by a light-activated G protein-coupled receptor. *J Biol Chem* **285**, 30825-30836, doi:10.1074/jbc.M110.147298 M110.147298 [pii] (2010).
43 Melyan, Z., Tarttelin, E. E., Bellingham, J., Lucas, R. J. & Hankins, M. W. Addition of human melanopsin renders mammalian cells photoresponsive. *Nature* **433**, 741-745, doi:nature03344 [pii] 10.1038/nature03344 (2005).

44 Qiu, X. *et al.* Induction of photosensitivity by heterologous expression of melanopsin. *Nature* **433**, 745-749, doi:nature03345 [pii]10.1038/nature03345 (2005).
45 Karunarathne, W. K., Giri, L., Kalyanaraman, V. & Gautam, N. Optically triggering spatiotemporally confined GPCR activity in a cell and programming neurite initiation and extension. *Proc Natl Acad Sci U S A* **110**, E1565-1574, doi:10.1073/pnas.1220697110 1220697110 [pii] (2013).
46 Bailes, H. J., Zhuang, L. Y. & Lucas, R. J. Reproducible and sustained regulation of Galphas signalling using a metazoan opsin as an optogenetic tool. *PLoS One* **7**, e30774, doi:10.1371/journal.pone.0030774 PONE-D-11-21928 [pii] (2012).
47 Karunarathne, W. K., Giri, L., Patel, A. K., Venkatesh, K. V. & Gautam, N. Optical control demonstrates switch-like PIP3 dynamics underlying the initiation of immune cell migration. *Proc Natl Acad Sci U S A* **110**, E1575-1583, doi:10.1073/pnas.1220755110 1220755110 [pii] (2013).
48 Masseck, O. A. *et al.* Vertebrate cone opsins enable sustained and highly sensitive rapid control of Gi/o signaling in anxiety circuitry. *Neuron* **81**, 1263-1273, doi:10.1016/j.neuron.2014.01.041S0896-6273(14)00072-5 [pii] (2014).
49 Spoida, K., Masseck, O. A., Deneris, E. S. & Herlitze, S. Gq/5-HT2c receptor signals activate a local GABAergic inhibitory feedback circuit to modulate serotonergic firing and anxiety in mice. *Proc Natl Acad Sci U S A* **111**, 6479-6484, doi:10.1073/pnas.1321576111 1321576111 [pii] (2014).
50 Cao, P. *et al.* Light-sensitive coupling of rhodopsin and melanopsin to G(i/o) and G(q) signal transduction in Caenorhabditis elegans. *FASEB J* **26**, 480-491, doi:10.1096/fj.11-197798j.11-197798 [pii] (2012).
51 Ellis-Davies, G. C. Caged compounds: photorelease technology for control of cellular chemistry and physiology. *Nat Methods* **4**, 619-628, doi:nmeth1072 [pii]10.1038/nmeth1072 (2007).
52 Callaway, E. M. & Katz, L. C. Photostimulation using caged glutamate reveals functional circuitry in living brain slices. *Proc Natl Acad Sci U S A* **90**, 7661-7665 (1993).
53 Banghart, M. R. & Sabatini, B. L. Photoactivatable neuropeptides for spatiotemporally precise delivery of opioids in neural tissue. *Neuron* **73**, 249-259, doi:10.1016/j.neuron.2011.11.016S0896-6273(11)01089-0 [pii] (2012).
54 Banghart, M. R., Williams, J. T., Shah, R. C., Lavis, L. D. & Sabatini, B. L. Caged naloxone reveals opioid signaling deactivation kinetics. *Mol Pharmacol* **84**, 687-695, doi:10.1124/mol.113.088096mol.113.088096 [pii] (2013).
55 Schonberger, M. & Trauner, D. A photochromic agonist for mu-opioid receptors. *Angew Chem Int Ed Engl* **53**, 3264-3267, doi:10.1002/anie.201309633 (2014).
56 Szobota, S. & Isacoff, E. Y. Optical control of neuronal activity. *Annu Rev Biophys* **39**, 329-348, doi:10.1146/annurev.biophys.093008.131400 (2010).
57 Kramer, R. H., Mourot, A. & Adesnik, H. Optogenetic pharmacology for control of native neuronal signaling proteins. *Nat Neurosci* **16**, 816-823, doi:10.1038/nn.3424nn.3424 [pii] (2013).
58 Niswender, C. M. & Conn, P. J. Metabotropic glutamate receptors: physiology, pharmacology, and disease. *Annu Rev Pharmacol Toxicol* **50**, 295-322, doi:10.1146/annurev.pharmtox.011008.145533 (2010).
59 Yamada, M., Inanobe, A. & Kurachi, Y. G protein regulation of potassium ion channels. *Pharmacol Rev* **50**, 723-760 (1998).
60 Honore, E. The neuronal background K2P channels: focus on TREK1. *Nat Rev Neurosci* **8**, 251-261, doi:nrn2117 [pii]10.1038/nrn2117 (2007).
61 Mathie, A. Neuronal two-pore-domain potassium channels and their regulation by G protein-coupled receptors. *J Physiol* **578**, 377-385, doi:jphysiol.2006.121582 [pii]10.1113/jphysiol.2006.121582 (2007).
62 Noel, J., Sandoz, G. & Lesage, F. Molecular regulations governing TREK and TRAAK channel functions. *Channels (Austin)* **5** (2011).
63 Heurteaux, C. *et al.* TREK-1, a K+ channel involved in neuroprotection and general anesthesia. *Embo J* **23**, 2684-2695 (2004).
64 Heurteaux, C. *et al.* Deletion of the background potassium channel TREK-1 results in a depression-resistant phenotype. *Nat Neurosci* **9**, 1134-1141 (2006).
65 Sandoz, G., Bell, S. C. & Isacoff, E. Y. Optical probing of a dynamic membrane interaction that regulates the TREK1 channel. *Proc Natl Acad Sci U S A* **108**, 2605-2610, doi:10.1073/pnas.1015788108 (2011).
66 Mazella, J. *et al.* Spadin, a sortilin-derived peptide, targeting rodent TREK-1 channels: a new concept in the antidepressant drug design. *PLoS Biol* **8**, e1000355, doi:10.1371/journal.pbio.1000355 (2010).

Chapter II: Optical control of metabotropic glutamate receptors

This chapter was published as a technical report in Nature Neuroscience volume 16, issue 4, pages 507-516 in March 2013 with me as first author.

Introduction:

Optogenetics has revolutionized neuroscience by making it possible to use heterologously expressed light-gated ion channels and pumps to stimulate or inhibit activity in genetically selected neurons and brain regions and thereby determine their roles in circuit function and behavior[1,2]. As the flow of information through neural circuits depends on the strength of synaptic transmission, and changes in synaptic strength are critical to neural processing as well as learning and memory, an important further development would be to bring optogenetics to the native pre- and postsynaptic receptors that control synaptic transmission and plasticity.

Of special interest are GPCRs, the largest class of membrane signaling proteins, which, because of their importance to disease, are the most explored drug targets in all of biology. GPCRs respond to a wide array of stimuli and contain a seven transmembrane domain that couples to heterotrimeric G proteins, including the Gq, Gs, Gt and Gi/o families, through which they regulate a variety of other signaling proteins[3]. Recent X-ray structures have increased our understanding of how GPCRs interact with external ligands and couple intracellularly with G proteins[4]. Despite these efforts, there remains a paucity of selective pharmacological tools for GPCRs, and the specific biochemical, physiological and behavioral roles of many GPCRs are not well understood. In neural systems, GPCRs are found mostly on sensory cilia and at synapses. The same GPCR may be found on both presynaptic excitatory and inhibitory nerve terminals, as well as on dendritic spines and associated glial processes[5], making it difficult to determine its specific function in each compartment and leaving the mechanism of induction of synaptic plasticity undefined. Even though multiple GPCRs in a cell may couple to the same G proteins, they often activate distinct targets as a result of molecular interactions that colocalize them in specific protein complexes, which can lead to unique patterns of regulation[3,6,7].

Thus, to determine the function of a GPCR, one needs specific tools for subtype-selective, cell type–specific, spatially precise, and, ideally, rapid and reversible manipulation. The ability to engineer individual full-length GPCRs that can be activated or blocked by remote control could provide a general solution for these problems. GPCRs have already been engineered to respond to non-native ligands, the so-called RASSLs and DREADDs, and used to orthogonally activate G protein pathways *in vitro*[8] and *in vivo*[9]. Because these receptors lack the spatiotemporal precision of optical manipulation, interest has remained in the development of light-activated GPCRs. Until now, effort has centered on naturally light-sensitive rhodopsin[10–12] and melanopsin[13–15] and chimeras that combine the transmembrane portions of rhodopsin with the cytoplasmic loops of adrenergic or serotonergic receptors that couple to other G proteins[16–20]. Although these foreign or chimeric receptors can be used to activate specific G proteins, they lack signaling specificity because they lack the complete sequence (and normal protein interactions) of the native GPCR. Moreover, as they require 11-*cis* retinal as a photoswitch, which is lost following photoisomerization, they cannot trigger either sustained or reproducible signals because of incomplete recovery following photo-stimulation[21].

To solve these problems, we developed an optochemical method for controlling native

mammalian GPCRs with light. We employed synthetic photoswitchable tethered ligands (PTLs) that could be targeted to genetically modified versions of native receptors[1,22], as has been done to light-block K+ channels[23] and to light-activate the ionotropic kainate receptor[24]. We targeted the eight-member mGluR family. mGluRs are class C GPCRs that are allosterically regulated by glutamate binding to a large extracellular clamshell ligand-binding domain (LBD)[5]. mGluRs respond to spatially confined, temporal patterns of synaptic and extrasynaptic glutamate to regulate neuronal excitability, transmitter release and synaptic plasticity[5,25,26]. They include presynaptic receptors, which provide feedback control over glutamate release from excitatory nerve terminals and control of GABA release from inhibitory nerve terminals, postsynaptic receptors that modulate synaptic signaling in dendritic spines, and receptors in astrocytic processes that are intimately associated with synapses and respond to neuronal activity in several ways, including gliotransmitter release[27,28]. The mGluRs are divided into three groups[5]. We focused on the group II mGluRs, mGluR2 and mGluR3, which couple to the Gi/o pathway to inhibit adenylyl cyclase[29], activate GIRK channels to reduce excitability and inhibit presynaptic voltage-gated calcium channels to inhibit neurotransmitter release[30,31]. These mGluRs operate in synaptic plasticity in multiple brain regions[25,26], participate in fundamental behavioral processes, including memory[32], and represent major drug targets for neuropsychiatric disorders[33]. We extended our engineering to the group III mGluR mGluR6, which also couples to Gi/o, but has distinct expression patterns, subcellular targeting and regulation, and, as a consequence, distinct roles in neural circuits[5].

We used a combination of structural analysis and synthesis of previously unknown compounds to develop new PTLs with maleimide at one end for cysteine attachment, a photoisomerizable azobenzene linker and glutamate as the ligand at the other end. Monte Carlo simulations enabled us to determine PTL attachment points such that photoisomerization of the azobenzene would toggle the PTL from a conformation that permits glutamate binding to one that does not. The approach was successful for both photo-agonism and photo-antagonism of mGluR2. Light rapidly, reversibly and reproducibly turned mGluR2 on and off. The photo-control was bistable and could be used to toggle excitability and presynaptic inhibition in cultured neurons and brain slices. *In vivo*, mGluR2 photo-agonism was able to reversibly and repeatedly modulate escape behavior in larval zebrafish, a fast control of a previously unknown native form of regulation of the acoustic startle response (ASR). The photo-control approach was generalizable, as we transferred it to mGluR3 and mGluR6. The introduction of photosensitivity into native GPCRs provides the means for probing their biological functions at a level of precision not previously available.

Results:

Tether model pharmacology and Monte Carlo simulations

To design photocontrol of mGluR2, we built a homology model of the mGluR2 LBD based on the mGluR3 crystal structure[34] (Supplementary Fig. 2.1a–c) and tested a series of test compounds, which we refer to as tether models (Fig. 2.1a). We found that, unlike the 4'L (γ carbon of glutamate) requirement at ionotropic glutamate receptors, 4'D stereochemistry was required for mGluR2 and that a short tether (D-Tether-0) acted as an agonist, whereas a longer tether (D-Tether-1) acted as an antagonist (Supplementary Fig. 2.1). These findings led us to synthesize D-MAG-0 and D-MAG-1 (D-maleimide azobenzene glutamate; Fig. 2.1b) with the goal of identifying attachment points for optical agonism (Fig. 2.1c) or antagonism (Fig. 2.1d). earlier experimentally determined coordinates that were validated computationally[35]. After manually positioning the glutamate group of D-MAG-0 in the binding pocket, the Monte-Carlo multiple minimum (MCMM) algorithm[36] was used to search the space accessible to D-MAG-0 with single-bond rotations as degrees of freedom. The MCMM algorithm generated 20,000 orientations and structures and, for each, automatically measured the distance from the cysteine-reactive maleimide group of MAG to every residue on the surface of the LBD. Simulations were performed for both *cis* and *trans* conformations of D-MAG-0 (Fig. 2.2a). The conformational search identified eight clusters of 3–8 residues that were frequently populated by the maleimide group of D-MAG-0 (Fig. 2.2b).

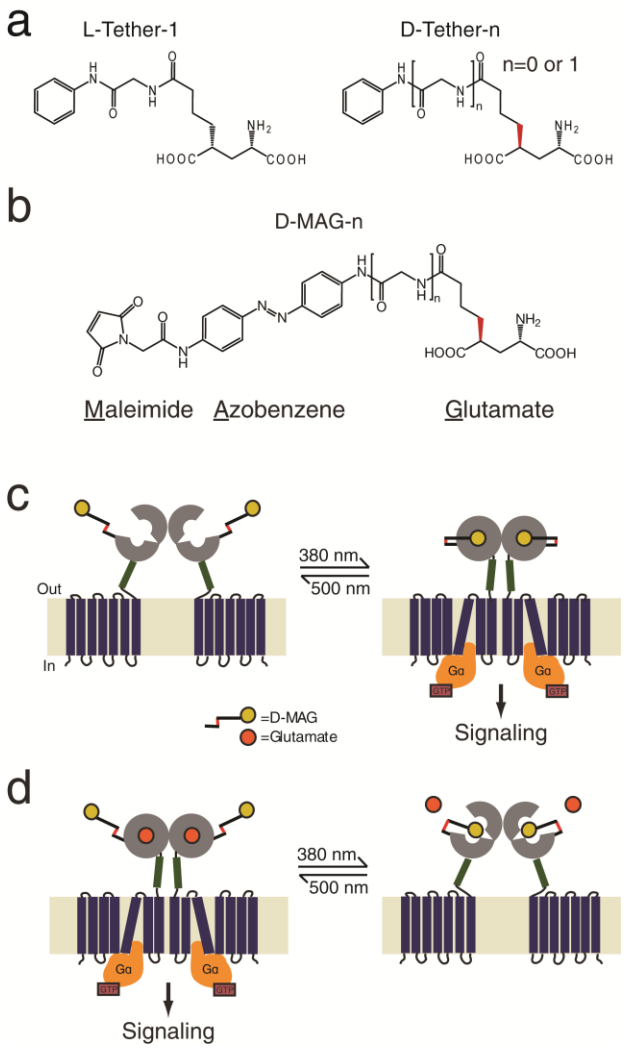

Figure 2.1, Design of photoswitches for light-control of mGluR2. a) Chemical structure of tether models including previously described L-Tether-1 and new 4′D versions with two different linker lengths (D-Tether-0 and D-Tether-1). b) Structure of D-MAG molecules. D-MAG is maximally isomerized to the *cis* state by 380-nm light and isomerized to the *trans* state by 500-nm light. Spontaneous thermal relaxation from *cis* to *trans* occurs over tens of minutes at 25 °C. c) Schematic view of light-induced agonism. mGluRs contain a ligand-binding clamshell domain (gray) that is coupled to a seven-transmembrane domain (dark blue) by a cysteine-rich domain (green). Agonist binding to the LBD initiates clamshell closure, which rearranges a dimer interface with a partner binding domain of a second subunit and transmits a conformational change via the transmembrane domain to the cytoplasmic domain, thereby activating G proteins. Under 380-nm illumination D-MAG enters the *cis* state and reorients the glutamate moiety into the ligand-binding site to drive clamshell closure and activate G protein and downstream signaling. d) Schematic of 380 nm–induced antagonism. Glutamate (dark orange circles) is shown in the bound, activated state of mGluR2. Following photoisomerization, the glutamate end of MAG enters the binding site and prevents clamshell closure, thereby deactivating the receptor.

To rationally design light-gated versions of mGluR2, we used Monte Carlo simulations to identify geometrically appropriate cysteine-attachment points for the conjugation of D-MAG-0. First, we built a homology model of mGluR2 in the open, glutamate-bound state using the mGluR1 open, glutamate-bound crystal structure (PDB ID: 1EWK) as a template. We then generated molecular models of D-MAG-0 with geometries of *cis*- and *trans*-azobenzene based on earlier experimentally determined coordinates that were validated computationally[35]. After manually positioning the glutamate group of D-MAG-0 in the binding pocket, the Monte-Carlo multiple minimum (MCMM) algorithm[36] was used to search the space accessible to D-MAG-0 with single-bond rotations as degrees of freedom. The MCMM algorithm generated 20,000 orientations and structures and, for each, automatically measured the distance from the cysteine-reactive maleimide group of MAG to every residue on the surface of the LBD. Simulations were performed for both *cis* and *trans* conformations of D-MAG-0 (Fig. 2.2a). The conformational search identified eight clusters of 3–8 residues that were frequently populated by the maleimide group of D-MAG-0 (Fig. 2.2b).

Based on the Monte Carlo simulations, we selected a subset of seven residues with orientations favorable for the maleimide end of MAG to conjugate and for its glutamate end to enter the ligand-binding site without steric clashes. Seven candidate sites were identified: Q42, D146, E373 and S376 in the upper lobe of the LBD, L300 and S302 on the lower lobe, and D215 at the hinge (Fig. 2.2c). Each site was individually substituted with cysteine and coexpressed with GIRK1 in HEK293 cells.

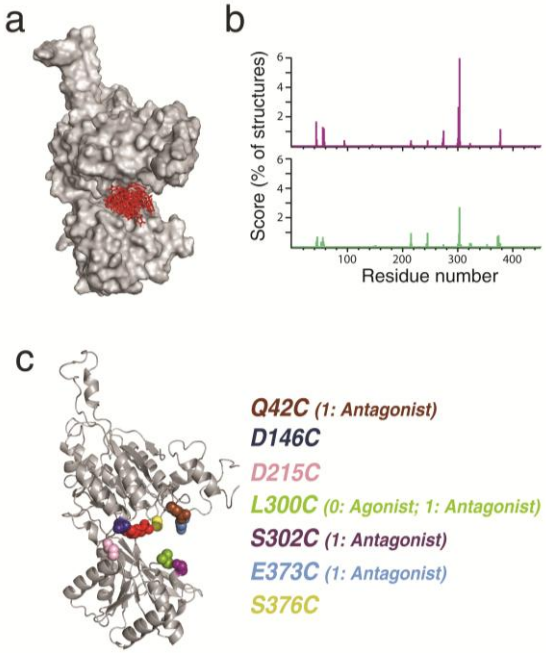

Figure 2.2. Monte Carlo simulations and cysteine-scanning of mGluR2 LBD. a) *cis*-D-MAG-0 (red stick depiction) with glutamate end bound in LBD (gray surface depiction) is shown in 20 superposed conformations calculated by Monte Carlo simulation using a homology model of the mGluR2 LBD in the open, glutamate-bound conformation. b) Results of D-MAG-0 simulations for *cis* and*trans* conformations. Lines indicate the frequency with which the maleimide end of MAG approached within 6Å of the Cα of a particular residue in the *cis* state (violet) and *trans* state (green). c) Open homology model of mGluR2 LBD showing native side chains of seven residues individually substituted to cysteine. Results of photoswitching of D-MAG-0 and D-MAG-1 attached at each of the positions where any photoresponse was observed are shown in parentheses. 0 indicates D-MAG-0 and 1 indicates D-MAG-1. Data are from ≥2 different coverslips for all conditions tested.

Photo-antagonism by D-MAG-1: LimGluR2-block

We initially focused on two of the MAG attachment sites, L300C and S302C, because of their high scores in the Monte Carlo simulations and their large photo-effects (Fig. 2.2b and Supplementary Table 2.1). Cells expressing either variant along with GIRK1 were labeled with either D-MAG-0 or D-MAG-1 (50–100 μM) for 30–60 min, patch-clamped in the whole-cell configuration and alternately challenged with 380-nm light to isomerize the photoswitch to *cis*

and 500-nm light to isomerize to *trans*. This was done in the absence of glutamate to determine whether there was photo-agonism or in the presence of glutamate to determine whether there was photo-antagonism. Notably, no photoeffects were observed in cells expressing wild-type mGluR2 and labeled with D-MAG-0 or D-MAG-1 (Supplementary Table 2.1).

Following labeling at S302C and L300C with D-MAG-1, we found that illumination at 380 and 500 nm had no effect on the current (Fig. 2.3a and Supplementary Fig. 2.2a). However, in the presence of glutamate, 380-nm light induced a marked decrease in the current that was reversed by illumination at 500 nm (Fig. 2.3a and Supplementary Fig. 2.2a). Repeated switching between 380- and 500-nm light toggled the glutamate-induced current between high and low levels. The percentage photo-antagonism was 21 ± 2% (n = 7) for D-MAG-1 at L300C and 53 ± 4% (n = 5) at S302C in 1 mM glutamate. At concentrations greater than 1 mM, photoantagonism was decreased (Supplementary Fig. 2.2b,c), indicating a competitive mechanism. D-MAG-1 antagonism is consistent with the antagonism of the D-Tether-1 compound, as described above. Because of the large potency of the 302C substitution in combination with D-MAG-1, we named this tool LimGluR2-block.

An advantageous property of the azobenzene photoswitches that we used is their thermal bistability, which makes it possible to produce persistent occupancy in the dark of the *cis* state following a photo-isomerizing light pulse[37,38]. Indeed, we found that brief light pulses at 380 nm induced antagonism that was stable in the dark until it was reversed by 500-nm illumination (Fig. 2.3b).

Photo-agonism by D-MAG-0: LimGluR2

We next turned to the version of MAG that was based on the agonist D-Tether-0, D-MAG-0. We focused on the combination of L300C and D-MAG-0 because of the utility of photo-activation, and referred to it as LimGluR2. The photo-activation of LimGluR2 by 380-nm light yielded currents about half as large as those evoked by saturating glutamate (48 ± 4% compared with 1 mM glutamate, n = 10; Fig. 2.3c). Illumination at 500 nm rapidly terminated the activation of the GIRK1 channels (Fig. 2.3c–f). Voltage ramps confirmed that the light activation of LimGluR2 at 380 nm was a result of the opening of the same inward-rectifying potassium conductance as was activated by glutamate (Supplementary Fig. 2.3a).

Notably, no antagonism of the glutamate response was induced by illumination at 380 nm (Fig. 2.3c and Supplementary Fig. 2.3c). This suggests that the lack of full activation by D-MAG-0 attached to L300C is not a result of partial agonism by *cis*-D-MAG-0. Application of glutamate following illumination at 380 nm increased the inward current above the level induced by light alone (Supplementary Fig. 2.3b). This result further indicates that MAG does not lock the LBD in a partially active conformation, but instead functions as a full agonist in a fraction of subunits. LimGluR2 maintained close to normal affinity for glutamate (Supplementary Fig. 2.3d) and retained the ability to be activated or antagonized by standard group II mGluR pharmacological agents (Supplementary Fig. 2.3e,f).

As with the bistability of LimGluR2-block, we found that brief activating light pulses at 380 nm evoked a period of GIRK activation that persisted for tens of seconds in the dark, and which could be rapidly turned off by illumination with 500-nm light (Fig. 3d). During this bout of protracted activation in the dark, the current declined by ~10–20%, which was similar to what was seen under continuous illumination of LimGluR2 at 380 nm, as well as in response to extended application of glutamate (Fig. 2.3a and Supplementary Fig. 2.4a). At moderate light

intensities (10–20 mW mm–2), bistable activation and deactivation were elicited by brief light pulses (250-ms pulse at 380 nm to activate and 1-s pulse at 500 nm to deactivate) of LimGluR2-induced GIRK currents with identical amplitude and kinetics to currents induced by extended illumination (Supplementary Fig. 2.4a–c). At higher light intensities (~40 W mm–2), signaling could be activated by sub-millisecond pulses of light (Fig. 2.3e), indicating that these brief pulses are sufficient to ligand the receptor and that the kinetics of effector activation and deactivation are rate-limited by subsequent signaling steps.

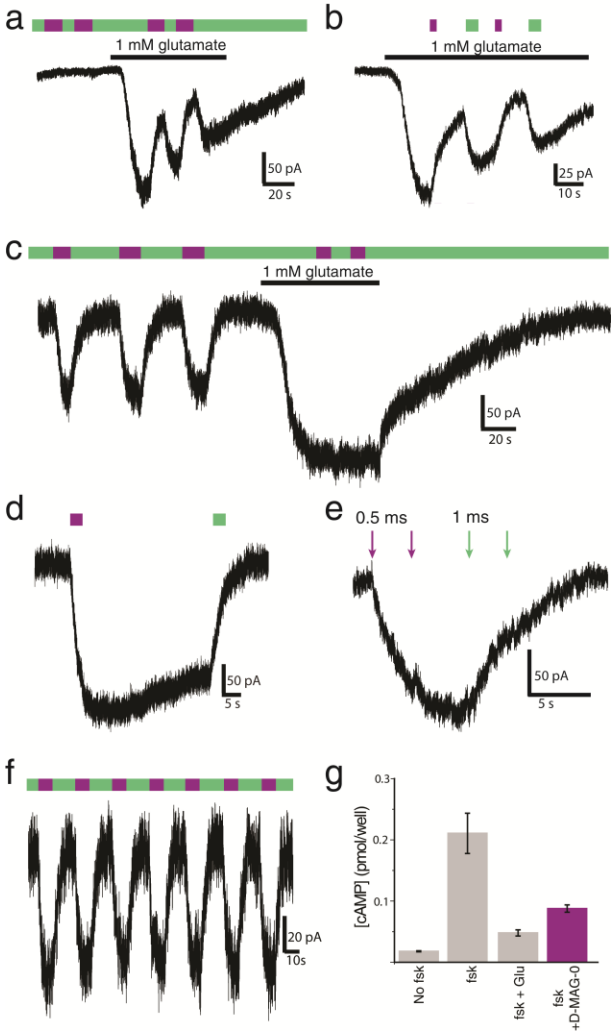

Figure 2.3. Photo-antagonism and photo-agonism of mGluR2. a–f) Effects of photoswitching D-MAG-0 and D-MAG-1 on the activation of GIRK1 current in HEK293 cells. a) When D-MAG-1 was attached to S302C (LimGluR2-block), light had no effect in the absence of glutamate, but 380-nm light evoked photo-antagonism in the presence of glutamate. Black bars indicate application of 1 mM L-glutamate. Green bars indicate illumination with 500-nm light and violet bars indicate 380-nm light. b) LimGluR2-block photo-antagonism is bistable. A brief flash of 380-nm light induced a decrease in glutamate-evoked current that was sustained in the dark until it was reversed by 500 nm. c) When D-MAG-0 was attached to L300C, 380-nm light evoked GIRK1 current on its own. The current remained activated until deactivation was initiated by 500-nm light. No photo-antagonism was seen in the presence of glutamate, indicating that D-MAG-0 was not a partial agonist of mGluR2-L300C. d) LimGluR2-mediated GIRK1 current showed sustained response in the dark following a brief illumination at 380 nm. e) At higher light intensities (~40 W mm^{-2}), 0.5-ms, 380-nm pulses could activate and 1-ms, 500-nm pulses could fully deactivate LimGluR2. The second 380-nm pulse showed minor further activation, indicating that the first pulse almost completely activated the receptors. f) GIRK1 current evoked by repetitive rounds of photo-activation and photo-deactivation of mGluR2-L300C–D-MAG-0 (LimGluR2) by pulses of 380-nm and 500-nm light, respectively. g) LimGluR2 activation reduced cAMP elevation induced by a 10-min application of 10 μM forskolin (fsk) with similar efficacy as the 1 mM glutamate application. Error bars represent s.e.m. for *n* = 3 coverslips per condition.

Repeated bouts of photoswitching of LimGluR2 yielded multiple rounds of photo-activation of GIRK1 channels without decline of the response (Fig. 3f), consistent with the lack of GRK-dependent desensitization of mGluR2[39,40]. Having observed the reproducibility of LimGluR2, we asked how it compares with previously described light-gated GPCRs that are made either of rhodopsin or of rhodopsin chimeras. To address this, we tested rhodopsin, the critical light-gated component of all of the previously described GPCRs. Rat rhodopsin, RO4, which also couples to GIRK1 channels[11], was expressed in HEK293 cells and the cells were incubated for 40 min in 1 μM 11-cis retinal in the dark. Illumination of cells coexpressing RO4 and GIRK1 with 490-nm light activated large inward GIRK currents (Supplementary Fig. 2.5a)

that were similar in amplitude and rise time to those evoked by LimGluR2 (Supplementary Fig. 2.5b). However, the GIRK1 deactivation speed of RO4 following light turn-off was much slower than that following light-driven deactivation of LimGluR2 (Supplementary Fig. 5a–c). As a result of the slow deactivation kinetics of RO4, repeated optical stimulation was limited to intervals of 90 s (Supplementary Fig. 2.5d). Even at this long interval, the RO4-mediated responses declined from pulse to pulse (Supplementary Fig. 2.5d,f). In contrast, LimGluR2 photo-responses were stable in amplitude (Fig. 2.3d and Supplementary Fig. 2.5e,f).

Having seen that LimGluR2 can photo-activate Gβγ-mediated signaling, as assayed with GIRK currents, we asked whether it could also photo-activate Gα-mediated signaling by measuring its ability to reduce cellular cAMP levels. When labeled with D-MAG-0 and stimulated with 380-nm light, LimGluR2 reduced the elevation of cAMP that was triggered by forskolin with an efficacy approaching that of 1 mM glutamate (Fig. 2.3g). This indicates that *cis*-D-MAG-0 activates mGluR2 in the same way as glutamate to induce native downstream signaling.

Generalization of photocontrol to mGluR3 and mGluR6

To determine whether the PTL approach could be generalized to other mGluRs, we tested cysteine substitutions in mGluR3, the other group II mGluR member, and mGluR6, a group III mGluR member, at residues that are homologous to L300 of mGluR2 (Fig. 2.4a). Optical control of mGluR3 is attractive because of the lack of agonists and antagonists that differentiate between mGluR2 and 3, with the exception of a recently described compound that agonizes mGluR2 and antagonizes mGluR3[41]. mGluR6 is an important target for photocontrol because of its central role in synaptic transmission from photoreceptors to ON bipolar cells in the retina.

Conjugation of mGluR3 Q306C with D-MAG-0 produced strong photo-agonism (LimGluR3) under 380-nm light (Fig. 2.4b). The photocurrents were 74 ± 12% (n = 6 cells) of the amplitude of 1 mM glutamate-evoked currents, indicating that LimGluR3 is even more efficient than LimGluR2. Conjugation of mGluR6-K306C with D-MAG-0 produced a strong photo-antagonism under 380-nm light (Fig. 2.4c). Photo-antagonism was 40 ± 3% (n = 5 cells, 1 mM glutamate) for D-MAG-0 at mGluR6-K306C. We termed this tool LimGluR6-block. Notably, photoswitching of D-MAG-0 anchored at sites of mGluR3 and mGluR6 that are homologous to mGluR2's L300 yielded similar photo-agonism in mGluR3, but photo-antagonism in mGluR6, providing a readout of the degree of geometric similarity near the LBD binding pocket.

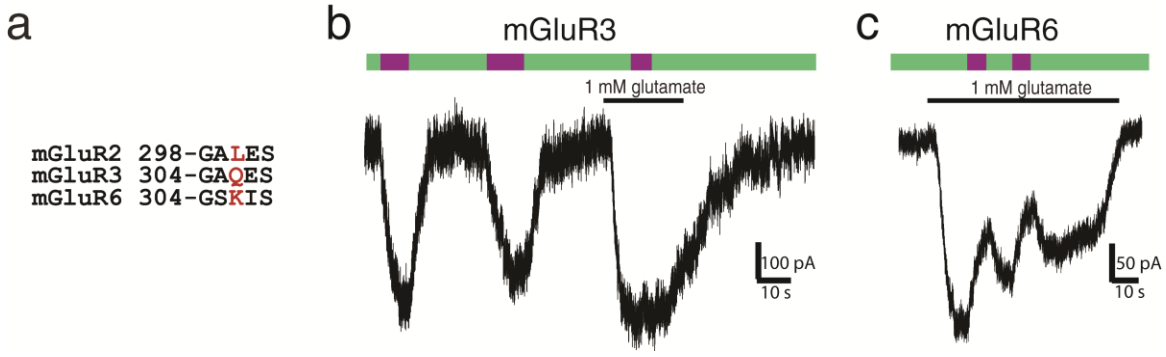

Figure 2.4, Extension of photoswitching from mGluR2 to mGluR3 and mGluR6. a) Local alignment of region containing D-MAG-0 anchoring sites in mGluR2 for LimGluR2 (red). b) When D-MAG-0 was attached to mGluR3-Q306C (LimGluR3), robust 380-nm light–induced agonism was observed. Similar to LimGluR2, no photo-antagonism was seen in the presence of glutamate. c) When D-MAG-0 was attached to mGluR6-K306C (LimGluR6-block) robust 380-nm light–induced photoantagonism was observed, indicating that the PTL approach can be extended to group III mGluRs.

Optical control of excitability in hippocampal neurons

In addition to the functional advantages over existing photoswitchable GPCRs, LimGluR2 is a native receptor that could make it possible to optically stimulate native mGluR2 targets with light. To test this, we examined the ability of LimGluR2 to optically modulate native downstream targets of mGluR2 in cultured hippocampal neurons. These targets include somatodendritic GIRK channels42 and voltage-gated calcium channels in the presynaptic nerve terminal[43,44], both of which should be within reach of mGluR2-L300C, which we found to distribute to the soma and many fine processes (Fig. 2.5a).

We first tested the expectation that activation by LimGluR2 of cell body GIRK channels would decrease excitability (Fig. 2.5b). In high extracellular potassium (60 mM) and under voltage clamp, illumination with 380-nm light evoked large inward currents that were deacti-vated by 500-nm light (Supplementary Fig. 2.6a). With illumination at a fixed intensity (0.4 mW mm–2 at 380 nm), photo-activation was ~5-fold faster in neurons than in HEK293 cells (single exponential fits: neurons, $\tau = 1.03 \pm 0.06$ s, $n = 5$; HEK293 cells, 5.69 ± 0.69, $n = 8$; unpaired, one-tailed *t* test, $P = 0.004$). This is consistent with previous observations of faster activation of GIRK channels by native GPCRs in cultured neurons compared with heterologously expressed receptors in GIRK-transfected HEK293 cells45 and suggests that LimGluR2 integrates into the native G-protein signaling machinery of neurons.

To test the ability of LimGluR2 to modulate neuronal excitability via GIRK channel activation, we performed current-clamp experiments. Neurons expressing LimGluR2 were labeled with D-MAG-0 and given depolarizing current injections, in 10-pA increments, under current clamp. This was done during alternating illumination with 380-nm and 500-nm light. Photo-activation of LimGluR2 at 380 nm decreased the number of action potentials evoked by each level of depolarization (Fig. 2.5c,d). This optical inhibition was highly reversible and repeatable (Fig. 2.5c,e,f and Supplementary Fig. 2.5b). The photo-currents were large enough to evoke a reversible 3–10-mV hyperpolarization at the resting potential (Fig. 2.5e) and, consistent with the bistability of the system, the hyperpolarization and silencing persisted for tens of seconds in the dark after activation of LimGluR2 by a brief 380-nm light pulse (Fig. 2.5e).

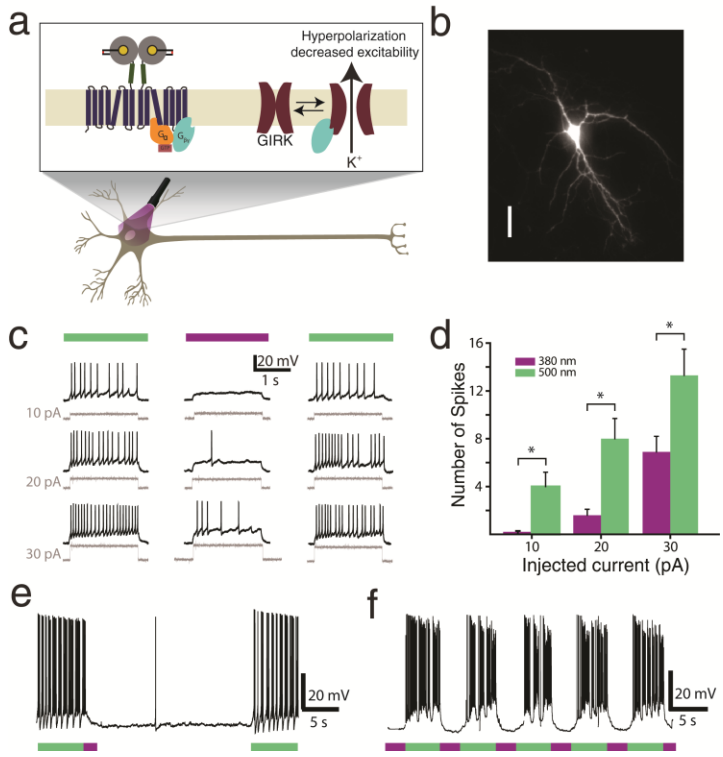

Figure 2.5, LimGluR2 hyperpolarizes and reduces excitability in cultured hippocampal neurons. a) LimGluR2-eGFP was widely distributed in cultured hippocampal neuron. Scale bar represents 50 µm. b) Schematic showing LimGluR2-mediated control of excitability via GIRK channels. Note that light was applied to entire field of view. c) Trains of spikes elicited by depolarizing current steps (gray traces) when LimGluR2 was off (500-nm illumination, green bar) were reversibly suppressed by activation of LimGluR2 (380-nm illumination, violet bar). Traces are from a representative cell. d) Summary of the current-step experiments shown in c for eight cells. Bars indicate the number of spikes in response to 2-s current injections under 380-nm (violet bar) or 500-nm (green bar) light and error bars indicate s.e.m. Asterisk indicates statistical significance (paired, one-tailed *t*-test, $P = 0.009$, 0.004 and 0.009 for currents of 10, 20 and 30 pA, respectively; $n = 7$ cells). e) LimGluR2-mediated hyperpolarization in a representative cell in response to brief (1 s) activation by 380-nm light (violet bar) persisted for tens of seconds in the dark before LimGluR2 deactivation by 500-nm light (green bar). The persistent activation in the dark effectively suppressed spikes. f) Representative trace showing repeatable spike silencing by photo-control of LimGluR2.

Optical control of synaptic transmission

Group II metabotropic glutamate receptors are known to traffic to presynaptic terminals and have inhibitory roles in synaptic transmission and plasticity[5,25]. We asked whether LimGluR2 would allow optical control of neurotransmitter release (Fig. 2.6a). We expressed mGluR2-L300C in low-density hippocampal cultures in which each neuron formed synapses onto itself (autapses). Cells were patch clamped and we recorded postsynaptic currents elicited by brief depolarization steps that elicited single action potentials. Excitatory postsynaptic currents (EPSCs) were detected in some cells (Fig. 2.6b) and inhibitory postsynaptic currents (IPSCs) were detected in others (Fig. 2.6c). Activation of LimGluR2 by 380-nm light rapidly and reversibly inhibited both the EPSCs (41 ± 5%, $n = 8$) and IPSCs (36 ± 3%, $n = 4$) (Fig. 2.6b,c).

In contrast with the potent inhibition by LimGluR2, there was no optical inhibition in either cells transfected with GFP instead of LimGluR2 or cells transfected with LimGluR2, but not labeled with D-MAG-0 (Fig. 2.6d). Moreover, there was no change in baseline PSC amplitude in labeled and transfected (LimGluR2) cells compared with GFP-transfected or unlabeled cells (LimGluR2, 223 ± 64 pA, $n = 12$; GFP, 262 ± 68 pA, $n = 5$; unlabeled, 232 ± 91 pA, $n = 5$). In addition, the optical inhibition of transmission by LimGluR2 produced no change in postsynaptic current (PSC) decay time (Supplementary Fig. 2.7a), time to peak (Supplementary Fig. 2.7b) or jitter (s.e.m. of time to peak), leaving the PSCs unchanged in shape (Supplementary Fig. 2.7c).

To test whether the LimGluR2-mediated optical inhibition of transmission proceeds through a presynaptic mechanism, we performed paired pulse experiments. The optical inhibition of transmission by illumination with 380-nm light was associated with a significant increase in

the relative size of the EPSC evoked by the second pulse (paired, one-tailed *t* test, $P = 0.01$; Fig. 2.6e–g). Similarly, during high-frequency (25 Hz) stimulation of autapses, 380-nm light increased short-term facilitation relative to during 500-nm light (Supplementary Fig. 2.7d–f). This indicates that activation of LimGluR2 inhibits postsynaptic currents by decreasing release probability, thereby increasing facilitation. This is exactly the mechanism by which native mGluR2 acts presynaptically via inhibition of N- and P/Q-type voltage-gated calcium channels, as has been observed for native group II mGluRs at the calyx of Held[43]. The paired pulse ratio in LimGluR2-positive cells was the same as that in GFP-transfected cells (LimGluR2, 1.5 ± 0.1, $n = 5$; GFP, 1.4 ± 0.3, $n = 4$), indicating that expression and labeling of LimGluR2 does not alter basal release.

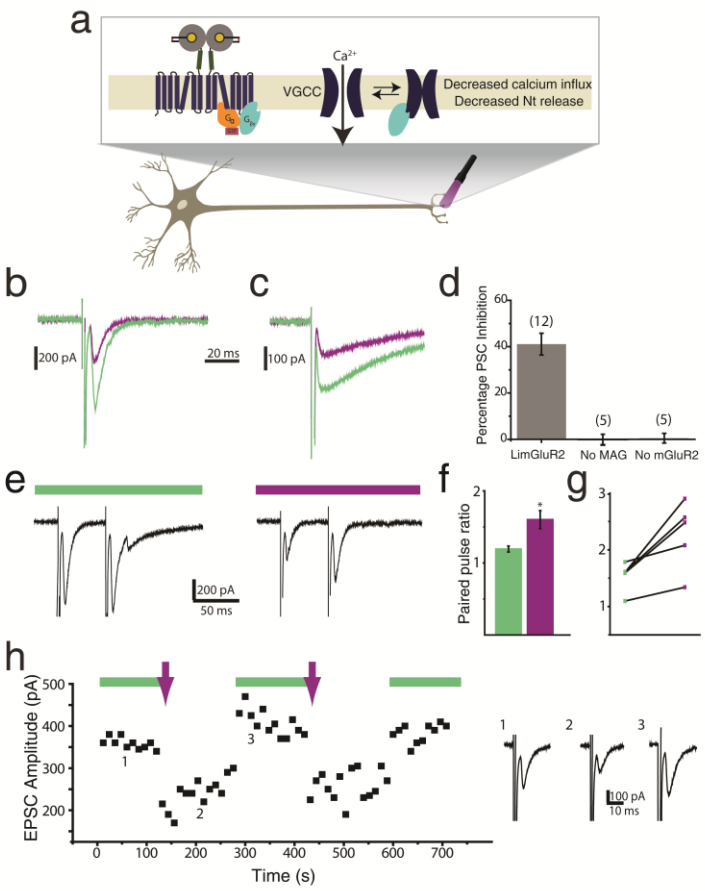

Figure 2.6, Optical activation of LimGluR2 reversibly decreases excitatory and inhibitory postsynaptic currents and increases paired pulse facilitation at hippocampal autapses. a) Schematic shows optical control of neurotransmitter (Nt) release via LimGluR2 triggered G protein suppression of opening of a presynaptic voltage-gated calcium channel (VGCC). b,c) Representative autaptic EPSC (b) and IPSCs (c) elicited by short (2 ms) depolarizing steps are decreased in amplitude by LimGluR2 activation by 380-nm light (violet traces) compared with deactivation by 500-nm light (green traces). d) Pooled inhibition of EPSCs and IPSCs by optical activation of LimGluR2 compared with controls in which mGluR2 (L300C) was expressed, but not labeled with D-MAG-0, and in which mGluR2 was not expressed. Values in parentheses denote the number of cells tested. Error bars represent s.e.m. e) Representative single sweeps of paired pulse recordings (50-ms inter-stimulus interval) of EPSCs under 500-nm light (green bar) followed by 380-nm light (violet bar). f) Summary of paired pulse ratio (PPR) values for representative cell. 380-nm light (violet bar) significantly increased the PPR compared with 500-nm light (green bar) ($n = 10$ sweeps per condition; paired, one-tailed *t* test, $^*P = 0.008$). Error bars represent s.e.m. g) Plot of average PPRs measured for five autaptic cells under 500-nm light (green symbols) and 380-nm light (violet symbols). h) Representative EPSC amplitudes from a cell showing repeatable, bistable optical inhibition of an excitatory autapse. Illumination at 500 nm to deactivate LimGluR2 was followed by brief (1 s) illumination at 380 nm (violet arrows), followed by a period of darkness, until illumination at 500 nm to deactivate LimGluR2 was resumed. Inserts (1–3) show EPSCs from the indicated times.

Finally, we tested the ability of LimGluR2 to produce multiple rounds of inhibition of transmission and recovery and for the inhibition to outlast the activating light pulse as a result of the bistable nature of the photoswitch. Brief photo-activation produced sustained inhibition of synaptic transmission that persisted in the dark for minutes and could be rapidly reversed by 500-nm illumination (Fig. 2.6h and Supplementary Fig. 2.7g). We found that LimGluR2 provided a

means for the reversible, repeatable optical control of presynaptic inhibition of neurotransmitter release.

Optical control of tonic inhibition by LimGluR2-block

We next assessed the ability of photoantagonism by LimGluR2-block to modulate receptor function in neurons in response to native glutamate. We tested whether photo-antagonism by LimGluR2-block could alter spike-firing patterns in cultured hippocampal neurons. In regions with high transfection efficiency (>1 transfected neuron per field of view), optical antagonism of mGluR2 with 380-nm light resulted in an increased firing frequency that was reversed by 500-nm light (Supplementary Fig. 2.8a,b). This suggests that LimGluR2-block is robust enough to alter neuronal signaling properties despite incomplete antagonism. Furthermore, this indicates that, under basal conditions, there is sufficient inhibitory tone produced by glutamate binding to mGluR2 to suppress spike firing.

We also tested LimGluR2-block in autaptic neurons. Under basal stimulation frequencies (0.1 Hz), photo-antagonism of mGluR2 induced an increase in EPSC amplitude (average increase in amplitude = 26 ± 8%, n = 6 cells; Supplementary Fig. 2.8c,d). This result is consistent with the observation that photo-antagonism of mGluR2 leads to an increase in spike-firing frequency and indicates that glutamate feedback at excitatory nerve terminals can provide inhibitory tone via mGluR2, even in a sparsely connected network. In contrast, at inhibitory autapses, LimGluR2-block did not induce a change in IPSC amplitude (average increase in amplitude = 1.0 ± 0.02%, n = 3 cells; Supplementary Fig. 2.8e,f), suggesting that inhibition of transmitter release via mGluR2 under sparse activity operates by local signaling at individual excitatory synapses, and that cross talk to inhibitory synapses may require high-frequency coordinate activity and global glutamate spillover.

Optical control of excitability in hippocampal slices

We tested LimGluR2 in organotypic hippocampal slices prepared from postnatal day 6–8 (P6–8) rats co-transfected with td-Tomato as a transfection marker. Slices were incubated with D-MAG-0 and whole-cell patch-clamp recordings were performed on cells up to two or three layers below the surface of the slice. At resting potential (–45 mV to –65 mV), LimGluR2 activation by illumination at 390 nm induced a reversible 3–8-mV hyperpolarization (Fig. 2.7a). In response to depolarizing current injections, illumination at 390 nm reproducibly decreased action potential firing (Fig. 2.7b,c), as was seen in the dissociated cultured neurons (Fig. 2.5c,d). Illumination with 500-nm light restored firing frequency to levels seen before LimGluR2 activation. In addition, LimGluR2 activation was able to decrease spontaneous spike firing (Fig. 2.7d) in a bistable, reversible and reproducible manner.

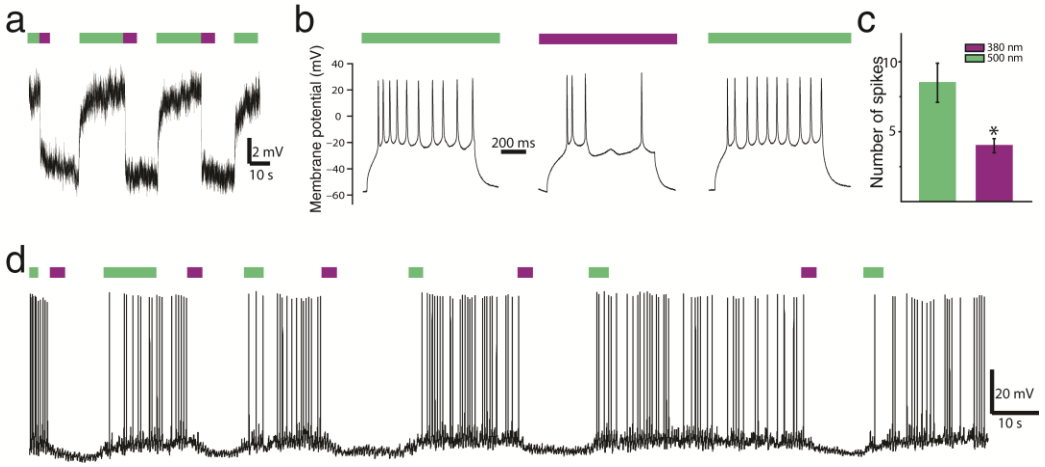

Figure 2.7, LimGluR2-mediated control of neuronal excitability in hippocampal slice. a) Hyperpolarization was triggered by illumination at 390 nm (violet bar) and reversed by illumination at 500 nm (green bar) in a representative cell. b) Representative cell recorded in whole-cell patch in cultured hippocampal slice showing spike firing in response to 1-s, 200-pA depolarizing current injections during 500-nm (green bars) or 380-nm (violet bar) illumination. LimGluR2 activation reversibly decreased the number of spikes. c) Summary of optical control of spike firing in response to current steps in LimGluR2-positive neurons (n = 6 cells). Asterisk indicates statistical significance (paired, one-tailed t test, P = 0.024) and error bars represent s.e.m. d) Representative trace showing reversible, bistable silencing of spontaneous activity by LimGluR2.

Notably, LimGluR2 expression and D-MAG-0 labeling did not adversely affect neurons, leaving the average resting membrane potential unaltered (Supplementary Fig. 2.9a). In addition, we found no photo-effects with D-MAG-0 in the absence of mGluR2-300C (Supplementary Fig. 2.9b,d) or in the presence of mGluR2-300C and absence of D-MAG-0 (Supplementary Fig. 2.9c), indicating that orthogonality is maintained in slices. These results indicate that expression, labeling and optical activation of LimGluR2 are attainable in intact tissue, providing a powerful means to probe the role of G protein signaling in general, and mGluRs in particular, in the native preparation. We next turned to *in vivo* experiments to determine whether LimGluR2 activation in neurons could alter behavior.

Optical control of zebrafish behavior

To determine whether LimGluR2 could be used *in vivo* to probe mGluR signaling in a behavioral context, we turned to the ASR of zebrafish (*Danio rerio*), a well-characterized behavior of teleosts that is similar to the mammalian startle response[46]. At 5–6 days post-fertilization (dpf), fish were individually mounted in a glass-well petri dish with the head embedded in agar and subjected to sound and vibration stimuli (900 Hz, 120 ms) ranging from low energy to high energy (0.1–10 mVpp, 0.5-mVpp increments). At lower energy levels (<2 mVpp), the sound and vibration stimulus induced forward swims, whereas higher energy levels elicited escape responses with the typical C bend[47]. We found that wild-type fish treated with the nonspecific group II mGluR agonist L-CCG-1 displayed a significantly decreased threshold of the ASR when compared with vehicle-treated fish (Mann-Whitney, $n_{ct} = n_{L\text{-}CCG\text{-}1} = 78$, $P < 0.02$, two tailed; Fig. 2.8a). This result indicates that activation of native group II mGluRs leads to a decrease in the threshold of the ASR in wild-type zebrafish.

Next, we examined whether optical activation of LimGluR2 could recapitulate the native

group II mGluR signaling effect of decreasing the threshold of the zebrafish ASR. We generated transgenic zebrafish in which LimGluR2(L300C) expression was driven by repeats of the *Gal4* upstream activating sequence (UAS). We crossed these *UAS-LimGluR2* zebrafish to *elavl3-Gal4; UAS-Kaede* fish to generate *elavl3-Gal4; UAS-Kaede; UAS-LimGluR2* zebrafish. The *elavl3* promoter (also known as *HuC*) drives pan-neuronal expression of Gal4, and, consequently, of LimGluR2, as well as the Kaede fluorescent protein, which served as a marker for the *elavl3-Gal4* transgene (Fig. 2.8b). *elavl3-Gal4; UAS-Kaede; UAS-LimGluR2* zebrafish were indistinguishable in swimming behavior at 5 dpf (Supplementary Fig. 2.10c–e) and ASR (Supplementary Fig. 2.10f) from *elavl3-Gal4; UAS-Kaede* fish, which contained the neuronal driver alone. Fish health and responses to touch were unaffected by the 45-min exposure to D-MAG-0 and 1-h recovery. The ASR was also not affected in a control transgenic line that did not express LimGluR2 and was treated with D-MAG-0 (Supplementary Fig. 2.10g). These results indicate that neither pan-neuronal expression of LimGluR2 nor D-MAG-0 treatment modify health or behavior.

LimGluR2 was photo-controlled by patterned illumination applied caudal to the eyes in a region covering the cranial nerves, hindbrain and the rostral portion of the spinal circuits that control the escape response. To activate LimGluR2, we illuminated the fish with 380-nm light for 400 ms; to deactivate it, we applied 510-nm light for 1s. Activation of LimGluR2 increased the probability of an escape response (Fig. 2.8c,d). This effect was reversed by 510-nm light and could be toggled back and forth by repeatedly activating and deactivating LimGluR2 (Fig. 2.8c). The behavior of fish expressing LimGluR2, but not labeled with D-MAG-0, was not altered by light (Fig. 2.8d). In addition, labeling of fish with D-MAG-0 did not alter the basal threshold for the ASR (Supplementary Fig. 2.10h). These results suggest a role for mGluR2 in the ASR and establish that LimGluR2 can be used to study mGluR2 signaling *in vivo*.

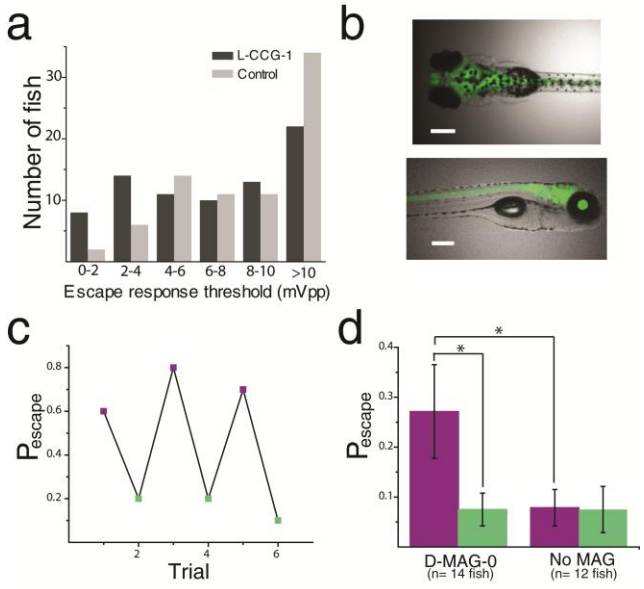

Figure 2.8, Agonism of endogenous group II mGluRs and photo-agonism of LimGluR2 increases escape response probability in zebrafish larvae. a) Treatment with the group II mGluR agonist L-CCG-1(10 μM) decreased the threshold of the wild-type zebrafish larvae ASR. The frequency distribution of minimum energy thresholds is shown. Class >10 mVpp represent fish that had an intact ASR, but that did not respond with a C bend at the highest sound energy attained by our experimental apparatus (10 mVpp). Comparison of the two groups was performed using the Mann-Whitney test ($z = 2.38$, $P < 0.02$, two-tailed distribution; $n_{control} = n_{L\text{-}CCG\text{-}1} = 78$ fish). b) UAS-GFP imaging revealed pan-neuronal expression in the *elavl3-Gal4* driver line. Scale bars represent 250 μm. c) Representative larva showing reversible modulation of escape response probability. Each data point represents the escape probability during a period of ten trials. Violet and green points represent trials after illumination at 510 and 380 nm, respectively. d) Summary of LimGluR2 modulation of escape response. Green bars indicate illumination with 510-nm light and violet bars indicate 380-nm light. Asterisks indicate statistical significance ($P = 0.007$ for comparison of 510-nm versus 380-nm illumination for MAG-labeled larvae with one-tailed paired *t* test; $P = 0.03$ for comparison of MAG-labeled and unlabeled larvae with one-tailed unpaired *t* test). Error bars represent s.e.m.

Discussion:

GPCRs represent the largest family of membrane signaling proteins and respond to a wide-array of stimuli. These seven transmembrane receptors couple to distinct classes of heterotrimeric G proteins, leading to the activation or inhibition of a large number of protein targets3. The diversity of signaling is vastly greater than can be accounted for by the four classes of G proteins to which GPCRs couple. The additional diversity comes from several factors, including localization into specific subcellular compartments, corralling into signaling nano-domains with particular effectors, assembly of preformed GPCR–G protein–effector complexes, heteromultimerization into complexes with specialized properties, and unique profiles of interaction with regulatory proteins[6,7].

To elucidate GPCR function, one needs a method that combines specific pharmacology with specificity for region, cell-type and subcellular compartment. At the same time, the approach needs to allow for the GPCR to be activated at physiological rates (that is, the millisecond timescale) and to be reversible and reproducible to mimic physiological signaling and permit quantitative analysis. All of this needs to be achieved on the full-length GPCR to maintain normal targeting and interaction with signaling partners and regulators. We overcame these obstacles by developing, via the rational design and synthesis of new PTLs called D-MAGs and a simple and fast Monte Carlo simulation approach to select anchoring sites for these PTLs, photo-agonizing and photo-antagonizing versions of three of the eight mGluRs, representing two of the three mGluR groups. These approaches can readily be adapted to other target proteins and PTLs.

We most thoroughly characterized the photo-agonism with D-MAG-0 at position L300C of mGluR2 (LimGluR2). Unlike rhodopsin, which is the basis of most of the previously described light-gated GPCRs, LimGluR2 can be actively toggled both on and off in less than 1 ms, enabling signaling to be controlled on a synaptically relevant timescale and providing for fast effector kinetics. Moreover, LimGluR2 permits repetitive stimulation at high rates without decline. Rhodopsin requires constant illumination to be activated, which increases the chance of tissue damage and can act as a confounding variable for behavioral studies, while LimGluR2 is bistable, eliminating the need for constant illumination. Notably, optical control of native GPCRs provides a unique opportunity to examine the specific synaptic and circuit functions of each receptor, which emerge from their restricted effector and regulatory profiles and cannot be deduced from widespread activation of the entire signaling pathway of the G protein to which they couple.

We found that, despite their limited homology (66% identity between mGluR2 and mGluR3 and 44% identity between mGluR2 and mGluR6), photo-control could be generalized in the mGluR family from mGluR2 to the other group II member mGluR3 and the group III member mGluR6, with the same D stereoisomer linkage to the glutamate of MAG being required. Differences in photo-switching with a particular MAG at homologous sites of these three mGluRs reveals differences between their LBDs. This information may be useful for designing additional photoswitches or other pharmacological ligands as well as for probing the mechanism of clamshell closure.

The LimGluRs provide rapid, reversible, bistable and highly reproducible control of excitability and synaptic transmission in dissociated cultured neurons and in brain slices, two of the prime *in vitro* systems in which synaptic transmission and plasticity in general, and mGluR

function in particular, are studied most extensively. Although the photo-agonism and photo-antagonism of LimGluR2 are not complete, the photo-agonism induced characteristic mGluR2-dependent modulation and the photo-antagonism prevented the induction of such changes by native glutamate release. The precise temporal control, which allows the agonist or antagonist to be toggled on and off in a time-coupled manner, repeatedly and reproducibly made it possible to observe small effects that would be difficult to distinguish with classical drugs. In the case of LimGluR2-block, the photoeffect in neurons was consistent with the behavior of most neurotransmitter-gated GPCRs, which tend to be localized outside of the synaptic cleft and experience subsaturating concentrations of the neurotransmitter. The success of the D-MAG labeling and photo-control of mGluRs in brain slice suggests that the approach should also work in the mammalian brain *in vivo*, as has been shown for a similar photoswitch directed to the ionotropic kainate receptor in the mouse retina *in vivo*[48]. Indeed, we found that LimGluR2 worked effectively *in vivo* in zebrafish when D-MAG was simply added to the zebrafish larvae E3 salt water medium. We used LimGluR2 to photo-manipulate mGluR2 signaling in the context of the zebrafish ASR, a widely studied behavior that is similar in architecture and pharmacological regulation to the mammalian ASR47. In rodents, mGluRs have been implicated in various forms of the startle response, including regulation of paired-pulse inhibition by group II mGluRs, using pharmacological manipulation[49]. It was recently shown that group II mGluRs are expressed across all main subdivisions of the zebrafish brain[50]. Indeed, we found that conventional agonism of group II mGluRs by L-CCG-1 lowers the zebrafish ASR threshold. The ability to target light to a subregion of the nervous system allowed us to localize the mGluR2-mediated effect on the ASR to the spinal cord and hindbrain and to find that optical activation of LimGluR2 also reduces ASR threshold; however, unlike L-CCG-1, this effect can result from acute activation of mGluR2 and can be reversed and repeated, suggesting that mGluR2 signaling could dynamically modulate escape threshold. Such information regarding the temporal dynamics of the ASR would not be possible to obtain using pharmacological approaches that require complete wash-out of ligands or addition of compounds whose activities are constrained by the pharmacokinetics of intact animals.

As with other GPCRs, mGluRs that couple to the same G protein often activate distinct effectors5 and are regulated distinctly[3,7]. Photo-agonism and photo-antagonism of group II and III mGluRs should make it possible to determine the precise spatial (pre- versus postsynaptic, synaptic versus perisynaptic versus astrocytic) and temporal properties of signaling by individual receptors to mediate lasting changes in synaptic strength. Furthermore, given that LimGluR2 maintains close to native ligand sensitivity, knock-in mice with a single point mutation to introduce a single cysteine anchor should allow for high resolution, specific photo-agonism or photo-antagonism while maintaining the receptor's native function. This would provide a new way to specifically probe the receptor's function in synaptic plasticity and learning, as well as in anxiety, depression and schizophrenia, for which they are major drug targets[33].

Methods:

Chemical synthesis.

The chemical synthesis of D-MAG-0, D-MAG-1 and D-tether models was carried out as described in the **Supplementary Chemical Synthesis**.

Homology modeling and Monte Carlo simulations.

Homology modeling was performed using ProMod II in the Swiss Model environment[51]. The target sequence was the rat mGluR2 LBD (residues 23–538, Uniprot ID: P31421) and the template was the open, glutamate-bound chain B of the rat mGluR1 structure (PDB ID: 1EWK) or the closed, glutamate-bound chain A of the rat mGluR3 structured (PDB ID: 2E4U). Energy minimization was performed using the Gromos96 force field in DeepView (Swiss PDB Viewer).

Models of MAG were built in Maestro 6.5 (Schrödinger) starting with the experimental structures of *cis*- and *trans*-azobenzene[35]. The MCMM search[36] (Macromodel 9.1, Schrödinger) considered all dihedral angles as degrees of freedom with the exception of those in glutamate and azobenzene. Solvent was treated implicitly using a generalized Born/surface area water model in the context of the OPLS-2005 force field[52]. Bond lengths, bond angles and dihedral angles of azobenzene were constrained to the experimental structures. Protein side chains were allowed to fluctuate while backbone atoms were frozen. After the simulation, all structures were exported from Maestro, checked for steric clashes using the command line version of MolProbity[53] and imported into Igor Pro (Wavemetrics). The distance of the maleimide group to all residues was measured for every structure and, for each residue, the number of structures with distances less than 6.5 Å was counted. Figures were made using PyMOL.

Molecular biology and gene expression in cultured cells.

Cysteine mutations were introduced into mGluR2, mGluR3 and mGluR6 cDNA in the pcDNA3.1 expression vector (CMV promoter) using the QuickChange mutagenesis kit (Agilent). GIRK1 (with F137S homotetramerization mutation[54]), eYFP and RO4 were also inserted into pcDNA3.1. HEK293 and HEK293T cells were transiently co-transfected using Lipofectamine 2000 (Invitrogen) with mGluR mutants, GIRK1-F137S (homotetramerization mutant) and eYFP at a ratio of 7.5:7.5:1 with 1.6 μg of DNA total per 18-mm cover slip. RO4-transfected cells were maintained in dark room conditions. Cultured hippocampal neurons were transfected using the calcium phosphate method. Each coverslip received 1.1 μg of mGluR2-L300C DNA (or S302C) and 0.2 μg of eGFP DNA or 1.3 μg of mGluR2-L300C-GFP. mGluR2-L300C and mGluR2-S302C were inserted into a plasmid under the control of a synapsin promoter (pcDNA3.1 with the human synapsin promoter) to target expression to neurons.

Cultured cell electrophysiology.

HEK293 cells were maintained in DMEM with 5% fetal bovine serum (vol/vol) on poly-L-lysine–coated glass coverslips. Dissociated hippocampal neurons were obtained from postnatal rats (P0–1) and plated at 75,000 cells per coverslip on poly-L-lysine–coated glass coverslips (12 mM). For autapse experiments, low density cultures of 25,000 cells per coverslip were used. Neurons were maintained in media containing MEM supplemented with 5% FBS, B27 (Invitrogen) and GlutaMAX (Invitrogen).

HEK293 and 293T whole-cell patch-clamp electrophysiology was performed 24–48 h

after transfection in high potassium solution containing 60 mM KCl, 89 mM NaCl, 1 mM MgCl2, 2 mM CaCl2 and 10 mM HEPES, pH 7.4. Glass pipettes of resistance between 3 and 6 MΩ were filled with intracellular solution containing 140 mM KCl, 10 mM HEPES, 3 mM Na2ATP, 0.2 mM Na2GTP, 5 mM EGTA and 3 mM MgCl2, pH 7.4. Cells were voltage clamped to –60 to –80 mV using an Axopatch 200A (Molecular Devices) amplifier.

Hippocampal neuron whole-cell patch-clamp electrophysiology was performed 3–6 d after transfection (12–15 d *in vitro*). For voltage-clamp recordings, a high potassium extracellular solution containing 79.5 mM NaCl, 60 mM KCl, 1.2 mM MgCl2, 2.5 mM CaCl2, 10 mM glucose and 5 mM HEPES, pH 7.4 was used. For all other experiments, extracellular solution contained 138 mM NaCl, 1.5 mM KCl, 1.2 mM MgCl2, 2.5 mM CaCl2, 10 mM glucose and 5 mM HEPES, pH 7.4. Intracellular solution contained 140 mM potassium gluconate, 10 mM NaCl, 5 mM EGTA, 2 mM MgCl2, 1 mM CaCl2, 10 mM HEPES, 2 mM MgATP and 0.3 mM Na2GTP, pH 7.2. For current-step experiments, cells were adjusted to –50 mV with current injection before current steps were initiated to normalize spike count comparisons between cells. Only cells with a resting potential ≤–45 mV were analyzed. For autapse experiments, cells were voltage clamped to –70 and stepped to 0 mV for 2 ms. Postsynaptic currents were delayed by 3 ms, which confirmed autaptic origins of transmission. Inter-stimulus intervals were ≥12 s. EPSCs and IPSCs were identified on the basis of the kinetics of decay with EPSCs approximately ten times faster than IPSCs (~5 ms versus 50 ms), as has been described previously[55]. All pharmacological compounds were obtained from Tocris and dissolved in extracellular buffers before application using a gravity-driven perfusion system.

For most experiments, illumination was applied to the entire field of view using a Polychrome V monochromator (TILL Photonics) through a 20• objective or a Lambda DG4 high-speed wavelength switcher (Sutter Instruments) with 380-nm and 500-nm filters through a 40• objective. For bistable switching the DG-4 was coupled to the microscope through a 40• objective. Ultrafast, submillisecond photo-switching was achieved using a laser spot illumination system, for which the output of a 375/488-nm dual laser diode module (Omicron LDM) was coupled into a multi-mode fiber (10 μm, NA 0.1). The light exiting from this fiber was collimated and directed to the back aperture of the objective (Olympus 40•, NA 0.6). Intensities in the sample plane were >40 W mm–2.

pClamp software was used for both data acquisition and control of illumination. To conjugate MAG, cells were incubated in 50–100 μM MAG for 30–60 min in the dark at 23–27 °C in standard extracellular cell buffers. For RO4 experiments cells were labeled with 1 μM 11-cis retinal for 40 min and experiments were performed under dark room conditions.

cAMP measurements.

Intracellular cAMP levels were assayed with an ELISA system from Applied Biosystems. HEK 293T cells grown to confluence on a 24-well plate were either exposed to D-MAG-0 (50 μM for 45 min in standard extracellular buffer) or to a similar volume of standard extracellular buffer. After washing (5•, 1 ml), cells were treated with forskolin and/or glutamate or 365-nm light and disrupted in lysis buffer 10 min later. For D-MAG-0–labeled cells, 365-nm illumination was controlled with a handheld lamp and applied for 10 s immediately after forskolin addition. Serial dilutions of cAMP served as standards. Samples of cell lysate and standards were incubated with antibody to cAMP and cAMP–alkaline phosphatase in a 96-well plate. The plate was then washed, incubated with substrate and finally chemiluminescence generated at the end of enzymatic reaction was measured in a luminometer, LmaxII 384 (Molecular Devices).

Hippocampal slice gene expression and electrophysiology.

Hippocampi were obtained from postnatal Sprague-Dawley rats (P7) and 400 μM slices were prepared and cultured as previously described[38]. After 3 d, slices were transfected by Biolistic gene transfer using a BioRad Helios Gene Gun and gold microcarriers coated with both mGluR2-L300C and tdTomato DNA.

Patch-clamp recordings were obtained after 6–9 d *in vitro*. Before recording, slices were incubated at 32 °C for 40 min with D-MAG-0 (50 μM) diluted in NMDG-labeling solution containing 150 mM NMDG-HCl, 3 mM KCl, 0.5 mM CaCl2, 5 mM MgCl2, 10 mM HEPES and 5 mM glucose, pH 7.4. Whole-cell patch-clamp recordings were performed on an upright Zeiss AxioExaminer using an Axopatch 200B amplifier (Molecular Devices). Pipettes of resistances 3–7 M were filled with solution containing 120 mM potassium-gluconate, 8 mM NaCl, 10 mM HEPES, 2 mM MgCl2, 2 mM MgATP, 0.3 mM NaGTP and 10 mM EGTA, pH 7.4. Artificial cerebrospinal fluid containing 119 mM NaCl, 2.5 mM KCl, 1.3 mM MgSO4, 1 mM NaH2PO4-H2O, 26.2 mM NaHCO3, 11 mM glucose and 2.5 mM CaCl2 was continuously perfused and bubbled with 95% O2/5% CO2. A DG-4 (Sutter Instruments) was coupled to the microscope for photoswitching through a 40• objective. Light intensity was approximately 20 mW mm−2 at 390 nm and 40 mW mm−2 at 500 nm.

Zebrafish transgenesis.

Expression of mGluR2-L300C was targeted to neurons using the UAS/GAL4 system. The transgenesis *UAS-LimGluR2(L300C)/cry:CER* construct contains the LimGluR2(L300C) open reading frame amplified from the expression vector pcDNA3.1. LimGluR2 expression is driven by an upstream sequence composed of 10• *UAS* repeats followed by the adenovirus E1b TATA box and a 5′ UTR from carp β-actin. The *UAS* sequence was amplified from the p5E-UAS vector, tol2 Kit[56]. The opposite strand contains a crystalline promoter sequence[57] driving expression of the cerulean fluorescent protein in the crystalline of the eye for easy screening of transgenic fish. The expression sequences are flanked by sites for the fish transgenesis system meganuclease Isce-1[58].

Wild-type embryos (AB line) were injected at the one-cell stage with 30 ng ml–1 *UAS-LimGluR2(L300C)/cry-CER* DNA, 10 units I-Sce1 (New England Biolabs R0694L), NEBuffer Isce-1 0.5•, and 0.1% Phenol Red (wt/vol). F1 embryos were raised and screened at 3 dpf by fluorescence microscopy for presence of cerulean fluorescent protein expression in the eye. F0 founder fish that generated *UAS-LimGluR2(L300C)/cry-CER*–positive F1 fish were crossed to wild-type fish to create stable lines. *UAS-LimGluR2(L300C)/cry-CER* fish were crossed to *HuC-Gal4; UAS-Kaede* (gift from the Baier laboratory, University of California, San Francisco) fish to generate *HuC-Gal4; UAS-Kaede; UAS-LimGluR2/cry-CER* fish in which Gal4 drives pan-neuronal expression of the Kaede fluorescent protein and LimGluR2(L300C).

Zebrafish behavioral assay.

D-MAG-0 was diluted to 50 μM in 1 ml of a 5% DMSO Ringer buffered solution 116 mM NaCl, 2.9 mM KCl, 1.8 mM CaCl2 and 5 mM HEPES, pH 7.2), and pre-illuminated with ultraviolet light (365 nm) for 45 s. The labeling solution was added to 5 dpf larvae (20–30 fish). The larvae were kept at 28.5 °C in the dark for 45 min. Next, the larvae were washed in fish medium E3 and kept in the presence of E3 in the dark for a recovery period of 1 h at 28.5 °C. Control fish were subjected to the same protocol, but in the absence of D-MAG-0. For

pharmacological experiments, L-CCG-1 (Tocris) was diluted in E3 solution to a final concentration of 20 μM. Experimental and control fish were kept overnight at 28.5 °C before mounting and testing for ASR.

Larvae were mounted in a glass well petri dish dorsal side up in 2% agar E3 solution at 36 °C. Agar was removed from a region caudal to the fish otic vesicle. All experimental larvae used in experiments had an intact ASR, as determined by a light tap in the dish containing the larvae. Tail-free mounted fish were attached with adhesive tape to the surface of an 8-Ohm mini-speaker (Radioshack, 273-092). Fish were illuminated from the side with attenuated white light. Images were captured at 30 Hz by a behavioral camera (IDS, USB 2 uEye). A square wave (900 Hz, 120 ms, controllable amplitude) stimulus was generated by a function waveform generator (Agilent, 33220A) connected to the mini-speaker. Sound- and vibration-induced escapes were determined by observation in behavioral movies of characteristic C bends induced by sound and vibration stimulus. Threshold was defined as the minimum energy capable of inducing >50% C bends in a ten trial test. All experiments were performed in a climate-controlled environment at 22 °C.

The illumination source was a Lambda DG4 high-speed wavelength switcher (Sutter). A digital micro-mirror device was used to pattern illumination through a 2.5• Zeiss objective. Illumination reached the larvae from the dorsal side and covered a region caudal to the eyes and reaching almost the whole length of the spinal cord. Activation and deactivation wavelengths were 380 and 15 nm, 0.09 mW mm–2 for 400 ms, and 510 and 20 nm, 0.49 mW mm–2 for 1 s, respectively. Larvae were sound and vibration stimulated 5 s after illumination. Ten stimuli with a 10-s inter-stimulus interval were performed for each condition. Illumination and behavioral set up were mounted on a 3i Marianas system with a spinning disk confocal (Yokagawa) mounted on a Zeiss microscope.

For the L-CCG-1 experiment, 5–6 dpf wild-type zebrafish larvae were treated overnight in 20 μM L-CCG-1- or vehicle-containing E3 solution. Trials were performed with a 10-s inter-trial interval and speaker voltage was increased in steps of 500 mVpp until the threshold was reached. All fish had an intact ASR as determined by a light tap to the dish.

For swimming and escape response control experiments, zebrafish larvae were kept in E3 in 48-well microplates mounted on a plexiglass box. For fish activity measurements, an infrared CCD camera (fire-i 780b, Unibrain) from above was used with trans-infrared illumination from below (Supplementary Fig. 2.10a,b). Sound stimuli were administered by two speakers (Visaton SC 5.9) screwed to the same plexiglass plate as the micro-well plate. Stimuli (powered by a 15-W amplifier) were sent to speakers using a Native Instruments PCI-6229 DAQ controlled by Matlab. Duration and frequency were 20 ms and 900 Hz, respectively. Escapes were detected using an in-house movement threshold algorithm. The acoustic stimulus was applied 110 ms after start of the movie. A successful escape response was counted if the difference of the integrated pixel values of the two frames immediately after the stimulus was statistically higher ($P < 0.01$) than the distribution of pixel-change values in the preceding 109 frames of recorded spontaneous activity. The accuracy of this algorithm was verified by visual inspection of movies. Animal experiments were approved by the University of California Animal Care and Use Committee.

Statistics and data analysis.

Data was analyzed using Clampfit (Axon Instruments) and Origin (OriginLab) software. Statistical analysis was performed using Microsoft Excel. All values reported are mean ± s.e.m.

References:

1 Szobota, S. & Isacoff, E.Y. Optical control of neuronal activity. Annu. Rev. Biophys. 39, 329–348 (2010).

2 Deisseroth, K. Optogenetics. Nat. Methods 8, 26–29 (2011).

3 Pierce, K.L., Premont, R.T. & Lefkowitz, R.J. Seven-transmembrane receptors. Nat. Rev. Mol. Cell Biol. 3, 639–650 (2002).

4 Kobilka, B.K. Structural insights into adrenergic receptor function and pharmacology. Trends Pharmacol. Sci. 32, 213–218 (2011).

5 Niswender, C.M. & Conn, P.J. Metabotropic glutamate receptors: physiology, pharmacology and disease. Annu. Rev. Pharmacol. Toxicol. 50, 295–322 (2010).

6 Bockaert, J., Perroy, J., Becamel, C., Marin, P. & Fagni, L. GPCR interacting proteins (GIPs) in the nervous system: roles in physiology and pathologies. Annu. Rev. Pharmacol. Toxicol. 50, 89–109 (2010).

7 Gainetdinov, R.R., Premont, R.T., Bohn, L.M., Lefkowitz, R.J. & Caron, M.G. Desensitization of G protein–coupled receptors and neuronal functions. Annu. Rev. Neurosci. 27, 107–144 (2004).

8 Pei, Y., Rogan, S.C., Yan, F. & Roth, B.L. Engineered GPCRs as tools to modulate signal transduction. Physiology (Bethesda) 23, 313–321 (2008).

9 Alexander, G.M. et al. Remote control of neuronal activity in transgenic mice expressing evolved G protein–coupled receptors. Neuron 63, 27–39 (2009).

10 Zemelman, B.V., Lee, G.A., Ng, M. & Miesenbock, G. Selectie photostimulation of genetically chARGed neurons. Neuron 33, 15–22 (2002).

11 Li, X. et al. Fast noninvasive activation and inhibition of neural and network activity by vertebrate rhodopsin and green algae channelrhodopsin. Proc. Natl. Acad. Sci. USA 102, 17816–17821 (2005).

12 Gutierrez, D.V. et al. Optogenetic control of motor coordination by Gi/o protein–coupled vertebrate rhodopsin in cerebellar Purkinje cells. J. Biol. Chem. 286, 25848–25858 (2011).13. Melyan, Z., Tarttelin, E.E., Bellingham, J., Lucas, R.J. & Hankins, M.W. Addition of human melanopsin renders mammalian cells photoresponsive. Nature 433, 741–745 (2005).

14 Qiu, X. et al. Induction of photosensitivity by heterologous expression of melanopsin. Nature 433, 745–749 (2005).

15 Lin, B., Koizumi, A., Tanaka, N., Panda, S. & Masland, R.H. Restoration of visual function in retinal degeneration mice by ectopic expression of melanopsin. Proc. Natl. Acad. Sci. USA 105, 16009–16014 (2008).

16 Yamashita, T., Terakita, A. & Shichida, Y. Distinct roles of the second and third cytoplasmic loops of bovine rhodopsin in G protein activation. J. Biol. Chem. 275, 34272–34279 (2000).

17 Yamashita, T., Terakita, A. & Shichida, Y. The second cytoplasmic loop of metabotropic glutamate receptor functions at the third loop position of rhodopsin. J. Biochem. 130, 149–155 (2001).

18 Kim, J.M. et al. Light-driven activation of beta 2-adrenergic receptor signaling by a chimeric rhodopsin containing the beta 2-adrenergic receptor cytoplasmic loops. Biochemistry 44, 2284–2292 (2005).

19 Airan, R.D., Thompson, K.R., Fenno, L.E., Bernstein, H. & Deisseroth, K. Temporally precise in vivo control of intracellular signalling. Nature 458, 1025–1029 (2009).

20 Oh, E., Maejima, T., Liu, C., Deneris, E. & Herlitze, S. Substitution of 5-HT1A receptor signaling by a light-activated G protein–coupled receptor. J. Biol. Chem. 285, 30825–30836 (2010).

21 Bailes, H.J., Zhuang, L.Y. & Lucas, R.J. Reproducible and sustained regulation of Galphas signaling using a metazoan opsin as an optogenetic tool. PLoS ONE 7, e30774 (2012).

22 Fehrentz, T., Schonberger, M. & Trauner, D. Optochemical genetics. Angew. Chem. Int. Edn Engl. 50, 12156–12182 (2011).

23 Banghart, M., Borges, K., Isacoff, E., Trauner, D. & Kramer, R.H. Light-activated ion channels for remote control of neuronal firing. Nat. Neurosci. 7, 1381–1386 (2004).

24 Volgraf, M. et al. Allosteric control of an ionotropic glutamate receptor with an optical switch. Nat. Chem. Biol. 2, 47–52 (2006).

25 Anwyl, R. Metabotropic glutamate receptor–dependent long-term potentiation. Neuropharmacology 56, 735–740 (2009).

26 Lüscher, C. & Huber, K.M. Group 1 mGluR-dependent synaptic long-term depression: mechanisms and implications for circuitry and disease. Neuron 65, 445–459 (2010).

27 Panatier, A. et al. Astrocytes are endogenous regulators of basal transmission at central synapses. Cell 146, 785–798 (2011).

28 Bradley, S.J. & Challiss, R.A. G protein–coupled receptor signaling in astrocytes in health and disease: a focus on metabotropic glutamate receptors. Biochem. Pharmacol. 84, 249–259 (2012).
29 Tanabe, Y., Masu, M., Ishii, T., Shigemoto, R. & Nakanishi, S. A family of metabotropic glutamate receptors. Neuron 8, 169–179 (1992).
30 Saugstad, J.A., Segerson, T.P. & Westbrook, G.L. Metabotropic glutamate receptors activate G protein–coupled inwardly rectifying potassium channels in *Xenopus* oocytes. *J. Neurosci.***16**, 5979–5985 (1996).
31 Ikeda, S.R., Lovinger, D.M., McCool, B.A. & Lewis, D.L. Heterologous expression of metabotropic glutamate receptors in adult rat sympathetic neurons: subtype-specific coupling to ion channels. *Neuron* **14**, 1029–1038 (1995).
32 Altinbilek, B. & Manahan-Vaughan, D. A specific role for group II metabotropic glutamate receptors in hippocampal long-term depression and spatial memory. *Neuroscience* **158**,149–158 (2009).
33 Marek, G.J. Metabotropic glutamate 2/3 receptors as drug targets. *Curr. Opin. Pharmacol.* **4**,18–22 (2004).
34 Muto, T., Tsuchiya, D., Morikawa, K. & Jingami, H. Structures of the extracellular regions of the group II/III metabotropic glutamate receptors. *Proc. Natl. Acad. Sci. USA* **104**, 3759–3764(2007).
35 Tsuji, T., Takashima, H., Takeuchi, H., Egawa, T. & Konaka, S. Molecular structure and torsional potential of trans-azobenzene. A gas electron diffraction study. *J. Phys. Chem. A***105**, 9347–9353 (2001).
36 Chang, G., Guida, W.C. & Still, W.C. An internal coordinate Monte-Carlo method for searching conformational space. *J. Am. Chem. Soc.* **111**, 4379–4386 (1989).
37 Gorostiza, P. *et al*. Mechanisms of photoswitch conjugation and light activation of an ionotropic glutamate receptor. *Proc. Natl. Acad. Sci. USA* **104**, 10865–10870 (2007).
38 Janovjak, H., Szobota, S., Wyart, C., Trauner, D. & Isacoff, E.Y. A light-gated, potassium-selective glutamate receptor for the optical inhibition of neuronal firing. *Nat. Neurosci.* **13**,1027–1032 (2010).
39 Iacovelli, L. *et al*. Regulation of group II metabotropic glutamate receptors by G protein–coupled receptor kinases: mGlu2 receptors are resistant to homologous desensitization. *Mol. Pharmacol.* **75**, 991–1003 (2009).
40 Raveh, A., Cooper, A., Guy-David, L. & Reuveny, E. Nonenzymatic rapid control of GIRK channel function by a G protein–coupled receptor kinase. *Cell* **143**, 750–760 (2010).
41 Hanna, L. *et al*. Differentiating the roles of mGlu2 and mGlu3 receptors using LY541850, an mGlu2 agonist/mGlu3 antagonist. *Neuropharmacology* **66**, 114–121 (2013).
42 Ehrengruber, M.U. *et al*. Activation of heteromeric G protein–gated inward rectifier K+ channels overexpressed by adenovirus gene transfer inhibits the excitability of hippocampal neurons. *Proc. Natl. Acad. Sci. USA* **94**, 7070–7075 (1997).
43 Takahashi, T., Forsythe, I.D., Tsujimoto, T., Barnes-Davies, M. & Onodera, K. Presynaptic calcium current modulation by a metabotropic glutamate receptor. *Science* **274**, 594–597(1996).
44 Shigemoto, R. *et al*. Differential presynaptic localization of metabotropic glutamate receptor subtypes in the rat hippocampus. *J. Neurosci.* **17**, 7503–7522 (1997).
45 Leaney, J.L. Contribution of Kir3.1, Kir3.2A and Kir3.2C subunits to native G protein–gated inwardly rectifying potassium currents in cultured hippocampal neurons. *Eur. J. Neurosci.* **18**,2110–2118 (2003).
46 Koch, M. The neurobiology of startle. *Prog. Neurobiol.* **59**, 107–128 (1999).
47 Burgess, H.A. & Granato, M. Sensorimotor gating in larval zebrafish. *J. Neurosci.* **27**,4984–4994 (2007).
48 Caporale, N. *et al*. LiGluR restores visual responses in rodent models of inherited blindness.*Mol. Ther.* **19**, 1212–1219 (2011).
49 Grauer, S.M. & Marquis, K.L. Intracerebral administration of metabotropic glutamate receptor agonists disrupts prepulse inhibition of acoustic startle in Sprague-Dawley rats.*Psychopharmacology (Berl.)* **141**, 405–412 (1999).
50 Haug, M.F., Gesemann, M., Mueller, T. & Neuhauss, S.C. Phylogeny and expression divergence of metabotropic glutamate receptor genes in the brain of zebrafish (*Danio rerio*).*J. Comp. Neurol.* Published online, doi:10.1002/cne.23240 (10 October 2012).
51 Bordoli, L. et al. Protein structure homology modeling using SWISS-MODEL workspace. Nat. Protoc. 4, 1–13 (2009).
52 Kaminski, G.A., Friesner, R.A., Tirado-Rives, J. & Jorgensen, W.L. Evaluation and reparametrization of the OPLS-AA force field for proteins via comparison with accurate quantum chemical calculations on peptides. J. Phys. Chem. B 105, 6474–6487 (2001).
53 Davis, I.W. et al. MolProbity: all-atom contacts and structure validation for proteins and nucleic acids. Nucleic Acids Res. 35, 375–383 (2007).
54 Vivaudou, M. et al. Probing the G-protein regulation of GIRK1 and GIRK4, the two subunits of the KACh

channel, using functional homomeric mutants. J. Biol. Chem. 272, 31553–31560 (1997).
55 Bekkers, J.M. & Stevens, C.F. Excitatory and inhibitory autaptic currents in isolated hippocampal neurons maintained in cell culture. Proc. Natl. Acad. Sci. USA 88, 7834–7838 (1991).
56 Kwan, K.M. et al. The Tol2kit: a multisite gateway-based construction kit for Tol2 transposon transgenesis constructs. Dev. Dyn. 236, 3088–3099 (2007).
57 Kurita, R. et al. Suppression of lens growth by alphaA-crystallin promoter–driven expression of diphtheria toxin results in disruption of retinal cell organization in zebrafish. Dev. Biol. 255, 113–127 (2003).
58 Grabher, C. & Wittbrodt, J. Meganuclease and transposon mediated transgenesis in medaka. Genome Biol. 8 (suppl. 1), S10 (2007).

Supplementary Figures:

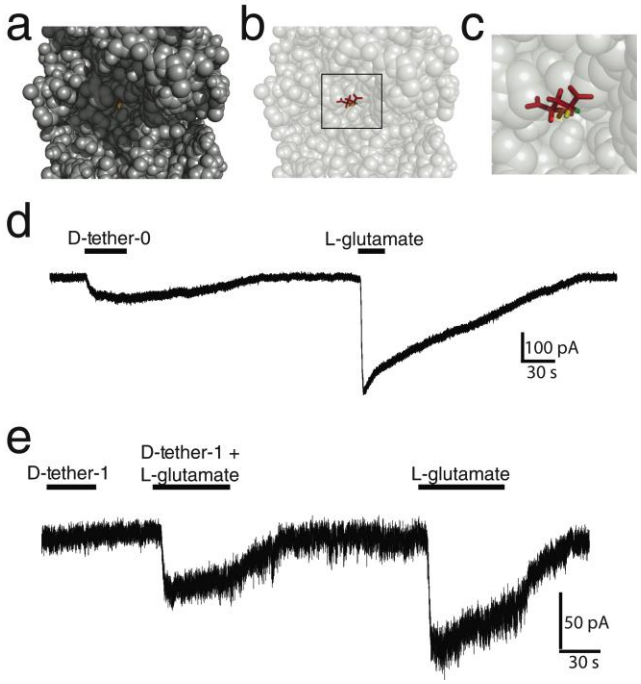

Figure S2.1, Design of photoswitches for control of mGluR2: Apparent access channel and tether model screening. a) Homology model of mGluR2 ligand binding domain in the closed, glutamate-bound, conformation (based on structure of mGluR3, PBD: 2E4U) reveals an access channel through which glutamate (red) is seen from the surface of the protein. The 4' D hydrogen of glutamate (yellow) is visible through the access channel, but the L hydrogen (green) is not. b,c) Stick representation of glutamate shows the directions in which 4'D and L substituents may project. The protein is transparent to illustrate that the orientation is the same as in A. While the 4'D position points away from the protein surface, the 4'L position points into the protein suggesting accessibility only of the former. d, e) D-Tether models of differing lengths have distinct effects on mGluR2 activation of GIRK1 channels in HEK293 cells. d) 1 mM D-Tether-0 activates mGluR2 (i.e. functions as an agonist), evoking GIRK1 current that is smaller (26 ± 5%, n=6) than that evoked by 1 mM glutamate. e) 1 mM D-Tether-1 does not activate mGluR2, but co-application with 1 mM glutamate reduces the response (45 ± 1%, n=4) compared to glutamate alone, indicating antagonistic activity.

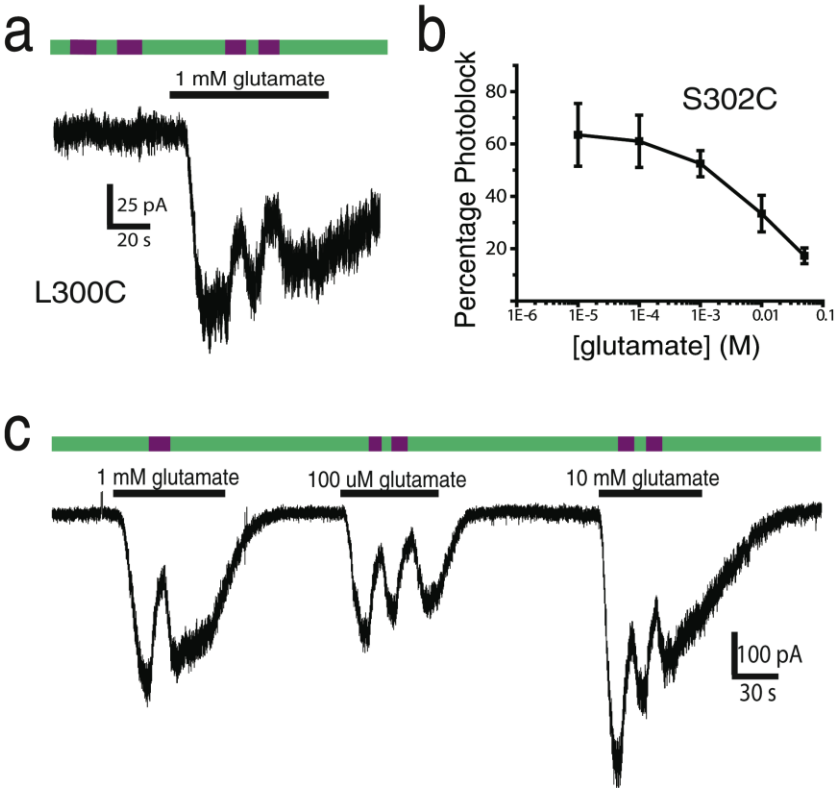

Figure S2.2, Photo-antagonism of mGluR2. a) Representative trace of currents in mGluR2-L300C after labeling with D-MAG-1. Similarly to LimGluR2-block (S302C) 380 nm light (violet bar) does not induce current in the absence of glutamate, but after application of 1 mM glutamate (black bar) induces a decrease in current amplitude. b) Glutamate-concentration dependence of photoantagonism by LimGluR-block (n=6 cells). c) Representative trace showing extent of photoblock by LimGluR2-block over a range of glutamate concentrations. After application of 10 mM Glutamate, photo-antagonism is reduced, indicating a competitive mechanism of antagonism.

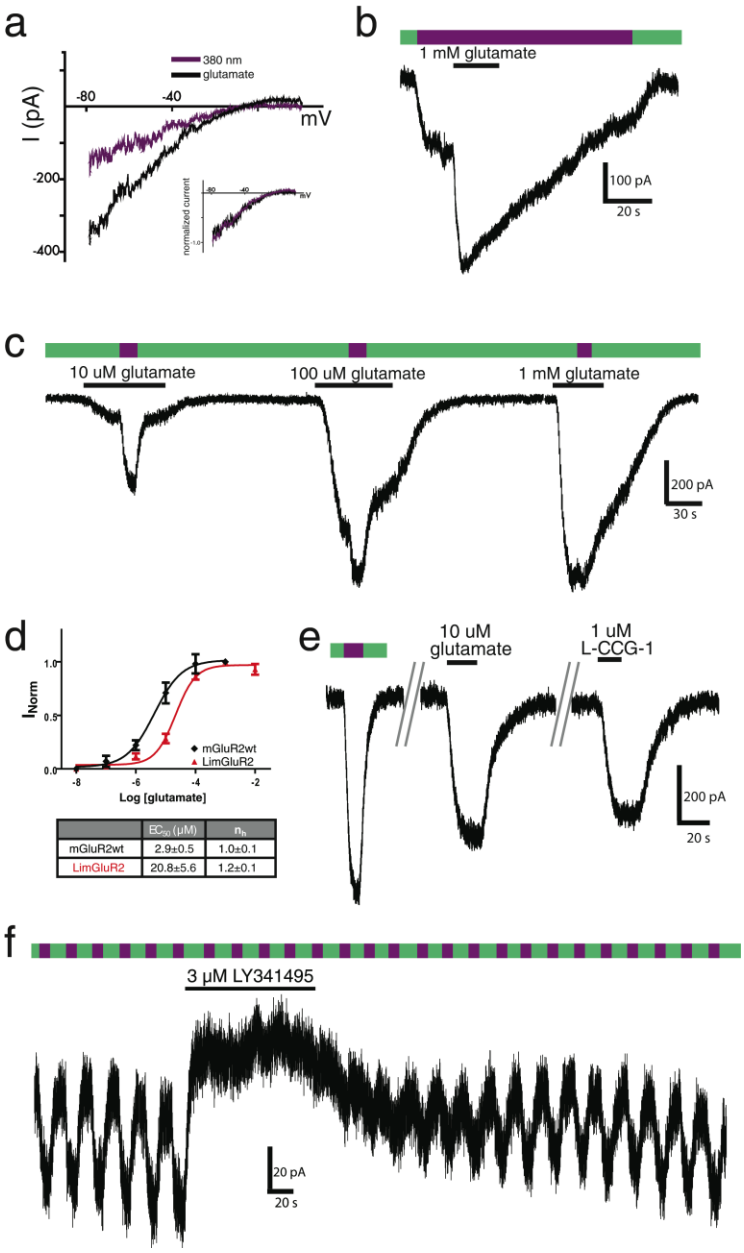

Figure S2.3, Photo-agonism of mGluR2. a) Representative trace of currents induced by either 380 nm illumination or application of 1 mM glutamate in LimGluR2 during voltage ramps from -80 to +20 mV. Ramp currents were subtracted from baseline ramps taken in absence of illumination or glutamate. Currents show inward rectification typical of GIRK current. Inset shows close overlay of normalized traces. b) When glutamate is applied after 380 nm illumination (violet bar), a further increase in inward current is seen, indicating that D-MAG-0 functions as a full agonist and does not occlude glutamate activation. Green bars indicate 500 nm illumination. c) Application of glutamate at a range of concentrations followed by photoswitching indicates that D-MAG-0 never functions as an antagonist. At sub-saturating concentrations, MAG increases inward current further indicating that it functions as a full agonist. d) Glutamate titration curves for mGluR2 and LimGluR2 indicate a minor decrease in glutamate affinity for LimGluR2. Titration curves for individual cells were fit and EC_{50} and n_h values were averaged. (n=6 cells each). e) LimGluR2 maintains sensitivity to L-CCG-1, a commonly used group II mGluR agonist. f) LimGluR2 maintains sensitivity to LY341495, a commonly used group II mGluR competitive antagonist.

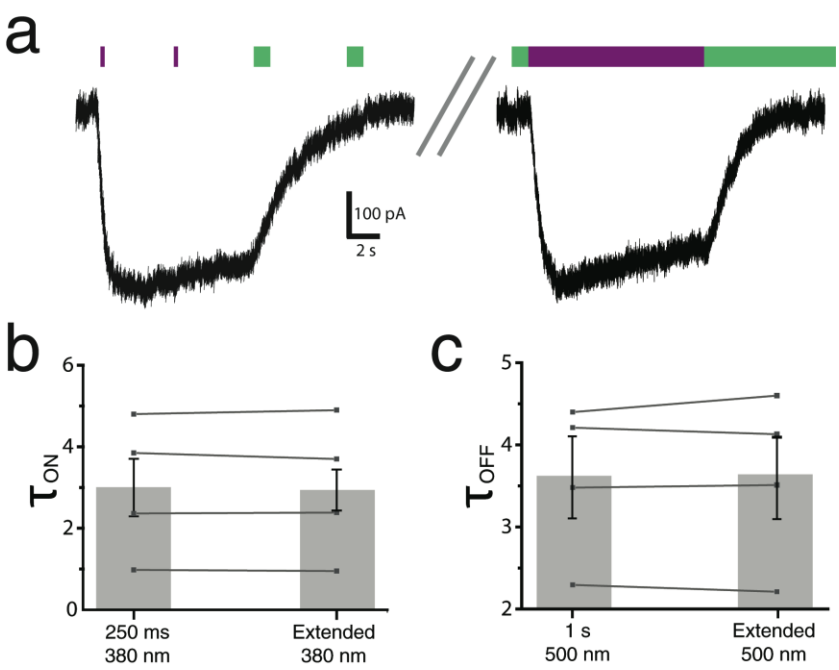

Figure S2.4, Characterization of LimGluR2 bistability and the kinetics of its activation and deactivation of GIRK. a) Representative trace showing that activation of LimGluR2 using a 250 ms pulse of illumination at 380 nm (15 mw/mm^2) and deactivation by a 1 s pulse at 500 nm (20 mw/mm^2) produce GIRK currents of similar amplitude and kinetics (of activation desensitization and deactivation) as does switching illumination between the wavelengths for extended times. b) Summary comparison of GIRK activation kinetics evoked by short pulses of illumination (250 ms at 380 nm) *versus* long exposures ($\underline{\geq}$ 5 s at 380 nm). c) Summary comparison of GIRK deactivation kinetics evoked by short pulses of illumination (1 s at 500 nm) *versus* long exposures ($\underline{\geq}$ 10 s at 500 nm). b, c) Lines show values for individual cells and bars show averages.

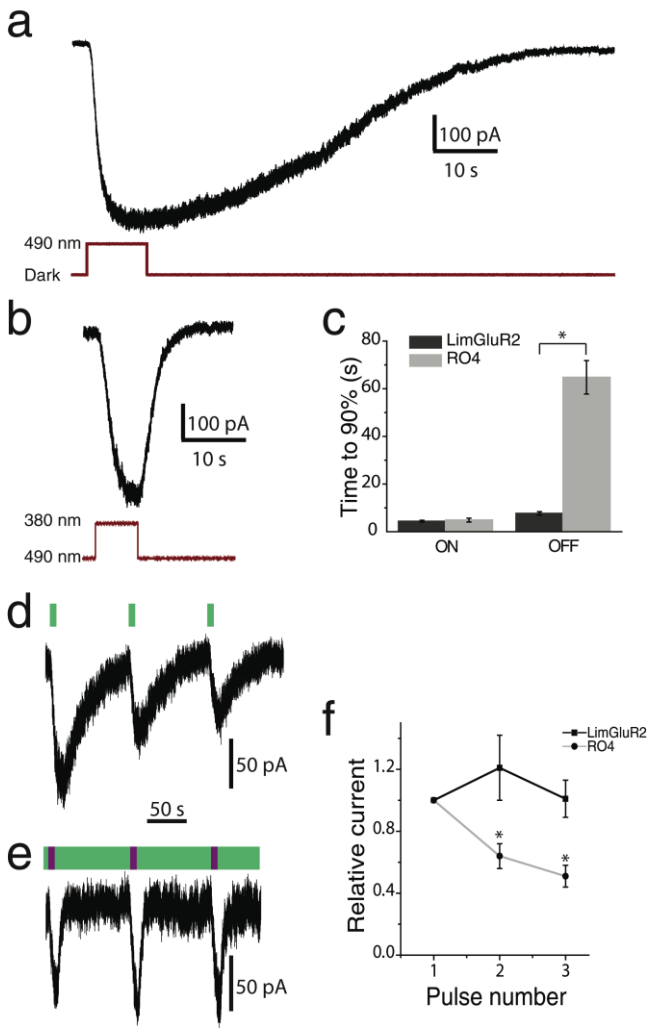

Figure S2.5, Comparison between the activation of GIRK1 channels by optical activation of rat rhodopsin (RO4) and LimGluR2 in HEK293 cells. a, b) Representative currents in response to light pulses for RO4 (a) and LimGluR2 (b) in cells co-expressing GIRK1. c) Summary of on and off kinetics for GIRK1 currents evoked by optical activation of RO4 and LimGluR2. The time to 90% off was significantly longer in RO4 (unpaired, 1-tailed t test, p=4x10^{-5}). d, e) Representative currents in response to repetitive optical activation (bouts of 10 s activation, followed by 90 s deactivation) of RO4 (d) and LimGluR2 (e). f) Summary of peak current amplitudes elicited by repeated optical activation of RO4 and LimGluR2. A significant run-down of photo-current amplitude was seen for RO4 but not LimGluR2 (* indicates p=0.016 for paired, 1-tailed t test).

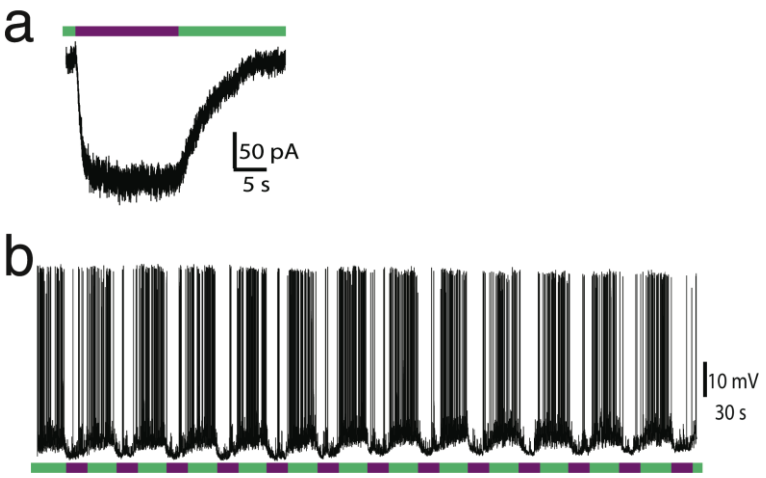

Figure S2.6, LimGluR2 mediated control of neuronal excitability. a) Representative trace of photo-current induced by illumination at 380 nm (violet bar) and extinguished by illumination at 500 nm (green bar) in a whole cell voltage-clamped neuron in 60 mM $[K^+]_o$ extracellular solution. b) Representative trace showing many rounds of repetitive suppression of spiking activity by photo-activation of LimGluR2.

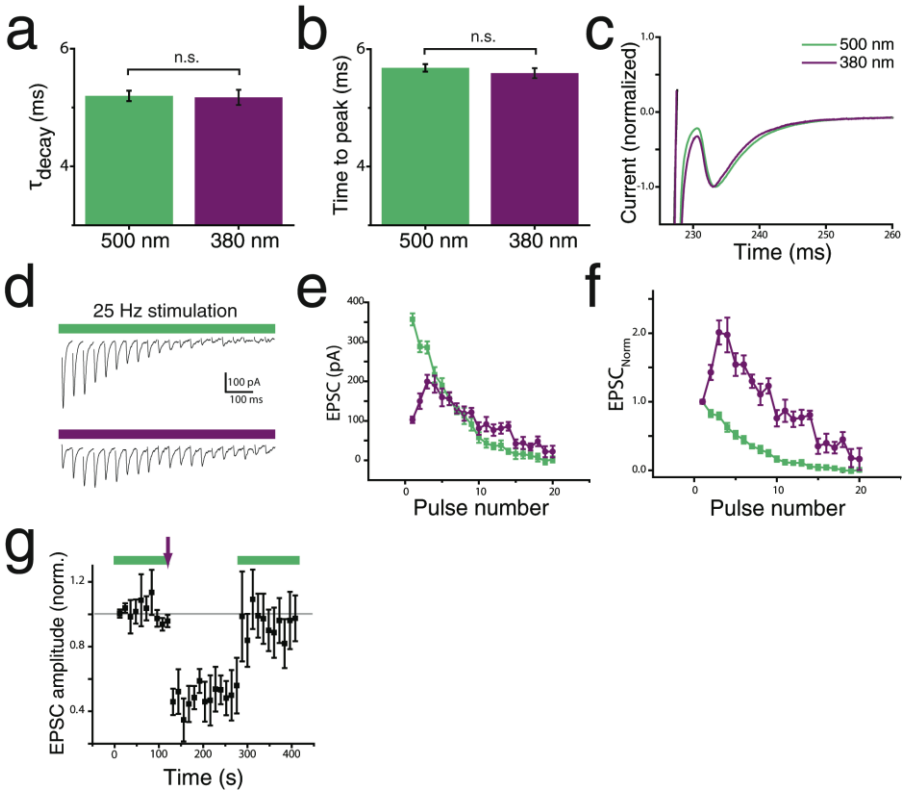

Figure S2.7, LimGluR2 inhibition of autaptic synaptic transmission. a-c) EPSC kinetics (a: decay time; b: time to peak, c: normalized overlay) are constant despite decrease in amplitude induced by optical activation of LimGluR2. a) EPSC decay time constant unchanged in 500 nm vs. 380 nm illumination (paired, 2-tailed t-test, p=0.91; n=15 sweeps/condition). b) Time to peak (time from peak of pre-synaptic spike to peak of EPSC) and jitter (S.E.M. of time to peak) are unchanged in 500 nm vs. 380 nm illumination (paired, 2-tailed t-test, p=0.74; n=15 sweeps/condition). c) Overlay of normalized average of 15 sweeps for both 380 nm and 500 nm illumination indicates no significant change in timing or shape of EPSC. Note, EPSC amplitude was reduced by 40% in this cell under 380 nm illumination. d) Representative behavior of autapse during 25 Hz stimulation under illumination with either 500 nm light (green bar) or 380 nm light (violet bar). Each trace is an average of 8 trains. e, f) Average EPSC amplitude (e) or normalized amplitude (f) during a 25 Hz train under 380 or 500 nm illumination. g) Summary of bistable inhibition in n=4 cells under the same protocol as (d): 2 minutes at 500 nm followed by 1 second of illumination at 380 nm (violet arrow) and 3 minutes in the dark before returning to 500 nm illumination for 2 more minutes.

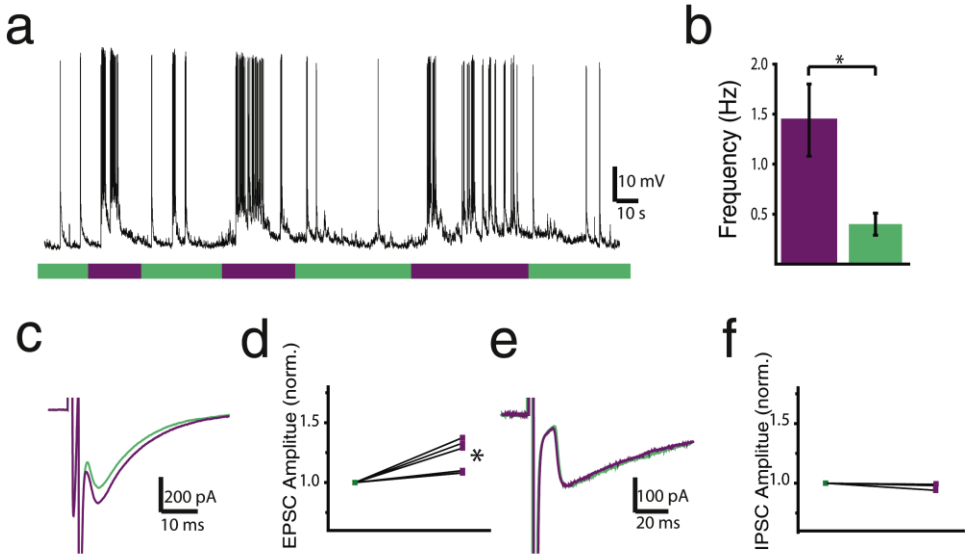

Figure S2.8, LimGluR2-block mediated modulation of excitability and transmission. a) Representative trace showing photoswitching of LimGluR2-block in a current-clamped neuron. Blockade of mGluR2 under 380 nm light increased firing frequency and was reversed by 500 nm illumination. b) Summary of firing frequency modulation in a representative cell. Firing frequency was determined for each round of photoswitching (5-20 s per photoswitch) over a 10 minute recording. (paired, 2-tailed t-test, p=0.028). c) Representative EPSCs in response to 380 nm (violet trace) or 500 nm illumination (green trace) in autaptic neurons expressing LimGluR2-block. Each trace is an average of 12 sweeps for each illumination condition. d) Summary of LimGluR2-block enhancement of EPSC amplitude. Each line reperesents a single cell and the violet point indicates the amplitude in 380 nm light and the green point indicates the amplitude in 500 nm light. All values were normalized to the amplitude in 500 nm. e) Representative IPSCs in response to 380 nm (violet trace) or 500 nm illumination (green trace) in autaptic neurons expressing LimGluR2-block. Each trace is an average of 12 sweeps for each illumination condition. f) Summary of LimGluR2-block enhancement of IPSC amplitude. IPSCs were unaffected by LimGluR2-block.

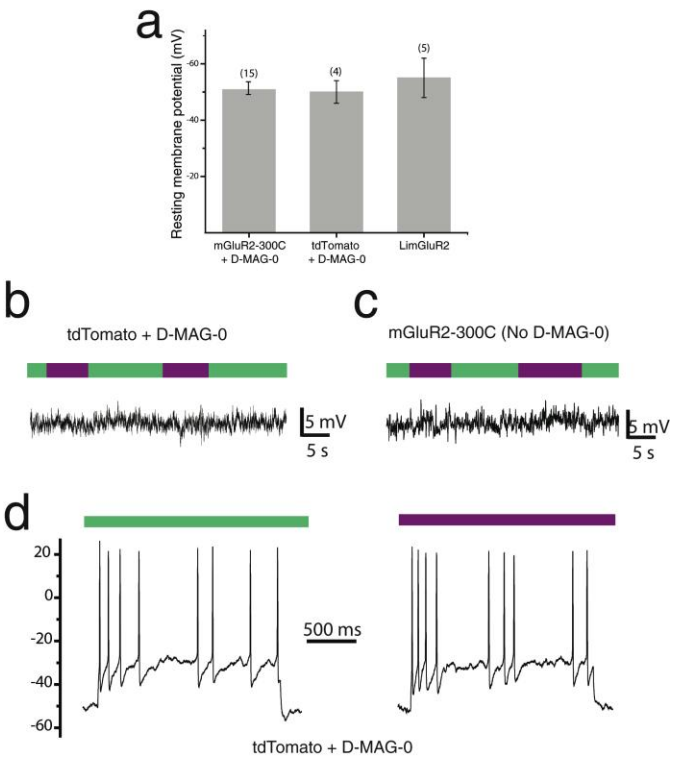

Figure S2.9, **Hippocampal slice controls indicate that LimGluR2 does not harm cell health and is orthogonal.** a) Average resting potential is not altered in cells expressing LimGluR2 and labeled with D-MAG-0 relative to cells with D-MAG-0 but without mGluR2-300C or unlabeled mGluR2-300C expressing cells. b) No photoswitching was seen in tdTomato-transfected cells labeled with D-MAG-0 or c) cells expressing LimGluR2 (mGluR2-300C) but not labeled with D-MAG-0. d) tdTomato-expressing cells labeled with D-MAG-0 show no change in spike firing in response to current injection when illuminated with 380 nm or 500 nm.

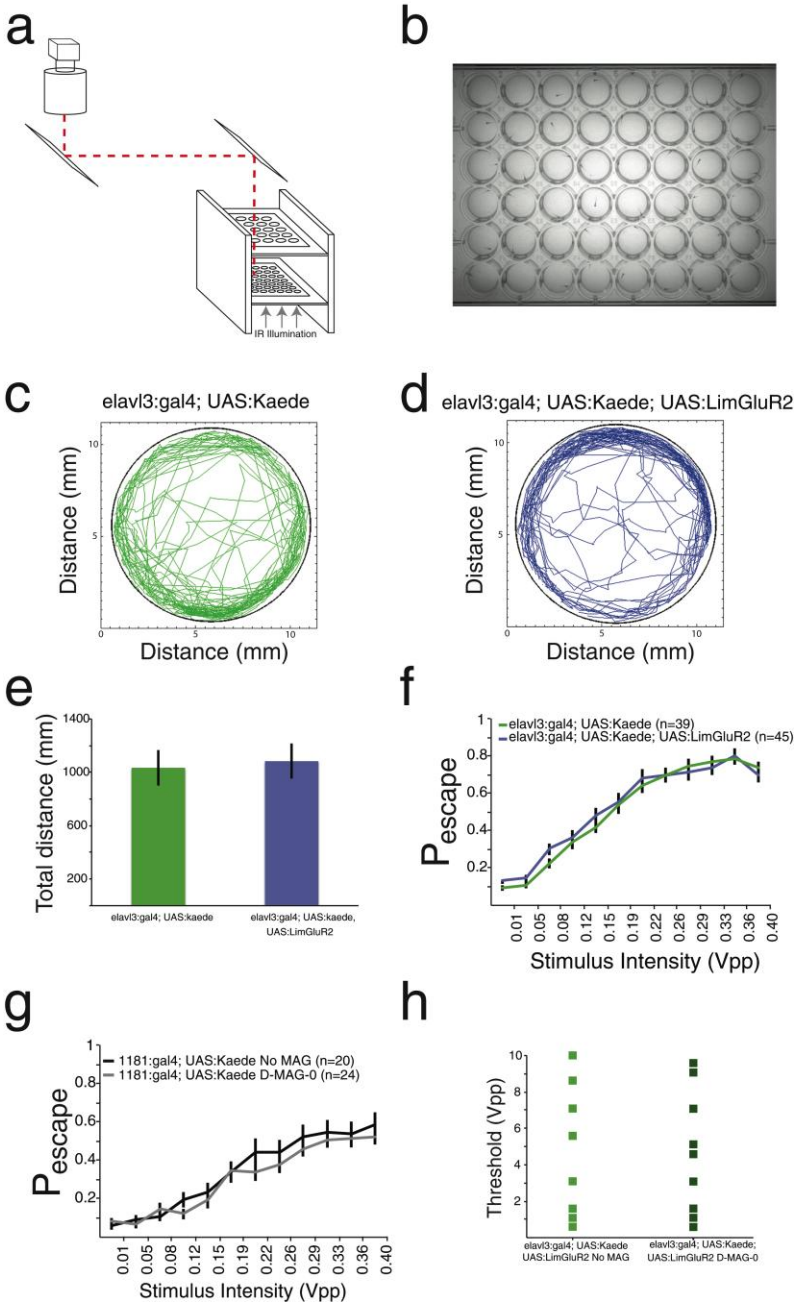

Figure S2.10. Pan-neuronal expression of LimGluR2 and labeling with D-MAG-0 do not modify basal activity levels and escape response threshold. a) Schematic of system used for measurement of swimming behavior and escape response in 48 well plates for different genetic lines with or without D-MAG-0 labeling (see Online Methods for details). b) Representative image of individual zebrafish in wells of a 48-well plate during tracking of swimming. c,d) Representative tracks of single zebrafish larvae with either GAL4 pan-neuronal driver driving Kaede fluorescent protein alone (*elavl3*:gal4; UAS:kaede control) (a) or also containing LimGluR2 (*elavl3*:gal4; UAS:kaede; UAS:LimGluR2) (b). (Tracking performed with an in-house written Matlab script.) e) Total distance travelled at 5-6 dpf by *elavl3*:gal4; UAS:kaede control (n = 24) or *elavl3*:gal4; UAS:kaede; UAS:LimGluR2 (n = 24). Larvae were imaged for 25 minutes under infrared illumination at 30fps in 48-well microplates. Total distance swum was measured by the tracking of the centroid of each fish for the duration of the recording. f) Sound stimulus intensity-probability of escape curve is not affected by LimGluR2 expression. The escape threshold of 5-6 dpf zebrafish larvae was determined by administering a randomized sequence of 120 sound stimuli at 10 different voltage levels, with a 30 second inter-stimulus interval (ISI) for *elavl3*:gal4; UAS:kaede control and *elavl3*:gal4; UAS:kaede; UAS:LimGluR2. Stimuli duration and frequency were 20ms and 900Hz, respectively. Experiment performed in a 48-well microplate, under infrared illumination and recorded at 30fps. Prior to testing larvae were acclimated for 30 minutes. Escapes were automatically determined by subtraction and thresholding of the first two frames after the stimulus. Accuracy of the detection method was verified by visual inspection of movies. g) Sound stimulus intensity-probability of escape curve is not affected by D-MAG-0 treatment. 1181:gal4; UAS:kaede 5-6dpf zebrafish larvae were treated with D-MAG-0 or control medium. Curve was determined as described above for (f). h) Labeling of *elav3*:gal4; UAS:kaede; UAS:LimGluR2 fish with D-MAG-0 does not modify ASR threshold before receptor activation with 380 nm light. Individual head-mounted fish, D-MAG-0-labeled or controls, were exposed to stimuli of increasing amplitude stimulit with an ISI of 10 seconds. The threshold was defined as the lowest sound able to initiate an escape response in >50% of trials. Graph shows the initial threshold of individual fish in the two groups.

Construct	D-MAG-0	D-MAG-1
mGluR2wt	x	x
Q42C	x	Antagonist (9±4%; n=4)
D146C	x	x
D215C	x	x
L300C	Agonist (48±4%; n=10)	Antagonist (21±2%; n=7)
S302C	x	Antagonist (53±4%; n=5)
E373C	Antagonist (5±2%;n=3)	Antagonist (4±1%; n=4)
S376C	x	x

Table S2.1, Cysteine screen of mGluR2. Results of photoswitching of D-MAG-0 and D-MAG-1 attached at each of the 7 positions tested. "x" indicates no photoresponse. Agonistic and antagonistic effects are quantified relative to 1 mM glutamate. Data from $\geq$ 2 different coverslips for all conditions tested.

Chapter III: Further development and *in vivo* application of photoswitchable metabotropic glutamate receptors

Introduction:

Mechanistic questions and further engineering of LimGluRs

Metabotropic glutamate receptors are an extremely diverse and physiologically important class of neuromodulatory GPCRs[1]. Despite their importance, which has been established through coarse techniques such as genetic knockout and pharmacology, classical approaches have been limited in their ability to define the precise spatial and temporal activation profiles of specific mGluRs in the brain. We recently used a chemical optogenetic approach to develop a subtype-specific means for optically agonizing or antagonizing group II mGluRs, mGluR2 or mGluR3, with high spatiotemporal precision[2]. These new tools, collectively termed LimGluRs, employ a previously described approach based on site-specific attachment of a chemical photoswitch which contains a functional group that can reversibly bind to a protein's allosteric site in response to different wavelengths of light. While initial results showed different attachment point/photoswitch combinations that produced photoagonism or photoantagonism of mGluR2 and 3, many questions remain about the molecular properties of this unique non-soluble ligand. A deeper understanding of the mechanism of photoswitching may allow for a better application of LimGluRs in both neurophysiological and biophysical contexts. The major questions about the mechanism of photoswitching are the relative efficacy and affinity of MAG on mGluR2 and 3 and the pharmacological sensitivity of LimGluRs to different types of drugs. Furthermore, a deeper understanding and tuning of the spectral and other optical properties of LimGluRs may be key to their successful application.

While it has been demonstrated that LimGluR2, as was previously shown for LiGluR[3] and Hylighter[4], is functional *in vivo* in the model vertebrate system of larval zebrafish[2], a major step forward for the technique would be to establish the ability to optically control LimGluRs *in vivo* in rodents. The ability to control LimGluRs and LiGluRs with light in awake mice would open the door to the ability to probe the role of specific receptors in defined brain regions and cell types during a wide repertoire of behaviors and models of neurological disorders. In order to establish photoswitchable glutamate receptors in mice, a number of technological obstacles must be overcome including *in vivo* expression and MAG-labeling and the development of a means of two-color illumination via optical fibers. Finally, the ultimate application of LimGluRs, which would not be possible using opsin-based optogenetic approaches, is the development of a knock-in mouse where the cysteine-substituted version of an mGluR can be substituted for the native gene. This transgenic approach would ideally allow for the optical control of specific mGluRs in their native expression pattern.

Motivation for optical control of group I mGluRs

The ability to photocontrol group I mGluRs would be an extremely powerful means of manipulating G_q pathway signaling in addition to proposing the precise properties of mGluR1 and 5. mGluR1 and mGluR5 have been shown to be key molecules in the induction and expression of long term synaptic plasticity in a number of brain regions, including the

hippocampus and basal ganglia[5]. Consistent with this, using genetic or pharmacological manipulations they have both been implicated in learning and memory[6,7] and addiction[8,9]. In addition, mGluR5 has recently emerged as an extremely promising drug target for both fragile X mental retardation[10] and Alzheimer's disease[11]. However, our understanding of the group I mGluRs and the mechanisms of their role in the aforementioned phenomena has been limited by many of the same factors that initially motivated development of group II mGluRs. The drugs that target mGluR1 and 5 are slow, hard to reverse, and unable to be spatially or genetically targeted. For example, mGluR5 is expressed in astrocytes where it is believed to be a key glutamate-sensor that controls calcium oscillations and ultimately gliotransmitter release[12,13], but any drug that targets mGluR5 is likely to also target receptors on nearby neurons making it difficult to decipher the distinct role of the neuronal or glial populations. While there are considerably more pharmacological agents that target group I mGluRs than group II or III, there are key challenges still remaining in isolating mGluR1 or mGluR5[1]. Most importantly, there is a lack of subtype specific orthosteric agonist since it was recently reported that CHPG, which was believed to be specific for mGluR5, is not able to distinguish between the two group I receptors[14]. It is worth noting that there are a number of specific antagonists or allosteric drugs that can distinguish between mGluR1 and 5, but these drugs still suffer from poor spatial and temporal targeting which would make it difficult to use them to understand something very precise like group I mGluR-mediated spine swelling or shrinking.

Currently the only optical means of manipulating G_q signaling are the chimeric optoXRs[15], which suffer from slow kinetics and poor repeability and, as such, have not been widely adopted[16]. Furthermore, group I mGluRs offer the unique property of dual coupling to G_s and G_q pathways[17] which makes it necessary to build a photoswitch off of the entire receptor in order to truly probe its properties. In addition group I mGluRs have unique synaptic targeting within the post-synaptic density that is key for recapitulating their signaling outputs and may allow them to be very powerful synaptic tools[18]. The ability to photocontrol mGluR1 and 5 would allow for the manipulation of proteins directly involved in native forms of long term synaptic plasticity and pave the way to a powerful means of probing the relationship between synaptic plasticity in key regions like CA1 and the ventral tegmental area and important behavioral paradigms such as memory and addiction. All of these reasons make extending photoagonism and photoantagonism to group I mGluRs extremely desirable.

Motivation for optical control of group III mGluRs

The final group of mGluRs, group III, present many interesting properties that make them an attractive complementary target for optical control. In particular, mGluR7 has many unique properties, which make it the most attractive target within this group. mGluR7 is the most prominently expressed of the group III mGluRs and is found presynaptically in many brain regions where it was identified as the major L-AP-4 sensitive receptor [19,20]. Unlike all of the mGluRs which have an EC_{50} for glutamate in the 1-20 μM range, mGluR7 has a greatly reduced affinity which results in an EC_{50} of ~ 1mM[1,21]. This is believed to reflect the fact that mGluR7, unlike most other presynaptic mGluRs which are located perisynaptically, is located directly in the synapse where it is believed to play the role of a low pass filter that inhibits transmission once glutamate has reached high levels in the synapse[22,23]. This low affinity, however, makes it difficult to target mGluR7 pharmacologically, especially orthosterically where very high concentrations of agonists or antagonists are required. In theory, the high local concentration

induced by covalent attachement of MAG, may allow for the low inherent affinity of mGluR7 to be overcome. mGluR7, like the other group III mGluRs, is expressed somewhat less than group I and II mGluRs, but is still found at a number of synapses throughout the brain, largely in the presynaptic compartment. Further adding to its uniqueness, mGluR7 is highly regulated in its intracellular C-terminal tail[24]. A number of proteins have been shown to bind and control mGluR7 trafficking, G protein coupling, and synaptic targeting. For instance, calmodulin (CaM) binding to mGluR7 has been shown to be required for $G_{\beta\gamma}$-mediated signaling and inhibition of hippocampal autapses[25]. Most notably, interactions between mGluR7 and the synaptic protein PICK1 (protein interacting with C kinase 1) have been shown to cluster mGluR7 and synapses[26,27,28] and mediate a protective role against absence epilepsy, which is observed either when mGluR7 is knocked-out[29] or the PICK1-mGluR7 interactions is disrupted in thalamo-cortical regions[30]. All of these properties make mGluR7 another attractive target for chemical optogenetic control.

Results:

Further characterization and modification of group II LimGluRs

LimGluRs provide a unique perspective on the tethered photoswitch approach due to their complex pharmacology that contains orthosteric ligands that work through the native glutamate binding site, and allosteric ligands, that work through other regions of the receptor to modulate signaling. We sought to use a combination of mutations and drugs that target either orthosteric or allosteric sites of mGluR2 and 3 to gain a deeper insight into the mechanism of photoswitching.

Recent work using a similar approach on ionotropic glutamate receptors has shown that the functional glutamate group of the chemical photoswitch MAG (Maleimide Azobenzene Glutamate) [31] is present in a local concentration exceeding 10 mM based on the required concentration of a competitive antagonist to block photoswitch activation. It was also previously shown that photoactivation of LimGluR2 with MAG does not display any apparent photoantagonism in the presence of glutamate (Fig. 2.3C, S2.3C) indicating that it is not a partial agonist despite its partial activation relative to glutamate which is believed to be due to partial cysteine labeling. An alternative explanation would be that the glutamate moiety of MAG is actually not in a high enough local concentration to compete off glutamate at high enough concentrations. In this scenario, MAG could be a partial agonist, just with a low affinity/local concentration. To test this we mutated the orthosteric glutamate binding site of LimGluR2 and assessed whether the reduced affinity of the receptor would reduce the efficacy of the photoswitch. We used the previously published R57A mutation of mGluR2 which removes an electrostatic interaction with the carboxyl group of glutamate [32]. Mutation R57A in the mGluR2-L300C background shifted the apparent affinity of mGluR2-300C for glutamate from ~20 uM to ~700 uM as assayed by GIRK activation in HEK 293T cells (Fig. 3.1A). This mutant, termed "low affinity" LimGluR2 or LA-LimGluR2, showed large photoactivation following conjugation that maintained bistability (Fig. 3.1B) and showed the same efficacy relative to saturating glutamate of LimGluR2 (Fig. 3.1C,D). This result indicates that despite the nearly millimolar EC_{50} of LA-LimGluR2, the local concentration of MAG is sufficiently high that its efficacy is not altered. This provides further evidence that MAG is in fact a high affinity, high efficacy agonist of mGluR2 despite partial labeling. Furthermore, LA-LimGluR2 provides a useful variant of LimGluR2 that may be used for neurobiological application. The shifted affinity of LA-LimGluR2 means that it would not be activated by extrasynaptic levels of glutamate in most brain regions. This could eliminate potentially deleterious effects of heterologous overexpression of a glutamate-activated receptor. In addition, the homologous mutant in LimGluR3 (R64A), to produce LA-LimGluR3, produced an even larger affinity shift in mGluR3 than mGluR2 (~1,000-fold vs. ~50-fold) while not obviously altering photoswitch efficiency (Fig. S3.1).

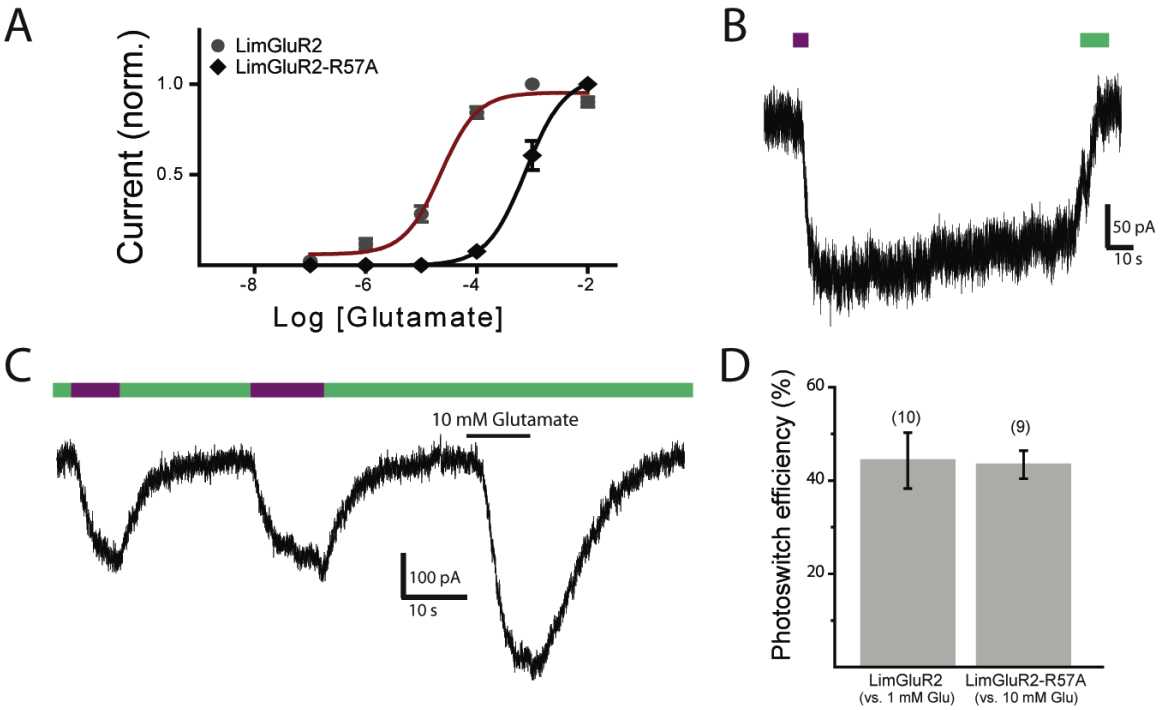

Fig. 3.1, A low-affinity variant of LimGluR2, LA-LimGluR2, displays efficient photoactivation. A) Dose response curves obtained for LimGluR2 and LimGluR2-R57A ("LA-LimGluR2") using the GIRK current assay in HEK 293 cells. The EC_{50} for LimGluR2 was 21± 2 μM and the EC_{50} for LA-LimGluR2 was 750 ± 180 μM. n=7 and n=5 cells for each condition, respectively. B) Representative trace showing bistable photoactivation of mGluR2 signaling by LA-LimGluR2. C) LA-LimGluR2 shows repeatable photoactivation that is 40-50% as large as 10 mM glutamate. D) Summary of photoswitch efficiency experiments show that decreasing the affinity of mGluR2 does not decrease the photoswitch efficiency which is defined as (photocurrent amplitude)/(Glutamate current amplitude) x100. The number of cells tested for each condition is shown in parentheses.

Since LA-LimGluR2 experiments provided strong evidence for D-MAG-0 as a high affinity, full agonist of mGluR2 we wondered how LimGluR2 photoactivation would respond to antagonism using non-competitive drugs termed negative allosteric modulators (NAMs). NAMs bind to a site in the TMD of mGluRs to indirectly block the activation via glutamate or other agonists [33]. The mechanism of NAM-mediated block is poorly understood and we, thus, wondered if a unique ligand like MAG with a very high local concentration could overcome a NAM more easily than a soluble agonist. RO64-5229 is an mGluR2-specific NAM with a reported IC_{50} of 110 nM for blocking glutamate activation. Application of 1 μM RO640-5229 was able to fully block photoactivation of LimGluR2 but not LimGluR3 (Fig. 3.2). A similar concentration of RO640-5229 was required to block glutamate-mediated activation (data not shown). Along with previous data showing that LimGluR2 photoactivation was fully blocked by the competitive antagonist LY341495a (Fig. S2.3f), this experiment provides further evidence that MAG activates mGluR2 in a manner that is very similar to its native agonist, further supporting the value of LimGluR2 as a tool to study mGluR2 function.

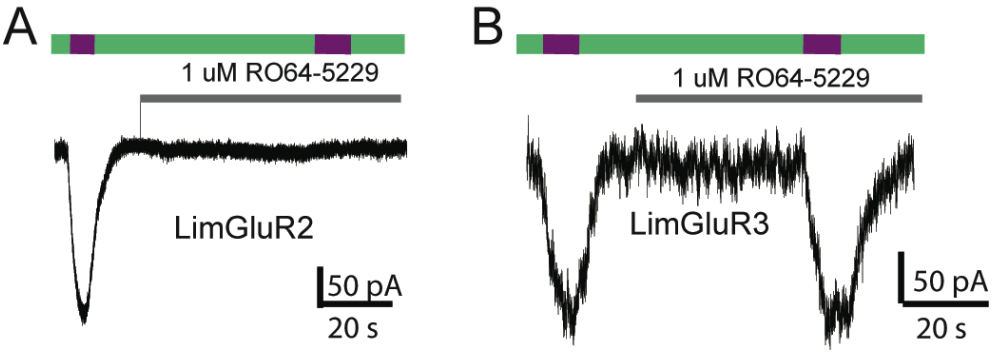

Fig. 3.2. LimGluR2, but not LimGluR3, is blocked by the NAM RO64-5229. A,B) Representative traces showing complete block of LimGluR2 (A) by 1 µM RO64-5229 which has no effect on LimGluR2 photocurrents (B). Reversal was extremely slow for LimGluR2 making it difficult to assess if a NAM could be fully removed following binding.

While the ability to optically control mGluRs is major step forward in expanding the optogenetic toolset for GPCRS, many issues still remain with producing efficient photoactivation in a variety of settings. The putative wavelengths used for photoswitching of LimGluR2 are 380 nm for turning on (*trans* to *cis*) and 500 nm for turning off (*cis* to *trans*). Unfortunately, 380 nm is not a widely available laser wavelength and may also pose problems for tissue penetration *in vivo*. We decided to look more closely at the precise wavelength required for activation of LimGluR2. By varying the activation wavelength in the range of 375 nm to 405 nm, we found that activation efficiency rapidly decreased as we approached visible light (Fig. 3.3A). Most notably, 405 nm, which is a widely available laser wavelength, was only able to activate LimGluR2 with ~50% efficiency relative to 380 nm (Fig. 3.3B). This result indicates that 405 nm lasers may be used for photoactivation of LimGluR2 but at a cost in terms of relative efficacy of activation. In order to further accommodate LimGluRs for use with visible light we next turned to a recently synthesized compound D-MAG-0_{460} (Fig. 3.4B). D-MAG-0_{460} is based on a recently published compound with L stereochemistry that was used to photoactivate LiGluR with visible light with a peak at 460 nm [34]. This compound is activated in the light, but unlike D-MAG-0, rapidly relaxes in the dark. We tested D-MAG-0_{460} on both LimGluR2 and LimGluR3 and found essentially no photoactivation of LimGluR2 and clear photoactivation of LimGluR3 following illumination with 445 nm light. The photoactivation of LimGluR3 was significantly larger than mGluR2 but was also much smaller than what is usually measured for LimGluR3 with D-MAG-0 (>60%). This may be due to the limited solubility of the compound that prevented labeling at a concentration above 10-20 µM. Ultimately, D-MAG-0_{460} provides an interesting lead for further tweaking of the optical properties of LimGluRs and an interesting hint into a surprising specificity for mGluR3 over mGluR2.

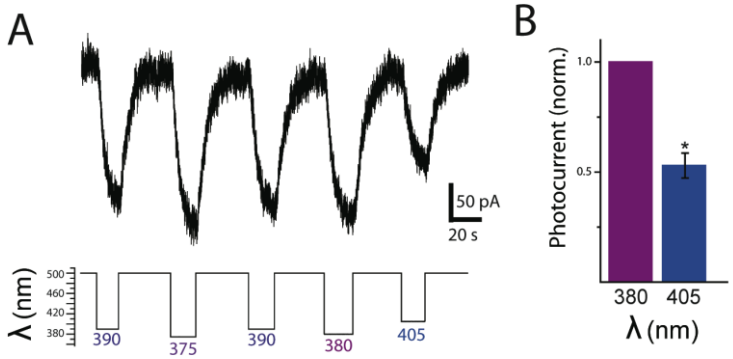

Fig. 3.3. Wavelength-dependence of LimGluR2 activation in the near UV. A) Representative GIRK current trace showing reduced photoactivation of LimGluR2 at longer wavelengths than 375 nm. B) Summary of photocurrent amplitude for 380 nm and 405 nm illumination shows a ~50% reduction for 405 nm. * indicates statistical significance (Paired T test, $P<0.05$; n= 4 cells).

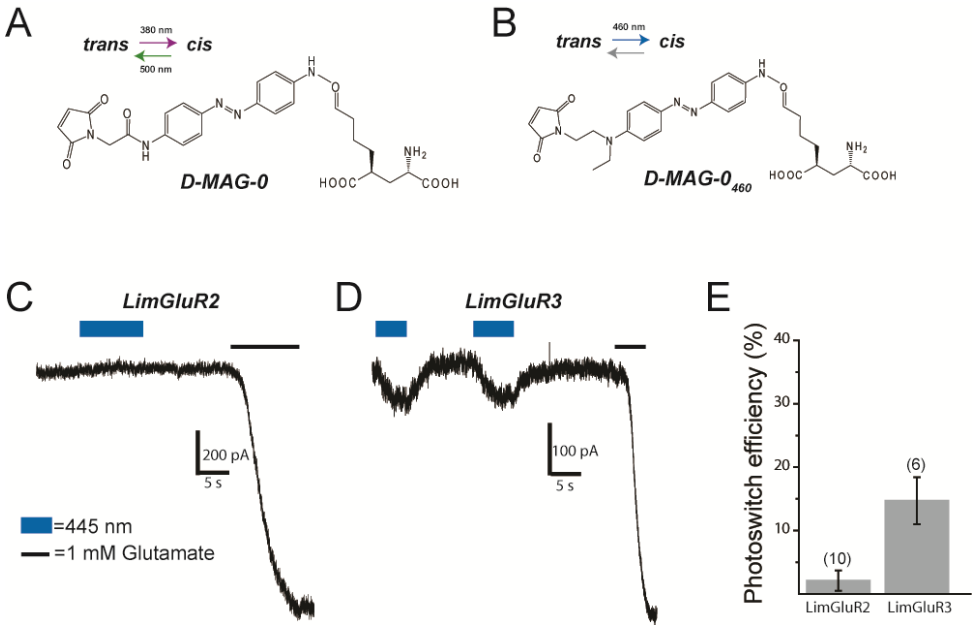

Fig. 3.4, Optical control of LimGluR3, but not LimGluR2, with D-MAG-0_{460}. A) Chemical structure of D-MAG-0 in trans state. D-MAG-0 requires near UV illumination to undergo *trans* to *cis* isomerization and visible illumination to undergo *cis* to *trans* isomerization. B) Chemical structure of D-MAG-0_{460} shows slight differences relative to D-MAG-0 in the linker between the maleimide group and the azobenzene. D-MAG-0_{460} undergoes *trans* to *cis* isomerization in the presence of visible light and relaxes back to *trans* rapidly in the dark. C, D) Representative traces showing the D-MAG-0_{460} does not photoactivate LimGluR2, but does photoactivate LimGluR3. E) Summary of photoactivation efficiency relative to 1 mM glutamate for LimGluR2 and LimGluR3 conjugated to D-MAG-0_{460}. The number of cells tested for each condition is shown in parentheses.

in vivo optical control of glutamate receptors in mice

While many very useful studies may be performed in culture and slice systems, as well as in model organisms such as zebra fish, it would ultimately be very powerful to be able to optically control glutamate receptors in behaving mammals. In order to move toward this goal we first developed adeno-associated viruses (AAV) that would allow for the targeted expression of LimGluR2 in the brains of mice. We produced a number of constructs with various promoters including human synapsin (hsyn) and chicken actin (CAG) in order to drive LimGluR2 expression. Fig. 3.5a shows expression of GFP-tagged LimGluR2 in slices taken from mice stereotactically-injected with AAV9 or AA7M8 viruses in medial prefrontal cortex, dentate gyrus, or visual cortex. After 3-4 weeks LimGluR2 is present in many cells and is spread out throughout fine processes. To gain further power for targeted expression we developed a FLEX version of LimGluR2 that may be used to target expression to Cre-expressing cells (citation). This expression system opens the door for a finer targeting of expression to specific cell types, which is not achievable with direct promoters. We expressed an AAV9 version of the FLEX LimGluR2-GFP in both Cre: Camkii and Cre: GAD mice and saw distinct expression profiles targeting either excitatory or inhibitory neurons, respectively (Fig. 3.5b). We also developed a virus for LimGluR3-GFP to allow for targeting of LimGluR3 to glial cells because of the native expression of mGluR3, but not mGluR2, in astrocytes[35]. Using the GFAP promoter we produced

an AAV9 virus that allowed expression of LimGluR3-GFP in astrocytes of CA1 (Fig. 3.5C). However, this promoter had some off target effects in CA1 neurons as identified by morphology.

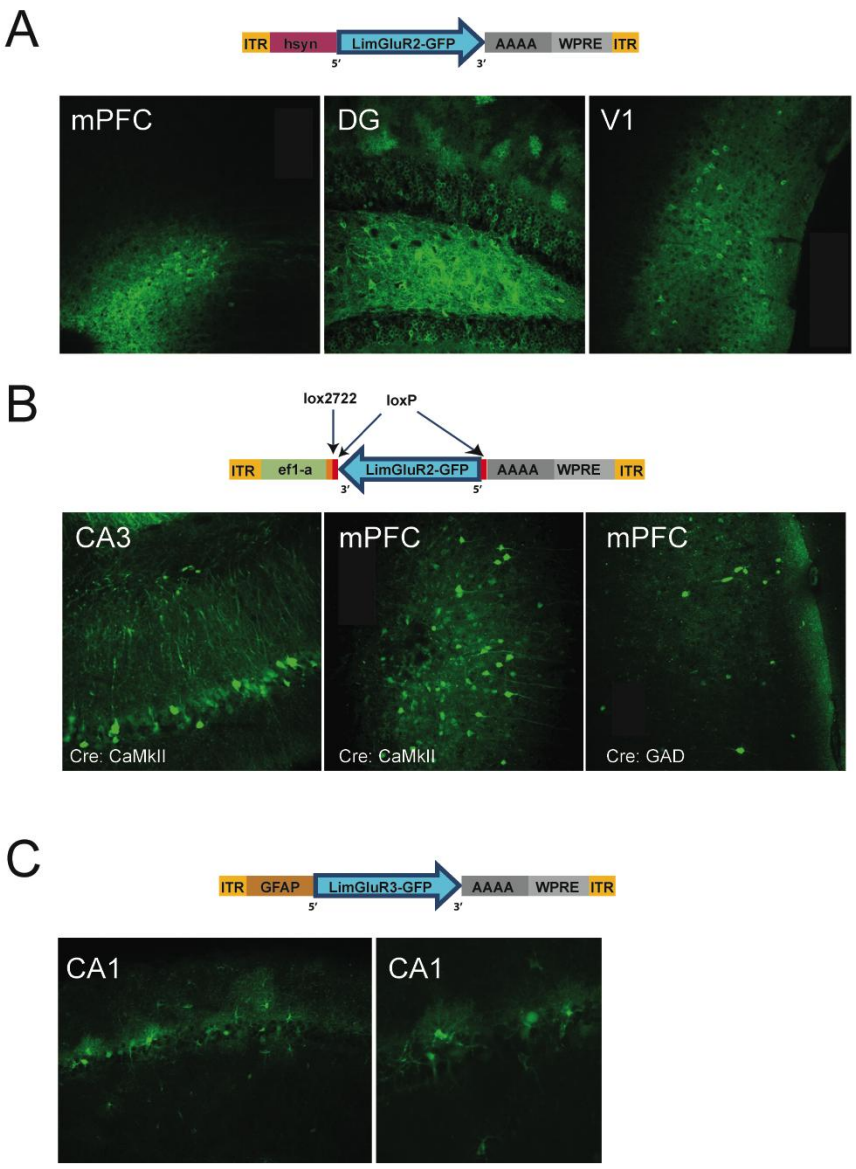

Fig. 3.5, AAV-mediated expression of LimGluR2 and LimGluR3 in mouse hippocampus and cortex. A) Above, vector map showing hsyn viral construct used for production of LimGluR2-GFP AAV9 or AAV7M8 viruses. Below, reperesentative expression of LimGluR2-GFP in neurons of mouse medial prefrontal cortex (mPFC), dentate gyrus (DG), or visual cortex (V1). B) Above, vector map showing FLEX viral construct used to produce an AAV9 virus for LimGluR2-GFP. Below, representative expression of LimGluR2-GFP specifically in excitatory neurons in CA3 or mPFC of Cre:CamkII mice or inhibitory, GABAergic neurons in mPFC of Cre:GAD mice. C) Above, vector map showing GFAP viral construct used for production of LimGluR3-GFP AAV9 virus. Below, representative expression of LimGluR3-GFP in astrocytes in the CA1 region of hippocampus. Note: a number of cells with neuronal morphology are observed indicating some lack of specificity of the promoter.

In order to test the ability to label and photoactivate MAG-based tools *in vivo*, we turned to the V1 visual cortex. V1 is a good brain region for testing these tools because it is easily targetable for expression and electrode placement, and easily stimulated in order to produce a response that may be inhibited by activation of an inhibitory tool like LimGluR2. Before testing LimGluR2, we first turned to LiGluR6, the light-activated ionotropic receptor because it is a simpler system that would allow for direct excitation of neurons without the need for a visual stimulus. We expressed an AAV2 virus under the control of the hsyn promoter in V1 (Fig. 3.6A). 3 weeks later we stereotaxically injected L-MAG-0 and then inserted an optrode connected to a dual laser system composed of a 375 nm and a 532 nm laser. Importantly, we waited 3 hours to allow the MAG to label receptors and to be cleared from the area by the flow of cerebrospinal

fluid. Following a flash of 375 nm a subset of cells showed a robust elevation in firing rates that was sustained in the dark and reversed by 532 nm illumination (Fig. 3.6B-D). Photoactivation was repeatable and observed at depths ranging from 200 uM to ~1 mM into the neocortex. The measured intensity at the tip of the 200 µM fiber was ~25 mW/mm2 and was able to drive photoactivation in less than 100 ms (Fig. 3.6D). We next tested LimGluR2-GFP using a similar experimental setup. However, LimGluR2 experiments required a visual stimulus in order to elevate neuronal activity (Fig. 3.6E). We delivered a 2hz full field flash of white light for 2s followed by either 375 or 532 nm illumination at the optrode. Following 375 nm illumination the response to visual stimuli was decreased relative to 532 nm illumination (Fig. 3.6F, G). These results indicate that MAG-based photoswitch systems may be labeled and photoswitched *in vivo* in awake mice.

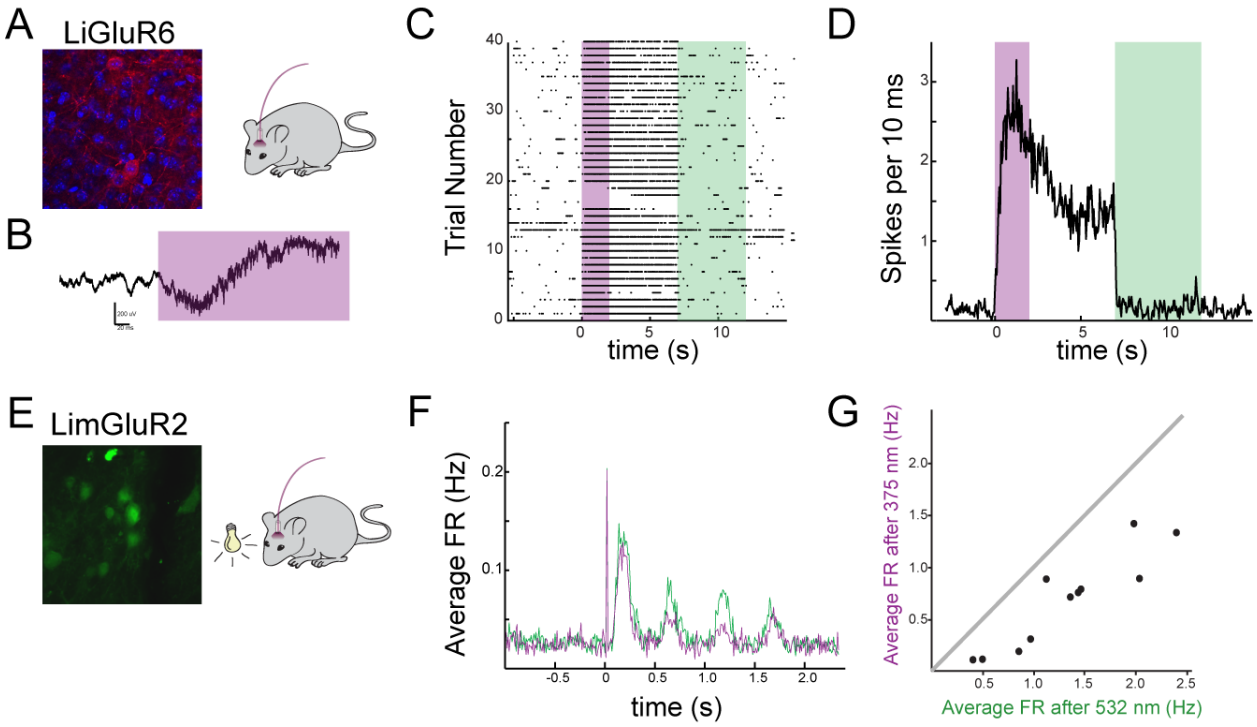

Fig. 3.6. *in vivo* optical control of LiGluR6 and LimGluR2 in visual cortex of awake mice. A) Antibody stain showing expression of LiGluR6 in V1. DAPI stain is shown in blue and the secondary antibody is shown in red. B) Raw recording showing a field response to 375 nm illumination (violet) in LiGluR6-infected cortex. In the presence of 375nm light higher frequencies are observed which include individual spikes which are rapid downward deflections. C) Raster plot showing repeatable spike firing in response to LiGluR6 activation by 375 nm light that is sustained in the dark and reversed by 532 nm illumination (green). D) Average firing rate for many cells showing the rapid increase and decrease in firing rate following illumination with 375 nm or 532 nm, respectively. E) Expression of LimGluR2-GFP in V1 near site of electrode implant. F) Average firing rate (FR) of V1 neurons in response to a 2 Hz, 2 s visual stimulus following brief 375 nm (violet) or 532 nm (green) illumination shows a modest decrease in visual response following LimGluR2 activation. G) Comparative firing rates for individual cells following 375 nm or 532 nm illumination shows a net decrease in firing following LimGluR2 activation.

Finally, we sought to develop a knock-in mouse that would express mGluR2-L300C in the native mGluR2 expression pattern. We first tested the mouse variant of mGluR2 to confirm that the L300C mutant was able to be photoactivated by D-MAG-0 in the same way. Following conjugation with D-MAG-0 the mouse version of LimGluR2 showed 45 ± 7% photoactivation

relative to 1 mM glutamate (n=5 cells) (Fig. S3.2A) and maintained bistability (Fig. S3.2B). Similar to the original rat LimGluR2, the mouse LimGluR2 showed a modest decrease in affinity for glutamate relative to wild type (Fig. S3.2C). In order to produce the LimGluR2 knock-in mouse, the FLP recombination system was used (Fig. 3.7). Homozygote mice carrying the 300C mutation in both copies of the gene are viable and show no gross phenotype relative to wild type. Future experiments will test the relative expression of mGluR2 and ultimately, the feasibility of these mice for optogenetic studies of mGluR2.

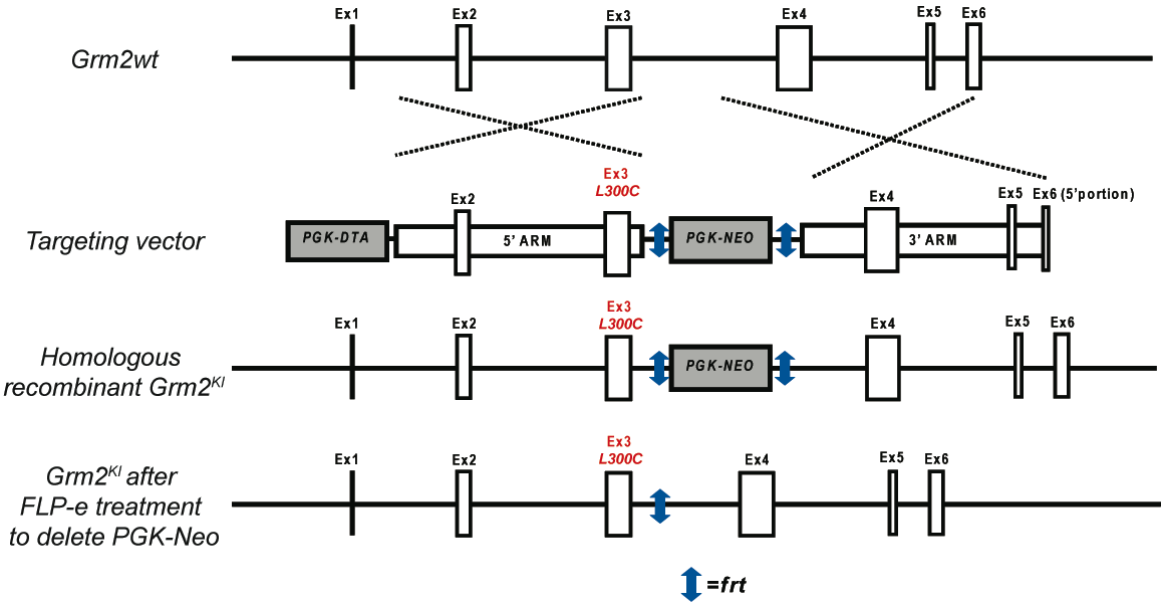

Fig. 3.7, Design of LimGluR2 knock-in mice via a sequence replacement strategy to mutate Leucine 300 to cysteine. The construct used to introduce the mutation ("Targeting vector") contains the mutation located in exon 3. This mutated exon 3 is located in the 3'end of the 5'ARM of homology. The construct also consists of a 5.3 kb 5' arm of homology (containing exons 2 & 3), a 4.9 kb 3' arm of homology (containing exons 4-6), a Diphtheria Toxin A (DTA) cassette, and a Neomycin (Neo) cassette flanked by frt sites for selective deletion. The Neo element permitted positive selection in ES cells, while the DTA element permitted negative selection in ES cells. After homologous recombination of the targeting vector to produce the "Homologous recombinant $Grm2^{KI}$", the PGK-Neo was excised via Flp-e administration to produce the final Grm2 300C mice.

Extension of optical control to group I and III mGluRs

Following the success of group II LimGluRs, we aimed to extend optical control throughout the mGluR subfamily. Due to its role in a variety of forms of synaptic plasticity and neurological disorders, as well as the limitations of its pharmacology, we first attempted to develop a photoswitchable mGluR1. A photoswitchable mGluR1 would also extend LimGluRs into the Gq and Gs-coupled Group I subfamily and provide a new general tool for control of those pathways. In order to achieve this we first tested tether models to see if mGluR1 would be better suited for L or D-MAGs which differ by the stereochemistry of the attachment to the 4' carbon of the glutamate moiety. Unlike mGluR2, D-tether models did not show any agonism of mGluR1 (data not shown). However, application of L-Tether-1, the basis for L-MAG-1, showed clear agonism in both the GIRK current assay (Fig. S3.3A) and in a calcium imaging assay(data not shown) when applied at 1 mM. This current was 10-30% in amplitude relative to saturating

glutamate, but this discrepancy in amplitude may indicate that L-tether-1 is not saturating at 1 mM. We next turned to homology with LimGluR2 and tested the R323C mutant of mGluR1, which is analogous to L300C, the MAG attachment point of LimGluR2 (Fig. S3.3B). We used calcium imaging with the dye Fura-2 to measure Gq activation by mGluR1. Prior to conjugation with MAG, mGluR1-R323C showed clear calcium responses to 100 μM glutamate. However, following conjugation of L-MAG-1 (or 0), but not D-MAG-1, responses to 100 μM glutamate were fully abolished (Fig. S3.3C). This result is unlikely due to activation of mGluR1 by L-MAG and depletion of calcium stores because during MAG conjugation there was not an observed increase in intracellular calcium concentration. Photoswitching of L-MAG-1 between *cis* and *trans* did not alter this phenotype (data not shown). The simplest explanation for this result would be that L-MAG-1 is able to antagonize mGluR1-R323C in both cis and trans states and prevent glutamate from either binding or activating the ligand binding domain of mGluR1. Consistent with this, application of >5 mM glutamate was able to elicit small calcium responses from L-MAG-1 labeled mGluR1-R323C (data not shown). This MAG/mutant combination may be useful for a subtype specific knockout of mGluR1, but to produce a reversible, photoswitchable version of mGluR1 we next turned to the crystal structure of the receptor.

Using a combination of data from previous Monte Carlo simulations (Fig. 2.2a,b), homology with mGluR2, and direct analysis of the structure, 22 potential cysteine substitution sites were identified in the LBD of mGluR1 (Table S3.1, Fig. 3.8A). 14 of these have been tested using the GIRK assay with a G-protein chimera that allows a Gq receptor to signal via the Gi/o-pathway[36]. Clear photoantagonism has been observed at 4 different residues at unique regions of the structure (Fig. 3.8). The most efficient photoantagonism has been observed for mGluR1-E325C, the analog of LimGluR2block (mGluR2-S302C), and W110C, a novel site identified via the structure (Fig. 3.8B-D). Both sites showed photoantagonism of 1 mM glutamate induced-currents of 30-50% with both L-MAG-0 and L-MAG-1. Conjugation of D-MAG-0 or D-MAG-1, and an elongated version of L-MAG termed L-MAG-2, also produced photoantagonism of similar efficiency in mGluR1-E325C. This is consistent with proper 4' L stereochemistry only being required for photoagonism, but not photoantagonism. Interestingly, the S166C substitution showed length-dependent photoantagonism. When MAG-0 (D or L) was conjugated, cis-MAG antagonized the receptor whereas following MAG-1 conjugation trans-MAG was able to antagonize the receptor with a similar efficacy (~20%). The final residue that showed photoantagonism, H55C displayed relatively weak antagonism compared to the other residues (<10%). Further screening of the remaining sites may yield photoagonism or photoantagonism with increased potency. In addition, homology may allow E325C or W110C analogs to be photoantagonized in the other group I mGluR, mGluR5. Finally, a full screen of all of the identified residues may yield insight into the structure and conformational changes of the mGluR1 LBD, especially as compared to mGluR2.

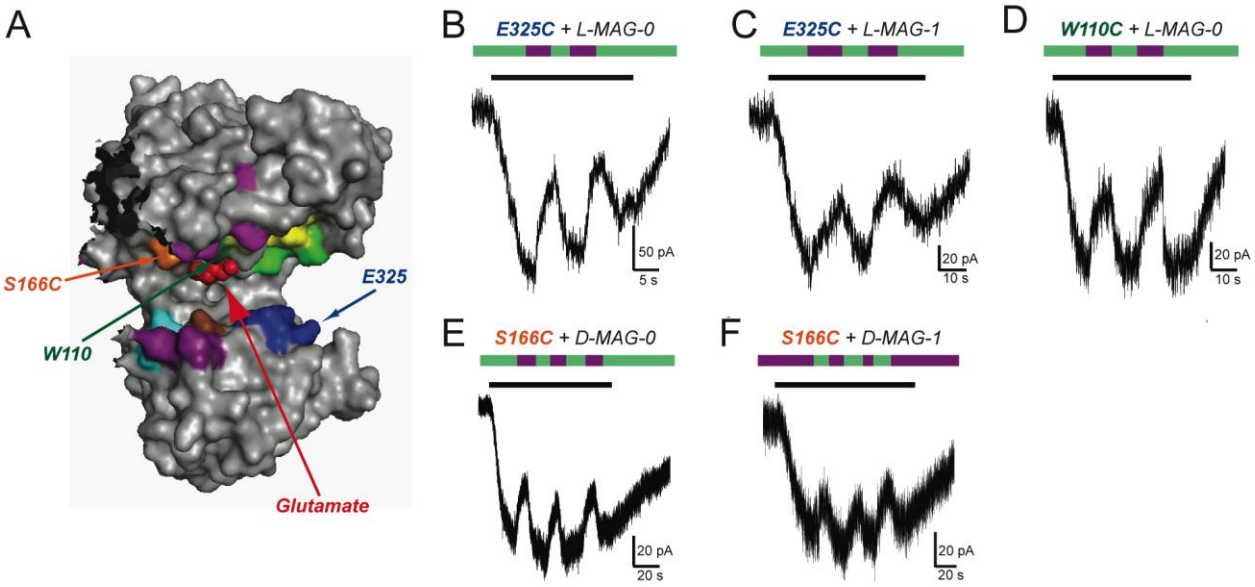

Fig. 3.8. Photoantagonism of mGluR1 by MAG attachment to residues in distinct structural regions. A) Structure of the mGluR1 LBD in the open state, in the presence of glutamate (PDB ID: 1EWK) showing glutamate in red. Residues individually mutated to cysteine to be tested for photoswitching are shown in various colors with residues that displayed the most potent photoswitching labeled. B-F) Representative traces showing photoantagonism of E325C (B,C), W100C (D), or S166C (E,F) using the GIRK current assay in HEK 293T cells.

We also sought to extend optical control to group III mGluRs. Initially we focused on mGluR7 due to its unique pharmacological properties, important role in diseases like absence epilepsy, and its well-studied regulation via its C-terminal tail. We first tested the analogous residue to L300C in mGluR2, K319C (Fig. 3.9A). In contrast to LimGluR2, when conjugated to D-MAG-0, mGluR7-K319C displayed large currents in response to 500 nm illumination that were reversed by 380 nm illumination which was consistent with trans-agonism of the receptor (Fig. 3.9B,C). Despite the reversed wavelength sensitivity of LimGluR7 (K319C + D-MAG-0), bistability was still achieved. mGluR7 could either remain active in the dark following 500 nm illumination or remain off in the dark following 380 nm illumination (Fig. 3.9D, E). Notably, photocurrents elicited by mGluR7 were ~2-3-fold larger than currents elicited by 10 mM glutamate, which is saturating in the wild-type mGluR7. To further investigate this we performed glutamate titrations under different conditions. Before MAG conjugation K319C and mGluR7wt showed identical dose response curves (Fig. S3.4A,B). However, following MAG conjugation the glutamate affinity was shifted to the point where no glutamate-evoked currents were observed at concentrations less than 10 mM (Fig. S3.4C). Concentrations exceeding 10 mM give unreliable currents that are plagued by artifacts so we were unable to perform a full glutamate titration on LimGluR7. Nonetheless, these experiments show that D-MAG-0 induces an affinity shift in addition to the ability to endowing the ability to be photoactivated.

Surprisingly, unlike mGluR2 and 3, when wild-type (wt) mGluR7 was incubated with D-MAG-0 photocurrents were observed that displayed trans-agonism. mGluR7wt photoactivation was more variable than LimGluR7 but could reach magnitudes of up to 40% relative to 10 mM glutamate (Fig. 3.9F). Based on the amplitude of currents evoked by 10 mM glutamate it appeared that mGluR7wt conjugated to D-MAG-0 did not display a major affinity shift. Similar to results with group II mGluRs, L-MAG-0 was unable to photoswitch either LimGluR7 or

mGluR7wt (data not shown). Similar wild type photoswitching was also observed with mGluR6 (data not shown). This result raises many questions about how the wild-type receptor can photoswitch and what this implies for the mechanism of photoswitching of LimGluR7. Mutation of native cysteines to alanine resulted in poor expression and were therefore inconclusive in determining the native residue responsible for photoswitch conjugation. Mutation of K319A maintained photoswitching, indicating that the weak nucleophilic nature of a lysine side chain was not the means of wild type photoswitching. Future work will be necessary to determine how the wild-type is able to conjugate MAG and perhaps devise a means of preventing this from happening so photoswitching of native group III mGluRs does not obscure other experiments that are based on D-MAG-0. Initial experiments testing potential wild type photoswitching of the other group III mGluRs, mGluR4 and 8, were inconclusive due to poor receptor expression.

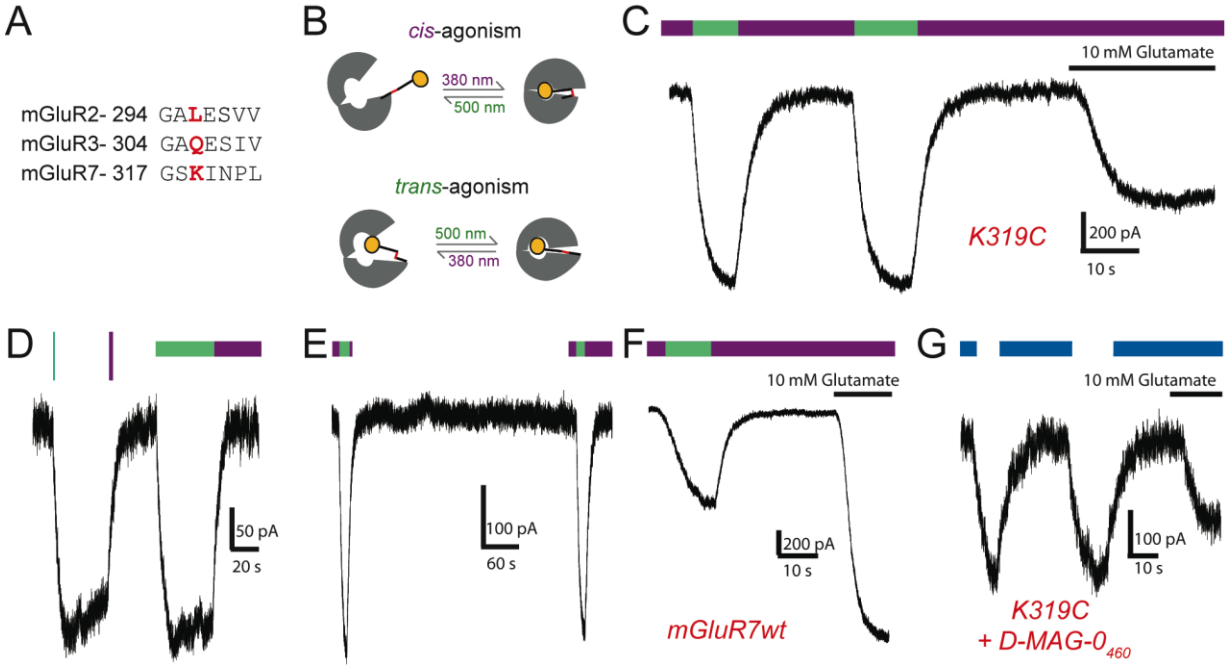

Figure 3.9, Optical control of mGluR7 reveals trans-agonism. A) Local alignment showing residues in the vicinity of the MAG attachment point for LimGluR2 and LimGluR3. B) Schematic showing two opposite means of photoagonism of a ligand-binding domain. In the case of *cis*-agonism (top) 380 nm light induces ligand binding, clamshell closure and activation whereas in the case of *trans*-agonism (bottom) 500 nm light induces activation. C) Representative trace showing very efficient photoactivation of LimGluR7 by D-MAG-0 relative to 10 mM glutmate. D,E) Bistability of LimGluR7. Brief flashes of light activate and deactivate LimGluR7 similarly to constant illumination (D) and the receptor can stay off in the dark following deactivation for minutes (E). F) Conjugation of D-MAG-0 to mGluR7wt produces trans-agonism with smaller amplitude relative to 10 mM glutamate than LimGluR7, which may be due to a lack of a drastic affinity shift. G) Conjugation of D-MAG-0460 to LimGluR7 results in dark evoked currents that are reversed by visible light (445 nm) and are large in amplitude relative to 10 mM glutamate.

Due to the unique reversed wavelength sensitivity of LimGluR7, it was intriguing to see how the red-shifted, fast relaxing D-MAG-0_{460} would perform when conjugated to mGluR7. Unlike LimGluR2 and 3, D-MAG0_{460} displayed large light-dependent activation of mGluR7 (Fig. 3.9G). In the presence of blue (~445 nm) light, mGluR7 was off, but turning off the light resulted in dark-evoked currents with a similar amplitude to 10 mM glutamate. This result is

consistent with trans-MAG agonism of mGluR7. However, this light-dependence is not ideal for a physiological experiment due to the need to constantly illuminate to keep the receptor off. However, this experiment reveals that mGluR7 may be less sensitive to subtle changes in photoswitch structure than mGluR2 or 3 and may be a good receptor on which to target future photoswitches.

Given the efficient photoswitching of LimGluR7 and the range of existing physiological questions about mGluR7 signaling at the synapse, we chose to further pursue LimGluR7 as a tool in the context of neurons. LimGluR7 was expressed in cultured hippocampal neurons and, unlike LimGluR2, displayed no clear hyperpolarizing effect on membrane potential following photoactivation with 500 nm light (Fig. 3.10A-C). When LimGluR7 was expressed in low-density cultures that were able to form autapses, a large 500 nm-induced inhibition of EPSCs was observed (Fig. 3.10D). Similar to LimGluR2 experiments, photoswitching at the autapse was rapid and reversible (Fig. 3.10E) and was accompanied with a change in paired pulse ratio (Fig. 3.10F), indicating that a presynaptic mechanism is involved. This result is consistent with a role for mGluR7 in presynaptic inhibition at a variety of synapses, including those in hippocampus (citation). This synapse-specific inhibition may either be due to synapse-specific targeting of mGluR7, or from weaker expression of LimGluR7 and a lower expression threshold for obtaining synaptic inhibition compared to membrane hyperpolarization.

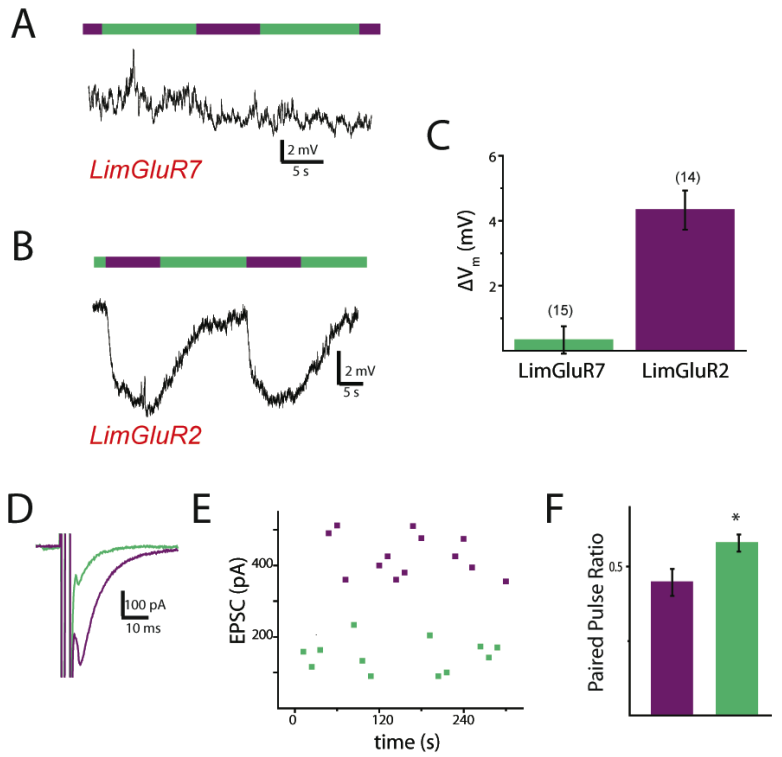

Figure 3.10. Photoactivation of LimGluR7 in hippocampal neurons reveals synapse-specific inhibition. A, B) Representative traces showing photoswitching responses of LimGluR7 and LimGluR2 in cultured hippocampal neurons. C) Summary bar graph showing reliable light-driven hyperpolarization by LimGluR2 but not LimGluR7. The number of cells tested per condition are shown in parentheses. D) Representative autaptic EPSCs showing 500 nm (green) light that is reversed by 380 nm light (violet) induced inhibition in LimGluR7-expression cells. E) Representative time course showing reversible and repeatable 500 nm light induced synaptic inhibition. F) 500 nm light-induced inhibition is accompanied by a small increase in paired pulse ratio (pulse 2/pulse 1) indicating a decrease in release probability.

We next attempted to further understand how the C-terminal domain (CTD) of mGluR7 plays a role in its ability to traffic and activate G proteins, especially at the synapse. Fig. 3.11A shows a map of the functional sites identified in the CTD of mGluR7. In the proximal part of the CTD, a binding site for $G_{\beta\gamma}$ has been identified as well as a partially overlapping site for calcium/calmodulin (Ca^{2+}/CaM) [25,37,38]. In the same subregion, residue S862 has been shown to

be targeted for phosphorylation by protein kinase C which can alter activation properties and expresson levels by disrupting Ca^{2+}/CaM binding [28]. In addition, many GPCRs have an 8th helix in the proximal region of the CTD that, in some cases, is necessary for aspects of signaling[39]. Finally, at the extreme distal end of the CTD the final 3 residues of mGluR7 have been identified as key for binding to PICK1, which can facilitate targeting of mGluR7 to the synapse and is necessary for synaptic inhibition in Cerebellar granule cells[26,27,28]. When the PICK1 binding site was removed in LimGluR7 photocurrents in HEK cells were unaffected (Fig. 3.11B). Similarly, when the CaM binding (residues 864-876) site was removed photocurrents were also unaffected in sharp contrast to the initial study which proposed that CaM binding is required for GIRK activation in HEK cells and synaptic inhibition in hippocampal neurons [25] (Fig. 3.11C). In contrast, when the entire CTD (LimGluR7ΔCTD) was removed no current was observed (Fig. 3.11D). Fig. 3.11E summarizes the glutamate evoked current amplitudes for the LimGluR7 variants described and shows no clear effect of removal of the CaM or PICK1 site. In order to understand whether the LimGluR7ΔCTD construct shows no current is because it is non-functional or because it doesn't reach the membrane we used previously described constructs that contain an N-terminal SNAP tag which allows for attachment of benzylguanine-conjugated dyes[40]. Since dye does not cross the plasma membrane, fluorescence is a reporter of receptor expression. When SNAP-mGluR7 was expressed and cells were labeled with ALEXA-647 clear fluorescence was observed around the plasma membrane, but when SNAP-mGluR7ΔCTD was expressed no fluorescence was seen indicating that CTD is required for surface expression (Fig. 3.11F). In contrast, SNAP-mGluR2ΔCTD was clearly expressed on the plasma membrane and gave large glutamate-evoked currents (Fig. 3.11G). This result indicates that a C-terminus is not required for mGluR signaling generally, but in the case of mGluR7 it is required for membrane targeting.

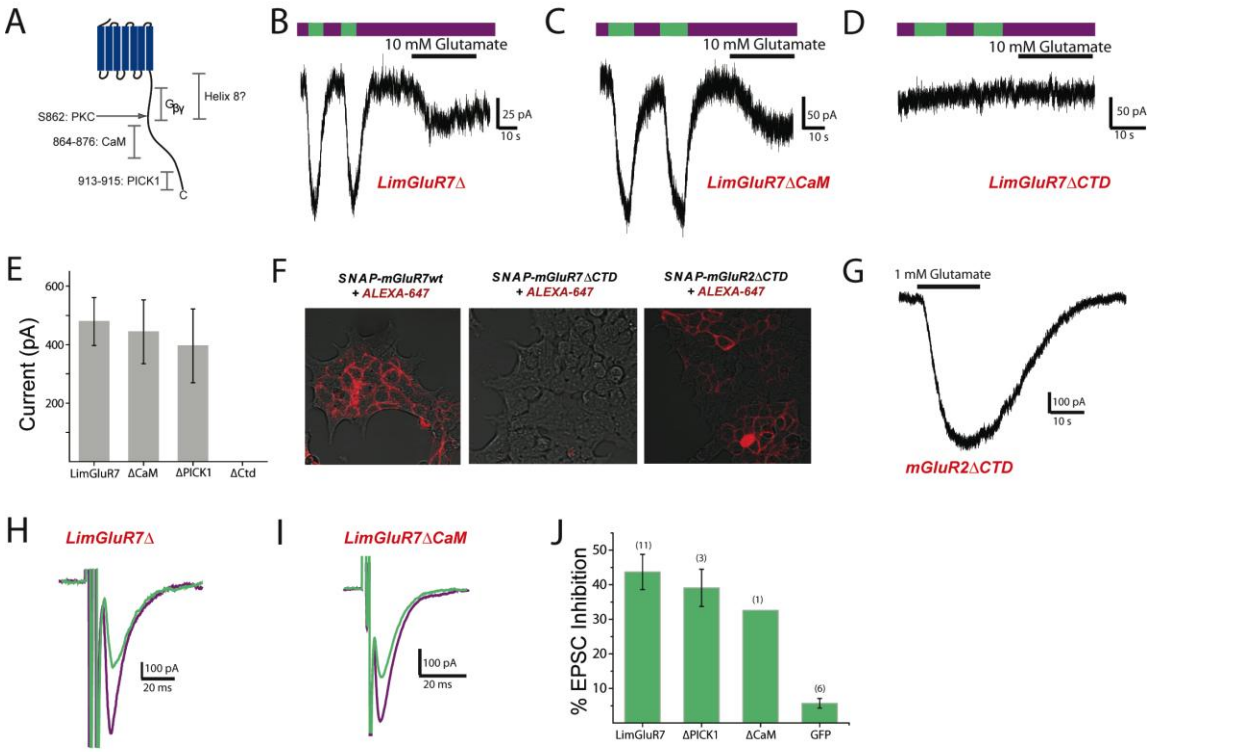

Figure 3.11. mGluR7 does not require a PICK1 or CaM binding site, but does require a CTD for signaling. A) Schematic showing location of identified binding sites and potential eight helix of mGluR7. The extracellular domain is not shown for simplicity. B-D) LimGluR7 shows normal photocurrents without the PICK1 (B) or CaM (C) binding site, but requires a CTD (D) in order to get currents. (E) Summary of current amplitudes in response to 10 mM glutamate for mGluR7 CTD variants. F) Images showing expression levels of mGluR7, mGluR7ΔCTD, and mGluR2ΔCTD. All images were taken with the same expression and imaging conditions. G) Representative trace showing large currents evoked by glutamate in mGluR2ΔCTD. H,I) LimGluR7ΔPICK1 and LimGluR7ΔCaM show 500 nm induced synaptic inhibition . J) Summary of synaptic inhibition in neurons expressing LimGluR7 and Ctd variants. The number of cells tested per condition are shown in parentheses.

We next tested the ability of LimGluR7ΔPICK1 and LimGluR7ΔCaM to inhibit transmission at hippocampal autapses. Both constructs showed 500 nm-induced synaptic inhibition with similar amplitude to LimGluR7 (~30-40%) (Fig. 3.11H-J). As a control, when neurons were transfected with GFP only a very small 500 nm-induced inhibition (<10%) was seen, which may be due to D-MAG-0 targeting of native group III mGluRs. Overall, this result shows that in both HEK cells and hippocampal synapses neither a PICK1 or CaM binding site is required for mGluR7 function.

Discussion:

Further characterization of group II LimGluRs

The experiments presented in this chapter provide a further analysis of LimGluR2, and to a lesser extent LimGluR3, as optogenetic and biophysical tools to understand G protein signaling and mGluR-specific function. We show that, as previously hypothesized, D-MAG-0 is a high affinity, high efficacy agonist of LimGluR2 and LimGluR3 that activates the receptor in a very similar way to glutamate. This was confirmed by experiments showing that decreasing the affinity of either receptor did not alter photoswitching and experiments that showed that NAMs block LimGluR2-mediated signaling in the same way as glutamate-mediating signaling. Further unpublished experiments have shown that high-affinity, partial agonists like DCG-IV and L-CCG-1 do not occlude photoswitching at supersaturating concentrations indicating that D-MAG-0 can compete off ligands with nM or low μM affinity to further activate mGluR2. In addition to their use in characterizing the mechanism of photoswitching, LA-LimGluR2 and LA-LimGluR3 may be useful variants for optical control of receptors without introducing a glutamate-sensitive receptor. This may be useful in cases where overexpression of either receptor causes deleterious effects. LA-LimGluR2 and LA-LimGluR3 are essentially orthogonal receptors that will only respond to light and will otherwise be silent, except for minor ligand-independent basal activity, when expressed heterologously.

To further expand the optical properties of LimGluRs, we also developed a variant of LimGluR3 that may be activated by visible light and turned off in the dark by D-MAG-0_{460}. While the bistability and extremely precice temporal control of receptor function afforded by the dual wavelength photoswitching of D-MAG-0 is often desirable, D-MAG-0_{460} provides a number of advantages that may be desirable depending on the application. The ability to activate a receptor with just one wavelength of visible light simplifies experimental protocols, which may make it easier to achieve photoactivation. Furthermore, by only using one wavelength, the range of the visible spectrum used for LimGluR3 activation with D-MAG-0_{460} may enable easier complexing of LimGluRs with other optical tools. For instance, red-shifted opsins may be activated with light of wavelengths larger than 560 nm[41] that would allow them to be activated without photoisomerizing D-MAG-0_{460} [34]. This may be an interesting platform for optically controlling metabotropic and ionotropic signaling in the same cell or spatially overlapping populations of cells. This would be difficult with existing rhodopsins because they have wide activation spectra that would likely interfere with each other. Furthermore, this type of experiment would be difficult with D-MAG-0 because the >490 nm light used to photoswitch from *cis* to *trans* would be likely to activate most channelrhodopsin variants. Finally, future work may be needed to develop a red-shifted variant of D-MAG-0 that is able to optically activate LimGluR2, rather than just LimGluR3, as was observed for D-MAG-0_{460}.

In addition to strengthening the base of understanding of the mechanism of photoswitching and expanding the toolset of LimGluRs, as has been done for LiGluRs, it is important to test and evaluate if LimGluRs may be used *in vivo* in the rodent brain. This is key because mGluRs are native receptors in mice and rats where their importance is established but many key questions remain. One useful example is the role of group II mGluRs as drug targets for schizophrenia. It has been shown that injection of group II mGluR agonists can reverse the psychotic phenotype induced by non-competitive NMDA receptor antagonists[42], which is an

increasingly relevant rodent model of schizophrenia[43].This result has become the basis of clinical trials in schizophrenic humans where there have been promising results[44]. However, because of the limited spatial and temporal control afforded by pharmacological agonists it has been difficult to identify which brain region or regions are mediating this effect and to, subsequently, find the circuit basis of these phenotypes. If LimGluRs could be established *in vivo* in mice it would be possible to probe, with greatly improved precision, how group II mGluRs can reverse psychosis. Finally, it is important generally for the MAG-based chemical optogenetic technique to establish *in vivo* photoswitching in mice in order to further motivate the development and application of these ionotropic and metabotropic tools.

In this chapter we report the first example of optical control of LiGluR and LimGluR2 in awake mice through an optical fiber. The use of an optical fiber for these experiments is key because this is the means of light delivery required for freely moving experiments, which are used in most behavioral optogenetics studies[45]. We show that LiGluR6 activation can increase neuronal firing in V1, while LimGluR2 can inhibit visual responses in the same region. This shows that sufficient AAV-mediated expression and labeling may be achieved. Future work will be needed to test for off-target or damaging effects of MAG injection, which were not obvious in initial experiments. The ultimate test will be to see if behavior may be manipulated by these tools in order to confirm that a large enough populations of neurons are able to be manipulated at once. Finally, MAG_{460} variants may provide improved light tissue penetration and should also be tested *in vivo*.

Optical control of group I mGluRs

We report initial attempts to optically control mGluR1. We first established that L, but not D, tether models can activate mGluR1 which indicates that L-MAGs will likely be required for photoagonism. In addition, we have identified a unique L-MAG specific phenotype in mGluR1-R323C which allows for the irreversible, subtype-specific antagonism of mGluR1. Future work will be needed to further understand the mechanism of this effect and to see if it may be extended to mGluR5. One intriguing possibility is if L-MAG labeling of R323C may be cis or trans-MAG dependent which could allow for the spatial targeting of receptor knockout by affinity labeling, which has been demonstrated with LiGluR[31].

Further screening of mGluR1 cysteine attachment sites has yielded robust photoantagonism, especially at positions E325C and W110C and, to a lesser extent, at H155C and S166C. E325C, in particular, seems promising, in part, because of its homology to LimGluR2-block, which has been established as a powerful means of controlling mGluR2. Future experiments will address if MAG-conjugated E325C is able to antagonize G_q signaling using calcium imaging and if it can block a physiological signal induced by mGluR1, such as LTD in CA1. Unexpectedly, E325C shows no MAG stereochemistry or length-dependence, unlike other residues such as S166C. A full screen of the identified candidate sites will show a number of patterns of photoswitching and MAG length-dependence, which may be useful for the formation of a structural map of mGluR1 ligand binding and clamshell closure. Furthermore, screening of novel sites and sites near those that have revealed photoantagonism, may result in a photoagonistic combination which would be the ultimate tool to emerge from this study.

Optical control of group III mGluRs

We also report results demonstrating optical control of mGluR7, which extends photoagonism into group III mGluRs. Initial results showed extremely robust *trans*-photoagonism of mGluR7-K319C which was accompanied by a large affinity shift making LimGluR7 a highly-orthogonal tool. However, it was found that mGluR7wt, without the introduction of a cysteine, was also able to photoswitch. This wt photoswitching was somewhat weaker and not accompanied with a large glutamate affinity shift, but maintained *trans*-agonism indicating that there may be a common mechanism with LimGluR7. One possible mechanism would be that D-MAG-0 attaches to the same point on both mGluR7wt and mGluR7-K319C to induce photoswitching, but that attachment of another MAG to K319C facilitates improved photoswitching and an accompanied affinity shift in LimGluR7. If this were to be the mechanism, it would be crucial to find the native residue for conjugation. Unfortunately, experiments have been inconclusive so far although there are a number of cysteines present on the LBD of mGluR7. However, most of these cysteines are conserved between all mGluRs and have been shown via crystal structures to be paired in disulfide bonds. An alternative possibility could be that D-MAG-0 attaches to a native lysine, although K319 has been ruled out. Ultimately, it will be important to identify the means of wild type photoswitching as this will be key in being able to avoid it native systems, including *in vivo*.

Wild-type photoswitching of mGluR7, which may or may not indicate that mGluR4 and 8 are also photoswitchable, poses many potential problems for the application of LimGluR2 or any other system based on D-MAG-0. Thankfully, mGluR7wt photoswitching is D-MAG dependent indicating that this is not an issue for experiments that use L-MAGs such as LiGluR or potential photoswitchable group I mGluRs. There are, fortunately, a number of potential ways to try to avoid this effect and its potential to introduce artifacts into experiments performed where native mGluR7 may be expressed. First of all, this finding further reinforces the need to always perform controls where MAG is applied without the transgene of interest as has become standard for the technique. Fortunately, the photoswitching of mGluR7 and LimGluR2 are of opposite wavelength-dependence making it easy to distinguish them and instilling confidence in any 380 nm-induced inhibitory effects as being mediated by LimGluR2. Also, the *trans*-MAG photoagonism of mGluR7 means that mGluR7 will be constantly activated and potentially desensitized during incubation periods as has been observed by treatment of mGluR7 with agonists in hippocampal neurons[46]. This may explain why no or weak wild-type photoactivation of wild-type mGluR7 has been observed in hippocampal cultures (Fig. 3.11J). As a further precaution, in the event that wild type mGluR7 (or other group III mGluR) photoswitching is observed, a group III mGluR-specific antagonist may be applied to isolate the desired group II effect. Future work will be needed to confirm that group III antagonists such as CPPG or UBP112 can block mGluR7 wild-type photoswitching. Labeling conditions may also be used to favor labeling of desired receptors, such as LimGluR2, over mGluR7 by either labeling with MAG in *cis* or at low concentrations or in the presence of a group III mGluR antagonist. The ultimate means of avoiding this problem may be to develop new variants of MAG. One option is to replace the glutamate moiety by a group II-specific agonist to prevent any potential effect on group III mGluRs. Many group II mGluR agonists show very weak, low affinity agonism on group III mGluRs but this may be enhanced if they are convalently attached and in high local concentration. However, both L-CCG-1 and DCG-IV are high affinity agonists for group II

mGluRs but low affinity antagonists of group III mGluRs, making them excellent candidates to replace the glutamate moiety of MAG. Alternatively, in the future it will be useful to evalutate alternative labeling chemistries to maleimide-cysteine coupling that may be more fully orthogonal and could allow complexing of multiple photoswitches that can target different receptors. Finally, the wild-type photoswitcing effect, while mostly disconcerting as a potentially confounding factor in future experiments, may be useful in some systems where group III mGluRs are prominently expressed such as the retina[47] or spinal cord[48]. Future experiments will be needed to look into the suitability of such experiments.

Despite the drawbacks introduced by the puzzling wild type photoswitching phenotype of mGluR7, LimGluR7 was used to gain some insight into mGluR7 function. First, we found that heterologous expression of LimGluR7 in hippocampal neurons led to synaptic inhibition that was not accompanied by the somatodendritic hyperpolarization observed with LimGluR2 photoactivation. This is surprising and indicates that not all $G_{i/o}$–coupled GPCRs will behave the same way but rather that expression level, subcellular targeting, and effector coupling are likely to be different for every receptor. In the event that LimGluR7 could be targeted without also labeling wild-type receptors, this would produce a very powerful tool for synapse-specific inhibition. Notably, we unequivocally show that, in contrast to what was previously believed[25], mGluR7 does not require CaM binding in order to activate the $G_{\beta\gamma}$-driven process of GIRK activation or presynaptic inhibition. It was previously reported that removal of the CaM binding site resulted in normal surface expression, but a complete inability to activate GIRK, which was believed to be due to the inability to release $G_{\beta\gamma}$[37]. We hypothesize that there may be some affinity shift in the absence of CaM, which may be easily tested, but that at saturating conditions there is no difference in activation. As has also been reported, removal of the CaM binding site may alter receptor desensitization or expression level[28], which will have to be tested more closely. In addition we show that PICK1 binding to mGluR7 is also not required for GIRK activation or synaptic inhibition. This is less surprising given that PICK1 is believed to be important for receptor targeting[26,27,28], not G protein activation. This result does, however, imply that the PICK1-dependence of mGluR7 targeting may be brain region-dependent. It is, of course, a possibility that heterologously-expressed LimGluR7ΔCaM or ΔPICK1 are able to co-assemble with wild-type mGluR7, which could facilitate proper targeting. Experiments in neurons from mGluR7 knockout mice will be required to fully test this. Finally, we show that mGluR7, but not mGluR2, requires a CTD for receptor targeting to the membrane. In contrast to results with ΔCaM and ΔPICK1 constructs, this result indicates that the mGluR7 CTD is indeed crucial for receptor function. However, the finding that mGluR2ΔCTD still traffics and functions indicates that an mGluR CTD is not absolutely necessary and that it is unlikely that a helix 8 is present or needed for G protein coupling. Overall, these results challenge existing notions of CTD regulation of mGluR7 and show that closely related GPCRs may have distinct regulatory properties as was observed for CTD deletions in mGluR7 and mGluR2. Future work will be needed to fully understand the role of CaM and PICK1 binding to mGluR7 and the crucial part of the mGluR7 CTD required for receptor expression.

This chapter demonstrates the many directions in which the field of optical control of mGluRs can grow and develop including: application *in vivo* and extending to group I and III receptors, At the same time this work poses many questions and obstacles that will need to be overcome including: non-ideal wavelength conditions, difficulty in finding attachment positions for every subtype, and potentially confounding off-target photoswitching of wild type receptors. Ultimately, the successful application of these techniques will hinge on finding questions and

systems that maximize the advantages of LimGluRs while limiting the difficulties associated with the technique.

Methods:

Chemical synthesis

Chemical synthesis was performed as previously described[2].

Cultured cell electrophysiology

HEK 293 or 293T cell and hippocampal neuron electrophysiology was performed as previously described[2]. In some HEK293T cell patch experiments the extracellular KCl concentration was increased from 60 mM to 120 mM to increase current amplitudes. NaCl was decreased from 89 mM to 29 mM to maintain osmolarity. For mGluR1 GIRK activation experiments, the previously described $G\alpha_{iq}$ was coexpressed at a receptor: channel: G protein: YFP ratio of 7:7:5:1. For LimGluR7 experiments in neurons, D-MAG-0 was converted to *cis* using a 365 nm handheld lamp after 15 minutes of labeling to prevent receptor desensitization by *trans* D-MAG-0. Labeling proceeded for another 15-30 minutes before experiments began. Precaution was taken to keep D-MAG-0 in *cis* as much as possible before patching cells and photoswitching. Light-induced hyperpolarization comparisons were made in the same batches of cells from the same neuron preps. Hyperpolarization was measured at -50 mV.

Calcium imaging

HEK 293 or 293T cells were loaded with 5 μM fura-2AM for 20 minutes and imaged after 10 minutes of wash in extracellular solution containing (in mM): 135 NaCl, 5.4 KCl, 2.5 $CaCl_2$, 1 $MgCl_2$, 10 Hepes, pH 7.4. Cells were alternately excited with 340 and 380 nm using a Xenon lamp. Emission was imaged with a 500 nm longpass filter. The ratio of emission between the two excitation wavelengths was used as a measure of intracellular calcium concentration. Glutamate was applied with a gravity-driven perfusion system.

Viral production and expression

AAV production was carried out using standard methods[49]. Injection was performed stereotaxically in isoflurane-anesthetized mice ranging from 4 weeks to 10 weeks old. Coordinate used were: +1.9 (AP), ±0.4 (ML), and -1.5 (DL) for mPFC (from bregma), for -1.9 (AP), ±1.5 (ML), and -1.3 (DL) for CA1(from bregma), -1.8 (AP), ±1.2 (ML), and -1.9 (DL) for DG (from bregma), and +0.4 (AP), ±2.2 (ML), and -0.8 (DL) for V1(from lambda). Injection was performed with a Drummond nanoninjector with ~20 nL injected every 10s for 3-5 minutes. Mice were sacrificed >3 weeks after injection to assess expression.

in vivo electrophysiology

Following virus injection, mice were implanted with screws and metal bars for head fixing in a custom made chamber. Following injection and implantation, mice were gradually trained in head-fixing to reduce movements which introduce electrical artifacts. After >3 weeks expression, an optrode was prepared that included up to 8 unique tungsten electrodes for

recording of individual units. The electrodes extended just beyond the optical fiber so that illumination would target the cells being recorded from. Optrodes were connected to a custom dual laser system consisting of a 532 nm laser and 375 nm laser that were coupled into the same fiber. Laser illumination and visual stimuli were controlled via Matlab. Visual stimuli were full field flashes of white light directly in front of the mice. Analysis was performed in Matlab to identify the spikes of individual cells and to determine firing rates under different conditions.

Knock-in mouse generation

Knock-in mice were generated by the UC Davis mouse biology program. Briefly, a target vector was made which carried the L300C mutation which was injected into embryos and underwent homologous recombination. A PGK-Neo cassette flanked by frt sites was used to select for mice with insertion. Following insertion, FLP-e was applied to remove the cassette. Genotyping was performed using primers that selectively amplified around the 300C site.

Imaging of SNAP-mGluR constructs

SNAP-mGluR7 and SNAP-mGluR2 constructs were provided by Jean-Phillipe Pin (Univ. of Montpellier). ΔCTD constructs were produced by introducing a stop codon via site-directed mutagenesis at residue Q857 in mGluR7 and residue P821 in mGluR2.Constructs were expressed, as previously described, in HEK293T cells for 36 hours and then incubated in 2.5 μM benzylguanine-Alexa-647(Invitrogen) for 45 minutes at room temperature in standard extracellular solution. Following labeling cells were mounted on an upright, scanning confocal microscope (Zeiss LSM 780) and imaged with a 20x objective and 561 nm excitation. All constructs were tested on the same day with the same labeling and imaging conditions.

References:

1 Niswender, C. M. & Conn, P. J. Metabotropic glutamate receptors: physiology, pharmacology, and disease. *Annu Rev Pharmacol Toxicol* **50**, 295-322, doi:10.1146/annurev.pharmtox.011008.145533 (2010).

2 Levitz, J. *et al.* Optical control of metabotropic glutamate receptors. *Nat Neurosci* **16**, 507-516, doi:10.1038/nn.3346nn.3346 [pii] (2013).

3 Szobota, S. *et al.* Remote control of neuronal activity with a light-gated glutamate receptor. *Neuron* **54**, 535-545, doi:S0896-6273(07)00344-3 [pii]10.1016/j.neuron.2007.05.010 (2007).

4 Janovjak, H., Sandoz, G. & Isacoff, E. Y. A modern ionotropic glutamate receptor with a K(+) selectivity signature sequence. *Nat Commun* **2**, 232, doi:10.1038/ncomms1231ncomms1231 [pii] (2011).

5 Luscher, C. & Huber, K. M. Group 1 mGluR-dependent synaptic long-term depression: mechanisms and implications for circuitry and disease. *Neuron* **65**, 445-459, doi:10.1016/j.neuron.2010.01.016S0896-6273(10)00041-3 [pii] (2010).

6 Aiba, A. *et al.* Reduced hippocampal long-term potentiation and context-specific deficit in associative learning in mGluR1 mutant mice. *Cell* **79**, 365-375, doi:0092-8674(94)90204-6 [pii] (1994).

7 Lu, Y. M. *et al.* Mice lacking metabotropic glutamate receptor 5 show impaired learning and reduced CA1 long-term potentiation (LTP) but normal CA3 LTP. *J Neurosci* **17**, 5196-5205 (1997).

8 Bellone, C. & Luscher, C. Cocaine triggered AMPA receptor redistribution is reversed in vivo by mGluR-dependent long-term depression. *Nat Neurosci* **9**, 636-641, doi:nn1682 [pii]10.1038/nn1682 (2006).

9 Kalivas, P. W. The glutamate homeostasis hypothesis of addiction. *Nat Rev Neurosci* **10**, 561-572, doi:10.1038/nrn2515nrn2515 [pii] (2009).

10 Michalon, A. *et al.* Chronic pharmacological mGlu5 inhibition corrects fragile X in adult mice. *Neuron* **74**, 49-56, doi:10.1016/j.neuron.2012.03.009S0896-6273(12)00272-3 [pii] (2012).

11 Um, J. W. *et al.* Metabotropic glutamate receptor 5 is a coreceptor for Alzheimer abeta oligomer bound to cellular prion protein. *Neuron* **79**, 887-902, doi:10.1016/j.neuron.2013.06.036S0896-6273(13)00552-7 [pii] (2013).

12 Panatier, A. *et al.* Astrocytes are endogenous regulators of basal transmission at central synapses. *Cell* **146**, 785-798, doi:10.1016/j.cell.2011.07.022S0092-8674(11)00820-8 [pii] (2011).

13 Sun, W. *et al.* Glutamate-dependent neuroglial calcium signaling differs between young and adult brain. *Science* **339**, 197-200, doi:10.1126/science.1226740339/6116/197 [pii] (2013).

14 Kammermeier, P. J. The orthosteric agonist 2-chloro-5-hydroxyphenylglycine activates mGluR5 and mGluR1 with similar efficacy and potency. *BMC Pharmacol* **12**, 6, doi:10.1186/1471-2210-12-61471-2210-12-6 [pii] (2012).

15 Airan, R. D., Thompson, K. R., Fenno, L. E., Bernstein, H. & Deisseroth, K. Temporally precise in vivo control of intracellular signalling. *Nature* **458**, 1025-1029, doi:10.1038/nature07926nature07926 [pii] (2009).

16 Bailes, H. J., Zhuang, L. Y. & Lucas, R. J. Reproducible and sustained regulation of Galphas signalling using a metazoan opsin as an optogenetic tool. *PLoS One* **7**, e30774, doi:10.1371/journal.pone.0030774PONE-D-11-21928 [pii] (2012).

17 Tateyama, M. & Kubo, Y. Dual signaling is differentially activated by different active states of the metabotropic glutamate receptor 1alpha. *Proc Natl Acad Sci U S A* **103**, 1124-1128, doi:0505925103 [pii]10.1073/pnas.0505925103 (2006).

18 Kennedy, M. B. Signal-processing machines at the postsynaptic density. *Science* **290**, 750-754, doi:8929 [pii] (2000).

19 Okamoto, N. *et al.* Molecular characterization of a new metabotropic glutamate receptor mGluR7 coupled to inhibitory cyclic AMP signal transduction. *J Biol Chem* **269**, 1231-1236 (1994).

20 Saugstad, J. A., Kinzie, J. M., Mulvihill, E. R., Segerson, T. P. & Westbrook, G. L. Cloning and expression of a new member of the L-2-amino-4-phosphonobutyric acid-sensitive class of metabotropic glutamate receptors. *Mol Pharmacol* **45**, 367-372 (1994).

21 Rosemond, E. *et al.* Molecular basis for the differential agonist affinities of group III metabotropic glutamate receptors. *Mol Pharmacol* **66**, 834-842, doi:10.1124/mol.104.002956mol.104.002956 [pii] (2004).

22 Shigemoto, R. *et al.* Differential presynaptic localization of metabotropic glutamate receptor subtypes in the rat hippocampus. *J Neurosci* **17**, 7503-7522 (1997).

23 Pelkey, K. A., Lavezzari, G., Racca, C., Roche, K. W. & McBain, C. J. mGluR7 is a metaplastic switch controlling bidirectional plasticity of feedforward inhibition. *Neuron* **46**, 89-102, doi:S0896-6273(05)00128-5 [pii]10.1016/j.neuron.2005.02.011 (2005).
24 Bockaert, J., Perroy, J., Becamel, C., Marin, P. & Fagni, L. GPCR interacting proteins (GIPs) in the nervous system: Roles in physiology and pathologies. *Annu Rev Pharmacol Toxicol* **50**, 89-109, doi:10.1146/annurev.pharmtox.010909.105705 (2010).
25 O'Connor, V. *et al.* Calmodulin dependence of presynaptic metabotropic glutamate receptor signaling. *Science* **286**, 1180-1184, doi:7977 [pii] (1999).
26 Boudin, H. *et al.* Presynaptic clustering of mGluR7a requires the PICK1 PDZ domain binding site. *Neuron* **28**, 485-497, doi:S0896-6273(00)00127-6 [pii] (2000).
27 Perroy, J. *et al.* PICK1 is required for the control of synaptic transmission by the metabotropic glutamate receptor 7. *EMBO J* **21**, 2990-2999, doi:10.1093/emboj/cdf313 (2002).
28 Suh, Y. H. *et al.* Corequirement of PICK1 binding and PKC phosphorylation for stable surface expression of the metabotropic glutamate receptor mGluR7. *Neuron* **58**, 736-748, doi:10.1016/j.neuron.2008.03.028S0896-6273(08)00302-4 [pii] (2008).
29 Sansig, G. *et al.* Increased seizure susceptibility in mice lacking metabotropic glutamate receptor 7. *J Neurosci* **21**, 8734-8745, doi:21/22/8734 [pii] (2001).
30 Bertaso, F. *et al.* PICK1 uncoupling from mGluR7a causes absence-like seizures. *Nat Neurosci* **11**, 940-948, doi:10.1038/nn.2142nn.2142 [pii] (2008).
31 Gorostiza, P. *et al.* Mechanisms of photoswitch conjugation and light activation of an ionotropic glutamate receptor. *Proc Natl Acad Sci U S A* **104**, 10865-10870, doi:0701274104 [pii]10.1073/pnas.0701274104 (2007).
32 Malherbe, P. *et al.* Identification of essential residues involved in the glutamate binding pocket of the group II metabotropic glutamate receptor. *Mol Pharmacol* **60**, 944-954 (2001).
33 Urwyler, S. Allosteric modulation of family C G-protein-coupled receptors: from molecular insights to therapeutic perspectives. *Pharmacol Rev* **63**, 59-126, doi:10.1124/pr.109.002501pr.109.002501 [pii] (2011).
34 Kienzler, M. A. *et al.* A red-shifted, fast-relaxing azobenzene photoswitch for visible light control of an ionotropic glutamate receptor. *J Am Chem Soc* **135**, 17683-17686, doi:10.1021/ja408104w (2013).
35 Petralia, R. S., Wang, Y. X., Niedzielski, A. S. & Wenthold, R. J. The metabotropic glutamate receptors, mGluR2 and mGluR3, show unique postsynaptic, presynaptic and glial localizations. *Neuroscience* **71**, 949-976, doi:0306-4522(95)00533-1 [pii] (1996).
36 Conklin, B. R., Farfel, Z., Lustig, K. D., Julius, D. & Bourne, H. R. Substitution of three amino acids switches receptor specificity of Gq alpha to that of Gi alpha. *Nature* **363**, 274-276, doi:10.1038/363274a0 (1993).
37 El Far, O. *et al.* Mapping of calmodulin and Gbetagamma binding domains within the C-terminal region of the metabotropic glutamate receptor 7A. *J Biol Chem* **276**, 30662-30669, doi:10.1074/jbc.M102573200M102573200 [pii] (2001).
38 Scheschonka, A. *et al.* Structural determinants of calmodulin binding to the intracellular C-terminal domain of the metabotropic glutamate receptor 7A. *J Biol Chem* **283**, 5577-5588, doi:M709505200 [pii]10.1074/jbc.M709505200 (2008).
39 Katritch, V., Cherezov, V. & Stevens, R. C. Structure-function of the G protein-coupled receptor superfamily. *Annu Rev Pharmacol Toxicol* **53**, 531-556, doi:10.1146/annurev-pharmtox-032112-135923 (2013).
40 Doumazane, E. *et al.* A new approach to analyze cell surface protein complexes reveals specific heterodimeric metabotropic glutamate receptors. *FASEB J* **25**, 66-77, doi:10.1096/fj.10-163147fj.10-163147 [pii] (2011).
41 Mattis, J. *et al.* Principles for applying optogenetic tools derived from direct comparative analysis of microbial opsins. *Nat Methods* **9**, 159-172, doi:10.1038/nmeth.1808nmeth.1808 [pii] (2012).
42 Moghaddam, B. & Adams, B. W. Reversal of phencyclidine effects by a group II metabotropic glutamate receptor agonist in rats. *Science* **281**, 1349-1352 (1998).
43 Moghaddam, B. & Javitt, D. From revolution to evolution: the glutamate hypothesis of schizophrenia and its implication for treatment. *Neuropsychopharmacology* **37**, 4-15, doi:10.1038/npp.2011.181npp2011181 [pii] (2012).

44 Patil, S. T. *et al.* Activation of mGlu2/3 receptors as a new approach to treat schizophrenia: a randomized Phase 2 clinical trial. *Nat Med* **13**, 1102-1107, doi:nm1632 [pii]10.1038/nm1632 (2007).
45 Zhang, F. *et al.* Optogenetic interrogation of neural circuits: technology for probing mammalian brain structures. *Nat Protoc* **5**, 439-456, doi:10.1038/nprot.2009.226nprot.2009.226 [pii] (2010).
46 Pelkey, K. A., Yuan, X., Lavezzari, G., Roche, K. W. & McBain, C. J. mGluR7 undergoes rapid internalization in response to activation by the allosteric agonist AMN082. *Neuropharmacology* **52**, 108-117, doi:S0028-3908(06)00229-2 [pii]10.1016/j.neuropharm.2006.07.020 (2007).
47 Brandstatter, J. H., Koulen, P. & Wassle, H. Diversity of glutamate receptors in the mammalian retina. *Vision Res* **38**, 1385-1397, doi:S0042698997001764 [pii] (1998).
48 Vilar, B. *et al.* Alleviating pain hypersensitivity through activation of type 4 metabotropic glutamate receptor. *J Neurosci* **33**, 18951-18965, doi:10.1523/JNEUROSCI.1221-13.201333/48/18951 [pii] (2013).
49 Grieger, J. C., Choi, V. W. & Samulski, R. J. Production and characterization of adeno-associated viral vectors. *Nat Protoc* **1**, 1412-1428, doi:nprot.2006.207 [pii]10.1038/nprot.2006.207 (2006).

Supplementary Figures:

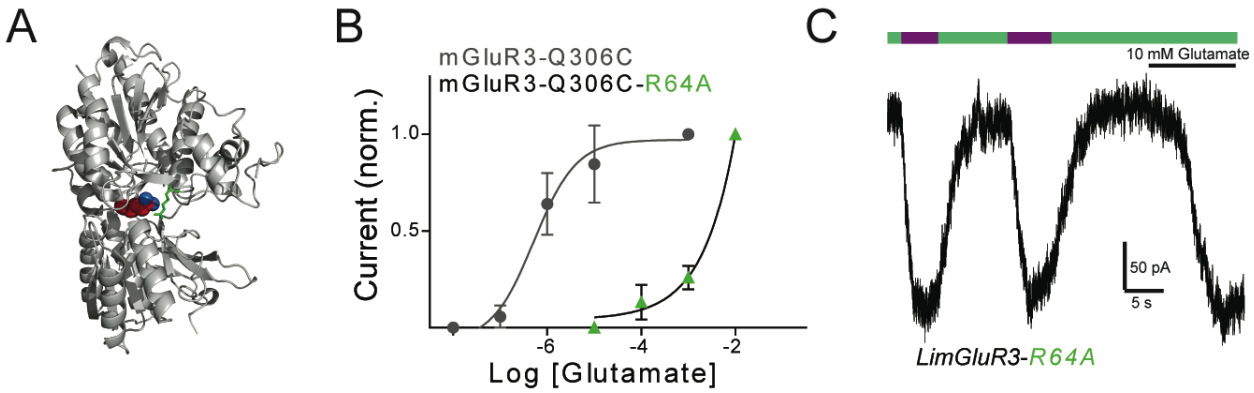

Figure S3.1, A low affinity variant of LimGluR3, LA-LimGluR3, reveals photoactivation despite a very large affinity shift. A) Crystal structure of mGluR3 ligand binding domain in the closed state (PDB ID: 2E4U) showing the locaton of residue R64 (green). Glutamate is shown in red with oxygen atoms of the carboxyl group shown in blue to highlight proximity to positively charged side chain of R64. B) R64A produces a large affinity shift in the mGluR3-Q306C background. The EC50 for LimGluR3 was 1 ± 2 μM and the EC_{50} for LA-LimGluR3 was not possible to determine because currents did not saturate. C) LA-LimGluR3 shows repeatable, efficient photoactivation with photocurrents that are nearly as large as currents evoked by 10 mM glutamate.

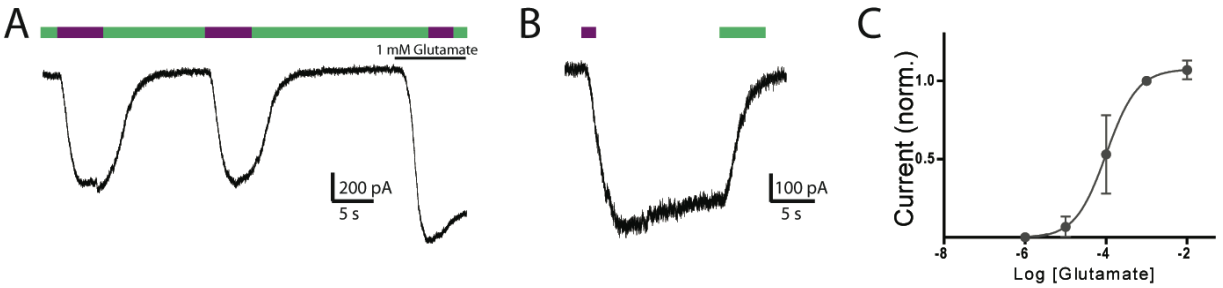

Figure S3.2. Conjugation of D-MAG-0 to the mouse variant of mGluR2-300C reveals efficient photoactivation that is comparable to LimGluR2. A) Representative trace showing repeatable photoactivation of mouse LimGluR2 which is comparable in amplitude to saturating glutamate. B) Mouse LimGluR2 shows large bistable photocurrents. C) Dose-response curve for mouse mGluR2-L300C shows an EC50 of 100± 28 μM (n=3 cells).

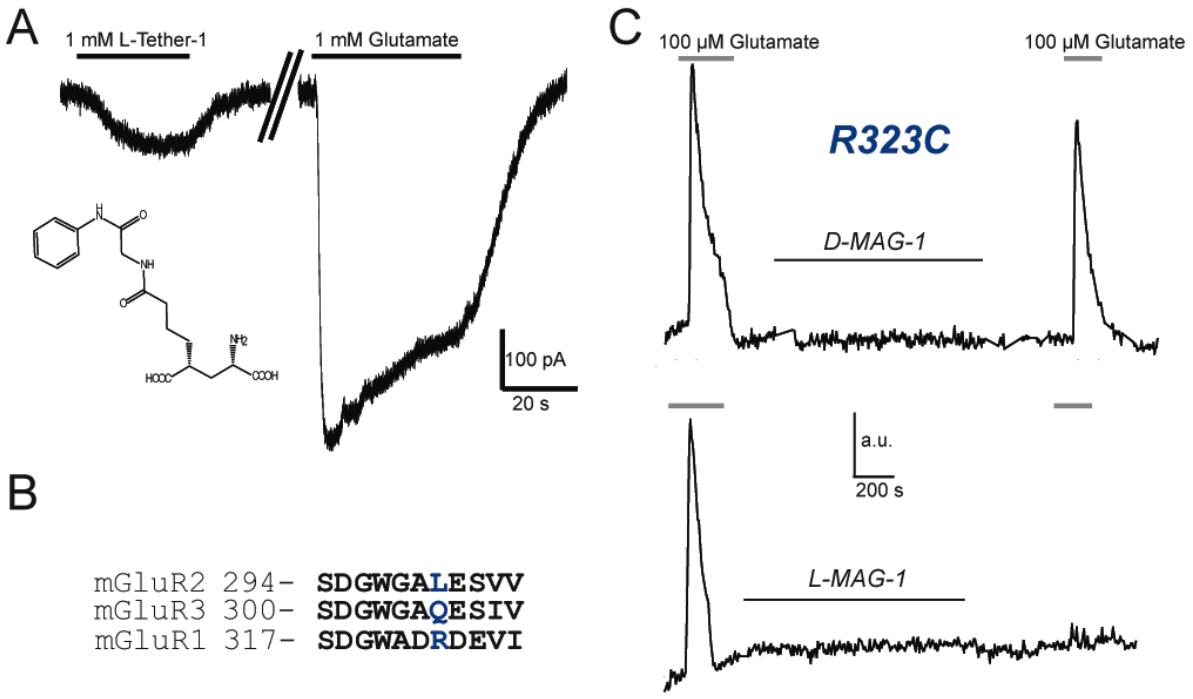

Figure S3.3, mGluR1 is activated by L-Tether-1, but the LimGluR2 analog, R323C, produces a knock-out phenotype. A) Representative GIRK current showing a small, inward current in response to 1 mM L-Tether 1 (shown as a chemical structure) that is ~20% the amplitude of saturating glutamate. B) Local alignment showing residues in the vicinity of the MAG attachment point for LimGluR2 and LimGluR3. C) Fura-2 calcium imaging experiments showing that conjugation of L-MAG-1 to mGluR1-R323C results in the abolition of responses to 100 µM glutamate. Each trace shows an average of ~20 cells that were simultaneously imaged.

Mutant	MAG-0	MAG-1
H54C	x	x
H55C	cis-antagonism	x
Q56C	-	-
A59C	x	
E60C	x	x
R71C		
W110C	cis-antagonism	
S165C		
S166C	cis-antagonism	trans-antagonism
V167C	x	x
A168C		x
G234C		
Y262C		
S263C		x
N264C		
E292C		
D322C	x	X
R323C	KO	KO
D324C	x	x
E325C	cis-antagonism	cis-antagonism
V405C	x	
Q406C		
D407C		x

Table S3.1, Summary of mGluR1 residues substituted to cysteine and tested for photoswitching with L-MAG-0 and L-MAG-1. X indicates that no photoswitching was observed, - indicates that no glutamate current was observed for this construct, and KO indicates the KO phenotype that was observed for R323C. Empty boxes indicate conditions that are yet to be tested.

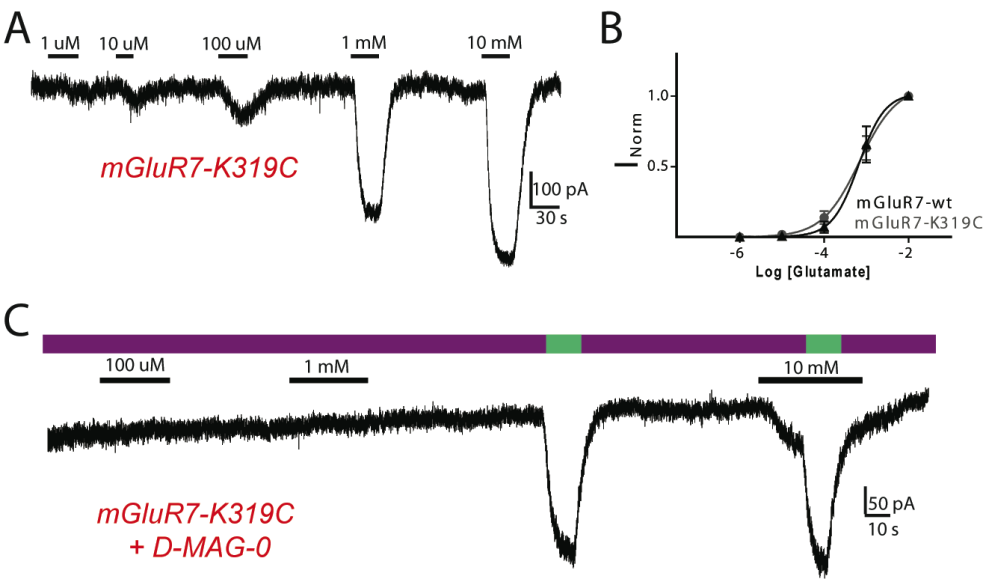

Figure S3.5, D-MAG-0 conjugation to mGluR7-K319C produces a large decrease in apparent glutamate affinity. A) Representative titration of mGluR7-K319C prior to conjugation of D-MAG-0. B) Glutamate dose response curves for mGluR7wt and mGluR7-K319C show nearly identical glutamate sensitivity. C) Following D-MAG-0 conjugation, LimGluR7 shows a drastically reduced glutamate affinity that is demonstrated that no glutamate evoked currents are observed at concentrations <10 mM.

Chapter IV: Conformational dynamics of metabotropic glutamate receptors

Introduction:

G protein-coupled receptors (GPCRs) constitute the largest family of membrane receptors in eukaryotes. GPCRs transduce a wide array of extracellular signals such as neurotransmitters, hormones, peptides or light through their interaction with intracellular guanosine nucleotide-binding proteins (G proteins). Due to their ubiquitous distribution throughout all tissues and their involvement in many physiological processes, GPCRs have become the largest family of drug targets in biology. GPCRs are characterized by a seven transmembrane helix domain that interacts intracellularly with G proteins to initiate downstream signaling. The recent boom in available crystal structures has greatly improved the understanding of how GPCRs interact with ligands and G-proteins[1-3]. However, despite their obvious value, structural approaches fail to capture the dynamics of GPCRs and only allow for the analysis of thermodynamically stable states which may be non-physiological. For this reason, X-ray crystallography has been limited in its ability to define a mechanism for receptor and G protein activation.

Recent molecular dynamics (MD) simulations have emphasized the importance of structural dynamics in determining GPCR activation properties[13,14]. However, different steps of GPCR activation occur over a large range of times from microseconds to seconds, making it impossible for MD studies to address all the relevant receptor dynamics[15,16]. Furthermore, it has been difficult to experimentally probe the conformational changes associated with receptor activation with high precision. Ensemble approaches based on the measurement of a physiological response, resonance energy transfer and other fluorescent methods have been widely used to measure the kinetics and protein-protein interactions associated with different aspects of GPCR signaling [17]. However, these methods report an average response from many receptors, which can obscure the heterogeneity inherent in receptor kinetics and are blind to rare or transient conformational subpopulations. In contrast to ensemble spectroscopic techniques, single molecule Forster resonance energy transfer (smFRET) allows for distinct conformations to be identified in single proteins and for the dynamic transitions between those states to be resolved over a range of time scales[18].

Metabotropic glutamate receptors (mGluRs) are members of the class C GPCR family, which form functional dimers, and are involved in modulation of synaptic transmission and neuronal excitability[4]. The eight different mGluRs are organized into groups I (mGluR1, 5), II (mGluR2, 3), and III (mGluR4, 6, 7, 8) based on sequence homology and G protein coupling profile. The distinctive structural feature of mGluRs is a large extracellular domain (ECD), consisting of a bi-lobed ligand binding domain (LBD) that contains the glutamate binding site, and a cysteine rich domain (CRD) that couples to a 7-transmembrane domain (TMD). Recent X-ray crystallography of the isolated TMD of mGluR1 has indicated a highly conserved fold relative to class A and B GPCRs, further indicating that despite the lack of sequence homology, mGluRs maintain many of the hallmark properties of all GPCRs [5]. Previous X-ray crystallography on the isolated ECD of mGluRs have shown “open” and “closed” LBD conformations as well as intersubunit reorientations between a “relaxed” and “active” state[6-8]. In the “active” conformation, the two LBDs rotate relative to each other, which brings the lower lobes of the LBD in close proximity. Initial structural work indicated that the “active” conformation (“closed-open/active” or “closed-closed/active”), which was observed with

mGluR1 LBDs in the presence of glutamate, corresponds to the functionally active state of the receptor[6,7]. However, subsequent structures have not always agreed. Notably, mGluR3 was crystallized in the "relaxed" intersubunit conformation even in the presence of two bound agonists which induced clamshell closure in both LBDs ("Closed-Closed/Relaxed")[8] and recently, mGluR1 was crystallized in the absence of ligand in the "active" state ("Open-Open/Active"; PDB: 3KS9). This raises the question of which intersubunit states are correlated with receptor activation and how many different orientations may be populated physiologically. Spectroscopic and functional studies have supported the idea of intersubunit reorientations within an mGluR dimer, but have so far not elucidated the precise mechanisms due to inherent limitations of ensemble and indirect techniques[9,10,11,12].

In order to understand how ligand binding mediates GPCR activation, we probed the motions between the N-terminal domains of group II mGluRs in real time using smFRET. Using this technique, in conjunction with functional assays, we have identified three distinct conformational states and propose a model of the structural transitions that lead to receptor activation.

Results:

Intersubunit FRET of mGluR2 reveals three distinct conformations

To assess the motions between subunits within an mGluR dimer, we used previously described N-terminally tagged SNAP-mGluR2 and CLIP-mGluR2 FRET constructs [19 20]. Crystal structures of the mGluR1 LBD with and without glutamate in the "relaxed" and "active" states, respectively, show an increase in distance between N-termini (Fig. 4.1A) [6]. SNAP and CLIP-tagged mGluR2 constructs were expressed in HEK 293T cells where they may be specifically labeled with donor (benzylcytosine-DY-547 for CLIP-mGluR2) and acceptor dye (benzylguanine-Alexa 647 for SNAP-mGluR2) (Fig. S4.1A-D), and show a FRET decrease upon receptor activation with glutamate which is consistent with previous work (Fig. 4.1B). Importantly, SNAP and CLIP-tagged mGluR2 were fully functional in a GIRK activation assay (Fig. S4.1E). Following receptor expression and dye labeling, cells were lysed and individual receptors were immobilized in detergent using the recently described SimPull technique [21] (Fig. 4.1C). Individual fluorescent spots were then imaged using total internal reflection microscopy (TIRF). Donor was excited and both donor and acceptor were simultaneously imaged (Fig. 4.1D; Methods) which showed many spots that exhibited FRET. Controls confirmed that mGluR2 was specifically pulled down (Fig. S4.1F) and dye labeling and imaging was specific for SNAP or CLIP (Fig. S4.1G, H). Individual dimeric receptors were identified by photobleaching in one step per channel. In spots where acceptor bleached before donor, fluorescence recovery was observed in the donor channel, confirming FRET (Fig. 4.1E).

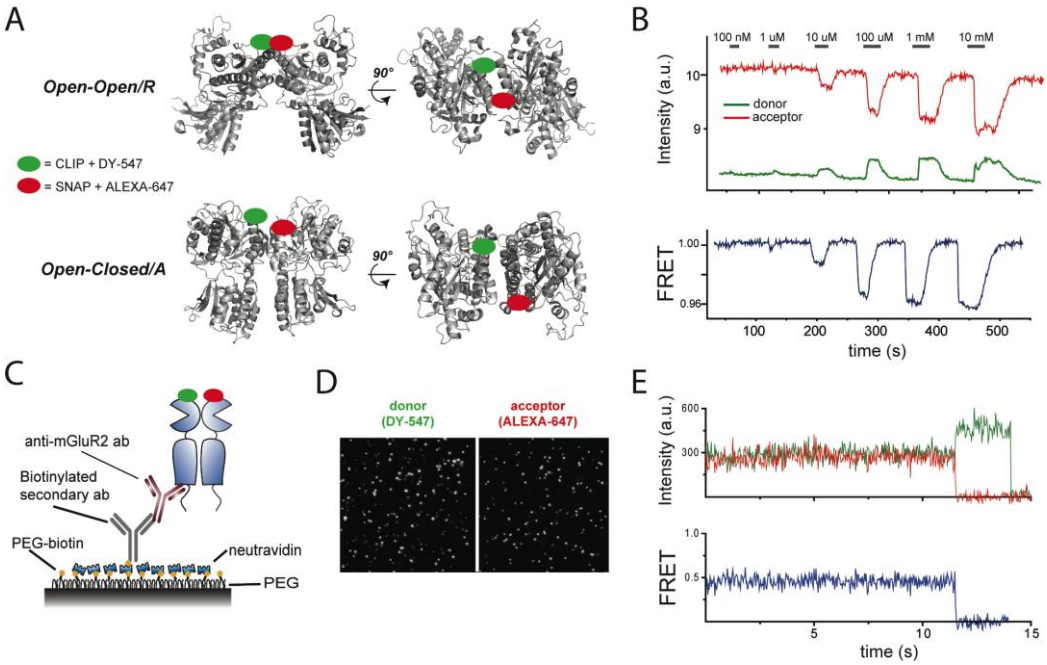

Figure 4.1, Ensemble and single molecule FRET between mGluR2 ligand binding domains. A) Structures of mGluR1 in the relaxed (above) or active (below) state show a relative reorientation of the N-termini which should bring fluorescent dyes farther apart. B) Ensemble FRET measurements in HEK 293T cells show a dose-dependent decrease in FRET upon glutamate application. C) Schematic of SimPULL pulldown of mGluR2 using a specific antibody on a passivated surface. D) Single molecules may be identified which undergo FRET. In these images only the donor is being excited. E) Representative FRET trace in basal (0 glutamate) conditions shows clear donor activation of acceptor and single step photobleaching.

We next measured FRET values for a variety of glutamate concentrations in order to assess if a FRET decrease could be observed as expected from ensemble measurements. In the presence of saturating glutamate, FRET was decreased to an average value of ~0.2 (Fig. 4.1A). Fig 4.1B shows histograms for many individual molecules under a wide range of glutamate concentrations which produces a number of peaks which may be identified. In the absence of glutamate a major FRET peak is observed at ~0.45. However, there is a clear shoulder produced by a small second peak with a FRET value of ~0.35 (Fig. S4.2A). Application of a saturating concentration of the competitive antagonist LY341495a does not alter the FRET histogram in the absence of glutamate indicating that this likely represents a fully inactive state of the receptor. As the concentration of glutamate increases the high FRET peak at 0.45 decreases and the low FRET peak at 0.2 increases until it is almost fully populated a saturating glutamate. At intermediate concentrations all three peaks (0.45, 0.35, 0.2) are present (Fig. S4.2B). We next examined the dynamics of the FRET using the cross-correlation between donor and acceptor channels which is an un unbiased means of quantifying dynamics without assuming a model. At 0 or saturating glutamate very little dynamics were observed (Fig. 4.1E, 4.2A), but at intermediate concentrations large cross-correlation was observed (Fig. 4.2C). This indicates that on the time scale of the measurement, which was 30 ms, there is little conformational dynamics except at intermediate concentrations. Consistent with this, in traces at 8 μM glutamate many anti-correlated transitions can be observed which correspond to changes in FRET. Individual traces showed transient population of 3 different FRET values of 0.2 0.35, and 0.45 (Fig. 4.2D) which further confirms the presence of at least three unique states. This data is most easily described with a 3-state model where high and medium FRET are inactive conformations, and low FRET is the active state of the receptor that gets stabilized by agonists.

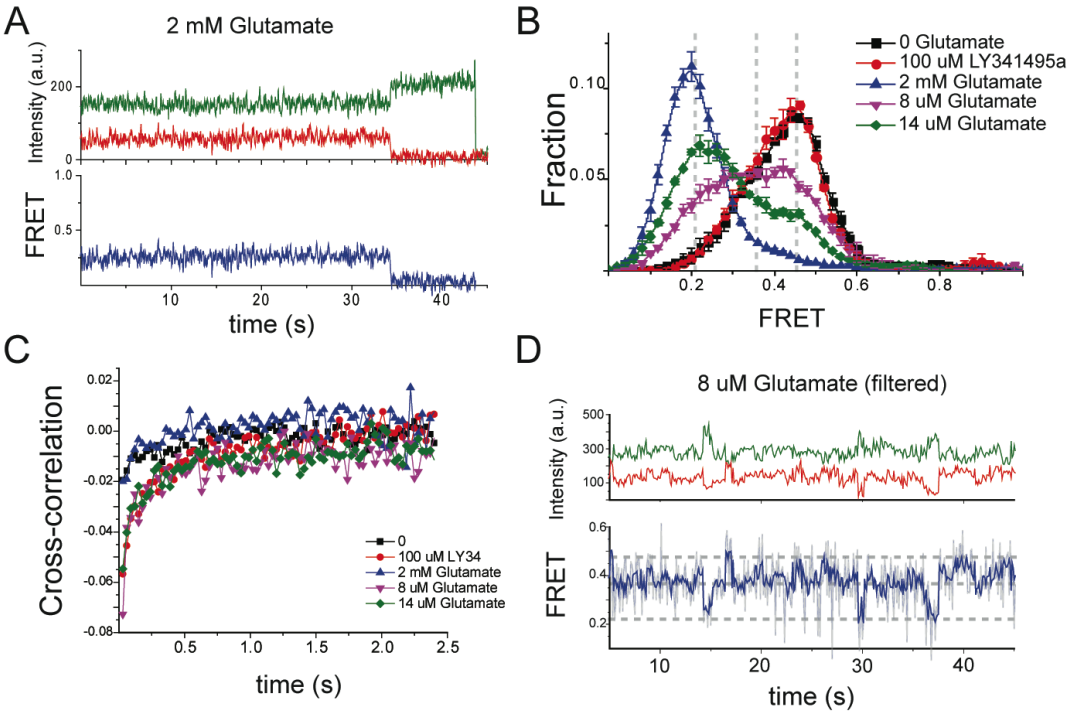

Figure 4.2, smFRET analysis of mGluR2 reveals dynamics between three states. A) Representative smFRET in the presence of saturating glutamate shows a decreased FRET value of 0.2. B) Histogram showing the FRET distributions for single molecules over a range of glutamate concentrations. Dotted lines show positions of 3 peaks used to fit the histograms. C) Cross-correlation analysis shows limited dynamics at 0 or saturating glutamate, but significant dynamics at intermediate concentrations. D) Representative trace at 8 uM glutamate shows transitions between 3 FRET states.

While glutamate is the native agonist of mGluRs, many synthetic agonists have been developed which allow for the selective targeting of subtypes. While a number of agonists show receptor activation, the overall level of activation is variable with some compounds defined as partial agonists while other are full agonists. Initial FRET measurements indicated that partial agonists induce a smaller maximal FRET decrease relative to glutamate despite having a higher affinity[20]. However, since these measurements were made in ensemble it is impossible to know if weak agonists stabilize a unique conformation or simply fail to fully stabilize the same conformation as glutamate or other full agonists. To test this, we turned to the agonist DCG-IV which gave a maximal ensemble FRET change of ~60% relative to glutamate (Fig. 4.3A, B). We then tested the effect of DCG-IV in smFRET and found that the same 3 peaks were present but that saturating concentrations of DCG-IV failed to fully populate the low FRET peak as well as glutamate (Fig. 4.3C, S4.3). Consistent with this, even saturating concentration of DCG-IV displayed greatly enhanced dynamics relative to 2 mM glutamate (Fig. 4.3D). This is consistent with the notion that DCG-IV is able to shift the conformational population toward the active state without locking the receptor in that state in the way a full agonist like glutamate does. Notably, at low or intermediate DCG-IV concentrations dynamics are enhanced relative to glutamate and a clear population of all three FRET states is clearly identifiable in the associated histograms (Fig. S4.3).

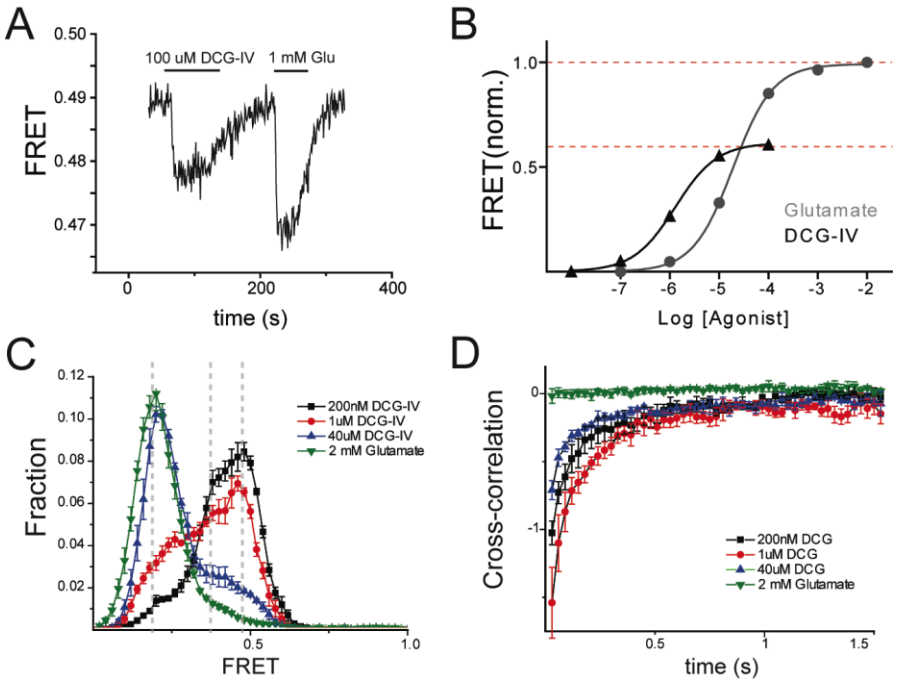

Figure 4.3, Partial agonist DCG-IV fails to fully stabilize active conformation. A) Representative ensemble FRET measurement in HEK cells shows a FRET decrease of ~60% for DCG-IV relative to glutamate. B) Dose response curve for DCG-IV and glutamate as measured by FRET. C) smFRET histogram for DCG-IV at a range of concentrations. At 40 uM, which is saturating, a large shoulder is observed at larger FRET values relative to glutamate. D) Cross-correlation analysis shows enhanced dynamics for DCG-IV relative to glutamate.

mGluR3 shows basal dynamics which are correlated to basal activity

To see if the conformational properties observed using smFRET on mGluR2 were generally true of mGluRs, we turned to the other group II mGluR, mGluR3. SNAP and CLIP-tagged mGluR3, like mGluR2, were functional and displayed an ensemble FRET decrease in HEK cells following glutamate application (Fig. S4.4A). mGluR3 also shows an increased apparent affinity for glutamate relative to mGluR3 despite their >70% amino acid sequence identity (Fig. S4.4B). When smFRET was measured in the absence of glutamate, mGluR3 showed a large shift in FRET values relative to mGluR2 (Fig. 4.4A). Similar to mGluR2, saturating concentrations of glutamate shifted the FRET values mostly into one peak at ~0.2. In contrast to mGluR2, in the absence of glutamate there was clear population of all 3 FRET peaks, including the low FRET peak of ~0.2. Application of the competitive antagonist LY341945a was able to shift the histogram toward higher FRET values and produce a distribution similar to mGluR2 in the absence of glutamate (Fig. 4.4A). Conflicting reports in the literature have indicated that mGluRs, including mGluR3 but not mGluR2, may be calcium-sensitive[22,23,24,25]. Since basal Ca^{2+} was maintained at 2 mM, we wondered if removal of Ca^{2+} would change the basal smFRET properties of mGluR3. In the absence of Ca^{2+} and presence of 10 mM EGTA, there was a shift in FRET values that was nearly as large as a competitive antagonist indicating that calcium plays a role in the basal decrease in FRET observed for mGluR3 relative to mGluR2. Elevation of Ca^{2+} to 10 mM did not further alter the FRET properties of mGluR2 (data not shown). It is important to note, given the extremely high affinity of mGluR3 for glutamate (<1 μM), that it is difficult to be fully confident that all glutamate has been removed from the experimental conditions. However, the Ca^{2+} dependence of the basal mGluR3 FRET indicates that even if there are sparse levels of glutamate, a physiological level of Ca^{2+} is still required to produce the bulk of the shift relative to mGluR2.

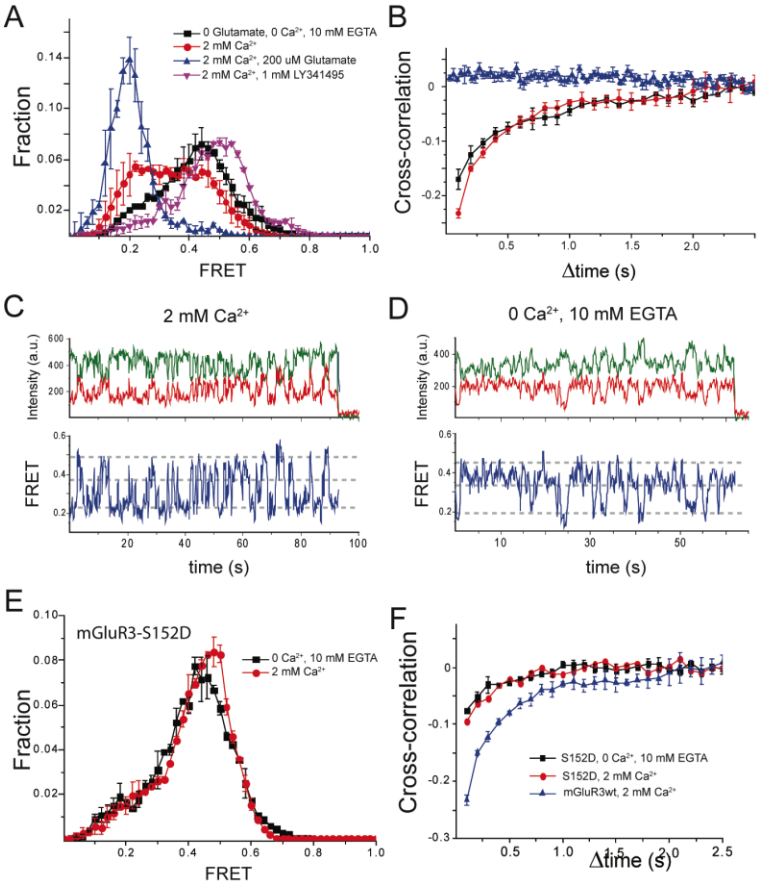

Figure 4.4, smFRET analysis of mGluR3 reveals Ca^{2+}-sensitive basal dynamics. A) Histograms for smFRET values of mGluR3 under a range of conditions with and without Ca^{2+} or glutamate. B) Cross-correlation analysis shows enhanced dynamics for mGluR3 in the presence or absence of Ca^{2+} relative to glutamate. Note: cross-correlation values are much larger than observed for mGluR2. C, D) Representative smFRET traces showing mGluR3 FRET values in the presence (C) or absence (D) of 2 mM Ca^{2+}. E) Histograms showing a lack of sensitivity to Ca^{2+} for mGluR3-S152D and an accompanying increase in basal FRET. F) Cross-correlation analysis shows decreased dynamics for S152D compared to mGluR3wt.

We next analyzed the dynamics of mGluR3 to gain more insight into its differences relative to mGluR2. Cross-correlation analysis indicated that at rest there is a large amount of dynamics that are only partially reduced by removal of Ca^{2+} (Fig. 4.4B). Notably, the cross-correlation values observed for mGluR3 were much larger than the maximal values observed for mGluR2 in the presence of glutamate (Fig. 4.2C). However, similar to mGluR2, application of saturating glutamate or LY341495 was able to largely abolish the dynamics of mGluR3 (Fig. 4.4B). Traces for individual molecule display the rapid dynamics relative to mGluR2 observed for mGluR3 in the presence or absence of Ca^{2+} (Figure 4.4C, D). When Ca^{2+} is fully removed there is still occasional population of the low FRET state, indicating that these conditions may lead to some activity that is either driven by the inherent dynamics of the system or by trace levels of glutamate. Finally, we tested the previously described mutation S152D which was reported to abolish Ca^{2+} sensitivity of mGluR1 and 3[22]. When mutated to S152D there was an increase in smFRET for mGluR3 that was accompanied by a lack of sensitivity to Ca^{2+}, as expected (Fig. 4.4E). Consistently, the histograms produced for S152D in the presence or absence of Ca^{2+} were both very similar to mGluR3 wild type in the absence of Ca^{2+} or presence of LY341495. Furthermore, S152D reduced the dynamics relative to wild type mGluR3 (Fig. 4.4F). In addition to abolishing Ca^{2+} sensitivity and increasing basal FRET, S152D showed a clear decrease in apparent glutamate affinity in ensemble FRET which may contribute to the reduction in basal dynamics (Fig. S4.5). Surprisingly, the reverse mutation in mGluR2, D146S, which was previously reported to induce Ca^{2+} sensitivity[22], failed to produce any basal FRET change or sensitivity to changes in Ca^{2+} concentration (data not shown). Overall, smFRET measurements of mGluR3 reveal basal dynamics that span all 3 FRET states, are calcium-dependent and may be abolished with the mutation S152D.

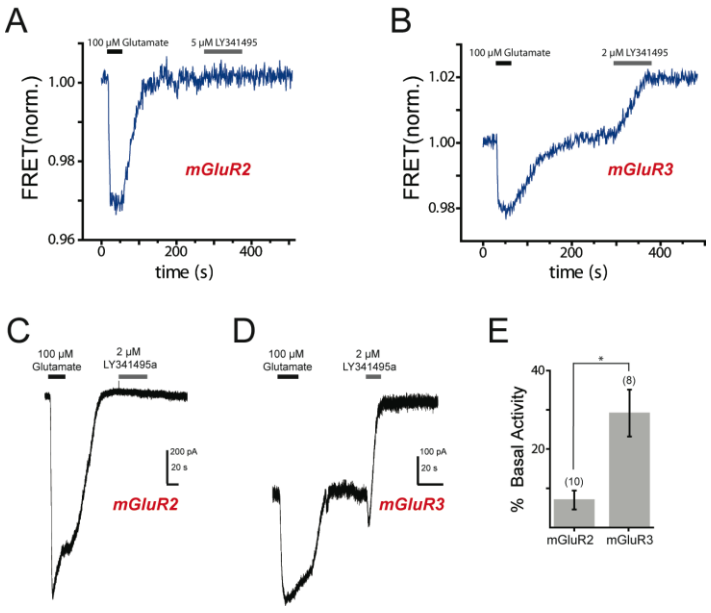

Figure 4.5, Basal dynamics of mGluR3 produce basal receptor activity. A, B) Ensemble FRET measurements in HEK 293T cells show a large increase in FRET upon application of an antagonist (LY341495) for mGluR3, but not mGluR2. C,D) mGluR3, but not, mGluR2 show a large response to LY341495 when measured in a GIRK current assay for Gi/o-activation. E) Summary of basal activity shows enhanced basal activity for mGluR3 relative to mGluR2. * indicates statistical significance (Unpaired, two-tailed T-test; $P<0.05$).

We next wondered if the basal dynamics and low FRET population of mGluR3 corresponded to basal activity of the receptor. First, we confirmed using ensemble FRET that there was a difference in basal FRET between mGluR2 and mGluR3 in living cells. Application of the antagonist LY341495 did not alter the basal level of FRET for mGluR2, but drastically

increased it for mGluR3 (Fig. 4.5A,B). We next turned to a GIRK current assay as a reporter for receptor activation. Similar to results observed with FRET, application of LY341495 induced a much larger outward current in mGluR3-transfected cells relative to mGluR2-transfected cells (Fig. 4.5C-E). This indicates that the basal conformational fluctuations of mGluR3 lead to basal activity that may be blocked with an antagonist. This finding agrees with the interpretation that the low FRET state, which is populated at rest by mGluR3 but not mGluR2, is indeed the active state of the receptor.

Allosteric modulation of mGluR2 ligand binding domains by G proteins

Having seen the effects of both orthosteric ligands and the divalent ion, Ca^{2+}, on mGluR FRET, we next wondered if G protein binding at the distant trans-membrane domain could alter the FRET properties of the mGluR2 LBD. Consistent with previous studies[20], we found that coexpression of the Gα subunit G_{oA} with the mutation G203T, which lowers affinity for nucleotides and locks the G protein in a high affinity state for the receptor[26], was able to increase the apparent affinity of mGluR2 for glutamate as measured by ensemble FRET (Fig. 4.6A). This affect was very subtle (<2 fold decrease in EC_{50}) and we wondered if a larger change could be observed for the partial agonist DCG-IV. Interestingly, we observed that co-expression of G_{oA}-G203T increased the affinity of mGluR2 for DCG-IV and also increased the maximal FRET change induced by DCG-IV when normalized to glutamate (Fig. 4.6B). This result indicates that G-protein binding can not only stabilize agonist binding, but actually allow a partial agonist to stabilize a more efficacious state than in the absence of bound G protein. As a control, when the wild-type G_{oA} was overexpressed no affinity or efficacy shift was observed (Fig. 4.6B). When we expressed the mGluR2 mutant F756D which has impaired G protein activation [27] and found that no shift in the DCG-IV FRET response was induced by G_{oA}-G203T (Fig. 4.6). Since SNAP and CLIP domains allow for the selective measurement of heteromers (Fig. S4.1), we next asked if F756D in only one subunit of a dimer could disrupt the apparent sensitivity shift induced by G_{oA}-G203T. Instead, we found that only one wild-type subunit was required to accommodate the effect of G protein binding to the dimer (Fig. 4.6D). This may indicate that only one G protein is required per dimer to influence the intersubunit conformational rearrangement associated with receptor activation. Future work may be able to recapitulate this complex in the smFRET assay to gain further insight into the means by which G protein allosterically regulates mGluR ligand sensitivity.

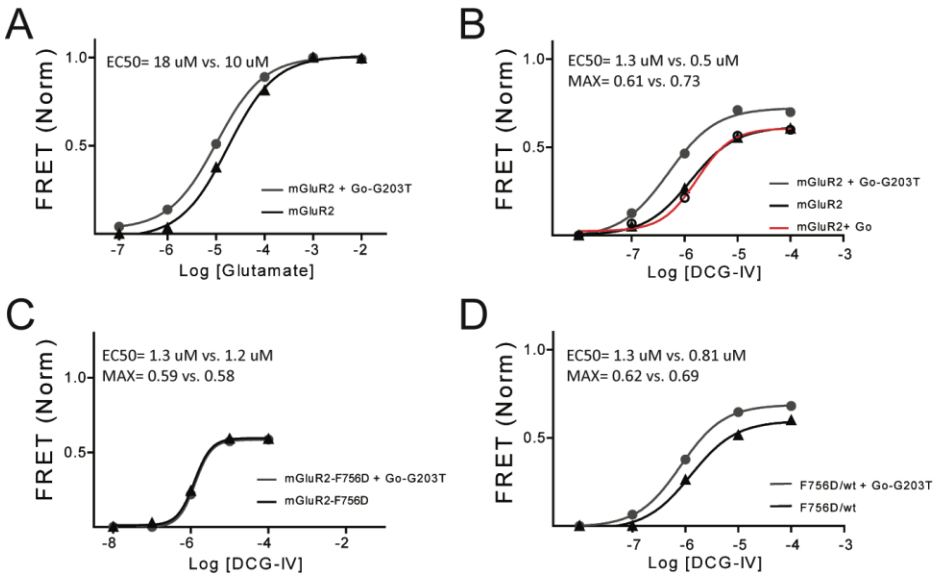

Figure 4.6, G proteins shift the apparent affinity and efficacy of mGluR2 agonists. A) Glutamate dose-response curve for mGluR2 in the absence of presence of co-expression Go-G203T shows a minor apparent affinity shift. B) Co-expression of Go-G203T, but not wild type Go, increase both the apparent affinity and efficacy of DCG-IV. C,D) Mutation of both (C) but not one (D) subunit to F756D prevents the affinity and efficacy shift induced by Go-G203T.

Discussion:

While many studies of GPCRs in general, and mGluRs in particular, have given great insight into how these receptors signal, a detailed molecular mechanism has so far been elusive. For example, crystallography of LBDs of mGluRs has given important clues about the potential conformations that these crucial domains may adopt. However, this body of work has shown a variety of conformations which are difficult to reconcile and due to the lack of dynamic information are difficult to incorporate into a simple functional model. Our work, which takes advantage of the enhanced resolution of smFRET has lent some insight into the conformational changes associated with ligand binding and receptor activation. Specifically, we have shown that three distinct FRET values are populated by mGluRs indicating that at least three intersubunit LBD conformations exist under physiological conditions that are stable enough to be resolved with 30-100 ms sampling. Fig. 4.7 shows a proposed model that may explain the three states observed for mGluR2 and 3.

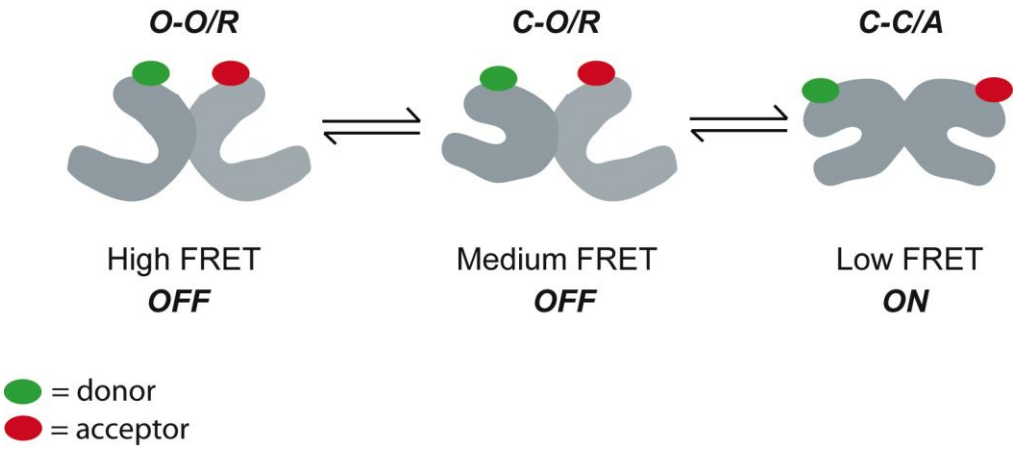

Figure 4.7, Structural model of three states observed by smFRET. Schematic showing three different structural states which correspond to different amounts of FRET as demonstrated by the relative distance between the N-terminal donor and acceptor dyes. In the active state the lower lobes of the LBDs are brought closer together which may facilitate closer association of the downstream CRDs or TMDs.

In this model three states are populated which are associated with high, medium, and low FRET peaks. Since both the high and medium peaks are populated in the absence of glutamate for mGluR2, which displays very limited basal activity, these states represent inactive states of the receptor. In the high FRET state both LBD clamshells remain open and the two subunits only interact at the upper lobe in the relaxed "R" mode. In the medium FRET state one LBD closes but the intersubunit orientation does not change, resulting in only a minor distance change between the two fluorophores. This state is occasionally visited in the absence of glutamate which is consistent with it representing an inactive conformation. The low FRET state, however, becomes populated upon application of glutamate and represents the active state of the receptor. In this state both ligand binding domain clamshells have closed and undergone a reorientation from "R" to "A" that brings the lower lobes together while drastically increasing the distance between fluorophores. This reorientation may facilitate the closer association of downstream

domains such as the CRDs which is consistent with recent work that showed that cross-linking of CRDs within a dimer induced receptor activity[11]. Based on the relative distances observed between the relaxed and active states of mGluR LBD structures (Fig. 1A) it is likely that the high and low states represent relaxed and active states, respectively. Furthermore, since the medium peak represents a more subtle distance change, we propose that this represents a relaxed orientation that corresponds to closure of just one LBD that is not accompanied by an intersubunit conformational change. It is important to note that this structural state does not necessarily mean that one agonist is bound, but only that one clamshell has closed. For instance, given its high affinity it is likely that, in this model, saturating DCG-IV stays bound in both subunits while the receptor interconverts between C-O/R and C-C/A. This is consistent with ligand binding models which show that agonists can bind to just the upper lobe of the LBD before stabilizing the closed state[28]. Future functional work will be needed to more closely associate different structural states to ligand occupancy to fully understand what occurs when only one ligand binds to a dimer. In addition, smFRET analysis with dyes at different points on the receptor, such as the lower lobe of the LBD, will allow for the testing of this structural model more thoroughly.

This model of FRET states supports the notion that the closed-closed/relaxed and open-open/active states observed in some crystal structures are likely never or very rarely populated in the full length receptor under physiological conditions. Further analysis of dynamics will have to assess whether the medium FRET state is indeed an intermediate between low and high FRET states, although this seems like the simplest explanation based on the available data (see Fig. 4.2D). An analysis of the dwell times for the different FRET states under different conditions will also give insight into the relative thermodynamic stability of each state.

In addition to defining the relative orientations of the two LBDs within an mGluR dimer, this work showed profound differences between two very closely related GPCRs: mGluR2 and mGluR3. While both receptors showed the same three states, mGluR3 showed greatly enhanced dynamics in the absence of agonist that led to an enhanced population of low and medium FRET states. Overall, the dynamics of mGluR3 were much larger than mGluR2, even for comparable conditions in terms of conformational ensemble as observed by histograms. In contrast with some studies that have challenged the notion of Ca^{2+} activation of mGluR3, we show that physiological Ca^{2+} is able to stabilize the active state of mGluR3, but not mGluR2. It has been difficult to determine the precise Ca^{2+} binding site since it has not been resolved with crystallography, but we have shown that the residue S152 likely is a contributor (Fig. 4.4E,F). However, this residue is located near both the glutamate binding site and the LBD dimer interface, making it difficult to determine if Ca^{2+} binds near the orthosteric site or in the dimer interface, as has been observed for Gd^{3+} [29]. The loss of Ca^{2+} sensitivity observed with the S152D mutation contradicts recent work proposing a novel binding site for Ca^{2+} that is adjacent to the glutamate binding site, far from from residue S152, and includes part of the bound glutamate itself [30]. However, mGluR3-S152D showed a reduced glutamate affinity which may, in part, underlie its loss of Ca^{2+} sensitivity.

The very high Ca^{2+} sensitivity of mGluR3, and the subsequent basal activity it produces, indicates that physiologically there is a basal tone provided to mGluR3. This basal activity difference may facilitate distinct roles for mGluR3 and mGluR2 in different compartments of the synapse in the brain [31]. It is worth mentioning that there may be trace levels of glutamate present that account for some of the differences between mGluR2 and mGluR3 that remain following removal of Ca^{2+}. However, these conditions likely mimic the *in vivo* conditions where glutamate

is unlikely to ever be fully removed from the extracellular solution. This indicates that our findings regarding mGluR3 basal activity likely reflect the physiological situation. Finally, future work will evaluate if the difference in dynamics between mGluR3 and mGluR2 lead to a difference in G protein activation and deactivation kinetics.

Ensemble experiments with co-expression of G proteins, indicate that inter-LBD FRET is a valid means for probing downstream coupling of mGluRs. We confirmed that G protein shifts the apparent affinity of mGluR2 for glutamate. We also saw that G protein shifts both the affinity and efficacy of the partial agonist DCG-IV. Furthermore, we show that only one functional TMD is required for this G protein-induced effect. This indicates that perhaps either one G protein can bind to a receptor or only one TMD can reach the activated conformation at a time, as has been previously suggested [32,33,34]. Alternatively, the G protein binding site of a mutated subunit may be rescued by coassembly with a wild type subunit. Extension of these experiments to the smFRET assay should provide further insight into what state G proteins induce or stabilize and how receptor dynamics are affected. In addition, positive allosteric modulators that bind to the transmembrane domains of mGluR2 may mimic the effect of G proteins since ensemble FRET work has shown that an mGluR2 PAM can also increase the affinity and efficacy of a partial agonist[20].

Overall, this work shows a new means of probing the biophysical properties of full length GPCRs in detergent without purification. We define a three state structural and functional model of mGluR LBD reorientation that refines previously irreconcilable findings from X-ray crystallography. We also demonstrate that the altered dynamics between mGluR3 and mGluR2 and treatment with partial versus full agonists, as revealed by smFRET, result in altered activation properties. This work is consistent with a wealth of recent work which indicates that receptor dynamics are key to understanding receptor function. Ultimately, this work will provide a foundation for further probing of the conformational dynamics of GPCRs in general, and mGluRs in particular. Furthermore, the ligand binding domains of mGluRs, which we show are highly amenable to smFRET studies, may be a valuable model system for understanding bilobed clamshell ligand binding domains, such as those of other Class C GPCRs like the $GABA_B$ receptor or ionotropic neurotransmitter receptors.

Methods:

HEK293T cell culture, molecular biology, and electrophysiology

HEK293T cells were maintained in DMEM with 5% FBS on poly-L-lysine-coated 18 mm glass coverslips and transfected with lipofectamine 2000 (Sigma). SNAP and CLIP-tagged DNA were provided by Jean-Phillipe Pin (Univ. of Montpellier). Each coverslip received 0.3-0.6 ug/DNA/well. For GIRK current experiments mGluR2 or 3, GIRK1-F137S, and YFP (as a transfection marker) were transfected at a 7:7:1 ratio with 0.7 ug/well for receptor and channel. Point mutations were introduced using the quick change mutagenesis kit. Whole cell patch clamp electrophysiology was performed 24-48 hrs after transfection as previously described in Chapter III.

Dye labeling and ensemble FRET measurements

Cells were briefly washed with an extracellular solution containing (in mM): 135 NaCl, 5.4 KCl, 2.5 $CaCl_2$, 1 $MgCl_2$, 10 Hepes, pH 7.4 and then labeled sequentially with 2.5 uM benzylguanine Alexa-647 (Invitrogen) for 45 minutes and 5 uM benzylcytosine DY-547 (Invitrogen) for 45 minutes. The dyes were diluted in extracellular solution and were washed in between labeling with acceptor and donor. Following labeling cells were mounted on an upright, scanning confocal microscope (Zeiss LSM 780) and imaged with a 20x objective. Excitation was performed using a 561 nm laser and images were taken in the donor and acceptor channels at 1hz. Clusters of cells were analyzed together and FRET was calculated as $FRET=(I_{Acceptor})/(I_{Donor}+I_{Acceptor})$ where I is intensity. FRET changes calculated for dose-response curves were normalized to saturating glutamate (1 mM or 10 mM) and dose-response curves were obtained from multiple cell clusters and averaged from multiple experiments. Fitting of dose-response curves was performed using Prism (Graphpad). All drugs were purchased from Tocris and delivered with a gravity-driven perfusion system.

Single Molecule Pulldown of mGluRs

For single molecule experiments, cells were recovered from the coverslip by incubating with Ca^{2+}-free PBS followed by gentle pipetting. Cells were then pelleted and lysed in lysis buffer consists of 10mM Tris, 150 mM NaCl, 1 mM EDTA, Protease inhibitor cocktail and 1% IGEPAL. Glass coverslips were coated with PEG and PEG-biotin at a ratio of ~100:1 as descibred in Jain et al, 2011. Prior to each experiment, coverslips were treated with neutravidin, followed by a biotinylated secondary antibody. Next, an mGluR2 or mGluR3-specific primary antibody was conjugated. Between each conjugation step, washing was performed to remove unlabeled compounds from coverslips. Lysate was then diluted in the same high potassium buffer used for functional experiments (ranging from 20x to 100x) and applied to coverslips. Fluorescence was monitored in real time to confirm sufficient receptor attachment. Once a sufficient number of receptors had immobilized on the surface, the coverslips were washed to remove excess, unbound fluorescently-tagged receptors from solution.

smFRET measurements

Following conjugation of receptors to antibodies, single molecule imaging was performed with an inverted microscope in TIRF mode using a 60x objective. To reduce photobleaching, imaging buffer consisting of 3 mM Trolox (Sigma) and an oxygen scavenging system (of glucose oxidase (165 U/ml), catalase (2,170 U/ml) and β-D glucose (0.4% wt/wt)) was supplied in the high potassium buffer. Excitation was performed with a 532 nm laser and emission was monitored in both donor and acceptor channels using a CCD camera. Fluorescence signal was recorded in real time using home-written Visual C++software either in 8 bit or 16 bits. The movies were analyzed using either a custom-written IDL or a C++ program. In brief, an average image is created by averaging few frames from the movie (5 to 12 frames). This averaging removes the noise and increases the detection accuracy. Then the fluorescent molecules that exhibit a Gaussian intensity profile are selected in the averaged image. These molecules are then tracked over time and their fluorescent intensity is recorded to build the intensity time trace for each molecule. The traces were then analyzed in MatLab. In brief, traces that showed single step donor and acceptor photobleaching and a constant total intensity were selected and filtered as previously described [35]. Traces from many selected molecules were compiled to build FRET histograms (200-500 molecules in each case). Cross correlation was calculated using the following formula:

$$\text{Cross-correlation } (\Delta t) \sim [I_{\text{donor }(t)} - \bar{I}_{\text{donor}}] \times [I_{\text{acceptor }(t+\Delta t)} - \bar{I}_{\text{acceptor}}]$$

Where Δt is the time interval, t is time, I is fluorescence intensity, and $\bar{I}$ is the average intensity.

References:

1 Rasmussen, S. G. *et al.* Crystal structure of the beta2 adrenergic receptor-Gs protein complex. *Nature* 477, 549-555, doi:10.1038/nature10361nature10361 [pii] (2011).

2 Katritch, V., Cherezov, V. & Stevens, R. C. Structure-function of the G protein-coupled receptor superfamily. *Annu Rev Pharmacol Toxicol* 53, 531-556, doi:10.1146/annurev-pharmtox-032112-135923 (2013).

3 Venkatakrishnan, A. J. *et al.* Molecular signatures of G-protein-coupled receptors. *Nature* 494, 185-194, doi:10.1038/nature11896nature11896 [pii] (2013).

4 Niswender, C. M. & Conn, P. J. Metabotropic glutamate receptors: physiology, pharmacology, and disease. *Annu Rev Pharmacol Toxicol* 50, 295-322, doi:10.1146/annurev.pharmtox.011008.145533 (2010).

5 Wu, H. *et al.* Structure of a class C GPCR metabotropic glutamate receptor 1 bound to an allosteric modulator. *Science* 344, 58-64, doi:10.1126/science.1249489 science.1249489 [pii] (2014).

6 Kunishima, N. *et al.* Structural basis of glutamate recognition by a dimeric metabotropic glutamate receptor. *Nature* 407, 971-977, doi:10.1038/35039564 (2000).

7 Tsuchiya, D., Kunishima, N., Kamiya, N., Jingami, H. & Morikawa, K. Structural views of the ligand-binding cores of a metabotropic glutamate receptor complexed with an antagonist and both glutamate and Gd3+. *Proc Natl Acad Sci U S A* 99, 2660-2665, doi:10.1073/pnas.052708599052708599 [pii] (2002).

8 Muto, T., Tsuchiya, D., Morikawa, K. & Jingami, H. Structures of the extracellular regions of the group II/III metabotropic glutamate receptors. *Proc Natl Acad Sci U S A* 104, 3759-3764, doi:0611577104 [pii] 10.1073/pnas.0611577104 (2007).

9 Brock, C. *et al.* Activation of a dimeric metabotropic glutamate receptor by intersubunit rearrangement. *J Biol Chem* 282, 33000-33008, doi:M702542200 [pii]10.1074/jbc.M702542200 (2007).

10 Tateyama, M., Abe, H., Nakata, H., Saito, O. & Kubo, Y. Ligand-induced rearrangement of the dimeric metabotropic glutamate receptor 1alpha. *Nat Struct Mol Biol* 11, 637-642, doi:10.1038/nsmb770 nsmb770 [pii] (2004).

11 Huang, S. *et al.* Interdomain movements in metabotropic glutamate receptor activation. *Proc Natl Acad Sci U S A* 108, 15480-15485, doi:10.1073/pnas.1107775108107775108 [pii] (2011).

12 Hlavackova, V. *et al.* Sequential inter- and intrasubunit rearrangements during activation of dimeric metabotropic glutamate receptor 1. *Sci Signal* 5, ra59, doi:10.1126/scisignal.20027205/237/ra59 [pii] (2012).

13 Dror, R. O. *et al.* Activation mechanism of the beta2-adrenergic receptor. *Proc Natl Acad Sci U S A* 108, 18684-18689, doi:10.1073/pnas.1110499108110499108 [pii] (2011).

14 Nygaard, R. *et al.* The dynamic process of beta(2)-adrenergic receptor activation. *Cell* 152, 532-542, doi:10.1016/j.cell.2013.01.008S0092-8674(13)00011-1 [pii] (2013).

15 Lohse, M. J., Maiellaro, I. & Calebiro, D. Kinetics and mechanism of G protein-coupled receptor activation. *Curr Opin Cell Biol* 27C, 87-93, doi:S0955-0674(13)00185-3 [pii]10.1016/j.ceb.2013.11.009 (2014).

16 Manglik, A. & Kobilka, B. The role of protein dynamics in GPCR function: insights from the betaAR and rhodopsin. *Curr Opin Cell Biol* 27C, 136-143, doi:S0955-0674(14)00009-X [pii]10.1016/j.ceb.2014.01.008 (2014).

17 Lohse, M. J., Nuber, S. & Hoffmann, C. Fluorescence/bioluminescence resonance energy transfer techniques to study G-protein-coupled receptor activation and signaling. *Pharmacol Rev* 64, 299-336, doi:10.1124/pr.110.004309pr.110.004309 [pii] (2012).

18 Joo, C., Balci, H., Ishitsuka, Y., Buranachai, C. & Ha, T. Advances in single-molecule fluorescence methods for molecular biology. *Annu Rev Biochem* 77, 51-76, doi:10.1146/annurev.biochem.77.070606.101543 (2008).

19 Doumazane, E. *et al.* A new approach to analyze cell surface protein complexes reveals specific heterodimeric metabotropic glutamate receptors. *FASEB J* 25, 66-77, doi:10.1096/fj.10-163147 fj.10-163147 [pii] (2011).

20 Doumazane, E. *et al.* Illuminating the activation mechanisms and allosteric properties of metabotropic glutamate receptors. *Proc Natl Acad Sci U S A* 110, E1416-1425, doi:10.1073/pnas.1215615110 1215615110 [pii] (2013).

21 Jain, A. *et al.* Probing cellular protein complexes using single-molecule pull-down. *Nature* 473, 484-488, doi:10.1038/nature10016nature10016 [pii] (2011).
22 Kubo, Y., Miyashita, T. & Murata, Y. Structural basis for a Ca2+-sensing function of the metabotropic glutamate receptors. *Science* 279, 1722-1725 (1998).
23 Francesconi, A. & Duvoisin, R. M. Divalent cations modulate the activity of metabotropic glutamate receptors. *J Neurosci Res* 75, 472-479, doi:10.1002/jnr.10853 (2004).
24 Nash, M. S., Saunders, R., Young, K. W., Challiss, R. A. & Nahorski, S. R. Reassessment of the Ca2+ sensing property of a type I metabotropic glutamate receptor by simultaneous measurement of inositol 1,4,5-trisphosphate and Ca2+ in single cells. *J Biol Chem* 276, 19286-19293, doi:10.1074/jbc.M007600200 M007600200 [pii] (2001).
25 Jiang, Y. *et al.* Elucidation of a novel extracellular calcium-binding site on metabotropic glutamate receptor 1{alpha} (mGluR1{alpha}) that controls receptor activation. *J Biol Chem* 285, 33463-33474, doi:10.1074/jbc.M110.147033M110.147033 [pii] (2010).
26 Barren, B. & Artemyev, N. O. Mechanisms of dominant negative G-protein alpha subunits. *Journal of Neuroscience Research* 85, 3505-3514, doi:Doi 10.1002/Jnr.21414 (2007).
27 Francesconi, A. & Duvoisin, R. M. Role of the second and third intracellular loops of metabotropic glutamate receptors in mediating dual signal transduction activation. *Journal of Biological Chemistry* 273, 5615-5624, doi:DOI 10.1074/jbc.273.10.5615 (1998).
28 Kunishima, N. *et al.* Structural basis of glutamate recognition by a dimeric metabotropic glutamate receptor. *Nature* 407, 971-977 (2000).
29 Tsuchiya, D., Kunishima, N., Kamiya, N., Jingami, H. & Morikawa, K. Structural views of the ligand-binding cores of a metabotropic glutamate receptor complexed with an antagonist and both glutamate and Gd3+. *P Natl Acad Sci USA* 99, 2660-2665, doi:DOI 10.1073/pnas.052708599 (2002).
30 Jiang, Y. S. *et al.* Elucidation of a Novel Extracellular Calcium-binding Site on Metabotropic Glutamate Receptor 1 alpha (mGluR1 alpha) That Controls Receptor Activation. *Journal of Biological Chemistry* 285, 33463-33474, doi:DOI 10.1074/jbc.M110.147033 (2010).
31 Petralia, R. S., Wang, Y. X., Niedzielski, A. S. & Wenthold, R. J. The metabotropic glutamate receptors, mGluR2 and mGluR3, show unique postsynaptic, presynaptic and glial localizations. *Neuroscience* 71, 949-976, doi:Doi 10.1016/0306-4522(95)00533-1 (1996).
32 Goudet, C. *et al.* Asymmetric functioning of dimeric metabotropic glutamate receptors disclosed by positive allosteric modulators. *Journal of Biological Chemistry* 280, 24380-24385, doi:DOI 10.1074/jbc.M502642200 (2005).
33 El Moustaine, D. *et al.* Distinct roles of metabotropic glutamate receptor dimerization in agonist activation and G-protein coupling. *P Natl Acad Sci USA* 109, 16342-16347, doi:DOI 10.1073/pnas.1205838109 (2012).
34 Hlavackova, V. *et al.* Evidence for a single heptahelical domain being turned on upon activation of a dimeric GPCR. *Embo Journal* 24, 499-509, doi:DOI 10.1038/sj.emboj.7600557 (2005).
35 Haran, G. Noise reduction in single-molecule fluorescence trajectories of folding proteins. *Chem Phys* 307, 137-145, doi:DOI 10.1016/j.chemphys.2004.05.017 (2004).

Supplemental Figures:

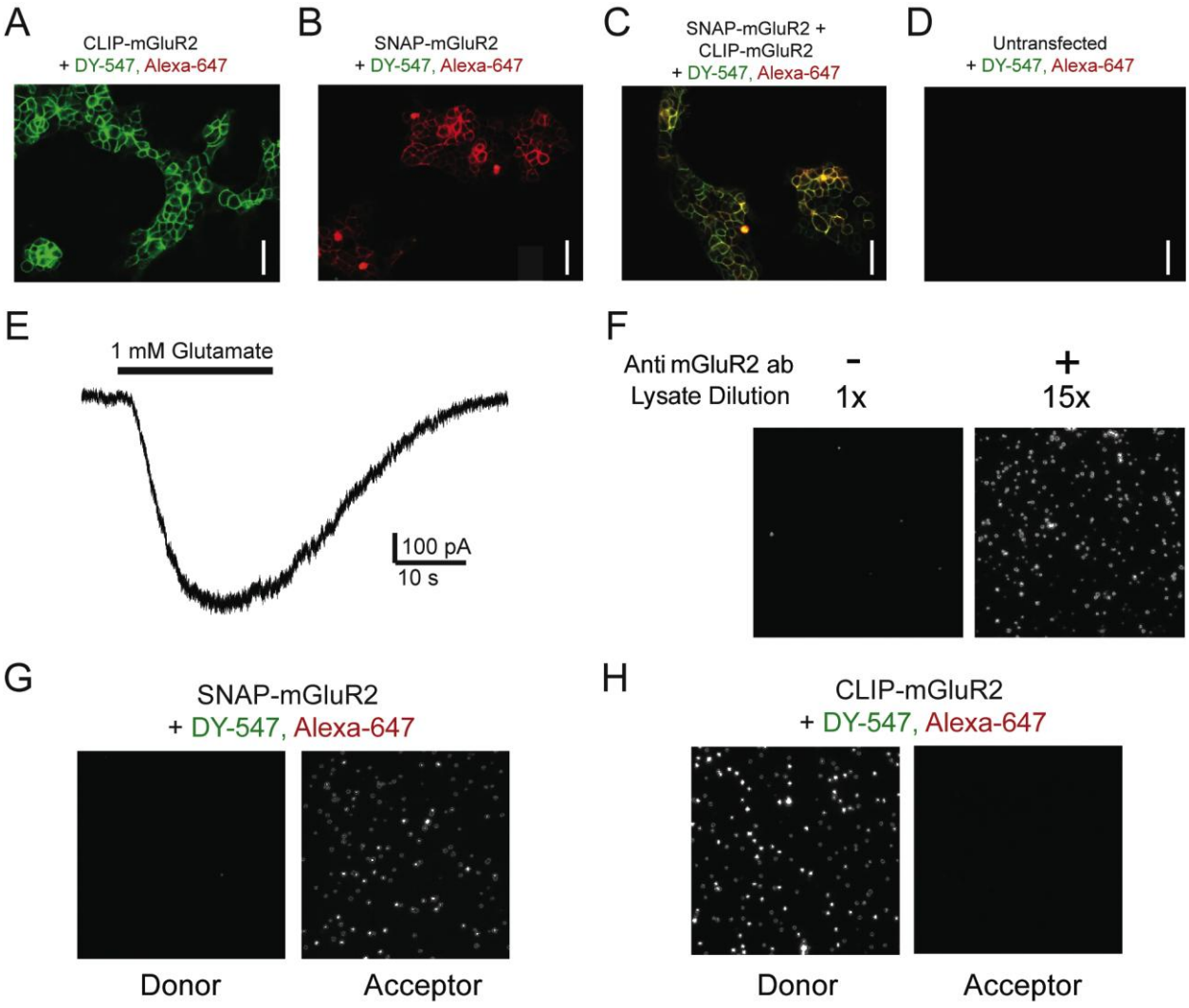

Figure S4.1, Controls show subtype-specific labeling of CLIP and SNAP-mGluR2. A-D) Labeling of HEK 293T cells expression CLIP-mGluR2 (A) , SNAP-mGluR2 (B) both (C) , or neither (D) with DY-547 and Alexa-647 show that labeling of each subunit is specific. E) SNAP-mGluR2 is functional in a GIRK assay in HEK 293T cells. F) Immobilization of mGluR2 on a passivated surface containing a secondary antibody requires an anti-mGluR2 primary antibody. G,H) Labeling of SNAP and CLIP-mGluR2 constructs is also specific when assayed using single molecule assay.

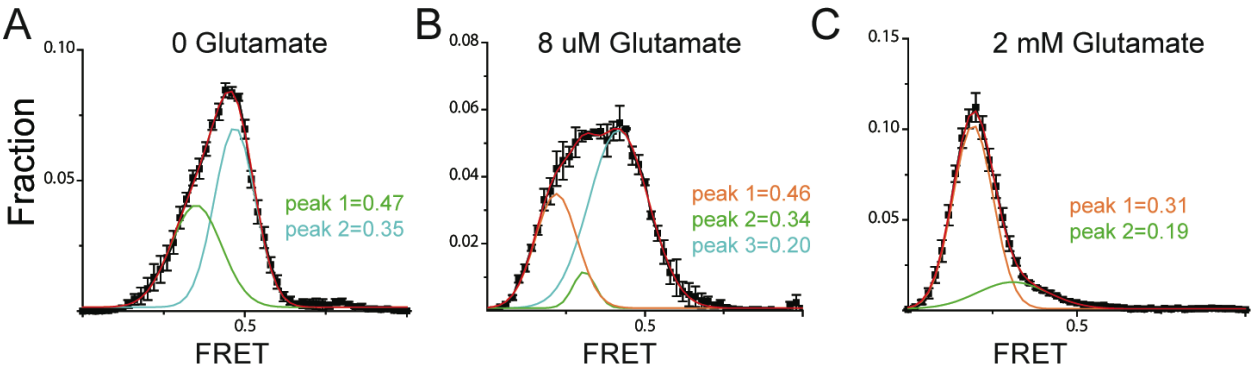

Figure S4.2, smFRET histograms for mGluR2 are fit with 3 different peaks. Histograms for mGluR2 smFRET values in the absence of 0 (A), intermediate (B), or saturating (C) glutamate show the identification of 3 distinct peaks with consistent values of ~0.45, 0.35, and 0.2.

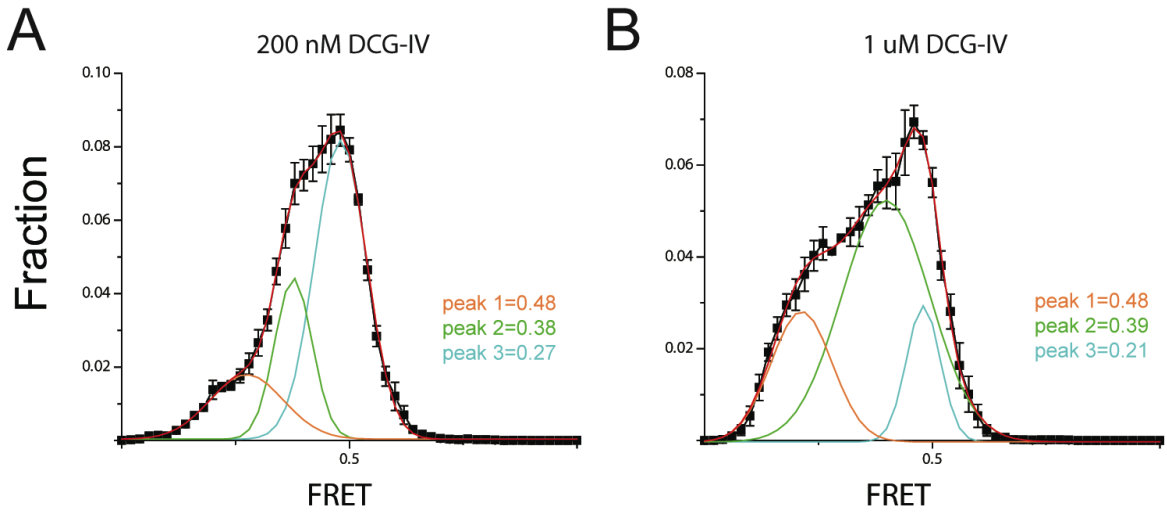

Figure S4.3, smFRET histograms for mGluR2 treated with DCG-IV show 3 peaks consistent with glutamate activation. Histograms for mGluR2 smFRET values in the presence of subsaturating DCG-IV show three distinct peaks that are consistent between conditions and correspond to values observed with glutamate.

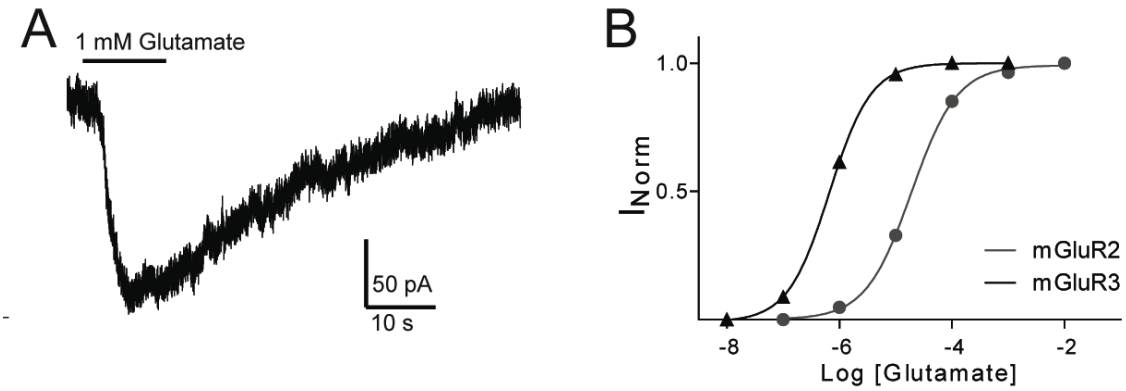

Figure S4.4, Functional control and ensemble FRET glutamate titration for mGluR3. A) SNAP-mGluR3 displays clear glutamate-evoked activation of GIRK channels indicating that this construct maintains the ability to activate G proteins. B) Dose response curves for glutamate-induced ensemble FRET changes for mGluR2 and mGluR3 show an increased apparent affinity for mGluR3.

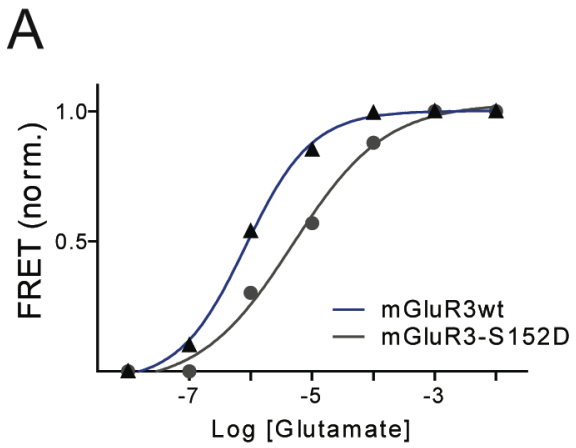

Figure S4.5, mGluR3-S152D shows a decreased glutamate affinity. A) Dose response curves for glutamate-induced ensemble FRET changes for mGluR3wt and mGluR3-S152D show a modest increase in EC_{50} from 0.8μM to 4.8 μM.

Chapter V: Optical analysis of stoichiometry and cooperativity of metabotropic glutamate receptors

Introduction:

Oligomerization of GPCRs

G protein-coupled receptors (GPCRs) are extremely important signaling molecules that respond to a wide array of extracellular stimuli and mediate many intracellular signaling pathways via G proteins. While the vast molecular diversity of GPCRs has been known for many years, a more recent observation has been that, in many cases, they can oligomerize into homomeric and heteromeric complexes. This higher order assembly provides a means for further diversifying the signaling capabilities of GPCRs by changing their sensitivity to stimuli, basal activity, regulation and desensitization, effector coupling, kinetics, subcellular targeting, and other properties[1,2,3,4 5]. Despite the great excitement aroused by the concept of GPCR oligomerization, such complexes have been difficult to observe and even more difficult to describe biophysically. Furthermore, while X ray crystallography is constantly expanding our structural understanding of GPCRs they have, so far, been limited in their ability to identify any common dimer interface that is in good agreement with functional data[6].

Many of the challenges associated with the characterization of GPCR oligomers are due to the possible transient nature of the associations as well as difficulty in determining receptor stoichiometry with precision in a cellular environment using ensemble techniques. A powerful technique for the characterization of membrane protein stoichiometry has emerged in recent years based on the expression of fluorescently tagged proteins in membranes and the subsequent counting of photobleaching steps in individual molecules as imaged with TIRF microscopy [7]. Most recently a number of groups have had success using single molecule fluorescence photobleaching and tracking techniques in living cells to observe GPCR oligomers[8,9]. In studies, most of which focused on class A GPCRs, a dynamic equilibrium between monomers and dimers was seen with varying dwell times for homo or heterodimers. These studies have been important in demonstrating GPCR oligomers but have failed to provide much insight into the nature of dimer interfaces or the functional consequence of dimerization.

Class C GPCRs are a unique subset of GPCRs because of the widely established fact of their oligomerization, which has been classically assumed to be strict dimerization[10,11]. This class includes, most notably, the metabotropic glutamate receptors (mGluRs) and $GABA_B$ receptors, which have been observed as oligomers in a variety of classical assays[12]. Most recently, Calebiro et al[8] used single molecule fluorescence techniques to observe dimers, tetramers, and octamers of the GABAB receptor, which along with other studies[13,14], challenges the idea of strict dimerization of class C GPCRs. However, work using ensemble time-resolved Forster resonance energy transfer (FRET) on mGluRs has failed to find evidence for higher order assembly[15].

mGluRs consists of three major domains which are the N-terminal bi-lobed ligand binding domain (LBD) which is coupled to a 7 helix trans-membrane domain (TMD) via an intermediate cysteine rich domain (CRD)[11,16]. Despite the constantly evolving understanding of how class C GPCRs assemble, the precise structural mechanism of mGluR dimerization has remained somewhat nebulous. Initial biochemical studies used denaturing gels to show that mGluRs form covalent dimers that may be disrupted by DTT treatment[17]. This covalent dimer

interface was identified as being mediated by an intersubunit disulfide bond formed by a conserved cysteine on the N-terminal LBD of mGluRs. Unfortunately, little characterization was performed on receptors with mutations at this residue other than to show that there is little change in the band pattern of native gels and that receptors were still functional[18-20]. Crystal structures of the LBDs of various mGluRs have failed to resolve the loop containing the conserved cysteine but have shown a clear interface between the upper lobes of the LBD, which is formed by helices B and C and appears to be largely hydrophobic[21]. There has been little functional work probing this interface, but one study reported a mutation at the hydrophobic interface in mGluR1, I120A, that prevented receptor activation[22]. A potential interface involving the TMDs has been even more elusive. Goudet et al[23] removed the extracellular domain of mGluR5 and observed altered basal G protein activation and response to allosteric drugs, but did not report on the oligomeric state. More recently, using a time resolved FRET strategy it was reported that a version of mGluR2 without the extracellular domain was a strict monomer but was still able to activate G proteins when reconstituted in nanodiscs[24]. In contrast, the recently reported crystal structure of the TMD of mGluR1 was arranged in dimers that were produced by an interface between TM1 helices that also involved cholesterol molecules[25]. Finally, much attention has recently been paid to reported heteromers between mGluRs and class A GPCRs, including most notably a complex between mGluR2 and the 5-HT_{2a} receptors[26]. The interface for this interaction has been proposed to primarily involve helices 4 and 5 and indicates that inter-GPCR interactions within the TMD of class C GPCRs are possible[27,28]. It remains to be seen if a similar interface is present in mGluR homodimers.

In addition to questions about the mechanism of homodimer assembly, recent work has indicated that mGluRs can form heteromers[15]. Original biochemical work failed to find evidence for interaction between the closely related mGluR1 and mGluR5 which led to the wide assumption that mGluRs are specific homodimers[17]. However, in a comprehensive study, Doumazane et al[15] used time resolved FRET to show evidence for heteromerization within and between group II and III mGluRs and within group I mGluRs. This was consistent with $G_{i/o}$ coupled mGluRs (Group II and III) being able to assemble with each other, but not with G_q coupled mGluRs (Group I). However, a more recent study used a similar approach and found evidence for interaction between mGluR2 and mGluR5, which argues for coassembly of group I and II mGluRs[29]. Finally, a powerful recent study found biochemical and pharmacological evidence for heteromers between mGluR2 and mGluR4 that may have physiological consequences in corticostriatal synapses[30].

We decided to use single molecule photobleaching assays to more closely determine the mechanism of dimerization of mGluRs and the specific rules of heteromerization in order to resolve discrepancies in the existing literature and to provide a platform for the dissection of the role of oligomerization in GPCR function.

mGluR cooperativity and activation mechanism

In addition to work on the dimerization of mGluRs, there is a wealth of studies on the activation mechanism of mGluRs. However, there has not been a clear consensus on how ligand binding couples to receptor activation. Initial work using radioligand binding observed negative cooperativity of glutamate binding in mGluR1[31]. This raised the question of how binding of ligands to either one or both subunit within a dimer would result in receptor activation. One body of work has argued that binding of glutamate to one subunit can activate mGluRs, but that two

activate more efficiently[32,33]. The same group has further shown that, using subunits with impaired G protein activation, ligand binding to one subunit can either activate its own TMD or cross-activate the adjacent subunit[32]. However, a competing group has argued that in mGluR1 binding of two ligands is required for activation[34] and that an uncoupled LBD can act as a dominant negative to a functional subunit[35]. Most recently, work on mGluR1 and mGluR2 has argued that the ability to activate with one ligand and to cross-activate within a dimer may depend on the G protein subtype involved[36]. In contrast, it has been firmly established that within a $GABA_B$ receptor heterodimer only one subunit binds the agonist, GABA, and the other subunit binds and activates G protein[37,38,39]. We recently showed, using smFRET, that the LBDs of mGluR2 exist in three different conformations which raises the question of which states are populated with binding of 1 vs. 2 subunits (Chapter 4). The challenge in all of the aforementioned studies has been the ability to precisely control ligand binding within a dimer without perturbing the system too drastically. All of these studies have used mutations to lower affinity in one subunit within a dimer in order to produce conditions that favor ligand binding to only the other subunit. However, this is complicated by the fact that a mutated subunit may have a drastically different affinity in the context of a heterodimer with wild type, thus obscuring the actual location of ligand binding. Furthermore, different mutations that alter binding affinity may also alter crucial LBD properties such as basal dynamics or the ability to undergo conformational dynamics. For this reason we sought to use the recently described LimGluRs to approach these key questions in the mGluR field[40]. LimGluRs are light activated mGluRs based on the covalent attachment of a photoswitchable ligand via a substituted cysteine. This photoswitchable tethered ligand (PTL), can rapidly and reversibly agonize or antagonize the subunit to which it is attached in response to different wavelengths of light. Using this system one can photoagonize or antagonize one subunit within an oligomeric protein while leaving the other subunits as wild type and, therefore not disrupt their native properties with mutations. This general approach has recently been used to disentangle the contributions of different subunits within a kainate receptor to produce desensitization[41]. In this study we used LimGluR2 and LimGluR3 to show that there is, indeed, subunit occupancy dependent activation of mGluRs that depends on receptor composition and dimer interface. By more precisely defining how ligand binding produces receptor activation, this work paves the way for a complete understanding of the process by which class C GPCRs allosterically couple a large extracellular domain to eventual G protein activation.

Results:

mGluRs form dimers that are mostly dependent on the ligand binding domain

In order to analyze mGluR oligomerization as a means of further understanding the activation mechanism of class C GPCRs, we turned to the single molecule subunit counting method in Xenopus oocytes. As described in the introduction, this technique allows for the analysis of membrane protein stoichiometry in the plasma membrane of living cells with single molecule precision. The ability to analyze single molecules gives access to statistics that can more accurately reflect the population of receptors than a simple bulk average which is used in techniques like ensemble FRET or western blots.

We expressed mGluR2 with a C-terminal monomeric eGFP and observed individual spots in the plasma membrane of Xenopus oocytes when imaged with TIRF microscopy (Fig. 5.1A). A patch of membrane was imaged until most of the spots had fully bleached. Most mGluR2-GFP spots were fully immobile making it easy to identify single molecules and observe their bleaching. Traces for individual molecules showed unique bleaching patterns with a majority bleaching in two distinct steps (Fig. 5.1B). Approximately 55% of spots bleached in two steps indicating that mGluR2 is, as expected, a dimer (Fig. 5.1C). However, 55% 2 step bleaching is lower than what would be expected for the previously reported GFP maturation rate of 80%[7]. The distribution observed in Fig. 5.1C is more easily fit with a maturation rate of 70% indicating that either GFP maturation is worse than expected in the context of mGluR2 or that there is a subpopulation of monomers that shifts the overall distribution. mGluR2-GFP was fully functional in oocytes as demonstrated by glutamate-mediated activation of GIRK channels. We also tested the subunit stoichiometry of mGluRs from group I (mGluR1 and mGluR5), group II (mGluR3), and group III (mGluR7) and found that all receptors gave bleaching step distributions consistent with dimerization (Fig. S5.1). Interestingly, the group I mGluRs were much more mobile than group II or group III making it more difficult to count them, but perhaps also underlying some physiologically-relevant differences in signaling mechanism.

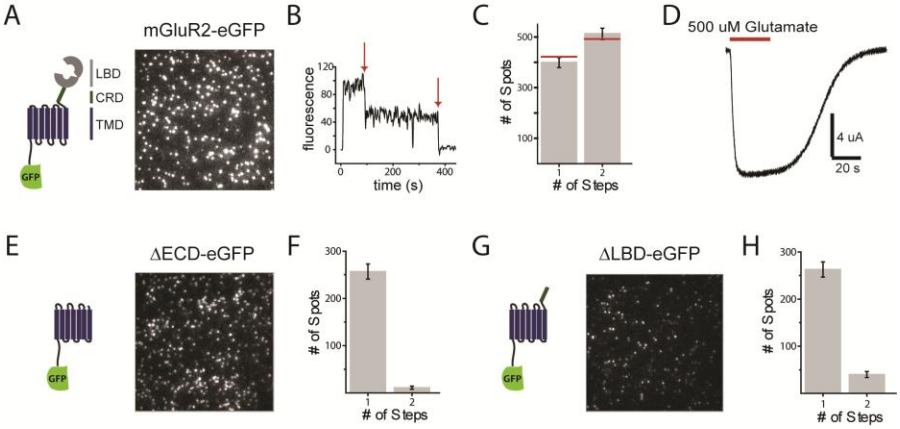

Figure 5.1, mGluR2 is ligand binding domain-dependent dimer in Xenopus oocytes. A) Schematic showing domain structure of mGluR2-eGFP construct and representative image showing expression of single receptors in oocytes. B) Representative trace showing typical 2-step photobleaching of mGluR2-eGFP. C) Distribution of 1 vs. 2 step photobleaching shows dimerization of mGluR2. Red lines indicated the expected distribution for a strict dimer with a 70% GFP maturation rate. D) Representative trace showing that mGluR2-eGFP construct is functional in GIRK current assay. E-H) mGluR2 dimerization is dependent on the LBD. ΔECD (E,F) and ΔLBD (G,H) constructs express in oocytes and show primarily single step photobleaching.

We next wondered which domains of mGluR2 mediate the dimerization observed in oocytes. We either removed the entire ECD (ΔECD-eGFP, Fig. 5.1E) or just the LBD (ΔLBD-eGFP, Fig. 5.1G) and, in both cases, saw a large reduction in the number of spots that bleached in two steps. The distributions for both of these constructs were consistent with full monomerization of the receptor (Fig. 5.1F, H), indicating that dimerization, at least at the low densities used for these experiments, is mediated by the LBDs. Application of negative or positive allosteric modulators, which bind in the TMDs, did not alter the stoichiometry of these constructs (data not shown).

To test our results in a different system we turned to the recently described SiMPull system [42] (Chapter 4). We expressed mGluR2-GFP in HEK 293T cells and then lysed the cells and specifically conjugated receptors to a passivated, antibody-treated surface and imaged single molecules (Fig. 5.2A,B). For the full length mGluR2-GFP we observed a very similar bleaching step pattern that was consistent with mGluR2 maintaining dimerization in this system (Fig. 5.2C). We then tested the ΔECD mGluR2-GFP construct (Fig. 5.2D, E) and saw a distribution that did not consist strictly of one step bleaching (Fig. 5.2F) as observed in oocytes (Fig. 5.1E). There were many spots that showed 2-step bleaching, although the overall distribution fell short of what would be expected for a strict dimer. This result indicates that at the higher concentrations used for SiMPull from HEK 293T cell lysate there is some weak dimerization between TMDs.

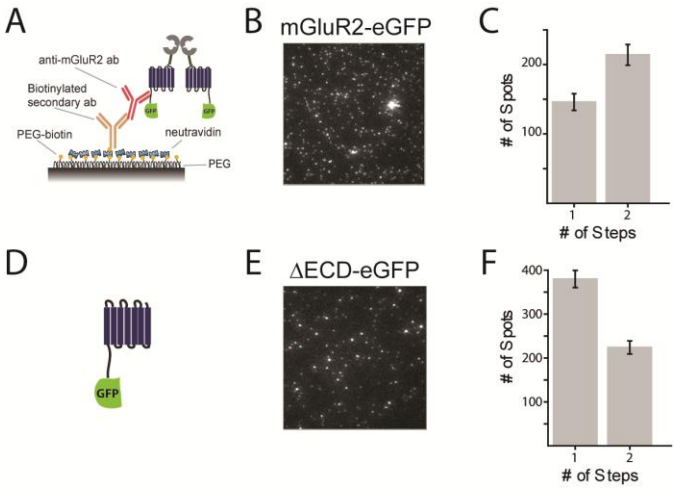

Figure 5.2, mGluR2 is a dimer in lysate from HEK293T cells and ΔECD shows weak dimerization. A) Schematic of pulldown of mGluR2-GFP using a passivated surface and specific antibodies. B) Representative image of surface with mGluR2-GFP. C) Distribution of bleaching steps show clear dimerization of mGluR2-GFP. D) Schematic of ΔECD-GFP construct. E) Representative image of coverslip surface with ΔECD-GFP. F) Distribution of bleaching steps shows many spots with 2-step bleaching but less than expected for a strict dimer.

Dimerization of mGluR2 results in cooperativity that depends on subunit occupancy

Since single molecule subunit counting showed that mGluRs are strict dimers, we next wondered what might be the functional consequences of dimerization. While many studies have addressed this using classical approaches, we turned to the recently described light-activated mGluR2, LimGluR2[40]. This receptor is based on the PTL, D-MAG-0, which covalently attaches to the receptor at position L300C. D-MAG-0 isomerizes between *trans* and *cis* in response to visible and near UV light, respectively (Fig. 5.3A). In the *cis*, but not the *trans* conformation, D-MAG-0 is able to agonize mGluR2 in a manner very similar to glutamate (Fig. 5.1B). As opposed to classical soluble agonists, PTLs offer the advantages of rapid control of ligand binding and unbinding and specific liganding of only subunits containing the cysteine substitution. It was previously shown that photoactivation of LimGluR2 can reach levels as high as 60% relative to saturating glutamate. Evidence points to the discrepancy in activation between

D-MAG-0 and glutamate as due to partial labeling of cysteines by the chemical photoswitch rather than partial agonism. When coexpressed with GIRK channels in HEK cells, LimGluR2 showed 380 nm induced activation (Fig. 5.3C). When LimGluR2 was photoactivated in the presence of subsaturating glutamate we observed a robust increase in photocurrent amplitude (Fig. 5.3C). This photocurrent potentiation was most strong around or just below the EC_{50} for glutamate for both wild type and low affinity variants of LimGluR2 (Fig. S5.2A). When photocurrent potentiation was measured in the presence of 10 μM glutamate there was a clear dependence on photoswitch efficiency which is a measure of D-MAG-0 labeling efficiency (Fig. 5.3D). In receptors where photocurrent was small compared with saturating glutamate (i.e. labeling was in a small percentage of subunits), the potentiation of photocurrent by 10 μM glutamate was largest. In addition, photoactivation in the presence of 10 μM glutamate was significantly faster that photoactivation in the absence of glutamate, further indicating some form of cooperativity (Fig. 5.3E). The simplest interpretation of this data is depicted in Fig. 5.3F. In LimGluR2 dimers where only one subunit is conjugated to D-MAG-0 photoactivation is very small or non-existent. However, at low glutamate concentrations the chance of the adjacent subunit being liganded increases which, when paired with photoactivation of the first subunit, results in a much larger activation (Fig. 5.3G). This model predicts that the relationship between number of subunits bound and activation level should be nonlinear (i.e. 2 subunits > (1 subunit x 2)). We sought to test the precise difference between ligand binding in 1 vs. 2 subunits to gain further insight into the cooperative activation of mGluRs and to resolve a long-standing debate in the mGluR field.

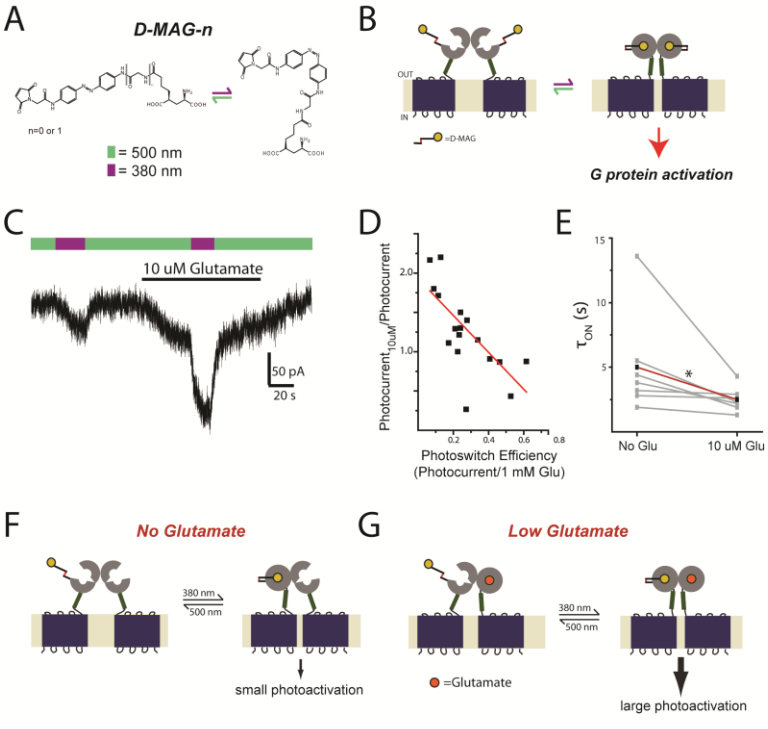

Figure 5.3, LimGluR2 demonstrates cooperativity in activation of GIRK currents. A) Chemical structure of D-MAG PTL. B) Schematic showing mechanism of photoactivation of LimGluR2 by D-MAG-0. C) Representative trace showing potentiation of photocurrent by 10 μM glutamate. D) Plot showing dependence on labeling efficiency for photocurrent potentiation in individual cells. E) Activation kinetics for individual cells in the absence or presence of 10 μM glutamate show a consistent decrease in τ_{ON}. Red line indicates the average of all cells. * indicates statistical significance (Paired T Test; $P<0.05$). F-G) Schematic showing interpretation of photoswitch potentiation. In partially labeled subunits weak or no photoactivation is observed (F), but in the presence of subsaturating glutamate photocurrents are larger due to non-linear coupling between ligands bound and activation level (G).

We next sought a means of testing how mGluR2 activation would proceed when either one or both subunits are bound to an agonist. PTLs provide ideal tools for such an experiment

because they can targeted unambiguously to specific subunits based on the presence of an engineered cysteine. Furthermore, as opposed to soluble ligand experiments which require mutations to one subunit to drastically lower affinity and potentially disrupt its other native properties, the unliganded subunit may be wild-type since there is no chance of it binding an agonist which is covalently tethered to the other subunit. In order to target D-MAG-0 to one or both subunits within an mGluR2 dimer we produced tandem dimers of mGluR2 that are connected by a transmembrane domain consisting of the β subunit of the Na/K ATPase (Fig. S5.3A). This approach has been previously reported for opsin tandem dimers [43]. These tandem dimers showed the expected molecular weight in western blots (Fig. S5.3B), the expected topology based on antibody staining of an extracellular GFP (Fig. S5.3C, D), and single molecule photobleaching consistent with the expected assembly in both HEK cell lysate (Fig. S5.3G,H) and oocytes (Fig. S5.3E, F). When the L300C mutation was introduced to one of the two subunits, very weak photoactivation was observed relative to saturating glutamate (Fig. 5.4A). Some cells showed no photocurrent but the average photoswitch efficiency was 8.4 ± 2.4 %. When both subunits were mutated to L300C, photoactivation showed a very similar efficiency to wild type LimGluR2 (Fig. 5.4B; 51.1 ± 6.2 %.) which is more than 5x larger than photoactivation with just one subunit. Fig. 5.4C summarizes the photoswitch efficiency for liganding of 0 vs. 1 vs. 2 subunits. Importantly, in the absence of introduced cysteines, no photocurrent was observed. Also, whether the location of the introduced cysteine on the first or second subunit did not alter photoswitch efficiency. These experiments show that, as predicted, there is a non-linear relationship between number of subunits bound to the receptor and level of activation. We next turned back to the dimerization of the receptor to look for clues about how crosstalk between subunits may mediate this strong cooperativity.

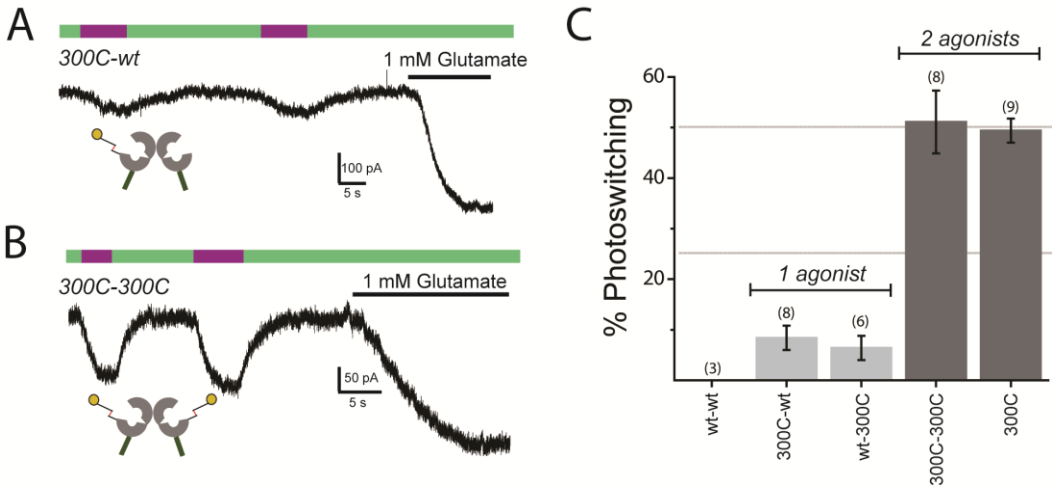

Figure 5.4, LimGluR2 tandem dimers show non-linear activation when 1 vs. 2 subunits are liganded. A-B) Photoactivation of LimGluR2 in tandem dimers when 1 (A) or 2 (B) subunits are labeled by D-MAG-0 show large difference in photoswitch efficiency relative to saturating glutamate. C) Summary of photoswitch efficiency for labeling of 0, 1, or 2 subunits with D-MAG-0. Dashed lines indicate expected values for linear coupling between ligand binding and receptor activation. % Photoswitching was defined as (photocurrent/1 mM glutamate current). The number of cells tested for each condition is shown in parentheses.

Further insight into the mechanism of mGluR2 dimerization

Since we showed that mGluR dimerization is primarily mediated by the LBD, with some weaker interactions in the TMD, we decided to look more closely at the specific interactions between the mGluR2 LBDs. Early biochemical studies on mGluR stoichiometry identified a conserved cysteine that was required for dimerization of mGluRs in a denaturing gel [17]. This has been an oft-cited residue that is believed to be important for dimerization, but it has been difficult to fully determine its role because few measurements have been made with this residue mutated in cells and since this region was not resolved in any of the LBD crystal structures. We mutated the aligned cysteine of mGluR2 to produce mGluR2-C121A and expressed a GFP-tagged version in oocytes (Fig. 5.5A). Surprisingly, we observed many spots with 2-step photobleaching. However, the overall distribution of photobleaching steps fell short of a strict dimer if 70% GFP maturation is assumed. This result indicates that dimerization is only partially mediated by an intersubunit cysteine, and that non-covalent interactions are likely major mediators of dimerization. Consistent with this, the amount of 2- step photobleaching observed for C121A was density dependent (Fig. 5.5C) indicating that there is some reversible non-covalent interactions involved in dimerization. Furthermore, treatment with 10 mM DTT was unable to decrease dimerization of mGluR2 indicating that once a dimer is formed, the non-covalent interactions are sufficient to keep the dimer together even in the absence of the intersubunit disulfide.

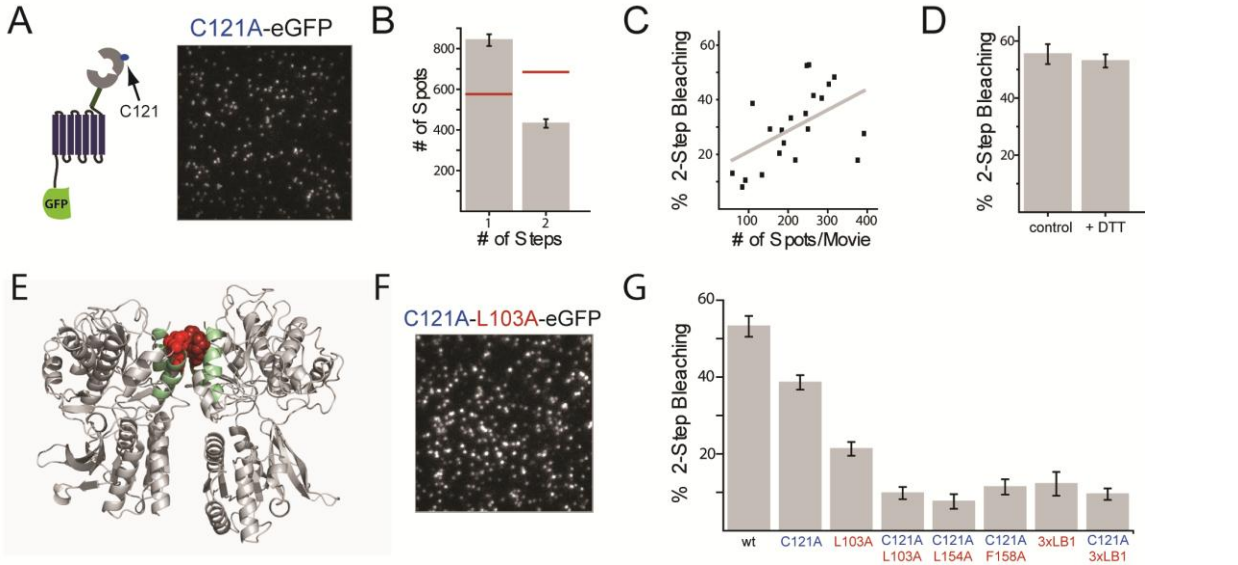

Figure 5.5, Mutations at the LB1 interface alter mGluR2 dimerization. A-B) Mutation of cysteine 121, which is believed to produce an intersubunit disulfide bridge leads to normal expression (A) but a decreased population of 2-step photobleaching (B). Red lines show expected distribution for a strict dimer with 70% GFP maturation. C) Density-dependence of dimerization of C121A. Each spot represents the value for one movie. The total # of spots includes both countable and uncountable D) Dimerization of mGluR2-GFP is not altered by incubation with 10 mM DTT. Each bar shows the average of >3 cells. E) Mutations to LB1 hydrophobic interface mapped onto mGluR1 LBD crystal structure (PDB: 1EWK). Mint green shows helices B and C and shades of red show the side chains of analogous residues to L103, L154, and F158 in each subunit. F) Mutation of residues at the hydrophobic interface and the intersubunit cysteine do not prevent expression of mGluR2. G) Summary of subunit stoichiometry for LBD interface mutants. Each bar is an average for $n \geq 2$ cells per condition.

In crystal structures of mGluR LBDs a common interface is observed between the upper lobes of the LBD (LB1) consisting of helices B and C [21](Fig. 5.5E). This interface is composed of hydrophobic residues and maintains a close association despite a large rotation between "Relaxed" and "Active" states. We individually mutated the three conserved residues L103 (which aligns with I120 of mGluR1), L154, and F158 to alanine either alone or in tandem with C121A and found a clear effect on dimerization. Mutation of any of the LB1 interface residues decreased dimerization of mGluR2 (Fig. 5.5F, G). When combined, despite normal expression and the presence of C121, these three mutations ("3xLB1) produced a photobleaching pattern consistent with monomerization of mGluR2. This result indicates that there is a hydrophobic interface between LB1 domains within a dimer that is weakened by mutation of L103, L154, and F157 to alanine.

Given the clear effects on mGluR2 dimerization, we wondered if any of the mutations would maintain the ability to activate G proteins. Surprisingly, all mutations tested, including "3xLB1" were able to mediate glutamate-induced GIRK currents in Xenopus oocytes (data not shown). It is important to note that for GIRK current measurements ~10x as much RNA must be injected into oocytes meaning that the functional measurements are done with receptors at a much higher density than subunit counting. The ability of LB1 mutants to function indicates that either monomeric full length mGluRs are still functional, which would contradict recent studies[24], or at higher densities mutants are able to dimerize. To test this we performed SiMPuLL experiments with expression of mGluR2-C121A-GFP and mGluR2-3xLB1 in HEK 293T cells. We found that both constructs exhibited photobleaching consistent with dimerization (Fig. S5.4). This finding argues for a shift in the density-dependence of dimerization for these mutants, rather than a complete monomerization.

We next wondered if mutations to either the intersubunit disulfide bridge (C121A) or the hydrophobic LB1 interface ("3xLB1") would alter receptor function in some way. We first turned to the intersubunit LBD FRET assay as a measure of the conformational changes between subunits using dye-labeled N-terminal SNAP and CLIP domains (Chapter IV). Consistent with the dimerization observed in SimPuLL (Fig. S5.4) both C121A and 3xLB1 showed clear FRET between subunits. We performed glutamate titrations and found that both constructs had altered glutamate sensitivities (Fig. 5.6A). Mutation of C121, and the associated disruption of the intersubunit disulfide bond, decreased the glutamate EC_{50}. On the other hand, mutation 3xLB1, which weakens the hydrophobic LB1 interface, resulted in an increased apparent affinity. Similar glutamate sensitivity shifts were observed when each construct was tested in a GIRK current assay (Fig. 5.6B). These results indicate that the dual dimer interfaces have distinct effects on receptor activation. Future work with smFRET and cooperativity measurements in a tandem dimer should provide further insight into the functional roles of the intersubunit disulfide bridge and the hydrophobic dimer interface.

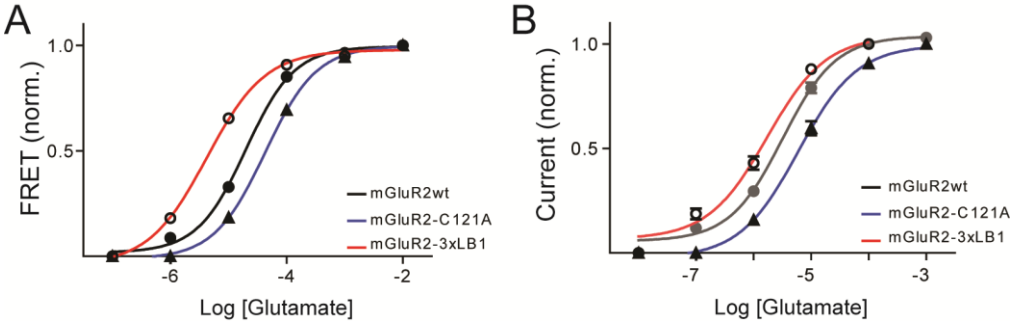

Figure 5.6, Mutations at the LB1 interface alter receptor conformational changes and activation. A) Glutamate titrations for mGluR2 LBD FRET sensors show apparent increase in affinity for 3xLB1 mutant (EC_{50}=4.2± 0.5μM) and apparent decrease in affinity for C121A mutant (EC_{50}=43± 3.3μM) compared to wild type (EC_{50}=20± 2.8μM). B) A similar relative affinity shift is observed when glutamate titrations are performed with a GIRK current functional assay. The EC50 for mGluR2wt, C121A, and 3xLB1 was 3.2 ± 0.3μM, 6.0 ± 0.7μM, and 1.7 ± 0.3μM, respectively.

mGluR2 forms intragroup and intergroup heterodimers

Having gained a clearer idea of how mGluRs form dimers via two distinct LBD interfaces, and perhaps a weaker TMD interface, we wondered if the single molecule photobleaching assays could provide some insight into the potential heteromerization of mGluR2. While early biochemical work argued against the formation of heteromers, recent work has indicated that there may be a variety of heteromers that can form within the mGluR family. To test this we co-expressed mGluR2-GFP with another mGluR, in its untagged form, at a ratio of 1:10. The rationale was that if a heteromer forms, the untagged subunit will coassemble with the tagged subunit and decrease the amount of spots that show two step photobleaching. As opposed to when expressed alone (Fig. 5.7A), when untagged mGluR3 was coexpressed, a decrease in 2-step photobleaching of mGluR2-eGFP was observed (Fig. 5.7B). Similar effects were observed when untagged mGluR2 or mGluR7 were coexpressed, but not when mGluR1 or mGluR5 were coexpressed (Fig. 5.7C). These experiments show that mGluR2 is able to coassemble with other group II and group III mGluRs, but not group I mGluRs, as was observed in recent trFRET studies[15].

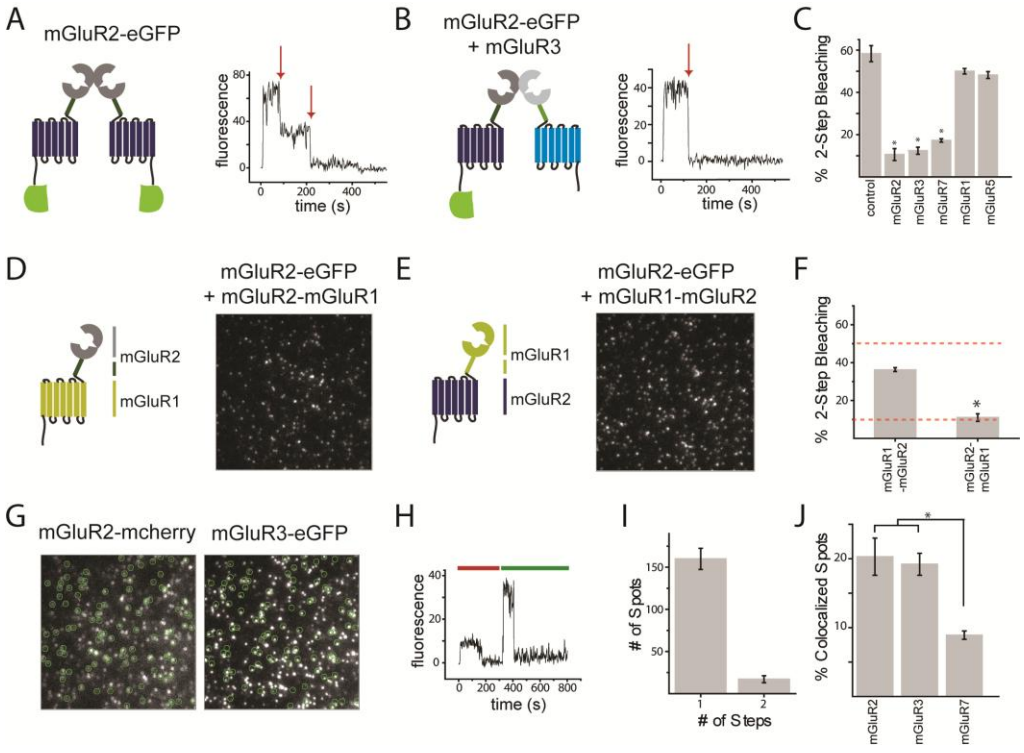

Figure 5.7, Heteromerization of mGluR2. A-B) Unlike expression by itself (A), coexpression with mGluR3 reduces 2-step photobleaching of mGluR2-GFP (B). (C) Summary of photobleaching of mGluR2-GFP in the presence of a number of untagged mGluRs shows specific interaction with mGluR2, 3, and 7 but not 1 and 5. D-F) Chimeras between mGluR2 and mGluR1 produce altered dimerization of mGluR2-GFP. 2-step mGluR2-GFP bleaching is decreased more strongly by a chimera between the ECD of mGluR2 and the TMD of mGluR1 (D) rather than the opposite (E). F) Summary of mGluR2-GFP in the presence of coexpressed chimeras. Red dashed lines show the values for mGluR2-GFP co-expressed with mGluR2 (lower) or mGluR1 (upper) from (C). (G) Colocalization between mGluR2-mcherry and mGluR3-eGFP. Colocalized spots are circled. Representative photobleaching trace for a colocalized spot between mGluR2-mcherry and mGluR3-eGFP. I) Summary of photobleaching steps for mGluR3-GFP in colocalized spots with mGluR2-mcherry. J) Average colocalization across all movies for mGluR2-mcherry with mGluR2, 3, and 7. * indicates statistical significance (unpaired T test, $P<0.05$).

We next wondered if we could identify how mGluR2 is able to heteromerize with some mGluRs but not others. In order to address this question, we made chimeras between mGluR1 and mGluR2 that contained the ECD of one receptor and the TMD of the other (Fig. 5.7D, E). Both of these constructs photobleached as dimers when GFP-tagged and expressed alone (Fig. S5.5). We then coexpressed untagged versions of either chimera with mGluR2-GFP and found that the mGluR2-mGluR1 chimera induced a larger decrease in 2-step photobleaching of mGluR2 (Fig. 5.7F). This result indicates that the specificity of heteromerization of mGluRs is primarily mediated by specificity in the interactions at the ECD and likely the LBDs. However, in the presence of either chimera mGluR2 did not fully photobleach as a dimer, which might mean that there is also some weak interaction between mGluR2 and mGluR1-mGluR2. This would be consistent with the finding that mGluRs are capable of some TMD-TMD interactions that can effect dimerization.

After establishing that mGluR2 can undergo both intragroup and intergroup heteromerization we wondered if such heteromers were strict dimers and if mGluR2 had any subtype preference. To test this we coexpressed mGluR2 with a C-terminal red fluorescent protein (mcherry) along with a GFP-tagged version of mGluR2, 3, or 7. When mGluR2-mCherry was coexpressed either with mGluR2-GFP or mGluR3-GFP many spots were identified in both the red and green channels that were colocalized within a diffraction-limited spot (Fig. 5.6G). Sequential photobleaching of the red and green channels showed single step bleaching for both subunits indicating that mGluR2/3 heteromers are strict dimers (Fig. 5.7H, I). A similar percentage of spots were colocalized when mGluR2-mcherry was coexpressed with mGluR2-GFP or mGluR3-GFP, but significantly less colocalized spots were observed when mGluR7-GFP was co-expressed (Fig. 5.7J). This result shows that, at least at the low expression densities used for single molecule colocalization, mGluR2 has no preference within group II but a preference for group II over group III.

We next wondered if the general heteromerization rules we observed at low densities in oocytes were maintained at higher densities in HEK cell lysate. Using SiMPull we saw that untagged mGluR2 was able to pulldown mGluR3-GFP but not mGluR1-GFP (Fig. S5.6). This agrees with the lack of crosstalk between mGluR2 and mGluR1 that was observed in oocytes (Fig. 5.7C). Given the prevalence of mGluR2/3 heterodimers in both oocytes and HEK cells, and the surprisingly different properties previously observed between mGluR2 and mGluR3 homodimers (Chapter 4), we decided to look more closely at this unique heteromeric GPCR.

mGluR2/3 heterodimers show unique activation properties

Since mGluR2 and mGluR3 readily heterodimerize heterologously (Fig. 5.7, S5.6) and have overlapping native expression patterns [44] that make them likely candidates for *in vivo* heteromerization, we decided to characterize the signaling properties of mGluR2/3 heterodimers. We first wondered if we could find functional evidence for their coassembly in mammalian cells. This would be very difficult classically because of the paucity of ligands that distinguish between the two subtypes. Even in cases where there are drugs that can distinguish between the two subtypes, it is dangerous to assume that they will work precisely as expected in a heteromeric receptor. To remove any ambiguity associated with soluble drugs we turned to LimGluR2 and LimGluR3[40]. We introduced the mutation F756D, which prevents G protein coupling[45], to LimGluR2 and saw no photocurrents when coexpressed with GIRK channels in HEK 293T cells (Fig. 5.9A). However, when mGluR2wt was co-expressed a modest photocurrent was observed indicating that cross-activation within a dimer can occur in mGluR2 (Fig. 5.9B). This agrees with previous work but provides less ambiguity about the location of bound agonists and gives more confidence in the interpretation about cross activation[36]. When mGluR3wt was co-expressed a clear photocurrent was also observed (Fig 5.9C) which indicates that mGluR2 and mGluR3 form functional dimers and are able to cross-activate. Attempts to photoactivate mGluR2wt with LimGluR3-F768D (the analog to F756D) were inconclusive because of poor expression of the LimGluR3 mutant.

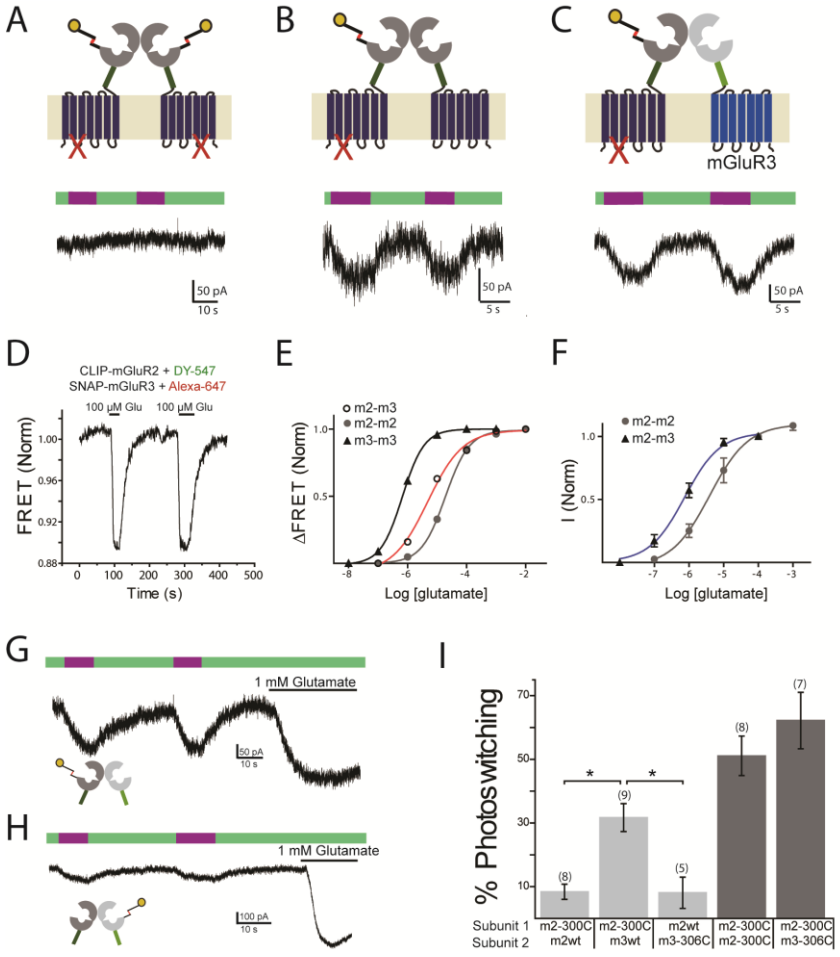

Figure 5.9, Functional mGluR2/3 heterodimers show cross-activation, altered glutamate affinity, and assymetrical cooperativity. A-C) Cross activation within group II mGluR dimers. LimGluR2-F756D is unable to activate G proteins (A) but is able to cross-activate within a dimer when it coassembles with mGluR2wt (B) or mGluR3 (C). D) CLIP-mGluR2 and SNAP-mGluR2 show FRET when labeled with donor and acceptor, respectively, that is decreased by glutamate activation. (E, F) mGluR2/3 heterodimers shown an intermediate glutamate affinity compared to mGluR2 and mGluR3 homodimers when measured with either intersubunit FRET (E) or tandem dimer GIRK activation (F). G-I) mGluR2/3 heterodimers show altered subunit occupancy-dependent activation compared to mGluR2 homodimers. MAG conjugation to mGluR2 produces robust photocurrents in mGluR2/3 heterodimers (G), but MAG conjugation to just mGluR3 produces very weak photocurrent. I) Summary og photoswitch efficiency (relative to 1 mM) for all conditions tested. * indicates statistical significance (Unpaired T test, $P<0.05$). The numbers of cells tested for each condition are shown in parentheses.

We next turned to the previously discussed inter-LBD FRET assay to measure specifically from heterodimers and determine their apparent glutamate affinity. A clear FRET signal was observed between CLIP-mGluR2 and SNAP-mGluR3 that was reversibly decreased by application of glutamate (Fig. 5.9D). When a full glutamate titration was performed, mGluR2/3 heterodimers had intermediate glutamate sensitivity when compared to the higher affinity mGluR3 and the lower affinity mGluR2 (Fig. 5.9E). We also examined the sensitivity of mGluR2/3 heterodimers to mGluR2-specific allosteric drugs and found weak sensitivity to both NAMs and PAMs (Fig. S5.7)

To probe the activation properties of mGluR2/3 more closely we made tandem dimers between mGluR2 and mGluR3 based on the same design used for mGluR2 tandem dimers (Fig. 5.3). mGluR2/3 tandem dimers were able to activate GIRK currents in HEK cells and showed an increased apparent affinity when compared with mGluR2 tandem dimers (Fig. 5.9F). We then turned to the cooperativity assay previously used to show that 1 ligand activates to a level of ~20% relative to 2 in mGluR2. Given that LimGluR3 shows increased photoswitch efficiency compared to mGluR2 (80% vs. 50%) and mGluR3 shows enhanced basal dynamics in smFRET, we wondered how photoswitching of mGluR2 or mGluR3 within a heterodimer would work. We introduced a cysteine for MAG conjugation to the mGluR2 subunit within a tandem heterodimer and saw robust photocurrents that were much more efficient than the photocurrents observed when only one subunit was activated within an mGluR2 dimer (Fig. 5.9G). This result told us that the enhanced photoagonism in LimGluR3 compared to LimGluR2 is probably not due to enhanced labeling, but rather due to enhanced activation of partially labeled receptors. Given the large single subunit activation observed when mGluR2 was agonized within mGluR2/3 we wondered if agonizing just mGluR3 would also give a large photoactivation. Surprisingly, when a cysteine was introduced only to the mGluR3 subunit, the photoactivation of the mGluR2/3 heterodimer was weaker than the reverse experiments (Fig. 5.9H). Figure 5.9I summarizes the photoswitch efficiency for all of the combinations tested. Most notably, there is an asymmetry within the mGluR2/3 heterodimer where activation of mGluR2 gives larger currents than mGluR3. Based on the larger photoactivation of LimGluR3 relative to LimGluR2 this indicates that the opposite subunit within a dimer determines the efficacy of one subunit. Also, maximal photoactivation when both mGluR2 and mGluR3 were labeled with D-MAG-0 showed a modest decrease compared to mGluR2 to a level intermediate between LimGluR2 and LimGluR3 (Fig. 5.9H).

Previous results have shown that mGluR3 displays prominent basal smFRET dynamics that result in basal receptor activity (Chapter 4). We showed that these basal dynamics are reduced by the mutation S152D which also abolishes Ca^{2+} sensitivity. We wondered if these

basal dynamics are the molecular basis of the enhanced photoactivation of mGluR2/3 heterodimers by liganding of just the mGluR2 subunit. As expected, when we introduced the mutation S152D to the mGluR3 subunit of a mGluR2/3 tandem dimer we saw reduced photoactivation by the mGluR2 subunit (Fig. 5.10). Consistent with this, LimGluR3-S152D showed reduced photoswitch efficiency relative to LimGluR3, indicating that the basal dynamics and Ca2+ sensitivity of mGluR3 is a major factor in its enhanced photoswitch efficiency compared to mGluR3. Finally, this result implies that mGluR2/3 heterodimers likely display basal activity, unlike mGluR2 homodimers. Future work will be needed to test this and to see if this results in altered kinetics for heterodimers compared to homodimers.

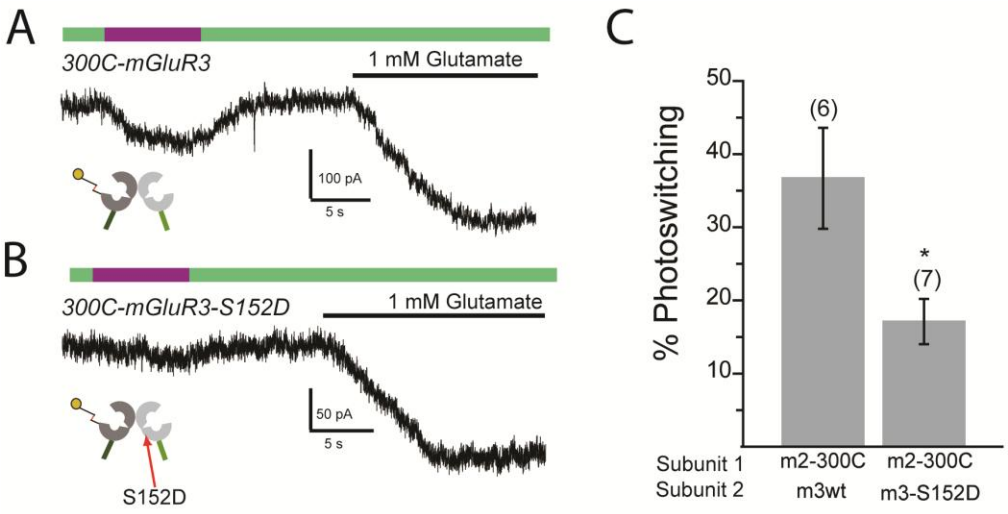

Figure 5.10, Mutation S152D, which removes mGluR3 basal dynamics, decreases single subunit activation of mGluR2/3 heterodimers. A,B) Reprsentative traces showing photoactivation of mGluR2 within an mGluR2/3 tandem heterodimer in the absence (A) or presence (B) of mutation S152D on the mGluR3 subunit. C) Summary of photoswitch efficiency for both conditions. * indicates statistical significance (unpaired T test, $P<0.05$). The number of cells tested for each condition is shown in parentheses.

Discussion:

Mechanism of dimerization of mGluRs

This work provides some clear insight into the mechanism by which mGluRs assemble. We show that group I, II, and III mGluRs are strict dimers when measured at the single molecule level in the plasma membrane of living Xenopus oocytes. Notably, a drastic difference in mobility was observed between group II/III and group I mGluRs although the functional consequences of this were unexplored. Using mGluR2 as a model mGluR, we found that dimerization is mediated by a number of interactions. The major determinant of dimerization is the clamshell LBD, which is stabilized as a dimer by an intersubunit disulfide bridge and a hydrophobic interface formed by helices B and C of the upper lobe (LB1). However, breaking these interactions disrupts dimerization at low densities but does not prevent receptors from forming dimers when expressed at high densities where they are functional. This indicates that the dimer interface is extensive and that dimerization natively may also be density dependent, even for wild type receptors. Furthermore, there appears to be an interface between TMDs of mGluR2 that is only evident at high expression levels. Further experiments which test the dimer interfaces proposed in crystal structures[25] or class C-class A GPCR heteromers[28] will be needed to fully understand this interaction. This TMD-TMD interaction may be important functionally for mediating interactions between subunits or as a weak contributor to dimerization specificity.

In addition to further elucidating the dimerization interfaces of mGluRs, we have shown a specific heterodimerization profile for mGluR2. mGluR2 is able to heterodimerize with the other group II or group III mGluRs, which share a common target of $G_{i/o}$ proteins, but not with the group I mGluRs, which primarily couple to G_q proteins. Using the precision afforded by single molecule colocalization, we also show that mGluR2 preferentially heterodimerizes with mGluR3 over mGluR7. Furthermore, mGluR2 shows no preference for homodimerization over heterodimerization with mGluR3, indicating that mGluR2/3 heterodimers may be a prevalent species *in vivo*. Future work may be able to use the SiMpull system to assay native systems for mGluR2/3 heterodimers by using fluorescently tagged antibodies. Preliminary results using untagged, heterologously expressed receptors in HEK cells have demonstrated the feasibility of this approach.

Mechanism of cooperative activation

While mapping the mGluR2 dimer interface has led to further insight into the structural interactions involved, cooperativity experiments using the PTL D-MAG-0 clearly demonstrated some of the consequences of dimerization. We have clearly shown, that when agonist binds to one subunit within an mGluR2 dimer there is clear, but weak activation. When two agonists are able to bind, however, activation is 5-6x larger than one agonist, which shows a strong cooperative effect. Due to the level of control afforded by D-MAG-0, this result is the clearest demonstration of the subunit occupancy dependent activation of mGluRs yet. Since *cis*-D-MAG-0 exists in a local concentration that may be viewed as saturating we are able to interpret these experiments as measuring receptor activation cooperativity rather than binding cooperativity. This distinction allows for a clearer interpretation of the experiment than those that rely on soluble ligands and mutations that disrupt ligand binding (and potentially also clamshell closure

or dynamics). Future experiments will be needed to compare the kinetics of activation for liganding 1 vs. 2 subunits, but experiments in figure 3 indicate that there is also an acceleration of activation when 2 subunits are bound compared to 1.

The clear demonstration of cooperativity raises the question of how subunits are able to interact and affect the activation efficacy of the other. Some clues came from examining the LBD dimer interface. Mutations that disrupted the ability to form an intersubunit disulfide bridge (C121A) decreased the apparent affinity for glutamate. This may indicate that this cross link provides a means for communicating between the two subunits that allows the active state to more easily be reached. Preliminary smFRET experiments with the C121A mutant were consistent with this idea by showing that this construct was not able to fully populate the low FRET peak as well as wild type mGluR2 in the presence of saturating glutamate. On the other hand, mutations that weakened the hydrophobic LB1 interface increased the apparent affinity of mGluR2. This may indicate that this interface plays a role in stabilizing the inactive state of the receptor in the absence of bound glutamate. Future smFRET experiments and tandem dimer cooperativity experiments will be needed to test these ideas about the different extracellular dimer interfaces.

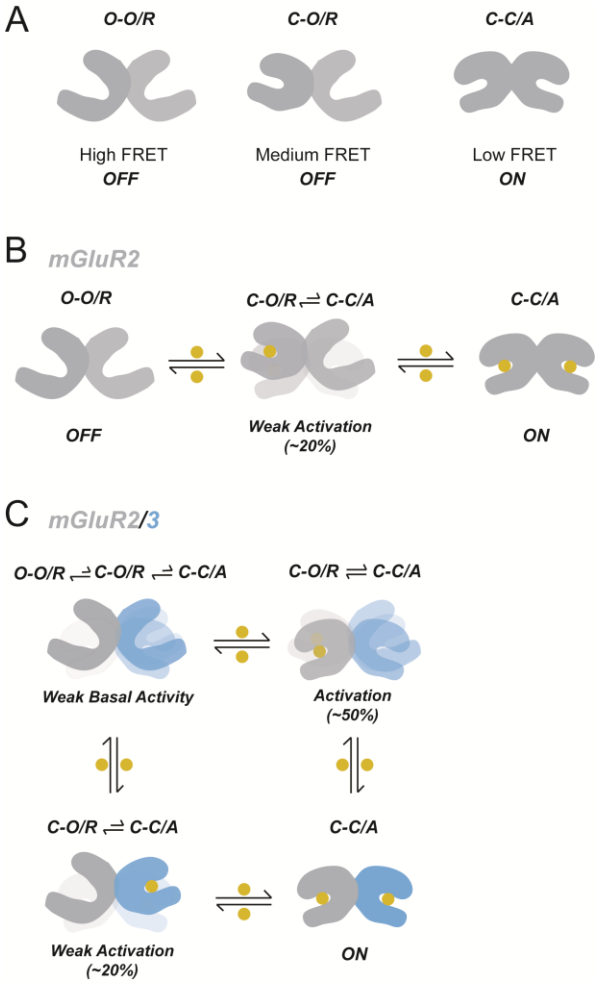

Figure 5.11, Model of cooperative activation of group II mGluRs. A) Three-state structural model previously proposed based on smFRET experiments. O and C represent open and closed states of each LBD while R and A represent relaxed and active intersubunit orientiations. The A state corresponds to a rotation that bring the LB2 domains closer together which facilitates downstream conformational changes that activate G proteins. B) Model of activation of mGluR2 homodimers by 1 or 2 ligands. At rest mGluR2 shows basically no dynamics and is in the relaxed state. When 1 ligand binds the receptor mainly goes to the C-O/R state but occasionally visits the C-C/A state (shown in light gray), which leads to some weak activation. When a second ligand bounds the active state is fully stabilized which leads to full activation. C) Model of activation of mGluR2/3 hterodimers. In the absence of agonist there is clear basal dynamics in the mGluR3 subunit that should induce enough dynamics in mGluR2 to produce some weak basal activity. When ligand binds to mGluR2 (top right), this combines with the basal fluctations of the mGluR3 subunit to produce frequent population of the active state and moderate receptor activation. When ligand binds to the mGluR3 subunit, the lack of basal dynamics of the mGluR2 subunit leads to weak activation that is similar to what is seen in mGluR2 homodimers. When ligand binds to both subunits the active state is fully stabilized and full activation is observed.

The most revealing cooperativity experiments have been those on mGluR2/3 heterodimers. These tandem dimers revealed a surprising asymmetry where agonizing only the mGluR2 subunit provided stronger activation than only agonizing the mGluR3 subunit. Initial smFRET experiments indicated that, like mGluR3 homodimers, mGluR2/3 heterodimers show enhanced basal dynamics compared to mGluR2 homodimers. The assymetrical photoswitching indicates that these dynamics are not distributed across the heterodimer, but rather limited to the mGluR3 subunit which, in turn, leads to enhanced activation via the mGluR2 subunit. Fig 5.11 shows a model of homodimer and heterodimer activation based on these results and the previously reported smFRET results (Chapter 4). In this model there are three structural states, based on the three FRET peaks observed in smFRET, where only one state represents the active state of the receptor (Fig. 5.11A). In this model, downstream activation of the receptor requires both subunits to close and facilitate the reorientation of the dimer interface from "relaxed" to "active". This makes it necessary that when one ligand is bound the other subunit can occasionally close and lead to weak activation (Fig 5.11B). In the mGluR2/3 heterodimer the enhanced basal dynamics, which are limited to the mGluR3 subunit, allow for the active state to be visited more when ligand is bound in mGluR2. In the reverse case, when mGluR3 clamshell closure is stabilized by an agonist, the weak dynamics of mGluR2 prevent much population of the active state and lead to an activation level that is similar to what is seen in mGluR2 homodimers. In the future smFRET experiments combined with photoswitching of one or both subunits will be the ultimate test of this model. Furthermore, this model predicts that in an mGluR3 homodimer activation of 1 subunit should be similar to activation of just the mGluR2 subunit in the heterodimer, because of the dynamics of the adjacent subunit. Initial attempts to test this have failed due to poor expression of mGluR3 tandem dimers.

While the work presented here has focused on interactions in the ligand binding domain, it will be interesting to understand how the inter-LBD conformational changes result in G protein activation. The simplest model is that once the active state is reached in the LBDs, the CRDs and/or the TMDs are brought in closer proximity which facilitates a conformational change in the TMDs that increases the affinity for G proteins. The precise mechanism of this is fairly hazy and will require a concerted effort to elucidate. The tandem dimer approach presented here should be a useful platform on which to add further perturbations to individual subunits to probe this mechanism. We show here that allosteric drugs that only target the mGluR2 subunit are able to elicit weak effects of mGluR2 heterodimers when assayed with LBD FRET. Experiment applying these drugs to mGluR2/3 tandem dimers that are liganded at mGluR2 or 3, or have G protein binding mutations in just one subunit, should be very valuable for integrating the LBD model into the framework of the entire receptor.

Overall this study shows the clear homo and heterodimerization of mGluRs, a model family of class C GPCRs. We show that dimerization produces interesting cooperative effects that can be significantly different between closely related receptors. Future work will be neded to apply these molecular biophysical differences to gain insight into the physiological differences between these closely related species. The techniques applied in this work should provide a working model for the means of study of oligomeric interactions in GPCRs.

Methods:

Single molecule subunit counting in Xenopus oocytes

Subunit counting was performed as previously described[7]. mGluR constructs were tagged with a C-terminal monomeric eGFP via a flexible 16 aa linker (TSGGSGGSRGSGGSGG). RNA for the construct of interest was injected in the evening and ~18-24 hours cells were imaged using a 100x objective on a TIRF microscope. Movies were acquired at 1 Hz using Andor software. Analysis was performed manually using house made software. Colocalization was performed by sequentially imaging the red channel and then the green channel. Red fluorescent proteins were fully bleached before imaging the green channel to prevent FRET between the two fluorophores. Colocalization was calculated as (# of colocalized spots/total spots). All conditions were tested in $\geq$ 2 separate injections.

Single molecule pulldown and subunit counting from HEK 293T cell lysate

Single molecule pulldown was performed as previously described (Chapter 4). Subunit counting with HEK 293T cell lysate was performed using the same system as Xenopus oocytes and analysis was performed in the same way. Gene expression was performed using Lipofectamine 2000 as previous described (Chapters 2, 3)

Ensemble FRET measurements

FRET measurements were performed as described in Chapter 4.

Tandem dimer constructs

Tandem dimers were based on previously reported tandem dimers [43]. The same linker previously used to connect eGFP to the C-terminus of mGluRs was also used as the linker between GFP and the β subunit of the Na/K ATPase, and the linker between the β subunit of the Na/K ATPase and the second GFP, and between the second GFP and the second mGluR subunit. The signal sequence of the second mGluR subunit was removed to prevent cleavage of the tandem dimer as confirmed by western blot.

Electrophysiology

Electrophysiology was performed as previously descibred (Chapter 2, 3).

References:

1 George, S. R., O'Dowd, B. F. & Lee, S. P. G-protein-coupled receptor oligomerization and its potential for drug discovery. *Nat Rev Drug Discov* **1**, 808-820, doi:10.1038/nrd913nrd913 [pii] (2002).

2 Terrillon, S. & Bouvier, M. Roles of G-protein-coupled receptor dimerization. *EMBO Rep* **5**, 30-34, doi:10.1038/sj.embor.74000527400052 [pii] (2004).

3 Gurevich, V. V. & Gurevich, E. V. GPCR monomers and oligomers: it takes all kinds. *Trends Neurosci* **31**, 74-81, doi:10.1016/j.tins.2007.11.007S0166-2236(07)00302-5 [pii] (2008).

4 Lohse, M. J. Dimerization in GPCR mobility and signaling. *Curr Opin Pharmacol* **10**, 53-58, doi:10.1016/j.coph.2009.10.007S1471-4892(09)00167-2 [pii] (2010).

5 Ferre, S. *et al.* G protein-coupled receptor oligomerization revisited: functional and pharmacological perspectives. *Pharmacol Rev* **66**, 413-434, doi:10.1124/pr.113.00805266/2/413 [pii] (2014).

6 Katritch, V., Cherezov, V. & Stevens, R. C. Structure-function of the G protein-coupled receptor superfamily. *Annu Rev Pharmacol Toxicol* **53**, 531-556, doi:10.1146/annurev-pharmtox-032112-135923 (2013).

7 Ulbrich, M. H. & Isacoff, E. Y. Subunit counting in membrane-bound proteins. *Nat Methods* **4**, 319-321, doi:nmeth1024 [pii]10.1038/nmeth1024 (2007).

8 Calebiro, D. *et al.* Single-molecule analysis of fluorescently labeled G-protein-coupled receptors reveals complexes with distinct dynamics and organization. *Proc Natl Acad Sci U S A* **110**, 743-748, doi:10.1073/pnas.12057981101205798110 [pii] (2013).

9 Kasai, R. S. & Kusumi, A. Single-molecule imaging revealed dynamic GPCR dimerization. *Curr Opin Cell Biol* **27**, 78-86, doi:10.1016/j.ceb.2013.11.008S0955-0674(13)00184-1 [pii] (2014).

10 Pin, J. P. *et al.* G-protein-coupled receptor oligomers: two or more for what? Lessons from mGlu and GABAB receptors. *J Physiol* **587**, 5337-5344, doi:10.1113/jphysiol.2009.179978jphysiol.2009.179978 [pii] (2009).

11 Rondard, P., Goudet, C., Kniazeff, J., Pin, J. P. & Prezeau, L. The complexity of their activation mechanism opens new possibilities for the modulation of mGlu and GABAB class C G protein-coupled receptors. *Neuropharmacology* **60**, 82-92, doi:10.1016/j.neuropharm.2010.08.009S0028-3908(10)00208-X [pii] (2011).

12 Kniazeff, J., Prezeau, L., Rondard, P., Pin, J. P. & Goudet, C. Dimers and beyond: The functional puzzles of class C GPCRs. *Pharmacol Ther* **130**, 9-25, doi:10.1016/j.pharmthera.2011.01.006S0163-7258(11)00023-4 [pii] (2011).

13 Comps-Agrar, L. *et al.* The oligomeric state sets GABA(B) receptor signalling efficacy. *EMBO J* **30**, 2336-2349, doi:10.1038/emboj.2011.143emboj2011143 [pii] (2011).

14 Comps-Agrar, L., Kniazeff, J., Brock, C., Trinquet, E. & Pin, J. P. Stability of GABAB receptor oligomers revealed by dual TR-FRET and drug-induced cell surface targeting. *FASEB J* **26**, 3430-3439, doi:10.1096/fj.12-203646fj.12-203646 [pii] (2012).

15 Doumazane, E. *et al.* A new approach to analyze cell surface protein complexes reveals specific heterodimeric metabotropic glutamate receptors. *FASEB J* **25**, 66-77, doi:10.1096/fj.10-163147fj.10-163147 [pii] (2011).

16 Niswender, C. M. & Conn, P. J. Metabotropic glutamate receptors: physiology, pharmacology, and disease. *Annu Rev Pharmacol Toxicol* **50**, 295-322, doi:10.1146/annurev.pharmtox.011008.145533 (2010).

17 Romano, C., Yang, W. L. & O'Malley, K. L. Metabotropic glutamate receptor 5 is a disulfide-linked dimer. *J Biol Chem* **271**, 28612-28616 (1996).

18 Ray, K. & Hauschild, B. C. Cys-140 is critical for metabotropic glutamate receptor-1 dimerization. *J Biol Chem* **275**, 34245-34251, doi:10.1074/jbc.M005581200M005581200 [pii] (2000).

19 Tsuji, Y. *et al.* Cryptic dimer interface and domain organization of the extracellular region of metabotropic glutamate receptor subtype 1. *J Biol Chem* **275**, 28144-28151, doi:10.1074/jbc.M003226200M003226200 [pii] (2000).

20 Romano, C. *et al.* Covalent and noncovalent interactions mediate metabotropic glutamate receptor mGlu5 dimerization. *Mol Pharmacol* **59**, 46-53 (2001).

21 Kunishima, N. *et al.* Structural basis of glutamate recognition by a dimeric metabotropic glutamate receptor. *Nature* **407**, 971-977, doi:10.1038/35039564 (2000).

22 Sato, T., Shimada, Y., Nagasawa, N., Nakanishi, S. & Jingami, H. Amino acid mutagenesis of the ligand binding site and the dimer interface of the metabotropic glutamate receptor 1. Identification of crucial

residues for setting the activated state. *J Biol Chem* **278**, 4314-4321, doi:10.1074/jbc.M210278200M210278200 [pii] (2003).
23 Goudet, C. *et al.* Heptahelical domain of metabotropic glutamate receptor 5 behaves like rhodopsin-like receptors. *Proc Natl Acad Sci U S A* **101**, 378-383, doi:10.1073/pnas.0304699101010304699101 [pii] (2004).
24 El Moustaine, D. *et al.* Distinct roles of metabotropic glutamate receptor dimerization in agonist activation and G-protein coupling. *Proc Natl Acad Sci U S A* **109**, 16342-16347, doi:10.1073/pnas.1205838109120583810 [pii] (2012).
25 Wu, H. *et al.* Structure of a class C GPCR metabotropic glutamate receptor 1 bound to an allosteric modulator. *Science* **344**, 58-64, doi:10.1126/science.1249489science.1249489 [pii] (2014).
26 Gonzalez-Maeso, J. *et al.* Identification of a serotonin/glutamate receptor complex implicated in psychosis. *Nature* **452**, 93-97, doi:10.1038/nature06612nature06612 [pii] (2008).
27 Fribourg, M. *et al.* Decoding the signaling of a GPCR heteromeric complex reveals a unifying mechanism of action of antipsychotic drugs. *Cell* **147**, 1011-1023, doi:10.1016/j.cell.2011.09.055S0092-8674(11)01272-4 [pii] (2011).
28 Moreno, J. L. *et al.* Identification of three residues essential for 5-hydroxytryptamine 2A-metabotropic glutamate 2 (5-HT2A.mGlu2) receptor heteromerization and its psychoactive behavioral function. *J Biol Chem* **287**, 44301-44319, doi:10.1074/jbc.M112.413161M112.413161 [pii] (2012).
29 Delille, H. K. *et al.* Heterocomplex formation of 5-HT2A-mGlu2 and its relevance for cellular signaling cascades. *Neuropharmacology* **62**, 2184-2191, doi:10.1016/j.neuropharm.2012.01.010S0028-3908(12)00030-5 [pii] (2012).
30 Yin, S. *et al.* Selective actions of novel allosteric modulators reveal functional heteromers of metabotropic glutamate receptors in the CNS. *J Neurosci* **34**, 79-94, doi:10.1523/JNEUROSCI.1129-13.201434/1/79 [pii] (2014).
31 Suzuki, Y., Moriyoshi, E., Tsuchiya, D. & Jingami, H. Negative cooperativity of glutamate binding in the dimeric metabotropic glutamate receptor subtype 1. *J Biol Chem* **279**, 35526-35534, doi:10.1074/jbc.M404831200M404831200 [pii] (2004).
32 Kniazeff, J. *et al.* Closed state of both binding domains of homodimeric mGlu receptors is required for full activity. *Nat Struct Mol Biol* **11**, 706-713, doi:10.1038/nsmb794nsmb794 [pii] (2004).
33 Brock, C. *et al.* Activation of a dimeric metabotropic glutamate receptor by intersubunit rearrangement. *J Biol Chem* **282**, 33000-33008, doi:M702542200 [pii]10.1074/jbc.M702542200 (2007).
34 Kammermeier, P. J. & Yun, J. Activation of metabotropic glutamate receptor 1 dimers requires glutamate binding in both subunits. *J Pharmacol Exp Ther* **312**, 502-508, doi:jpet.104.073155 [pii]10.1124/jpet.104.073155 (2005).
35 Beqollari, D. & Kammermeier, P. J. Venus fly trap domain of mGluR1 functions as a dominant negative against group I mGluR signaling. *J Neurophysiol* **104**, 439-448, doi:10.1152/jn.00799.2009jn.00799.2009 [pii] (2010).
36 Tateyama, M. & Kubo, Y. The intra-molecular activation mechanisms of the dimeric metabotropic glutamate receptor 1 differ depending on the type of G proteins. *Neuropharmacology* **61**, 832-841, doi:10.1016/j.neuropharm.2011.05.031S0028-3908(11)00233-4 [pii] (2011).
37 Kniazeff, J., Galvez, T., Labesse, G. & Pin, J. P. No ligand binding in the GB2 subunit of the GABA(B) receptor is required for activation and allosteric interaction between the subunits. *J Neurosci* **22**, 7352-7361, doi:22/17/7352 [pii] (2002).
38 Margeta-Mitrovic, M., Jan, Y. N. & Jan, L. Y. Ligand-induced signal transduction within heterodimeric GABA(B) receptor. *Proc Natl Acad Sci U S A* **98**, 14643-14648, doi:10.1073/pnas.251554798251554798 [pii] (2001).
39 Margeta-Mitrovic, M., Jan, Y. N. & Jan, L. Y. Function of GB1 and GB2 subunits in G protein coupling of GABA(B) receptors. *Proc Natl Acad Sci U S A* **98**, 14649-14654, doi:10.1073/pnas.251554498251554498 [pii] (2001).
40 Levitz, J. *et al.* Optical control of metabotropic glutamate receptors. *Nat Neurosci* **16**, 507-516, doi:10.1038/nn.3346nn.3346 [pii] (2013).
41 Reiner, A. & Isacoff, E. Y. Tethered ligands reveal glutamate receptor desensitization depends on subunit occupancy. *Nat Chem Biol* **10**, 273-280, doi:10.1038/nchembio.1458nchembio.1458 [pii] (2014).
42 Jain, A. *et al.* Probing cellular protein complexes using single-molecule pull-down. *Nature* **473**, 484-488, doi:10.1038/nature10016nature10016 [pii] (2011).

43 Kleinlogel, S. *et al.* A gene-fusion strategy for stoichiometric and co-localized expression of light-gated membrane proteins. *Nat Methods* **8**, 1083-1088, doi:10.1038/nmeth.1766nmeth.1766 [pii] (2011).
44 Petralia, R. S., Wang, Y. X., Niedzielski, A. S. & Wenthold, R. J. The metabotropic glutamate receptors, mGluR2 and mGluR3, show unique postsynaptic, presynaptic and glial localizations. *Neuroscience* **71**, 949-976, doi:0306-4522(95)00533-1 [pii] (1996).
45 Francesconi, A. & Duvoisin, R. M. Role of the second and third intracellular loops of metabotropic glutamate receptors in mediating dual signal transduction activation. *J Biol Chem* **273**, 5615-5624 (1998).

Supplementary Figures:

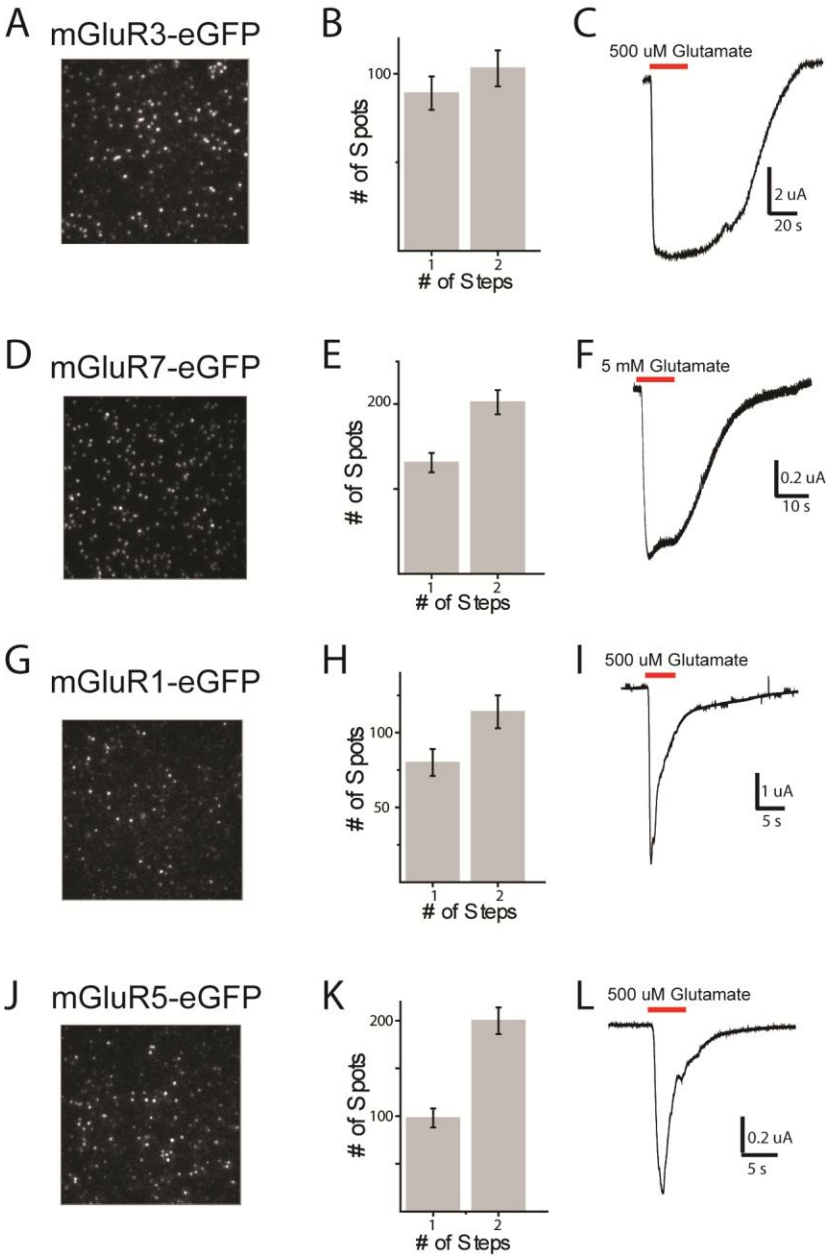

Figure S5.1, Group I,II, and III mGluRs are all dimers in Xenopus oocytes. A-L) All mGluRs tested show dimerization in single molecule photobleaching assay in oocytes. mGluR3-eGFP (A-C) and mGluR7-eGFP (D-F) express on the surface, show a photobleaching pattern consistent with dimerization, and activate co-expressed GIRK channels. mGluR1-eGFP (G-I) and mGluR5-eGFP (J-L) express on the surface, show a photobleaching pattern consistent with dimerization, and activate native calcium-activaeted chloride channels. Compared to group II and III mGluRs, the group I mGluRs, mGluR1 and mGluR5, show much more mobility on the surface of the cell.

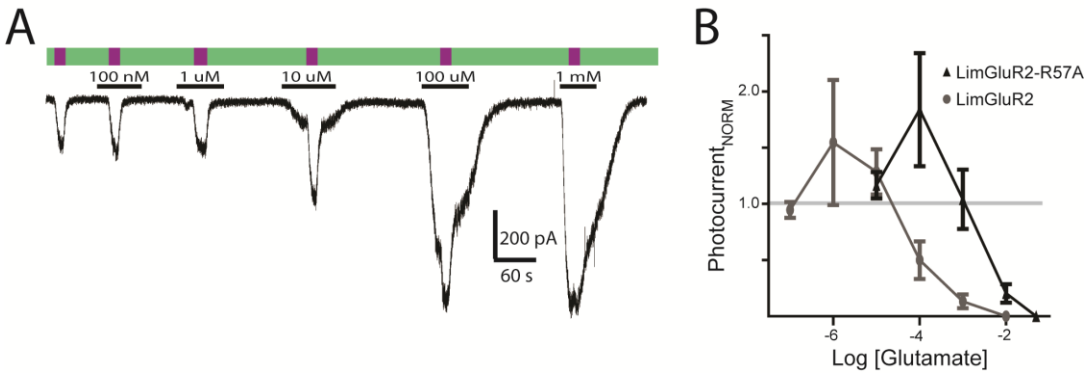

Figure S5.2, LimGluR2 cooperativity is dependent on glutamate concentration and affinity. A) Representative trace showing LimGluR2 photoswitching in the presence of a range of glutamate concentrations. In the presence of 10 μM the photocurrent is clearly enhanced relative to in the absence of glutamate. Higher concentrations of glutamate reduced the photocurrent. B) Concentration dependence of photocurrent amplitude for both LimGluR2 and LimGluR2-R57A, which has a reduced glutamate affinity. Photocurrent is normalized to the amplitude in the absence of glutamate. n=4 cells for each condition.

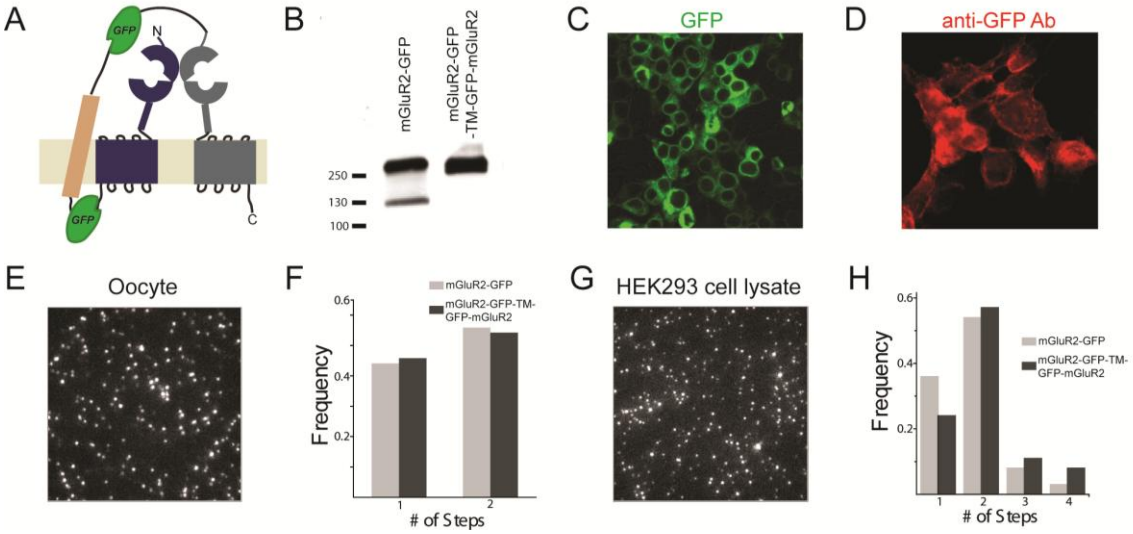

Figure S5.3, mGluR2 tandem dimers have the expected size, stoichiometry and topology. A) Schematic showing design of mGluR tandem dimers. A short, glycine-rich, flexible linker is shown between the first subunit (blue) and GFP and between the GFP and the β subunit of the Na/K ATPase (beige) which crosses the membrane. Another linker connects to another GFP, which is connected by a final linker to the second subunit (gray) which lacks a signal sequence to prevent cleavage. B) Western blot for mGluR2-GFP and the tandem mGluR2. Two bands are seen for mGluR2-GFP for both the dimer and monomer, respectively, whereas for the tandem dimer there is no monomer band because the subunits are covalently connected. C) Image of cells expressing mGluR2–GFP tandem dimers. D) Image of cells expressing mGluR2-GFP tandems fixed and stained with an anti-GFP antibody without permeabilization. This result indicates that the second GFP is extracellular, as expected. E-F) mGluR2-GFP tandem dimers show a similar photobleaching distribution to mGluR2-GFP in Xenopus oocytes, indicating that they assemble as expected and not into higher order complexes. G-H) In lysate from HEK 293T cells, tandem dimers show a similar photobleaching distribution to mGluR2-GFP indicating that assembly is as expected. In this system there are slightly more 3 and 4 step bleaching which could be due to the possibility of multiple receptors binding to the same antibody or multiple primary antibodies to the same secondary antibody.

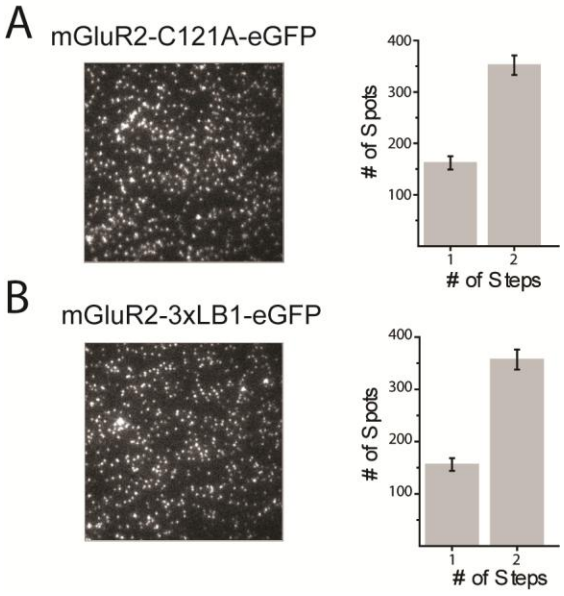

Figure S5.4, LB1 dimer interface mutants show dimerization in HEK 293T cell lysate. A,B) Expression of either mGluR2-C121A-eGFP (A) or mGluR2-3xLB1-GFP(B) in HEK 293T cells results in a photobleaching step distribution that shows clear dimerization.

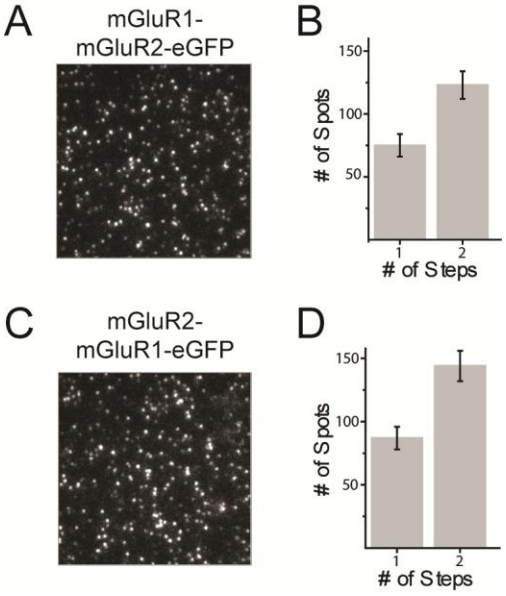

Figure S5.5, Chimeras between mGluR1 and mGluR2 are dimers in Xenopus oocytes. A,B) mGluR1-mGluR2-eGFP expresses (A) and shows a photobleaching step distribution consistent with dimerization (B). C,D) mGluR2-mGluR1-eGFP expressed (C) and shows a photobleaching step distribution consistent with dimerization (D).

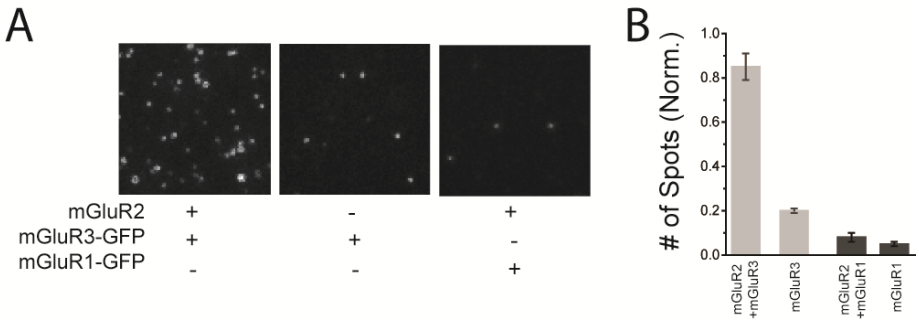

Figure S5.6, mGluR2 heteromerizes specifically with mGluR3 over mGluR1 in HEK 293T cell lysate. A-B) Single molecule pulldown shows that mGluR2 can interact with mGluR3, but not mGluR1. A) Representative images showing pulldowns of mGluR2 by an mGluR2-specific antibody. When mGluR2 was coexpressed with mGluR3 there was clear pulldown of mGluR3-GFP that was not observed when mGluR1-GFP was coexpressed or when the mGluR2 DNA was omitted. B) Summary of pulldown of mGluR3-GFP and mGluR1-GFP by mGluR2.

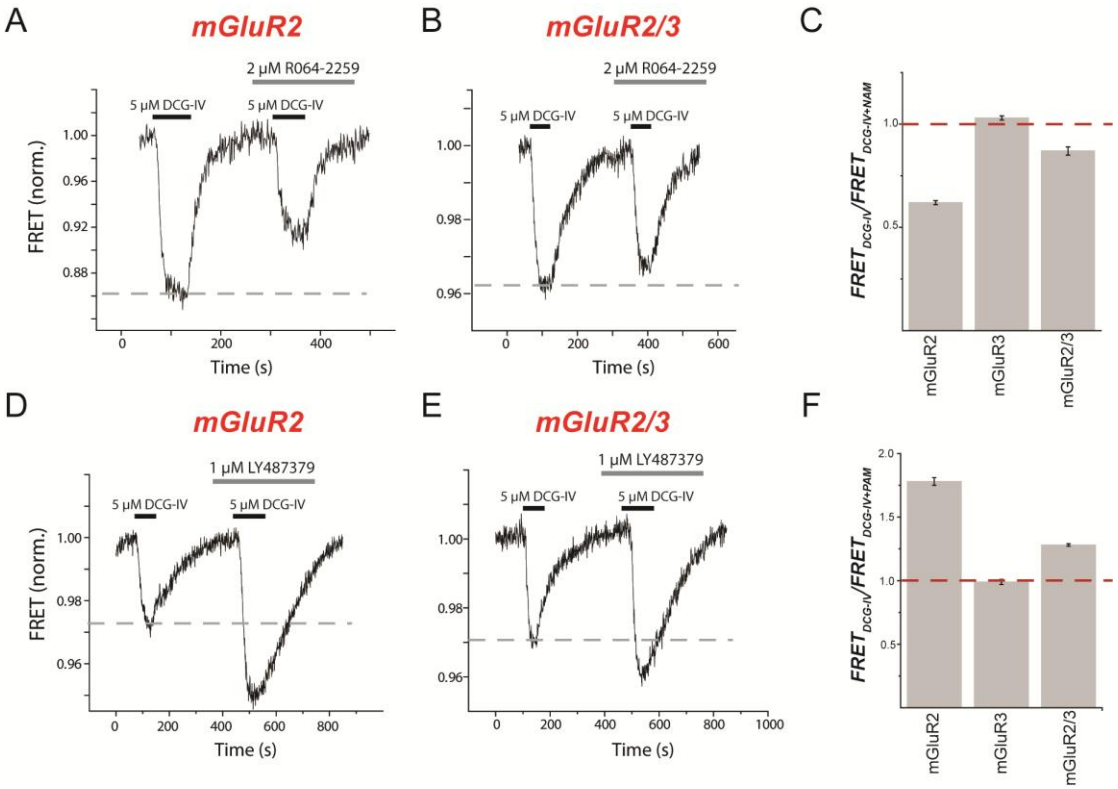

Figure S5.7, Weak sensitivity of mGluR2/3 heterodimers to mGluR2-specific allosteric modulators. A-C) Effects of the mGluR2-specific NAM R064-2259 on intersubunit LBD FRET for mGluR2, mGluR3, and mGluR2/3 heterodimers. RO64-2259 decreases the FRET decrease induced by the agonist DCG-IV for both mGluR2 (A) and mGluR2/3 (B). C) Summary of inhibition of FRET decrease induced by 5 μM DCG-IV for all three group II mGluR species shows weak sensitivity of heterodimers compared to strong and no sensitivity for mGluR2 and mGluR3, respectively. D-F) Effects of the mGluR2-specific PAM LY487379 on intersubunit LBD FRET for mGluR2, mGluR3, and mGluR2/3 heterodimers. LY487379 increases the FRET decrease induced by the agonist DCG-IV for both mGluR2 (D) and mGluR2/3 (E). D) Summary of enhancement of FRET decrease induced by 5 μM DCG-IV for all three group II mGluR species shows weak sensitivity of heterodimers compared to strong and no sensitivity for mGluR2 and mGluR3, respectively. Note: for both the mGluR2-specific PAM and NAM, the observed effect was less than half in the heterodimer compared to the mGluR2 homodimer.

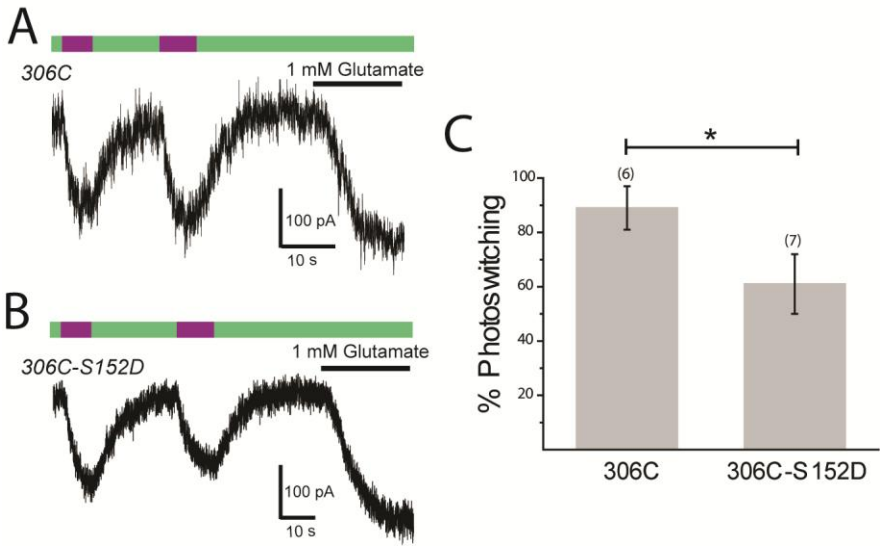

Figure S5.7, Mutation S152D decreases photoswitch efficiency of LimGluR3. A-B) Representative traces showing photoswitching of either LimGluR3 (A) or LimGluR3-S152D (B) in GIRK assay in HEK 293T cells. C) Summary of photoswitch efficiency relative to 1 mM glutamate for both constructs shows a significant decrease in photoswitch efficiency when the S152D mutation is present. * indicates statistical significance (Unpaired T test; $P<0.05$). The number of cells tested for each condition are shown in parentheses.

Chapter VI: Optical control of endogenous proteins with a photo-switchable conditional subunit reveals a role for TREK1 in GABAB signaling

This work was published in Neuron volume 74, issue 6 in 2012 with me as second author.

Introduction:

While the production of pharmacological reagents targeted to membrane signaling proteins has been a major objective for both academic laboratories and the pharmaceutical industry, many important membrane proteins are still without specific blockers. Moreover, where specific blockers exist, they often have high affinity and are selective only at low concentrations, so that the onset of their effect upon exposure takes a long time to develop and they bind so tightly that they are difficult to remove. The development of Photoswitched Tethered Ligands (PTLs) that are targeted to an introduced cysteine near ligand binding sites of membrane proteins opened the door to the reversible control of membrane signaling, by using two wavelengths to photoisomerize the tether between one state that permits ligand binding and a second state which prevents binding [1]. Because specificity derives from the unique geometric relationship between the ligand binding site and the engineered anchoring site, rather than from tight binding, photo-isomerization to the non-binding state rapidly removes the ligand. Moreover, the high effective concentration of the ligand near its binding site in the permissive state leads to rapid binding upon photoisomerization, itself a very rapid transition [1]. Together, these properties enable highly selective optical control of binding and unbinding on the millisecond time-scale and micron space-scale[1].

So far, optical control with PTLs has been applied to ion channels and receptors that are over-expressed in cells. Because the introduction of the anchoring site can usually be done with minimal perturbation to protein function[1], it should be possible to introduce the mutation into the native protein via genetic knock-in. Still, generation of a knock-in animal is laborious and expensive, making sense only when one is directly interested in the signaling by the targeted protein, but not for exploring the function of several candidate proteins as in typical pharmacological experiments. To address this, we developed a scheme for targeting optical control via a PTL to native proteins without the requirement for genetic knock-in. Our approach is to express a "photoswitchable conditional subunit" (PCS) that contains a PTL anchoring site and a mutation that retains the subunit inside the cell. This engineered subunit will not function in cells where native subunits are missing. However, in cells that express the native subunits that are required to form the functional protein complex, the native and engineered subunits will assemble inside the cell and the complex will be trafficked to the plasma membrane, thereby placing the native protein under optical control provided by the co-assembled engineered subunit.

$GABA_B$ receptors set the inhibitory tone, provide the critical feed-forward and feedback inhibition that shapes the spread of neural activity, regulates the filtering properties of neural circuits and prevents hyper-excitation and seizure[2,3]. In the hippocampus, the postsynaptic $GABA_B$ response was long thought to be mediated exclusively through Kir3 potassium channels[4-6], but the genetic knockout of Kir3 subunits has suggested that another channel might also contribute to $GABA_B$ inhibition[7]. The identity of this additional channel has not been revealed and its function in tissue from wild-type animals remains to be determined. Using the

PCS approach we show that TREK1, a 2P-potassium channel typically thought of as a leak channel, is an additional target of $GABA_B$ receptors in the hippocampus.

Results:

One interesting class of channels to consider for participation in hippocampal $GABA_B$ signaling is the large family of 2P-potassium channels. These channels are typically thought of as leak channels, whose function is to set the resting potential[8]. However, some of them can be regulated by GPCRs[8,9]. The physiological function of these channels has remained elusive due to a lack of specific blockers. One of the 2P-potassium channels, TREK2, was found recently to be involved in the $GABA_B$ control of spatial learning in the entorhinal cortex [9]. However, the entorhinal $GABA_B$ current deactivates more than ten times more slowly than the hippocampal $GABA_B$ current, suggesting that TREK2 is not the missing hippocampal channel. In the absence of specific pharmacological blockers of most 2P-potassium-channels, and because knock-out of specific genes can lead to compensatory expression of related genes, we searched for an alternative approach for selective pharmacology. We turned to the strategy of PTLs, which obtain their target selectivity not from the specificity of the ligand but from their selective attachment to the protein of interest and the precise geometric relation of the attachment site to the ligand binding site[1,10-12]. Because the PTLs are photo-isomerized between two conformations by distinct wavelengths of light and because only one of the conformations permits the ligand to bind, they can activate or block the target protein rapidly and reversibly. Thus, in principle, photo-block should provide a clear assay for when the channel is activated.

PTL for the TREK1 channel

We developed a light-blocked version of the 2P-Potassium Channel TREK1, using the PTL MAQ, which contains a maleimide (M) that tethers the molecule to a genetically engineered cysteine, a photoisomerizable azobenzene (A) linker and a pore-blocking quatenary ammonium group (Q) (Figure 6.1A, top). In its relaxed state, MAQ is in the *trans* configuration (Figure 6.1A and Figure 6.1B, left). It is rapidly photo-isomerized to the *cis* configuration by 380 nm light and rapidly photo-isomerized back to the *trans* form by 500 nm light (Figure 6.1B). MAQ was previously employed to photo-control the voltage-gated Shaker potassium channel [10].

We introduced single cysteine mutations as attachment sites at a series of different positions in portions of the first and second pore loops (P1 and P2) of TREK1 (Figure 6.1A) and expressed the channel in HEK293 cells. MAQ was applied in the external solution to each of these cysteine-substituted mutants and photoswitching was tested by measuring the modulation of the current when illumination was switched back and forth from 500 nm to 380 nm. We first examined cysteine substitutions at residue N122 in P1 and K231 in P2 of TREK1, since these are homologous to the optimal site for photo-block by MAQ in the Shaker channel (Shaker 422)[10]. While both sites showed photo-modulation, they had a different dependence on light, *i.e.* on the configuration of the MAQ photoswitch. TREK1(K231C-MAQ) produced photo-block in the *trans* state (500 nm illumination), as found in Shaker [10], but TREK1(N122C-MAQ) produced photo-block in the *cis* state (380 nm illumination) (Table 6.1). The opposite photoswitching at the two attachment positions indicates P1 and P2 differ structurally and that P2 more closely resembles the P loop of Shaker. This is interesting in view of the levels of homology of the conserved C-terminal portion of the P regions, where TREK1's P1 and P2 have 17% and 23% identity (55% and 57% similarity), respectively, to the P of Shaker, and a unique long loop precedes TREK's P1 (Figure S6.1).

Photo-modulation was also seen at two other MAQ attachment sites in P1 (Table 6.1). The strongest photo-modulation was at S121C (Table 6.1), which displayed 64 ± 3% (n = 14) block under 380 nm light and was unblocked by isomerization to *trans* under illumination at 500 nm (Figure 6.1C). Since MAQ thermally relaxes into the *trans* state, TREK1(S121C-MAQ) has the advantage that the channel is unblocked and can function normally in the dark.

Position and Mutation	**Photoswitch**	**380 nm**	**Light-gated current amplitude**
S121C	Yes	Block	124 ± 9 (6)
N122C	Yes	Block	59 ± 12 (7)
Q123C	No	-	0 (4)
H126C	Yes	Block	31 ± 4 (4)
K231C	Yes	Unblock	− 98 ± 13 (4)

Table 6.1, Effect of Mutation on MAQ Block under 380 nm Light. Values are reported as mean ± SEM with the number of determination in parenthesis. The block percentages are reported for 0 mV holding potential. To compare the blocking effects, the cells were recorded the same day with the same MAQ aliquot.

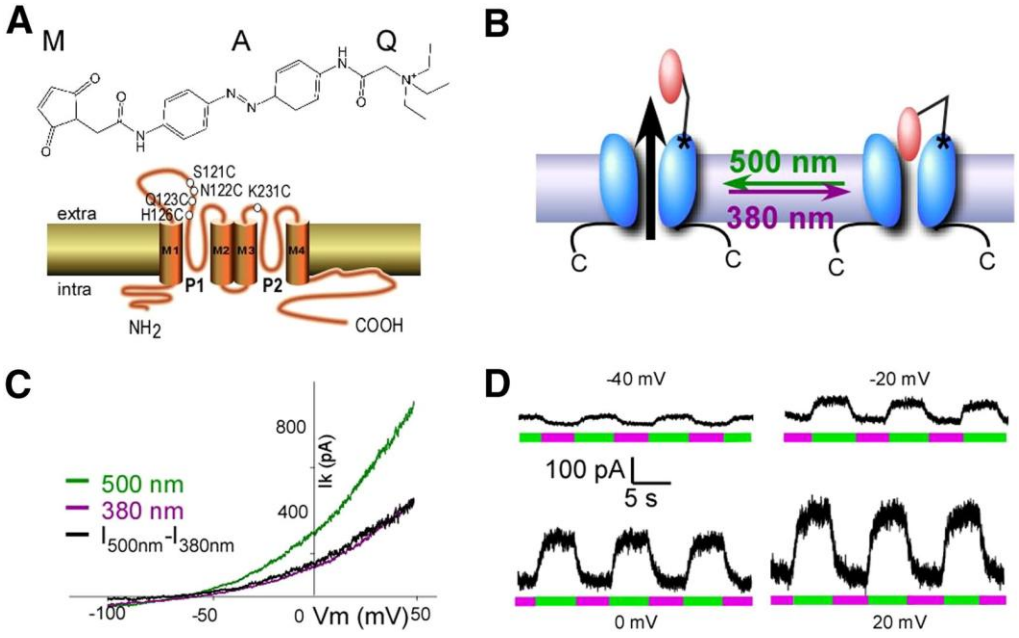

Figure 6.1, Light-gated TREK1. A) (Top) MAQ consists of a maleimide (M), which tethers the photoswitch to a cysteine introduced into the outer portion of the first P-loop of the channel (bottom), a photoisomerable azobenzene (A) linker and a quaternary ammonium (Q) pore blocker. (Bottom) Cartoon showing the membrane topology of TREK1 channel and the different position tested. B) Schematic representation of light-gated TREK1. MAQ is covalently attached to cysteine (S121C). MAQ blocks the pore in the *cis* configuration (380 nm light). Exposure to 500 nm light places MAQ in the *trans* state where the pore is unblocked. C,D) Whole-cell recording from HEK293T cell expressing TREK1(S121C) and labeled with MAQ. Current was elicited by voltage-ramps (from -100 to 50 mV, 1s in duration) (C). Alternating illumination at 500 nm (green) and 380 nm (magenta) reversibly blocks and unblocks constant outward current, as seen at different holding potentials (D).

Subunit replacement strategy

Cysteine-substituted versions of TREK1 that can be photo-blocked by MAQ could be introduced into neurons by transfection, but this would add the heterologous protein to the native protein and result in over-expression. One way around this would be to generate a genetic knock-in that replaces the native TREK1 with a version of TREK1 that is identical except for the single cysteine substitution. However, knock-in production is lengthy and costly. We therefore sought an alternative easier strategy for introducing the MAQ photoswitch into native channels.

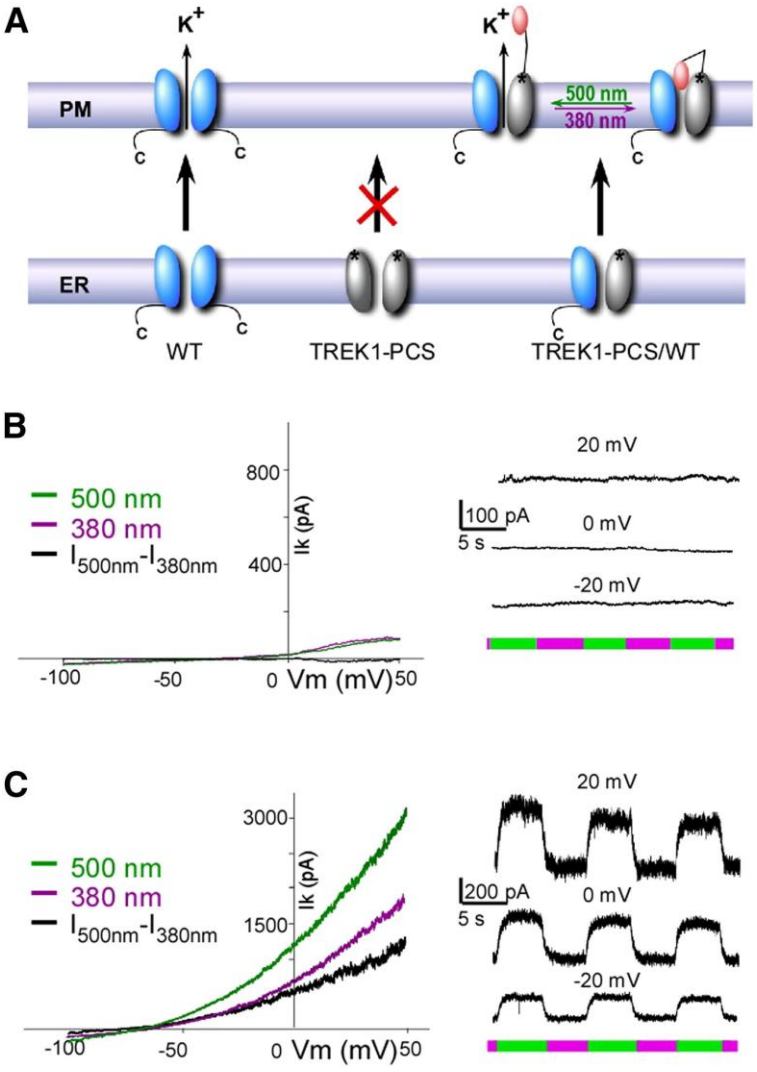

Figure 6.2, Development of a Subunit Replacement Strategy. A) Schematic representation of subunit replacement strategy. Deletion of the TREK1 carboxy-terminal tail (TREK1-PCS, gray) results in retention of the homomeric mutant channel in the endoplasmic reticulum. In contrast, the wild-type homomeric channel (WT, blue) traffics to the plasma membrane. Coexpression of TREK1-PCS with WT produces a heteromeric channel that traffics to the membrane because of the WT subunit and which can be light-gated because of MAQ attachment to the TREK1-PCS. B, C) Whole-cell recording from HEK293T cell expressing either TREK1-PCS alone (B) or coexpressed with WT (C) and labeled with MAQ. Current was elicited by voltage-ramps (from −100mV to 50mV, 1 s in duration) (left). Alternating illumination at 500 nm (green) and 380 nm (magenta) reversibly blocks and unblocks constant outward current, as seen at different holding potentials (right).

We developed a subunit replacement strategy to obtain optical control over a neuron's native TREK1 channels (Figure 6.2A). As shown earlier, deletion of the TREK1 carboxy-terminal tail (TREK1ΔC) results in retention of the channel in the endoplasmic reticulum[13]. In agreement with this, TREK1ΔC(S121C-MAQ) in HEK293 cells produced no detectable current above background: current amplitude at 0mV was 71 ± 37 pA (n=11) for TREK1ΔC-S121C-transfected HEK293 cells *versus* 68 ± 40 pA (n=7) for non-transfected cells. Moreover, following exposure to MAQ, alternating illumination between 380 nm and 500 nm produced no

change in the basal current in TREK1ΔC-S121C-transfected cells (Figure 6.2B). Because the cytoplasmic N-terminal domain and the first transmembrane segment (M1) of TREK1 are sufficient to dimerize with the full-length TREK1 channel[14], we hypothesized that TREK1ΔC would dimerize with the wildtype TREK1 channel (WT) and produce a functional channel (Figure 6.2A). In contrast with the lack of photo-modulation of current in MAQ-labeled cells expressing TREK1ΔC(S121C) alone (Figure 6.2B), co-expression of TREK1ΔC(S121C) with WT in HEK293 cells yielded a TREK1 current that was strongly photo-modulated (Figure 6.2C). This indicates that TREK1ΔC(S121C) assembles with the WT subunits and that the heteromeric channel goes to the cell surface, where the TREK1ΔC(S121C) subunit is labeled by the charged, membrane impermeant MAQ endowing the channel with regulation by light via photoisomerization of MAQ. From here on, we refer to the TREK1ΔC(S121C) subunit that contains the cysteine photoswitch attachment site and that is retained internally unless co-assembled with a WT native subunit as the TREK1 Photoswitchable Conditional Subunit (TREK1-PCS).

Heteromeric TREK1-PCS/TREK1 channel functions normally

For the approach to work as intended, the heteromeric TREK1-PCS/WT channel would need to retain normal functions of the TREK1 channel. We tested the TREK1-PCS/WT heteromeric channel to determine whether it was regulated by external and internal stimuli in the same way as WT. To do this, we examined the sensitivity to stimuli of total WT current in cells expressing WT alone and compared this to the photo-blocked current component from cells co-expressing the TREK1-PCS along with WT, where the light-sensitive current is attributed solely to the heteromeric TREK1-PCS/WT channel labeled with MAQ on the TREK1-PCS.

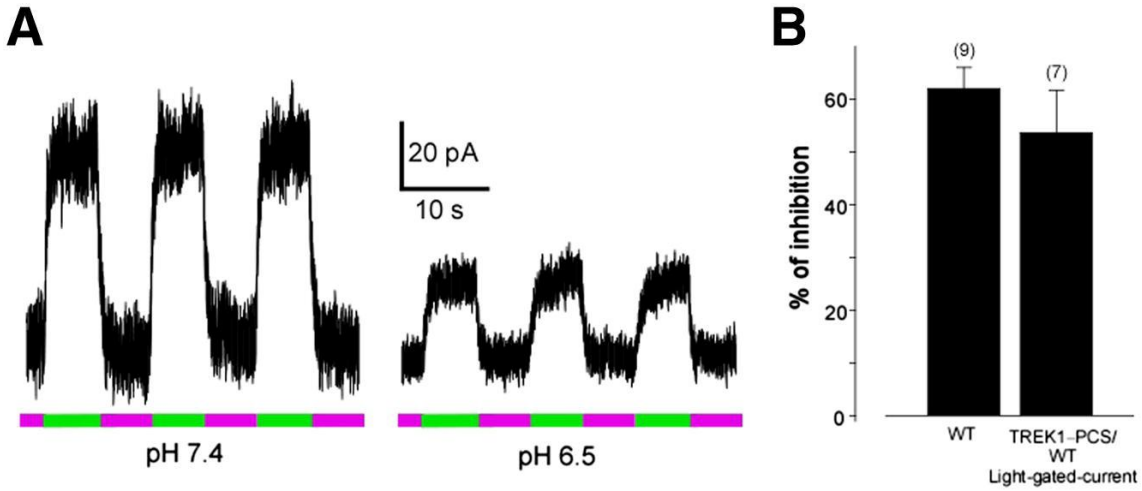

Figure 6.3, **Heteromeric channels formed by TREK1-PCS and WT retain normal regulation by external acidification.** A) Representative example of the effect of acidic pH on the light-gated current of TREK1-PCS/WT. Alternating illumination at 500 nm (green) and 380 nm (magenta) reversibly blocks and unblocks, respectively, the constant outward current, both at pH7.4 and pH6.5, but the amplitude of the photo-modulation is smaller at pH6.5. B) Inhibition by external acidification from pH7.4 to pH 6.5 of the photo-blocked current component of TREK1-PCS/WT heteromeric channels is similar to the inhibition of total WT current under the same condition. Numbers in parentheses above bars indicate number of cells tested.

TREK1 channels are inhibited by external acidification, due, it has been proposed, to titration of a histidine residue in P1[15,16], an effect which has been attributed to C-type inactivation[15-17]. We found that the light-gated current obtained from MAQ-labeled HEK293T cells co-expressing the TREK1-PCS and WT subunit is also inhibited by external acidification (Figure 6.3A). This inhibition of the photo-gated current in the TREK1-PCS/WT heterodimer was 53.6 ± 8 % (n=8), similar to the 60.6 ± 5 % (n=8) inhibition of total current in WT alone ($p > 0.7$, t-test).

We next investigated the regulation of the TREK1-PCS/WT heterodimer channel by internal modification induced by GPCR activation. Gi-coupled receptors have been shown to enhance TREK1 current[18]. We therefore tested the ability of the Gi-coupled $GABA_B$ receptor ($GABA_BR$) to regulate the light-gated current of the TREK1-PCS/WT heterodimer. Activation of $GABA_BR$ induced a 2.6 ± 0.3 (n=8) fold increase in total current in cells expressing WT alone. This value was similar ($p > 0.8$, t-test) to the 2.7 ± 0.3 (n=9) fold increase observed in the light-gated current from the heterodimeric channel in MAQ-labeled cells co-expressing the TREK1-PCS and WT subunits (Figure 6.4A, C).

Residue S333 of TREK1 is a phosphorylation site that has been shown to be involved in inhibition of current by PKA[19]. Moreover, it is the dephosphorylation of S333 that appears to underlie the enhancement of TREK1 current by Gi-coupled GPCRs[9,18]. Part of the evidence for this is that mutation of S333 reduces or eliminates the enhancement of current by Gi-coupled GPCRs[9,18]. We therefore examined the effect of the mutation S333D, which mimics the phosphorylated state of S333 and reduces current in homomeric WT channels[20]. Co-expression of the TREK1-PCS with TREK1(S333D) yielded a small light-gated current (44 ± 8 pA at 0 mV, n=5), approximately 3-fold smaller than the light-gated current of TREK1-PCS co-expressed with the WT subunit (128 ± 8 pA at 0 mV, n=8, $p < 0.05$; Figure 6.4A, B). In addition, as observed for total current from WT channels [9,18], the enhancement of the light-gated current by activation of $GABA_BR$ was considerably reduced by the S333D mutation (Figure 6.4C).

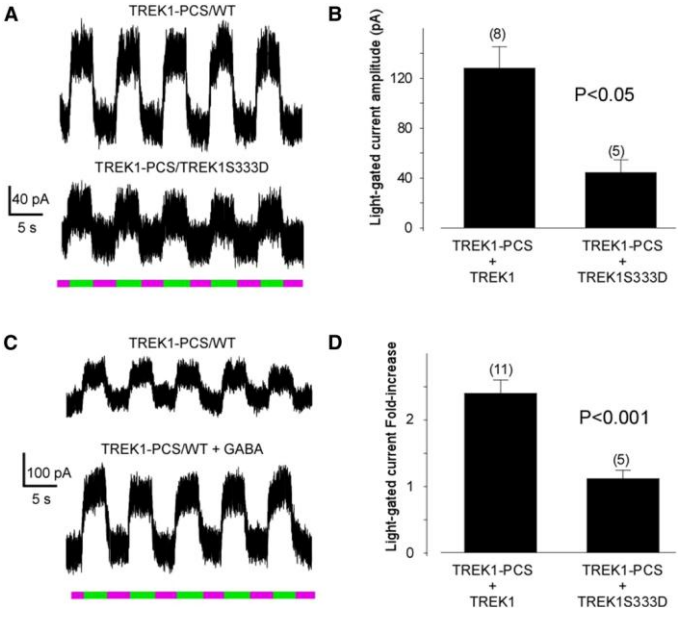

Figure 6.4, **Mutation of Serine 333 to Aspartate reduces the photoswitchable current and prevents its up-regulation by GiPCR activation**. The residue S333 has been reported to be a PKA phosphorylation site and mutation to aspartic acid (to mimic the phosphorylated state) has been shown to decrease TREK1 current. A) Alternating illumination between 380 nm (magenta) and 500 nm (green) reversibly blocks and unblocks constant outward current from TREK1-PCS/WT heterodimer (top) and from TREK1-PCS/TREK1S333D dimer (bottom). B) Bar graph representing the light-gated current recorded from HEK cells transfected by either TREK1-PCS + TREK1 or TREK1-PCS + TREK1S333D. The S333D mutation decreased the photocurrent. C) Alternating illumination between 380 nm (magenta) and 500 nm (green) reversibly blocks and unblocks constant outward current from TREK1-PCS/WT heterodimer before (top) and after GABA application (bottom). D) Bar graph representing the effect of activation of $GABA_B$ receptor in HEK cells transfected with $GABA_{B1}$ and $GABA_{B2}$ in combination with either TREK1-PCS + TREK1 or TREK1-PCS + TREK1S333D. The S333D mutation prevents regulation of photocurrent by $GABA_B$ activation.

Taken together, these results indicate that not only does the heteromeric TREK1-PCS/WT channel retain the typical TREK1 rectification (Figure 6.2), but it also retains TREK1's normal internal and external regulation (Figures 6.3 and 6.4). In other words, the TREK1-PCS approach endows the native channel with sensitivity to light while maintaining its normal function.

TREK1-PCS approach reveals a role of TREK1 in the hippocampal $GABA_B$ response

To investigate the role of TREK1 in neurons, we transfected TREK1-PCS into dissociated cultured hippocampal neurons, labeled with MAQ and examined the effect of light. While untransfected neurons labeled with MAQ were not responsive to light (Figure S6.2), light could be used to control the resting membrane potential of TREK1-PCS transfected neurons that were labeled with MAQ (Figure 6.5A, top). Photo-block by illumination with 380 nm light induced a small but reproducible depolarization of 4.0 ± 0.8 mV (n=29) (Figure 6.5B). This depolarization was sufficient to increase the rate of action potential firing in response to spontaneous excitatory synaptic potentials (EPSPs) (Figure 6.5C-D). A similar light-induced modulation of membrane potential was seen in TREK1-PCS transfected CA1 and CA3 pyramidal neurons of hippocampal slices, indicating that PCS expression, its assembly with native TREK1 subunits and labeling with MAQ can be achieved in tissue with intact circuitry (Figure 6.5A, bottom).

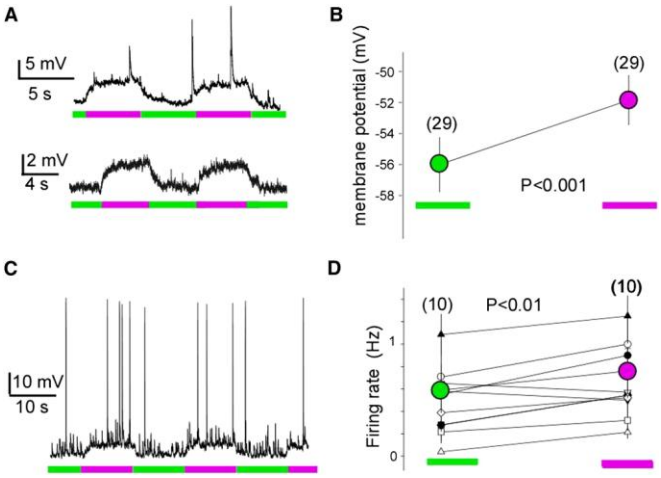

Figure 6.5, TREK1 in hippocampal neurons. A) Whole-cell recording from hippocampal neurons expressing TREK1-PCS in dissociated neuronal culture (top) and cultured hippocampal slice (bottom). Representative example of light modulation of the resting membrane potential, hyperpolarizing under 500 nm light (green), when TREK1 channels are unblocked, and depolarizing under 380 nm light (magenta) when the channels are blocked. B) Average of resting membrane potential measured under 500 nm light (green, unblocked) and 380 nm light (magenta, blocked). C) Photo-modulation of spontaneous firing of hippocampal neuron expressing TREK1-PCS and labeled with MAQ. D) Average of the spontaneous firing rate over several minutes (2-4 minutes while alternating 500 nm and 380 nm light for 5 s each). Statistical significance determined with paired t-test.

The postsynaptic $GABA_B$ response, described by Newberry and Nicoll in 1984[21] which is involved in GABA-induced slow inhibitory postsynaptic potential[22], has long been thought to be mediated by Kir3 potassium channels via activation of the $G_{i/o}$ pathway[4-6]. However, not all of the current induced by the $GABA_B$ agonist baclofen is blocked by external Ba^{2+}, a signature of Kir3 channels, and, moreover, there is a residual potassium current in Kir3.2 and Kir3.3 double knockout mice, suggesting that an additional, unidentified, K^+ channel may contribute to the $GABA_B$ response[7]. Since the TREK1 channe1 is expressed in hippocampal neurons[23] and is only weakly sensitive to Ba^{2+}[24], and, moreover, since it is enhanced by Gi-coupled receptors[18], we hypothesized that the TREK1 channel could be this unknown channel.

We found that TREK1-PCS transfected hippocampal neurons have no detectable photoswitched TREK1 current at rest (Figure 6.6C). However, the outward current induced by the $GABA_B$ receptor agonist balcofen included a component that was blocked by 380 nm light and unblocked by 500 nm light and represented 18.3 $\pm$ 3% (n = 6) of the total $GABA_B$ induced current (Figure 6.6B). The photoswitched component of the $GABA_B$ response could also be seen in organotypic hippocampal slice (Figure 6.6D; n=3 CA1 cells).

To isolate the photoswitched component of the baclofen response, we blocked Kir3. Addition of 1 mM external barium, which completely blocks Kir3 current[25] and only partially blocks TREK1 current[24], blocked a large component of the current and left a residual photoswitchable current (Figure S6.3). Finally, to address the specificity of $GABA_B$ activation, we used the competitive $GABA_B$ antagonist CGP55845. CGP55845 prevented induction of the photoswitched current by baclofen and stopped it once it had been already induced (Figure S6.4A, B). In addition, as expected for its ability to block signaling by $GABA_B$ receptors, pertussis toxin prevented induction of the photoswitched current by baclofen (n=5) (Figure S6.4C). Together, these results indicate that activation of hippocampal $GABA_B$ receptors activates not only Kir3 channels but also TREK1 channels, which are made light sensitive by the expression of the TREK1-PCS.

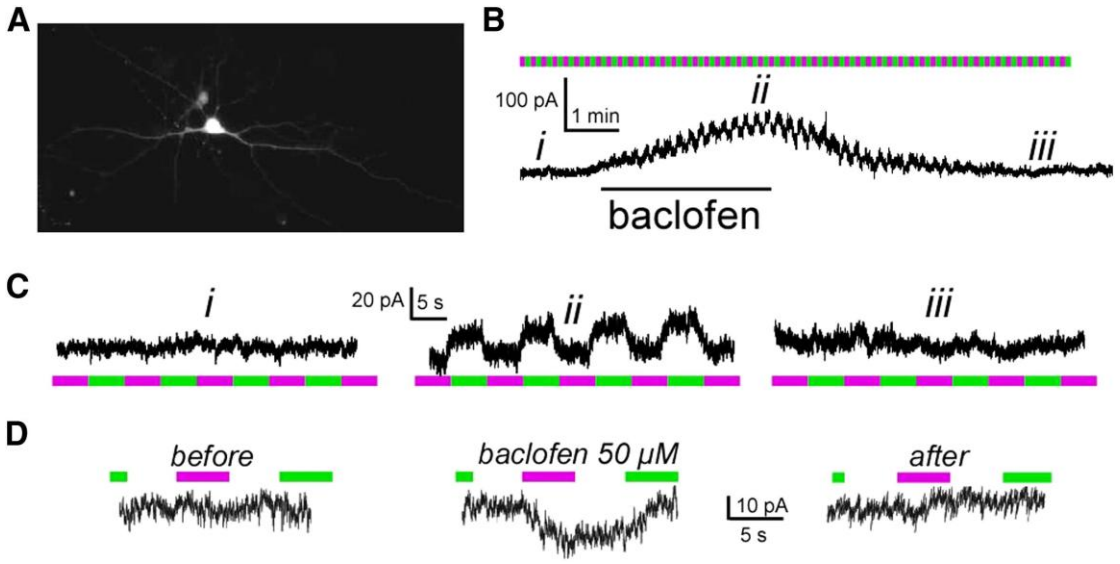

Figure 6.6, TREK1 is activated by $GABA_B$ in hippocampal neurons. A) Image of a cultured hippocampal neuron expressing TREK1-PCS and soluble Tomato. B) Representative current obtained from hippocampal neuron expressing TREK1-PCS. Application of baclofen (60 µM) induces an outward current, which can be reversed upon washout. During the baclofen response the current is modulated by light *(ii)*, indicating that TREK1 contributes to the $GABA_B$ receptor triggered current. C) Zoom-in of the recorded current in top right during periods marked as (*i*), (*ii*) and (*iii*). Illumination at 500 nm (green) and 380 nm (magenta). D) Representative current obtained from hippocampal neuron in organotypic slice expressing TREK1-PCS. During the baclofen response the current is modulated by light, indicating that TREK1 contributes to the $GABA_B$ receptor triggered current under conditions when the hippocampal circuit is intact.

As neurons where recorded after 3-6 days expression of the TREK1-PCS and its expression was driven by a strong promoter (CMV), it is likely that the PCS outnumbers the native (WT) TREK1 subunit and that most newly assembled channels plasma membrane targeted

channels will be PCS/WT (light-blocked) heterodimers. Assuming that the light-block of PCS/WT heterodimers will be the same in neurons as it is in HEK293 cells and taking into account that the MAQ block of TREK1 channels is approximately 64%, this suggests that approximately 30% of the $GABA_B$ induced current is carried by TREK1 channels. This value is in agreement with the amount of residual baclofen-induced current in the Kir3.1 knockout mouse and in Kir3.2 knockout mouse (26%), as well as in the Kir3.2/Kir3.3 double knockout mice (15%)[7]. The relative contribution of Kir3 and TREK1 channels depends, in part, on membrane voltage. Since Kir3 is an inward rectifier and TREK1 is an outward rectifier, a holding potential of -55 mV favors the TREK1 channel component, while at more negative potentials, such as -70 mV, the Kir3 component will be favored.

Discussion:

Photoswitched tethered ligands have opened the door to the selective, rapid and reversible optical control of membrane signaling through proteins that are normally insensitive to light[1]. We have developed a scheme for targeting optical control via a PTL to native proteins without the requirement for genetic knock-in. The approach is to express a PCS that contains an anchoring site for the photoswitch as well as a mutation that retains the subunit inside the cell. The engineered subunit does not traffic and so has no function unless native subunits are present, co-assemble with it and carry it to the cell surface. The PCS/WT complex is rendered light-sensitive once an externally applied membrane impermeant photoswitch is attached to the PCS, something possible only at the plasma membrane.

PCS strategy

To generate a PCS requires the fulfillment of three conditions. First, it is necessary to identify an appropriate site for cysteine modification on the extracellular face of the protein complex where the PTL will be covalently anchored so that its photoisomerization between *trans* and *cis* states results in liganding, and hence modulation of signaling, in one isomer state but not the other. Second, this cysteine-substituted subunit must be mutated in a manner that eliminates its cell-surface trafficking as a homomultimer, but which allows for its surface targeting when it is co-assembled with the wildtype subunit. Finally, the function of the heteromeric complex between the cysteine-substituted, trafficking deficient (PCS) subunit and the wildtype subunit must be efficiently gated by PTL(s) on the PCS subunit(s). We describe here how these conditions can be met.

The first step in developing a PCS—that of anchoring a PTL for photocontrol—has been successfully accomplished in a variety of proteins with a variety of ligands. The two main approaches have been steric block of an active site (either a pore of an ion channel or a catalytic site of an enzyme) or allosteric regulation by the PTL attached to a receptor's ligand binding domain [1,12,26]. The method that has been generalized the most so far is pore block of potassium channels using MAQ as a photoswitchable tethered quaternary ammonium that is attached via its maleimide to a cysteine that has been introduced near the outer mouth of the pore. This was initially demonstrated for the Shaker channel[10]. Because of the high degree of conservation of the pore region of potassium channels, photo-block by MAQ was readily generalized to a diverse set of additional potassium channels, including members of two subfamilies of classical voltage-gated channels (Kv1.3 and Kv3.1), the M-current channel (Kv7.2) and one of the Ca++-activated K+ channels that generates the long-lasting action potential afterhyperpolarization (SK2) [27]. A major reason for the ease of transferring the strategy to other channels is that the high effective concentration of the quaternary ammonium ligand near the pore in the blocking state assures efficient block, even if the affinity for the blocker is low. Moreover, the energy of the azobenzene isomerization is so large that it ensures efficient dissociation in the non-blocking state even if the affinity for block by quaternary ammonium ions is high. In the present study, photo-block with MAQ was successfully applied for the first time to a 2P potassium channel, the TREK1 channel, despite its low affinity for the most broadly used quaternary ammonium blocker, tetraethylammonium[28]. As further evidence of the generalizability of the approach, we also adapted MAQ photo-block to an additional 2P potassium channel target: TASK3. Based on

the success of MAQ so far, it seems likely that it will work on the majority of potassium channels.

Since the PCS approach requires that the photo-control work when only a subset of subunits (the PCS) carry the PTL, but the wildtype subunits do not, the approach is particularly well suited to photo-block of an enzyme active site or channel pore, because block can usually be accomplished by a single ligand, as is the case for quaternary ammonium block of potassium channels. However, the system should also work in cases where the protein complex is composed of more than one type of subunit, such as in the NMDA receptor. In this case the subunit that controls function, the NR2 subunit, would serve as the PCS and be controlled allosterically by a PTL attached to a cysteine introduced into the ligand binding domain.

The second condition that must be fulfilled for the PCS strategy to work is that the only PCS subunits to arrive at the plasma membrane are ones that have co-assembled with native subunits. To achieve this either the subunit must naturally require co-assembly with a distinct partner to traffic to the surface or mutation(s) need to be introduced into the PCS that result in its intracellular retention except in cells that express the wild-type subunit. In addition to the C-terminal deletion of TREK1 that we employed here, several other methods have been reported that provide for this kind of control. A variety of forward trafficking signals that drive localization to the plasma membrane have been identified and these can be disabled by mutation. In addition, it is possible to introduce retention signals that hold proteins in the endoplasmic reticulum. For the PCS approach to work, the effect of the mutation(s) must be rescued by co-assembly with a wild-type subunit. Of course, the mutation(s) must also not affect the function or regulation of the protein of interest.

An example of such a strategy is found in Kir2.1 mutation of the di-acidic forward trafficking site, which leads to retention in the endoplasmic reticulum, but where co-assembly of the di-acidic mutant with wildtype subunits traffics the heteromeric channel to the plasma membrane [29,30]. A summary of characterized retention and export signals is presented in Supplemental Table 6.1.

In some protein complexes there is no need to introduce a mutation in order to induce endoplasmic reticulum retention since one or more of the subunits naturally use this strategy to ensure that only heteromeric assemblies of a particular kind reach the cell surface. This is what is seen in Kir6 channels, where the channel forming subunit is retained inside the cell unless co-assembled with SUR [31 32]. It is also what is seen with the $GABA_B$ receptor, a GPCR that is composed of GB1 and GB2 subunits, in which RXR endoplasmic reticulum retention motifs, which prevent trafficking to the cell surface, are masked in a complementary manner to allow for surface trafficking in the GB1/GB2 heteromer [33]. A functionally analogous scheme operates in NMDA receptors, which are composed of two NR1 and two NR2 subunits, with neither subtype arriving on the cell surface on its own [34 35 36].

As long as the PTL is anchored to an introduced cysteine, one is limited to the use of charged PTLs that will not cross the plasma membrane, which are targeted to either secreted proteins or the extracellular face of membrane proteins. In this way one avoids conjugating the PTL to functionally important lone cysteines on cytoplasmic proteins, such as enzymes that have cysteine at their active sites. However, with several new strategies now available for the orthogonal attachment of probes to proteins [37 38 39 40] it should be possible to expand the PCS strategy to intracellular domains of multimeric membrane proteins. Moreover, orthogonal labeling inside the cell should make it possible to apply the approach to soluble intracellular proteins as long as they are obligate heteromultimers where the PCS cannot function without the

wildtype endogenous partner. It should be noted that if the PCS can heteromerize with more than one native subunit then the analysis becomes more complex, analogous to the complexity of interpreting subunit-specific pharmacological agents, knockout and dominant negative effects.

TREK1-PCS development

We generated a PCS of the TREK1 potassium channel. This is a member of the large 2P potassium channel family. Since their first isolation, the 2P potassium channels have posed a fascinating conundrum. On one hand, they are always open, leading to the impression that they are leak channels that "merely" set up the resting membrane potential. On the other hand, they are regulated by a very large number of signaling systems (including polyunsaturated fatty acids, phosphoinositides, pH, GPCRs, protein kinases, temperature and mechanical force), giving the impression that they are a vital hub of neuronal control. Adding to the mystery, their genetic knock-out often has only subtle effects, although in some cases intriguing specificity has emerged for different family members, for example in poly-unsaturated-fatty-acid-mediated neuroprotection, anesthesia, pain perception, and for a possible role in the treatment of depression[41-44]. Attempts at definitive determination of function have been hampered by a lack of specific, reversible pharmacological agents. Our TREK1-PCS paves the way for solving this pharmacological problem, since the 2P potassium channels show similar block by external quaternary ammonium moieties and this is the blocking ligand of the MAQ photoswitch.

In the present case of TREK1, the Shaker channel served as a successful guide for where to introduce the MAQ attachment site, even though, outside of the pore region, the 2P potassium channels have strongly diverged from the Shaker-type Kv channels. Our screen for MAQ attachment sites in the P regions of TREK1 provided one preferred position, at which block is relieved in the dark, conferred under 380 nm illumination (*cis* state) and relieved under 500 nm illumination (*trans* state). As with other azobenzene PTLs, on and off gating can be repeated many times without loss of efficacy and the switch is bistable, persisting for long periods without illumination in the higher energy *cis*-blocked state, but available for a rapid return to *trans* with light. Interestingly, in TREK1 we found differences in photo-block by MAQ when it was attached to homologous positions in the first (P1) pore region *versus* the second (P2) pore region. Recently obtained structures of the pore of 2P-potassium channels, TRAAK [45] and TWIK1 [46], have shown that the two-fold symmetry converges to an essential four-fold symmetric pore helix and selectivity filter. However, the regions homologous to our cysteine attachment sites in TREK1 are not seen in these crystal structures. Our finding that MAQ attachment to homologous positions in the P1 and P2 of TREK1 yield different blocking characteristics suggests that these portions of the pore region are not four-fold symmetric. The tandem coupling of pairs of subunits that characterizes 2P channels may serve to constrain this asymmetry.

TREK1-PCS reveals a role of TREK1 in hippocampal $GABA_B$ response

While TREK1 is highly expressed in the hippocampus, no hippocampal function had yet been identified. We took interest in the regulation of TREK1 by Gi-coupled GPCRs, since several transmitter-gated versions of these are found in the hippocampus[5]. Postsynaptically, hippocampal $GABA_B$ receptors can inhibit calcium channels[47], but they are primarily known to enhance the potassium channels that underlie the slow inhibitory postsynaptic potential (IPSP). The slow IPSP is known to involve G-protein-coupled inwardly-rectifying potassium (Kir3)

channels[4,22]. Baclofen is generally used to study the $GABA_B$ response (Dutar and Nicoll, 1988). Using baclofen, Koyrakh and colleagues showed evidences for an additional unidentified $GABA_B$ channel target[7]. Our PCS approach enables us to identify this channel as TREK1. As with Kir3 channels, TREK1 is also post-synaptic[23], where it is complexed with the post-synaptic machinery via interaction with AKAP150[48]. This is the second case where a 2P potassium channel has been implicated in GABAergic signaling, since TREK2 appears to mediate a different and much slower IPSP in entorhinal cortex[9].

These findings suggest that 2P potassium channels may have a broad role in synaptic signaling in the brain. It breaks with the traditional notions that Kir3 channels are the sole targets of postsynaptic $GABA_B$ receptors and that 2P-potassium channels serve simply as leak channels in the hippocampus. Our PCS approach offers an affordable and powerful strategy for identifying the molecular basis of unknown ionic currents and for obtaining a pharmacological foothold in multi-subunit signaling proteins.

Methods:

Molecular Biology and Gene Expression

Cysteine mutations were introduced into mTREK1 cDNA in the pIRES2EGFP expression vector using the QuickChange mutagenesis kit (Agilent). The PCR protocol used was 1 cycle (95°, 30 s), 16 cycles (95°, 30 s; 55°, 1 min; 68°, 12 min). TREK1-PCS has been made by PCR and introduced in pIRES2EGFP expression vector. HEK293 Cells were transiently cotransfected using Lipofectamine 2000 (Invitrogen) with TREK1 mutants or TREK1-PCS. For co-expression, TREK1 or TREK1-PCS are cotransfected with a ratio of 1:3 to 1:5 with 1.6 μg of DNA total per 18 mm diameter cover slip. Hippocampal neurons were transfected using the calcium phosphate method. Each 12 mm coverslip received 1.1 μg of TREK1-PCS DNA and 0.2 μg of Tomato DNA.

Cell Culture

HEK293 cells were maintained in DMEM with 5% FBS on poly-L-lysine-coated glass coverslips. Dissociated hippocampal neurons were obtained from postnatal rats (P0-1) and plated at 75,000 cells/coverslip on poly-L-lysine-coated glass coverslips (12 mM). Neurons were maintained in media containing MEM supplemented with 5% fetal bovine serum, B27 (Invitrogen), and GlutaMAX (Invitrogen).

Electrophysiology

HEK293 cell electrophysiology was performed 24-72 h after transfection solution containing (in mM): 145 mM NaCl, 4 mM KCl, 1 mM $MgCl_2$, 2 mM $CaCl_2$ and 10 mM HEPES. Glass pipettes of resistance between 3 and 6 MΩ were filled with intracellular solution containing (in mM): 140 KCl, 10 Hepes, 3 Na_2ATP, 0.2 Na_2GTP, 5 EGTA, 3 $MgCl_2$, pH 7.4. Cells were voltage clamped using an Axopatch 200A (Molecular Devices) amplifier in the whole cell mode.

Hippocampal neuron whole cell patch clamp electrophysiology was performed 3-6 days after transfection (DIV 12-15 for cultured neurons; DIV 6-8 for slices). For voltage and current clamp experiments in cultured neurons, extracellular solution contained (in mM): 138 NaCl, 1.5 KCl, 1.2 $MgCl_2$, 2.5 $CaCl_2$, 10 glucose, 5 Hepes, (plus 10 CNQX, 10 Bicucculine only for voltage clamp experiments), pH 7.4. In slices ACSF contained (in mM) 19 NaCl, 2.5 KCl, 1.3 $MgSO_4$, 1 NaH_2PO_4-H_2O, 26.2 $NaHCO_3$, 11 glucose and 2.5 $CaCl_2$ and was continuously perfused and bubbled with 95% O_2/5% CO_2. For all experiments, intracellular solution contained (in mM): 140 K-Gluconate, 10 NaCl, 5 EGTA, 2 $MgCl_2$, 1 CaCl2, 10 Hepes, 2 MgATP, 0.3 Na_2GTP, pH 7.2. For slice experiments MAQ was diluted in NMDG-labeling solution containing (in mM): 150 NMDG-HCl, 3 KCl, 0.5 $CaCl_2$, 5 $MgCl_2$, 10 HEPES and 5 glucose, pH 7.4. Only cells with a resting potential <-45 mV were analyzed. All pharmacological compounds for voltage clamp recording were dissolved in appropriate extracellular buffers before application using a gravity-driven perfusion system.

Illumination was controlled using a Polychrome V monochromator (TILL Photonics) through a 20x objective or with a Lambda DG4 high speed wavelength switcher (Sutter) with

380 nm and 500 nm filters through a 40x objective. pClamp software was used for both data acquisition and control of illumination. To conjugate MAQ, cells were incubated in 50-100 μM MAQ for 60 minutes in the dark at room temperature in standard extracellular cell buffer for either HEK293 cells or hippocampal neurons. The percentage of block was calculated from the current induced by a voltage-ramp at -20 mV as $(I_{500}-I_{380}/I_{500})*100$.

Preparation of cultured hippocampal slices

Hippocampi were obtained from postnatal Sprague-Dawley rats (postnatal days 6 and 7), cut into 400-μm slices and cultured on 0.4-μm Millicell culture inserts (Millipore) in Neurobasal-A medium (Gibco) supplemented with 20% horse serum (vol/vol), insulin, ascorbic acid, GlutaMAX (Gibco), penicillin/streptomycin, HEPES and Ara-C. Slices were transfected 2-3 d after isolation by Biolistic gene transfer using a BioRad Helios Gene Gun and gold microcarriers coated with both DNA encoding TREK1-PCS in Pires2EGFP and cytosolic tdTomato (to aid in the visualization of the transfected cells).

References:

1 Szobota, S. & Isacoff, E. Y. Optical control of neuronal activity. *Annu Rev Biophys* **39**, 329-348, doi:10.1146/annurev.biophys.093008.131400 (2010).

2 Semyanov, A., Walker, M. C., Kullmann, D. M. & Silver, R. A. Tonically active GABA A receptors: modulating gain and maintaining the tone. *Trends Neurosci* **27**, 262-269, doi:10.1016/j.tins.2004.03.005 (2004).

3 Kohl, M. M. & Paulsen, O. The roles of GABAB receptors in cortical network activity. *Adv Pharmacol* **58**, 205-229, doi:10.1016/S1054-3589(10)58009-8 (2010).

4 Luscher, C., Jan, L. Y., Stoffel, M., Malenka, R. C. & Nicoll, R. A. G protein-coupled inwardly rectifying K+ channels (GIRKs) mediate postsynaptic but not presynaptic transmitter actions in hippocampal neurons. *Neuron* **19**, 687-695 (1997).

5 Padgett, C. L. & Slesinger, P. A. GABAB receptor coupling to G-proteins and ion channels. *Adv Pharmacol* **58**, 123-147, doi:10.1016/S1054-3589(10)58006-2 (2010).

6 Ulrich, D. & Bettler, B. GABA(B) receptors: synaptic functions and mechanisms of diversity. *Curr Opin Neurobiol* **17**, 298-303, doi:10.1016/j.conb.2007.04.001 (2007).

7 Koyrakh, L. *et al.* Molecular and cellular diversity of neuronal G-protein-gated potassium channels. *J Neurosci* **25**, 11468-11478, doi:10.1523/JNEUROSCI.3484-05.2005 (2005).

8 Noel, J., Sandoz, G. & Lesage, F. Molecular regulations governing TREK and TRAAK channel functions. *Channels (Austin)* **5**, doi:16469 [pii] (2011).

9 Deng, P. Y. *et al.* GABA(B) receptor activation inhibits neuronal excitability and spatial learning in the entorhinal cortex by activating TREK-2 K+ channels. *Neuron* **63**, 230-243, doi:10.1016/j.neuron.2009.06.022 (2009).

10 Banghart, M., Borges, K., Isacoff, E., Trauner, D. & Kramer, R. H. Light-activated ion channels for remote control of neuronal firing. *Nat Neurosci* **7**, 1381-1386, doi:nn1356 [pii]10.1038/nn1356 (2004).

11 Volgraf, M. *et al.* Allosteric control of an ionotropic glutamate receptor with an optical switch. *Nat Chem Biol* **2**, 47-52, doi:nchembio756 [pii]10.1038/nchembio756 (2006).

12 Fehrentz, T., Schonberger, M. & Trauner, D. Optochemical genetics. *Angew Chem Int Ed Engl* **50**, 12156-12182, doi:10.1002/anie.201103236 (2011).

13 Chemin, J. *et al.* A phospholipid sensor controls mechanogating of the K+ channel TREK-1. *EMBO J* **24**, 44-53, doi:10.1038/sj.emboj.7600494 (2005).

14 Veale, E. L., Rees, K. A., Mathie, A. & Trapp, S. Dominant negative effects of a non-conducting TREK1 splice variant expressed in brain. *J Biol Chem* **285**, 29295-29304, doi:10.1074/jbc.M110.108423 (2010).

15 Cohen, A., Ben-Abu, Y., Hen, S. & Zilberberg, N. A Novel Mechanism for Human K2P2.1 Channel Gating: FACILITATION OF C-TYPE GATING BY PROTONATION OF EXTRACELLULAR HISTIDINE RESIDUES. *J Biol Chem* **283**, 19448-19455 (2008).

16 Sandoz, G., Douguet, D., Chatelain, F., Lazdunski, M. & Lesage, F. Extracellular acidification exerts opposite actions on TREK1 and TREK2 potassium channels via a single conserved histidine residue. *Proc Natl Acad Sci U S A* **106**, 14628-14633, doi:0906267106 [pii] 10.1073/pnas.0906267106 (2009).

17 Bagriantsev, S. N., Peyronnet, R., Clark, K. A., Honore, E. & Minor, D. L., Jr. Multiple modalities converge on a common gate to control K2P channel function. *EMBO J* **30**, 3594-3606, doi:emboj2011230 [pii]10.1038/emboj.2011.230 (2011).

18 Cain, S. M., Meadows, H. J., Dunlop, J. & Bushell, T. J. mGlu4 potentiation of K(2P)2.1 is dependant on C-terminal dephosphorylation. *Mol Cell Neurosci* **37**, 32-39, doi:10.1016/j.mcn.2007.08.009 (2008).

19 Patel, A. J. *et al.* A mammalian two pore domain mechano-gated S-like K+ channel. *EMBO J* **17**, 4283-4290, doi:10.1093/emboj/17.15.4283 (1998).

20 Lauritzen, I. *et al.* Cross-talk between the mechano-gated K2P channel TREK-1 and the actin cytoskeleton. *EMBO Rep* **6**, 642-648 (2005).

21 Newberry, N. R. & Nicoll, R. A. Direct hyperpolarizing action of baclofen on hippocampal pyramidal cells. *Nature* **308**, 450-452 (1984).

22 Dutar, P. & Nicoll, R. A. A physiological role for GABAB receptors in the central nervous system. *Nature* **332**, 156-158, doi:10.1038/332156a0 (1988).

23 Sandoz, G. *et al.* Mtap2 is a constituent of the protein network that regulates twik-related K+ channel expression and trafficking. *J Neurosci* **28**, 8545-8552 (2008).
24 Zhou, M. *et al.* TWIK-1 and TREK-1 are potassium channels contributing significantly to astrocyte passive conductance in rat hippocampal slices. *J Neurosci* **29**, 8551-8564, doi:10.1523/JNEUROSCI.5784-08.2009 (2009).
25 Hibino, H. *et al.* Inwardly rectifying potassium channels: their structure, function, and physiological roles. *Physiol Rev* **90**, 291-366, doi:10.1152/physrev.00021.200990/1/291 [pii] (2010).
26 Gorostiza, P. & Isacoff, E. Y. Optical switches for remote and noninvasive control of cell signaling. *Science* **322**, 395-399, doi:10.1126/science.1166022322/5900/395 [pii] (2008).
27 Fortin, D. L. *et al.* Optogenetic photochemical control of designer K+ channels in mammalian neurons. *J Neurophysiol* **106**, 488-496, doi:10.1152/jn.00251.2011jn.00251.2011 [pii] (2011).
28 Noel, J., Sandoz, G. & Lesage, F. Molecular regulations governing TREK and TRAAK channel functions. *Channels (Austin)* **5**, 402-409, doi:10.4161/chan.5.5.1646916469 [pii] (2011).
29 Ma, D. *et al.* Role of ER export signals in controlling surface potassium channel numbers. *Science* **291**, 316-319, doi:10.1126/science.291.5502.316291/5502/316 [pii] (2001).
30 Ma, D. *et al.* Diverse trafficking patterns due to multiple traffic motifs in G protein-activated inwardly rectifying potassium channels from brain and heart. *Neuron* **33**, 715-729, doi:S0896627302006141 [pii] (2002).
31 Sakura, H., Ammala, C., Smith, P. A., Gribble, F. M. & Ashcroft, F. M. Cloning and functional expression of the cDNA encoding a novel ATP-sensitive potassium channel subunit expressed in pancreatic beta-cells, brain, heart and skeletal muscle. *FEBS Lett* **377**, 338-344, doi:0014-5793(95)01369-5 [pii]10.1016/0014-5793(95)01369-5 (1995).
32 Zerangue, N., Schwappach, B., Jan, Y. N. & Jan, L. Y. A new ER trafficking signal regulates the subunit stoichiometry of plasma membrane K(ATP) channels. *Neuron* **22**, 537-548, doi:S0896-6273(00)80708-4 [pii] (1999).
33 Margeta-Mitrovic, M., Jan, Y. N. & Jan, L. Y. A trafficking checkpoint controls GABA(B) receptor heterodimerization. *Neuron* **27**, 97-106, doi:S0896-6273(00)00012-X [pii] (2000).
34 Okabe, S., Miwa, A. & Okado, H. Alternative splicing of the C-terminal domain regulates cell surface expression of the NMDA receptor NR1 subunit. *J Neurosci* **19**, 7781-7792 (1999).
35 Standley, S., Roche, K. W., McCallum, J., Sans, N. & Wenthold, R. J. PDZ domain suppression of an ER retention signal in NMDA receptor NR1 splice variants. *Neuron* **28**, 887-898, doi:S0896-6273(00)00161-6 [pii] (2000).
36 Xia, H., Hornby, Z. D. & Malenka, R. C. An ER retention signal explains differences in surface expression of NMDA and AMPA receptor subunits. *Neuropharmacology* **41**, 714-723, doi:S0028390801001034 [pii] (2001).
37 Boyce, M. & Bertozzi, C. R. Bringing chemistry to life. *Nat Methods* **8**, 638-642, doi:10.1038/nmeth.1657nmeth.1657 [pii] (2011).
38 Liu, D. S. *et al.* Diels-Alder cycloaddition for fluorophore targeting to specific proteins inside living cells. *J Am Chem Soc* **134**, 792-795, doi:10.1021/ja209325n (2012).
39 Yao, J. Z. *et al.* Fluorophore targeting to cellular proteins via enzyme-mediated azide ligation and strain-promoted cycloaddition. *J Am Chem Soc* **134**, 3720-3728, doi:10.1021/ja208090p (2012).
40 Cohen, J. D., Zou, P. & Ting, A. Y. Site-specific protein modification using lipoic acid ligase and bis-aryl hydrazone formation. *Chembiochem* **13**, 888-894, doi:10.1002/cbic.201100764 (2012).
41 Heurteaux, C. *et al.* TREK-1, a K+ channel involved in neuroprotection and general anesthesia. *Embo J* **23**, 2684-2695 (2004).
42 Noel, J. *et al.* The mechano-activated K+ channels TRAAK and TREK-1 control both warm and cold perception. *EMBO J* **28**, 1308-1318, doi:emboj200957 [pii]10.1038/emboj.2009.57 (2009).
43 Heurteaux, C. *et al.* Deletion of the background potassium channel TREK-1 results in a depression-resistant phenotype. *Nat Neurosci* **9**, 1134-1141 (2006).
44 Mazella, J. *et al.* Spadin, a sortilin-derived peptide, targeting rodent TREK-1 channels: a new concept in the antidepressant drug design. *PLoS Biol* **8**, e1000355, doi:10.1371/journal.pbio.1000355 (2010).
45 Brohawn, S. G., del Marmol, J. & MacKinnon, R. Crystal structure of the human K2P TRAAK, a lipid- and mechano-sensitive K+ ion channel. *Science* **335**, 436-441, doi:10.1126/science.1213808335/6067/436 [pii] (2012).

46 Miller, A. N. & Long, S. B. Crystal structure of the human two-pore domain potassium channel K2P1. *Science* **335**, 432-436, doi:10.1126/science.1213274335/6067/432 [pii] (2012).
47 Mintz, I. M. & Bean, B. P. GABAB receptor inhibition of P-type Ca2+ channels in central neurons. *Neuron* **10**, 889-898, doi:0896-6273(93)90204-5 [pii] (1993).
48 Sandoz, G. *et al.* AKAP150, a switch to convert mechano-, pH- and arachidonic acid-sensitive TREK K(+) channels into open leak channels. *Embo J* **25**, 5864-5872 (2006).

Supplementary Figures:

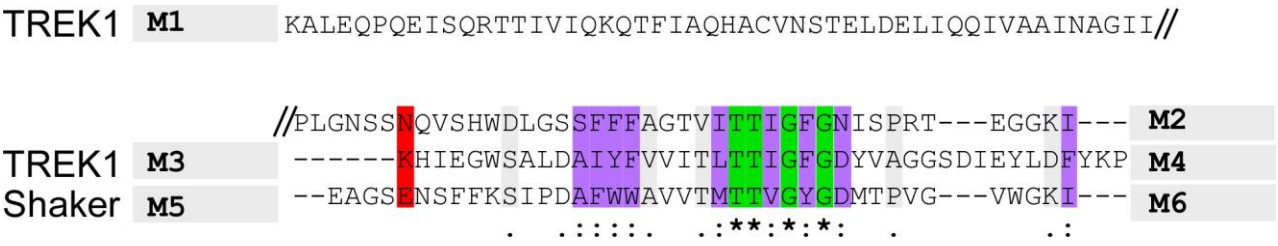

Figure S6.1, **Sequence alignment of shaker and TREK1 pore regions.** An ***** (green boxes) indicates positions which have a single, fully conserved residue. A **:** (pink boxes) indicates conservation between groups of strongly similar properties. A **.** (grey boxes) indicates conservation between groups of weakly similar properties. The red box indicates the E422 in shaker, the N122 in P1 and K231 in P2 of TREK1.

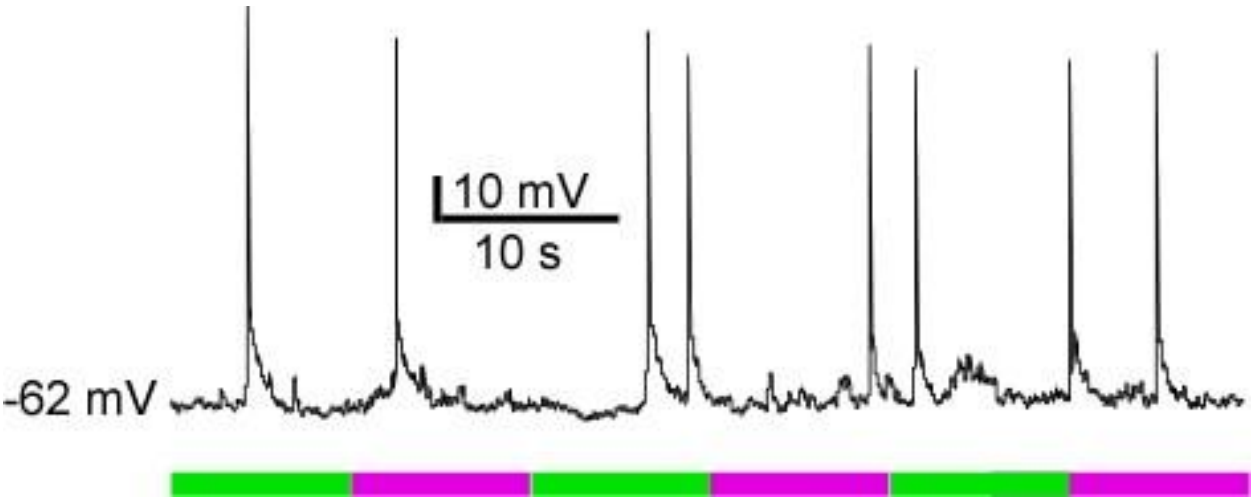

Figure S6.2, **Whole-cell recording from non-transfected MAQ-labeled hippocampal neuron.** Representative example of light modulation of the resting membrane potential which is not modified by alternating illumination at 500 nm (green) and 380 nm (magenta).

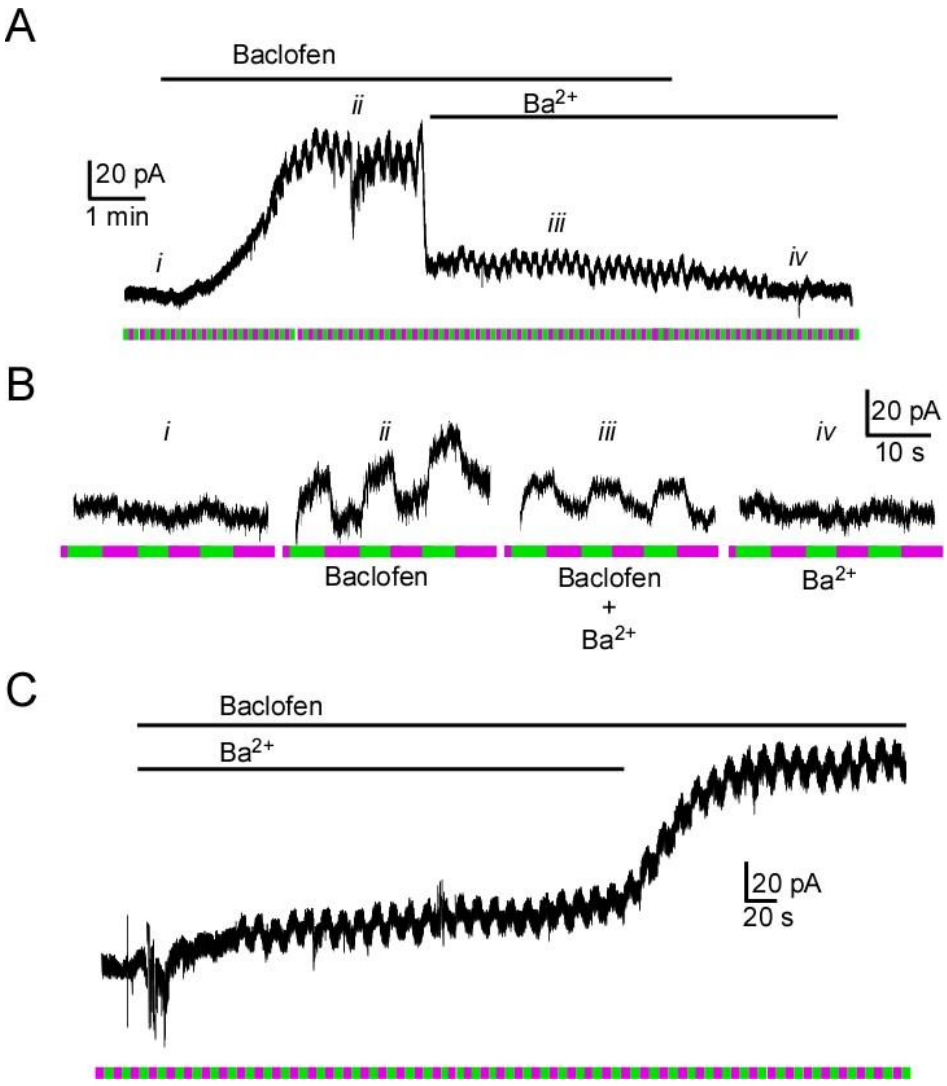

Figure S6.3, Representative current obtained from hippocampal neuron expressing TREK1-PCS. A) Application of baclofen (60 µM) induces an outward current with a component that was blocked by 380 nm light and unblocked by 500 nm light. Application of 1 mM external barium blocks most of the outward current (consistent with its known complete block of Kir3), and only partially blocks the photoswitchable component of the current (consistent with its known partial block of TREK1). The photoswitchable component of the current turns off upon baclofen washout. B) Zoom-in of the recorded current in (A) during periods marked as (*i*), (*ii*) (*iii*) and (*iv*). Illumination at 500 nm (green) and 380 nm (magenta). C) Co-application of Barium and baclofen induces an outward current that is blocked by 380 nm light and unblocked by 500 nm light. Barium washout relieves block of an outward current with little increase in the photoswitched component, consistent with unblock of Kir3.

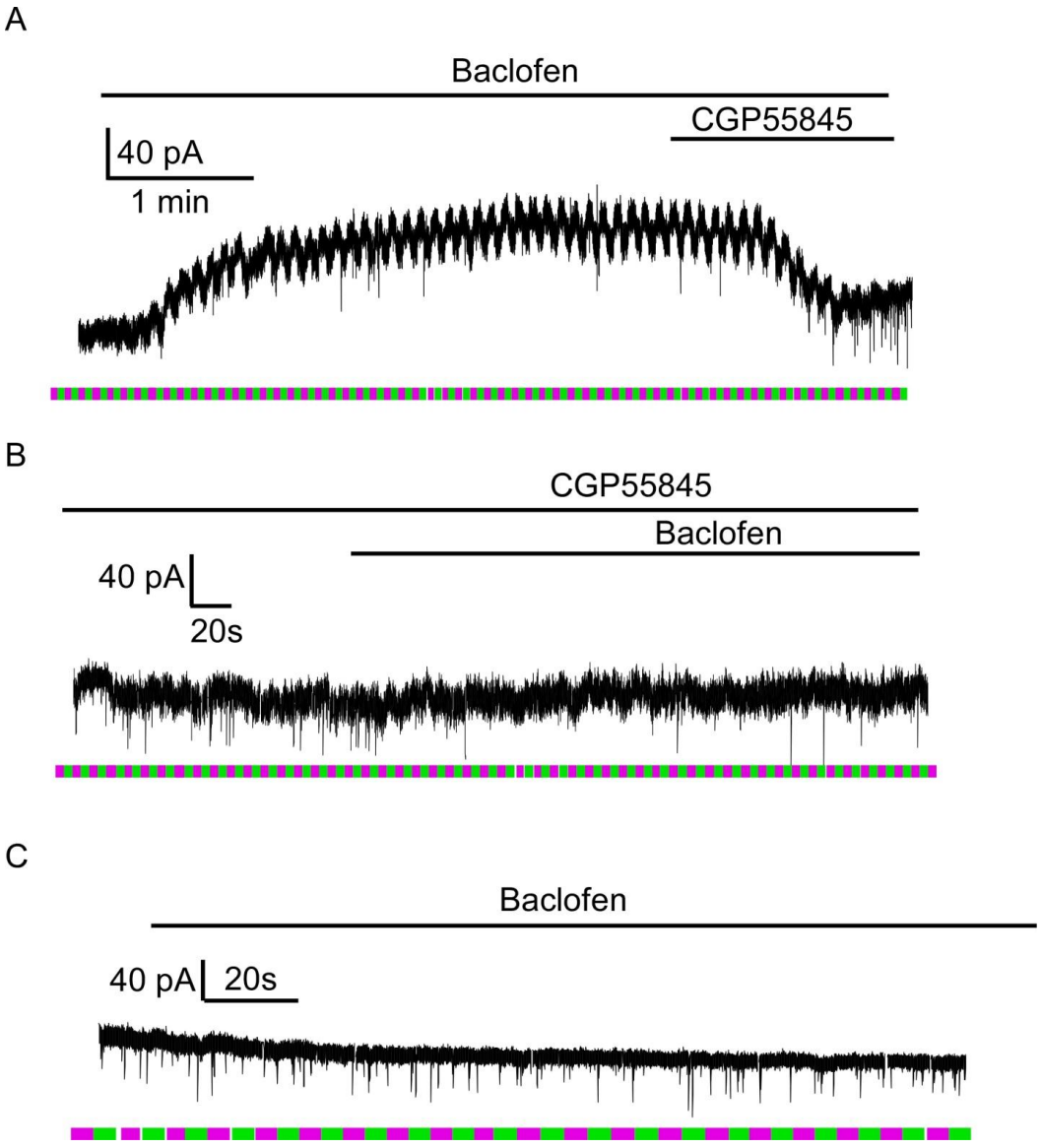

Figure S6.4, **CPG55845 and PTX prevent the baclofen induced-current.** A) Representative current obtained from hippocampal neuron expressing TREK1□C-S121C. Application of baclofen (60 µM) induces an outward current, which can be reversed by application of 5 µM of CPG55845 during the period of baclofen application. Before baclofen no photoswitched current is evident, but during the baclofen response the current is modulated by light, indicating that the baclofen-activated current is partly due to TREK-1 channels. Illumination at 500 nm (green) and 380 nm (magenta). B) Prior exposure to CPG55845 prevents induction of a baclofen induced current. C) PTX incubation for 36 hours prevents the baclofen induced current.

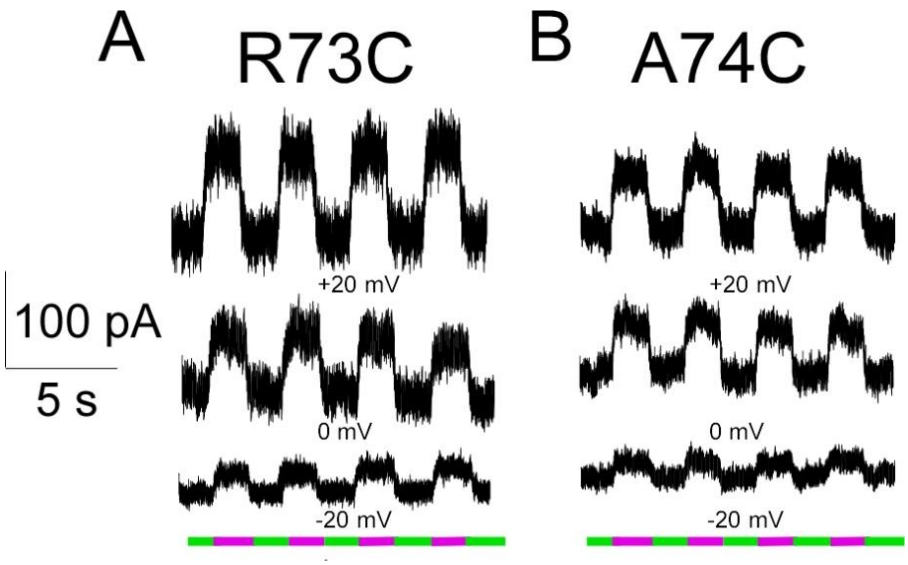

Figure S6.5, **Light-gated TASK3.** A) Whole-cell recording from HEK293T cell expressing TASK3(R73C) that has been labeled with MAQ. Current was elicited by alternating illumination at 500 nm (green) and 380 nm (magenta), which reversibly blocked and unblocked constant outward current, as seen at different holding potentials. B) Same as in A but for another MAQ anchoring site: TASK3(A74C).

Chapter VII: Phospholipase D2 specifically regulates TREK channels via direct interaction and local production of phosphatidic acid

This chapter is currently under review at the Proceedings of the National Academies of Science with me as co-first author. It is the product of a collaboration with the Sandoz lab at the University of Nice.

Introduction:

Growing evidence indicates that trafficking and function of membrane proteins, including ion channels and receptors, can be regulated by both their associated protein and lipid environments. Membrane lipids play a key role in intracellular signal transduction via lipid mediators that act as second messengers and docking sites for proteins. Membrane phospholipids, specifically, function as signaling molecules that are able to exert their effects on membrane proteins dynamically in conjunction with enzymes, such as phospholipases, which alter their phosphate head groups. Phospholipase D is an enzyme that catalyzes the hydrolysis of the membrane phospholipid phosphatidylcholine to produce phosphatidic acid (PA). PA, much like phosphatidylinositol-4,5-bisphosphate (PIP2), is a second messenger which is involved in a variety of cellular functions such as cell proliferation, cytoskeleton organization, morphogenesis and vesicle trafficking[1-3]. However, unlike PIP2, following its production by PLD, PA is extremely short lived and is rapidly converted to DAG by DAG kinase which raises the question of how PLD activity can effectively regulate cellular processes[4,5]. Notably, primary alcohols can compete with water as a substrate for PLD2 which can lead to the production of phosphatidylethanol (PEtOH) or phosphatidyl-butan-1-ol (P-1-BtOH) rather than PA[6]. There are two mammalian isoforms of PLD, PLD1 and PLD2, which share 50% amino acid identity and are both widely expressed in the nervous system[7].

The family of K_{2P} channels serves as a hub for the generation and regulation of a negative resting membrane potential throughout the nervous system. K_{2P} channels are dimers composed of subunits that contain 2 pairs of transmembrane segments which flank a pore domain (in the order: TM1, P1, TM2, TM3, P2, TM4)[8]. The activity of K_{2P} channels drives the membrane potential toward the K^+ equilibrium potential and therefore reduces cellular excitability via hyperpolarization. The members of the TREK channel subfamily of K_{2P} channels, TREK1, TREK2, and the more evolutionarily distant TRAAK channel, are widely expressed in the nervous system[9,10]. TREK channels display low basal activity but can be stimulated by various stimuli including phospholipids such as PA and PIP2[11-15], an increase in temperature, mechanical stretch, intracellular and extracellular pH[11,14-16], polyunsaturated fatty acids (PUFAs) such as arachidonic acid, and pharmacological agents such as volatile anesthetics and riluzole[16]. TREK1 gene knock out produces mice with reduced sensitivity to volatile anaesthetics[17], impaired neuroprotection afforded by PUFAs against ischemia[17] and altered pain perception[18]. In addition, loss of TREK1 renders mice resistant to depression, suggesting TREK1 as a candidate target for antidepressant medications[19]. While classical methods of genetic knockout or pharmacological approaches have been used for most work on TREK channels, we recently developed the photoswitchable conditional subunit (PCS) method that allows us to endow endogenous TREK1 channels with light sensitivity. The PCS technique allows for the study of native TREK1 channels without the need for transgenic manipulation or non-specific pharmacological agents.

Previously, we used the TREK1-PCS method to discover a role for TREK1 in mediating the hippocampal $GABA_B$ response[20].

In many cases, regulation of membrane proteins is mediated by the organization of complexes between various proteins and signaling molecules that serve to enhance both the speed and specificity of the regulation[21,22]. For example, TREK1 interacts with AKAP150, a scaffolding protein, which brings protein kinase A (PKA) into the proximity of TREK1 to facilitate specific regulation of the cytoplasmic domain of TREK1 by PKA-mediated phosphorylation[10,23-25]. In the case of phospholipids, one potential mechanism for specific regulation is spatiotemporal segregation where the local concentrations of specific phospholipids are either dynamically increased or decreased relative to the bulk of the membrane.

In this study, we report an inhibitory effect of protracted exposure to primary alcohols on TREK1 and TREK2 channels. We investigated the metabolic pathway involved in this indirect regulation and found that TREK1 and TREK2, but not TRAAK, are specifically potentiated by PLD2, but not PLD1. We also provide evidence that the specificity of this regulation is due to the direct binding of PLD2 to TREK channels. Furthermore, using a catalytically inactive mutant of PLD2 to compete with endogenous PLD2, we were able to reduce TREK current by decreasing the local PA concentration in the vicinity of the channel. We then studied the functional coupling of native TREK1 channels with endogenous PLD2 in hippocampal neurons and found that PLD2-mediated regulation is associated with tonic potentiation of the basal TREK current. These findings demonstrate a new mechanism of regulation of an ion channel by direct interaction with a phospholipase which is able to locally modulate the phospholipid composition of the membrane.

Results:

TREK1 is inhibited by protracted but not acute primary alcohol application

TREK channels can be stimulated by phospholipids, including directly applied PA[26] but so far there has been no determination of whether such PA-mediated activation is regulated. Since alcohols target PLD[6] and PLD catalyzes the production of PA[27], we wondered if alcohol might modulate TREK channels through PLD. A diverse population of potassium channels are directly regulated by ethanol, including BK[28], SK[29], K_V[30] and GIRK[31]. We initially investigated the possible regulation of TREK1 by alcohols in a heterologous system. We first tested primary alcohols and found that acute application of either 0.25 % butan-1-ol (27 mM) or 0.6 % ethanol (104 mM) for ~1 minute did not modify TREK1 current in HEK 293T cells (Fig. 7.1A, B). However, protracted ($\geq$1 hr) application of either of these primary alcohols reduced TREK1 current by around 50% (Fig. 7.1C, F; current densities were 39 ± 5 pA/pF for TREK1, 18 ± 5 pA/pF for TREK1 + ethanol; $P<0.05$ and 18 ± 4 pA/pF for TREK1 + butan-1-ol; $P<0.05$). We then tested secondary alcohols and found that, unlike ethanol or butan-1-ol, protracted application of 0.25 % butan-2-ol did not modify TREK1 current (Fig. 7.1D, E; current density was 43 ± 6 pA/pF, $P>0.4$).

We then investigated the potential regulation of native TREK1 current by alcohol in primary cultures of hippocampal neurons. We expressed an engineered TREK1-Photoconditionnal subunit (TREK1-PCS) to endow light sensitivity to the native TREK1 channels [32]. As in HEK293T cells, protracted ($\geq$1 hr) application of 0.6% of ethanol reduced TREK1 current by around 70% compared to untreated cells (Fig. 7.1F). These results suggest that primary alcohols modulate native and heterogously expressed TREK1 channels via an indirect mechanism, such as a metabolic effect on a second messenger that regulates TREK1.

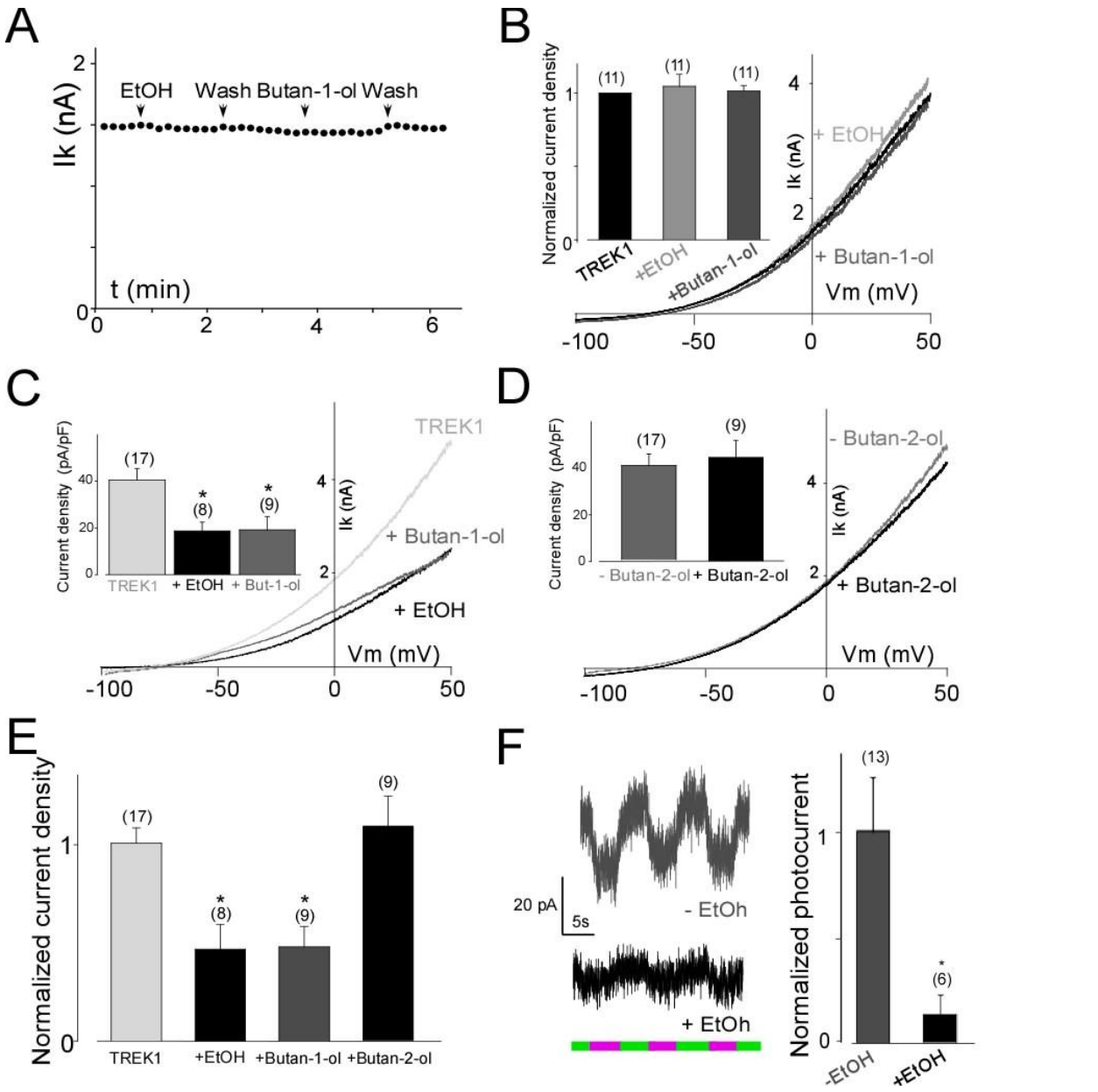

Figure 7.1. TREK1 is inhibited by protracted but not acute primary alcohol application. (A, B) Effect of acute primary alcohol application on TREK1 current. (A) Representative example of TREK1 current stability following brief (~1 minute) primary alcohol application in HEK 293T cells. (B) Summary of effect of acute primary alcohol application on TREK1 current. Current was elicited by voltage-ramps (from -100 to 50 mV, 1s in duration). Inset, normalized TREK1 current density after acute primary alcohol application. (C) Effect of protracted primary alcohol application on TREK1 current in HEK 293T cells. Current was elicited by voltage-ramps (from -100 to 50 mV, 1s in duration). Inset, normalized TREK1 current densities after acute primary alcohol application. (D) Effect of protracted butan-2-ol application. Insets, TREK1 current densities before and after protracted butan-2-ol application are shown. (E) Summary of normalized TREK1 current densities after protracted alcohol application. Student's *t* tests (*$P < 0.05$) shows the difference between TREK1 and TREK1 after ethanol, butan-1-ol or butan-2-ol application. The numbers of cells tested are indicated in parentheses. (F) Protracted ethanol application decreases native TREK1 photocurrent in hippocampal neurons. Left, representative examples of TREK1 photocurrent with (black trace) and without (gray trace) protracted (≥1 hr) ethanol application. Right, average normalized TREK1 photocurrent amplitudes with and without protracted ethanol application (≥1hrs).

PLD2-mediated potentiation of TREK1 current is reversed by protracted primary alcohol treatment and the PLD inhibitor FIPI

We next asked whether the observed effects of alcohol on TREK1 could be mediated by PLD. To address this question, we first set out to determine if PLD can regulate TREK activity. We tested this by co-expressing TREK1 and PLD2. We found that PLD2 co-expression increased TREK1 current by more than 4-fold (Fig. 7.2A, B; current densities for TREK1 and TREK1+PLD2 were 19 ± 2 pA/pF and 86 ± 9 pA/pF, respectively; $P<0.001$).

Since the production of PA by PLD2 is inhibited by primary alcohols, we wondered if protracted treatment with primary alcohols would affect the potentiation of TREK1 by PLD2. In the presence of co-expressed PLD2, protracted application of either ethanol or butan-1-ol reduced TREK1 current by 71% (Fig 2C, D; current densities were 39 ± 5 pA/pF for TREK1 alone, 139 ± 21 pA/pF for TREK1 + PLD2, 24 ± 5 pA/pF for TREK1 + PLD2 + ethanol, and 22 ± 5 pA/pF for TREK1 + PLD2 + butan-1-ol; $P<0.01$ for TREK1 + PLD2 vs. TREK1 + PLD2 + ethanol and $P<0.01$ for TREK1 + PLD2 vs. PLD2 + butan-1-ol). Notably, the current densities observed for TREK1 co-expressed with PLD2 and treated with ethanol or butan-1-ol were not significantly different than the current amplitude for TREK1 expressed alone after primary alcohol incubation (Fig. 7.2F; $P>0.4$ for TREK1 + ethanol vs. TREK1 + PLD2 + ethanol and $P>0.5$ for TREK1 + butan-1-ol vs. TREK1 + PLD2 + butan-1-ol). Consistent with the previous section, the secondary alcohol butan-2-ol failed to modify TREK1 current when co-expressed with PLD2 (Fig. S7.1; current density was 127 ± 44 pA/pF, $P>0.7$). In summary, primary but not secondary alcohols suppressed the ability of PLD2 to enhance current by TREK1 (Fig. 7.2F). Since primary alcohols, but not secondary alcohols, can serve as alternative substrates in PLD-catalyzed transphosphatidylation to produce phosphatidylalcohols instead of PA, these results suggest that the inhibition of TREK1 by primary alcohols is mediated by inhibition of the production of PA by PLD2. To confirm that the effect of alcohol on TREK1 is directly linked to inhibition of PA production, we used the recently developed, specific PLD inhibitor 5-fluoro-2-indolyl des-chlorohalopemide (FIPI)[33]. Incubation for one hour with FIPI reduced TREK1 + PLD2 current by 76% to a level similar to primary alcohol incubation (Fig. 7.2E, F; current density was 19 ± 4 pA/pF for TREK1 + PLD2 + FIPI, $P<0.01$ for TREK1 + PLD2 vs. TREK1 + PLD2 + FIPI). Furthermore, coapplication of primary alcohol and FIPI did not show an additional inhibitory effect indicating that both treatments may work through the same mechanism (Fig. 7.2F; current density was 24 ± 6 pA/pF, $P>0.4$ for TREK1 + PLD2+ FIPI vs. TREK1 + PLD2 + FIPI + EtOH and $P>0.6$ for TREK1 + PLD2+ EtOH vs. TREK1 + PLD2 + FIPI + EtOH). In addition, FIPI reduced TREK1 current densities to similar levels with or without PLD2 coexpression as was also observed for primary alcohol treatment (Fig. S7.2). These results strongly support the idea that PLD2 potentiates TREK1 channel activity through production of PA.

PLD2-mediated potentiation of TREK1 requires basic residues in the TREK1 C terminus

Our results so far indicate that the regulation of TREK1 channels by PLD2 depends on the production of PA by PLD2. To further test this idea, we turned our attention to the portion of the TREK1 channel that is known to be essential for PA regulation, and where PA has been conjectured to bind [26]. Stimulation of TREK1 by PA depends on five positively charged residues in the TREK1 carboxyl-terminal domain (Ctd) and the negative charge of the phosphate group of

PA. This modulation can be eliminated by mutation of the positively charged residues to produce "TREK1-pentaA".

To test if the ability to sense phospholipids is required for TREK1 to be potentiated by PLD2, we examined the effect of PLD2 co-expression on TREK1-pentaA. Unlike in wild-type TREK1, TREK1-pentaA was not potentiated by PLD2 co-expression (Fig. S7.3). Together with the suppression of PLD2 modulation of TREK1 by primary alcohols and FIPI, this result argues that enzymatic production of PA by PLD2 is required for stimulation of TREK1.

A catalytically inactive mutant of PLD2 decreases TREK1 current

Our findings that protracted exposure to primary alcohols and FIPI reduces TREK1 current in cells transfected with only TREK1, that the magnitude of this suppression is far greater when PLD2 is co-expressed and that the current that remains after primary alcohol or FIPI treatment is the same whether or not PLD2 is co-expressed, suggest that endogenous PLD2 tonically stimulates TREK1 and that this stimulation is suppressed by primary alcohols or FIPI. In order to test if TREK1 is regulated by endogenous PLD2, we co-expressed a catalytically inactive mutant of PLD2 (PLD2-K758R)[34,35]. Co-expression of PLD2-K758R significantly decreased the TREK1 current (Fig. 7.2G, H; current densities were 51 ± 7 pA/pF and 28 ± 3 pA/pF for TREK1 and TREK1 + PLD2-K758R, respectively; $P<0.05$). This suppression was similar to that elicited by protracted application of primary alcohols and FIPI (Fig. 7.1; Fig. S7.2). Moreover, protracted primary alcohol application did not further inhibit TREK1 current when PLD2-K758R was co-expressed (Fig. 7.2H; current densities were 30 ± 4 pA/pF for TREK1 + PLD2-K758R + ethanol and $P>0.6$ and 29 ± 4 pA/pF for TREK1 + PLD2-K758R + butan-1-ol; $P>0.7$) which is consistent with a dependency of primary alcohol regulation of TREK on PLD2.

The ability of the over-expressed catalytically-inactive form of PLD2 to prevent endogenous wild-type PLD2 from stimulating TREK1 could be explained by competition for localization to the vicinity of TREK1. We therefore examined this possibility by asking if the channel and enzyme directly associate.

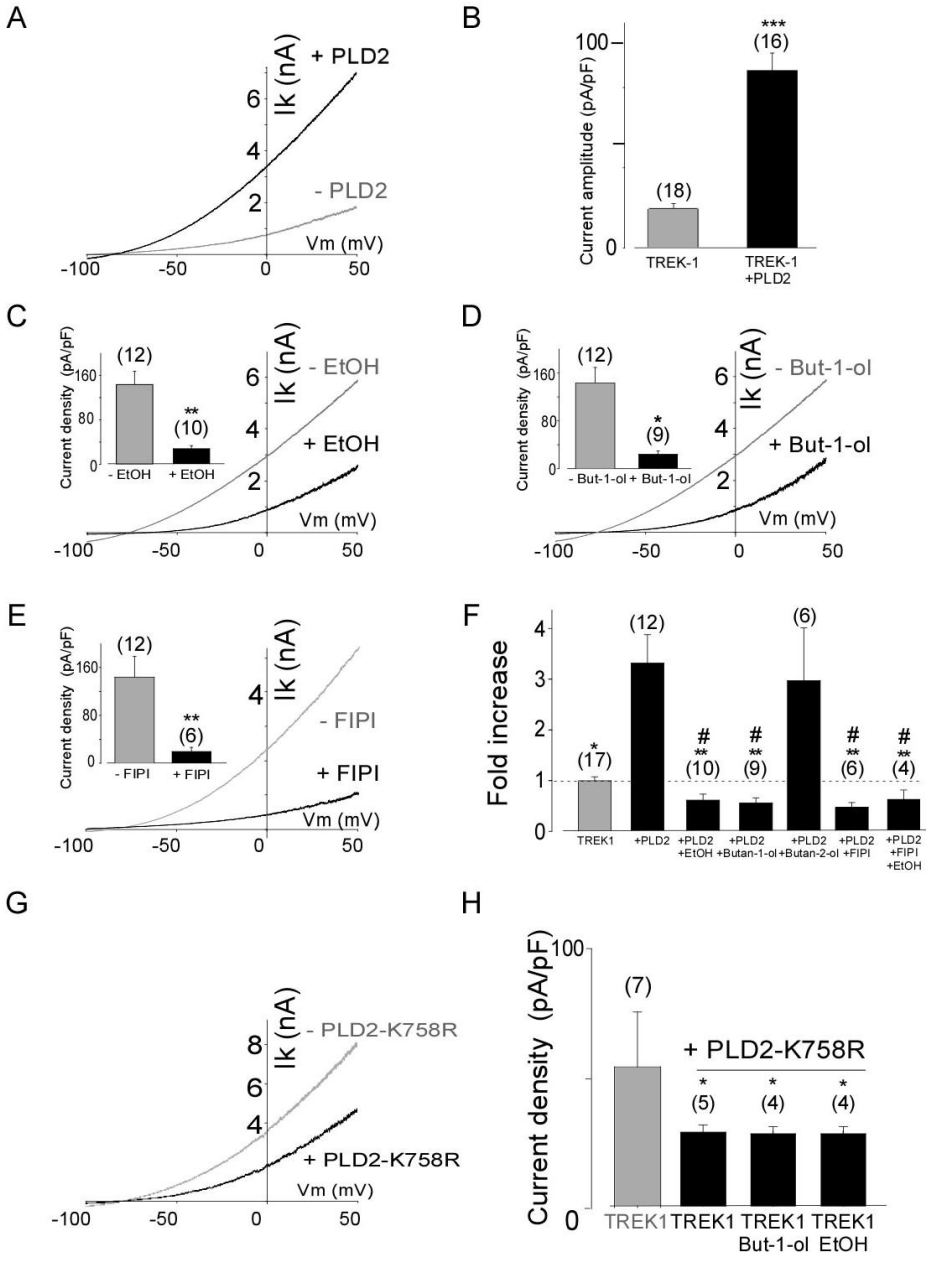

Figure 7.2. TREK1 is potentiated by PLD2 in a PA-dependent manner (A, B) TREK1 is potentiated by PLD2 co-expression. (A) Representative traces showing that PLD2 co-expression increases TREK1 current. (B) Bar graph showing the TREK1 current densities in the presence or absence of co-expression of PLD2. Student's *t* test (***P < 0.001) shows the difference between TREK1 and TREK1 co-expressed with PLD2. The numbers of cells tested are indicated in parentheses. (C-F) Primary alcohols and FIPI abolish the potentation of TREK1 current by PLD2. Representative traces showing effects of protracted ethanol (C), butan-1-ol (D), or FIPI (E) application on TREK1 current in the presence of PLD2. Insets, TREK1 current densities before and after treatments. (F) Summary of normalized amplitude of TREK1 current in the presence of PLD2 after protracted treatment with alcohol, FIPI or both. Student's *t* tests (*P < 0.05, **P < 0.01) show the difference between TREK1 co-expressed with PLD2 and after ethanol, butan-1-ol or butan-2-ol application. Student's *t* tests (#P < 0.05) show the difference between TREK1 and TREK1 co-expressed with PLD2 after either ethanol or butan-1-ol or butan-2-ol application. The numbers of cells tested are indicated in parentheses. (G, H) A catalytically inactive mutant of PLD2 (PLD2-K758R) decreases

TREK1 current. (G) Representative traces showing that coexpression of PLD2-K758R decreases TREK1 current. (H) Summary of TREK1 current densities in the presence or absence of co-expressed PLD2-K758R and before and after protracted primary alcohol application are shown. Student's *t* tests (*$P < 0.05$) show the difference between TREK1 and TREK1 co-expressed with PLD2-K578R with or without protracted primary alcohol exposure. The numbers of cells tested are indicated in parentheses.

PLD2, but not PLD1, specifically regulates TREK1 through direct interaction

Having found that PLD2 modulates TREK1, we asked whether a related phospholipase D, PLD1, has the same effect. Whereas co-expression of PLD2 significantly increased TREK1 current (Fig. 7.3A, B; current densities were 168 ± 28 pA/pF for TREK1 + PLD2 versus 41 ± 8 pA/pF for TREK1 alone; P<0.001), co-expression of PLD1 had no effect on TREK1 current (Fig. 7.3A, B; current density was 58 ± 9 pA/pF for TREK1 + PLD1; P>0.6).

We asked whether the ability of PLD2 but not PLD1 to stimulate TREK1 could be accounted for by direct association of only PLD2 with the TREK1 channel. PLD2 was co-immunoprecipitated with TREK1, but PLD1 was not (Fig. 7.3C). As a control, in the absence of TREK1 expression, anti-TREK1 antibodies did not precipitate PLD2 (Fig. 7.3C). Furthermore, using immunocytochemistry, we found that TREK1 and PLD2 co-localize in HEK293T cells (Fig. S7.4A), but TREK1 and PLD1 do not (Fig. S7.4B). Taken together, these results indicate that PLD2 interacts with TREK1 but that PLD1 does not and that this explains the exclusive modulation of the channel by PLD2.

PLD2 is able to potentiate TREK2, but not TRAAK

Having observed that PLD2 interacts with and regulates TREK1 but that PLD1 does not, we asked whether the interaction and modulation extend to other members of this K_{2P} subfamily of channels. To test this, we co-expressed PLD2 with TREK2 and the more distantly related TRAAK channel. TREK2 and TRAAK, like TREK1, are lipid and mechano-gated and display the same PA-sensitivity as TREK1[36,26] (Fig. S7.5). PLD2 co-expression significantly increased TREK2 current (Fig. 7.3D; current densities were 24 ± 3 pA/pF for TREK2 alone and 144 ± 29 pA/pF for TREK2 + PLD2; P>0.01) but did not significantly affect TRAAK current (Fig. 7.3E; current densities were 8 ± 3 pA/pF for TRAAK alone and 8 ± 3 pA/pF for TRAAK + PLD2; P>0.8). Consistent with these results, PLD2 was co-immunoprecipitated with TREK2 (Fig. 7.3F), but not with TRAAK (Fig. 7.3F). As a control, in the absence of TREK2 expression anti-TREK2 antibodies did not precipitate PLD2 (Fig. 7.3F), confirming the specificity of the assay. In addition, immunocytochemistry of PLD2 and TREK2 showed co-localization (Fig. S7.4C), while TRAAK and PLD2 showed no overlap (Fig. S7.4D). Futhermore, we found that PLD1 co-expression does not affect TREK2 current (Fig. S7.6E; current densities were 31 ± 11 pA/pF for TREK2 alone and 39 ± 21 pA/pF for TREK2 + PLD1; P>0.9 for TREK2 alone vs. TREK2 + PLD1). These results suggest that PLD2 interacts with, and hence regulates, TREK2, which is closely related to TREK1, but not the more distantly related TRAAK.

Having found that TREK2 resembles TREK1, we asked if it is also similar in the ability to be inhibited by protracted exposure to primary alcohols. We found that, like TREK1, TREK2 current is reduced by protracted exposure to primary alcohols (Fig. S7.6A, B; and, moreover, that this effect is potentiated when PLD2 is over expressed along with TREK2 (Fig. S7.6C, D). Unlike TREK1 and TREK2, TRAAK, which is not potentiated by PLD2 over-expression, is not sensitive to protracted exposure to primary alcohols (Fig. S7.7). In summary, TREK1 and

TREK2 are similar to one another and differ from the other TREK channel family member TRAAK in the ability to be specifically regulated by primary alcohols via PLD2 through specific interaction between channel and enzyme.

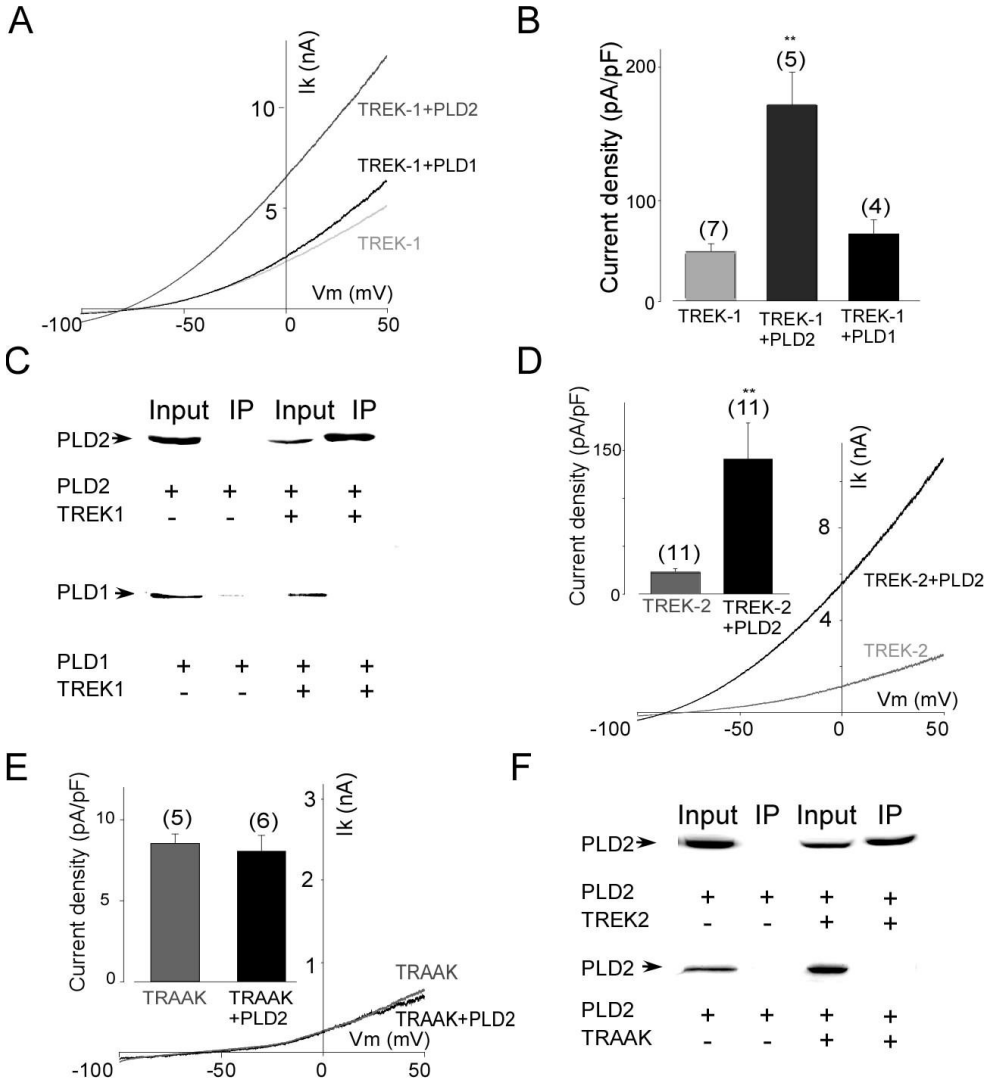

Figure 7.3. PLD2, but not PLD1, specifically regulates TREK1 and TREK2 but not TRAAK. (A-C) Unlike PLD2, PLD1 does not regulate TREK1. (A) Representative traces showing effects of PLD1 and PLD2 co-expression on TREK1 current. (B) Summary of TREK1 current in the presence or absence of either PLD1 or PLD2. Student's *t* tests (**$P < 0.01$) show the difference between TREK1 and TREK1 co-expressed with PLD2 or PLD1. The numbers of cells tested are indicated in parentheses. (C) Top, co-immunoprecipitation of PLD2 by anti-TREK1 antibodies from transfected HEK293T cells. Bottom, same as top for TREK1 and PLD1. (D-F) PLD2 specifically regulates TREK1 and 2, but not TRAAK. (D) PLD2 co-expression potentiates TREK2 current. Inset, TREK2 current densities in the presence or the absence of co-expressed PLD2. (E) PLD2 co-expression does not alter TRAAK current. Inset, TRAAK current densities in the presence or the absence of co-expressed PLD2. (F) Top, co-immunoprecipitation of PLD2 by anti-TREK2 antibodies from transfected HEK293T cells. Bottom, co-immunoprecipitation of PLD2 by anti-TRAAK antibodies from transfected HEK293T cells.

To further test the idea that direct interaction between enzyme and channel is necessary for the channel to be potentiated, we forced an interaction between TRAAK and PLD2 by fusing the proteins to one another to produce a PLD2-TRAAK tandem (Fig. 7.4A). PLD2-TRAAK showed significantly increased current compared to TRAAK alone (Fig. 7.4B; current densities were 5.5 ± 2 pA/pF for TRAAK alone and 51 ± 13 pA/pF for PLD2-TRAAK; $P<0.01$). Similarly to TREK1 and TREK2, protracted application of ethanol reduced the current density of PLD2-TRAAK to the amplitude observed for TRAAK alone indicating that PLD2-mediated production of PA is required for the potentiation observed with PLD2-TRAAK (Fig. S7.8). These results are consistent with the notion that anchoring of PLD2 to the channel enables it to regulate the channel's activity via its local enzymatic activity.

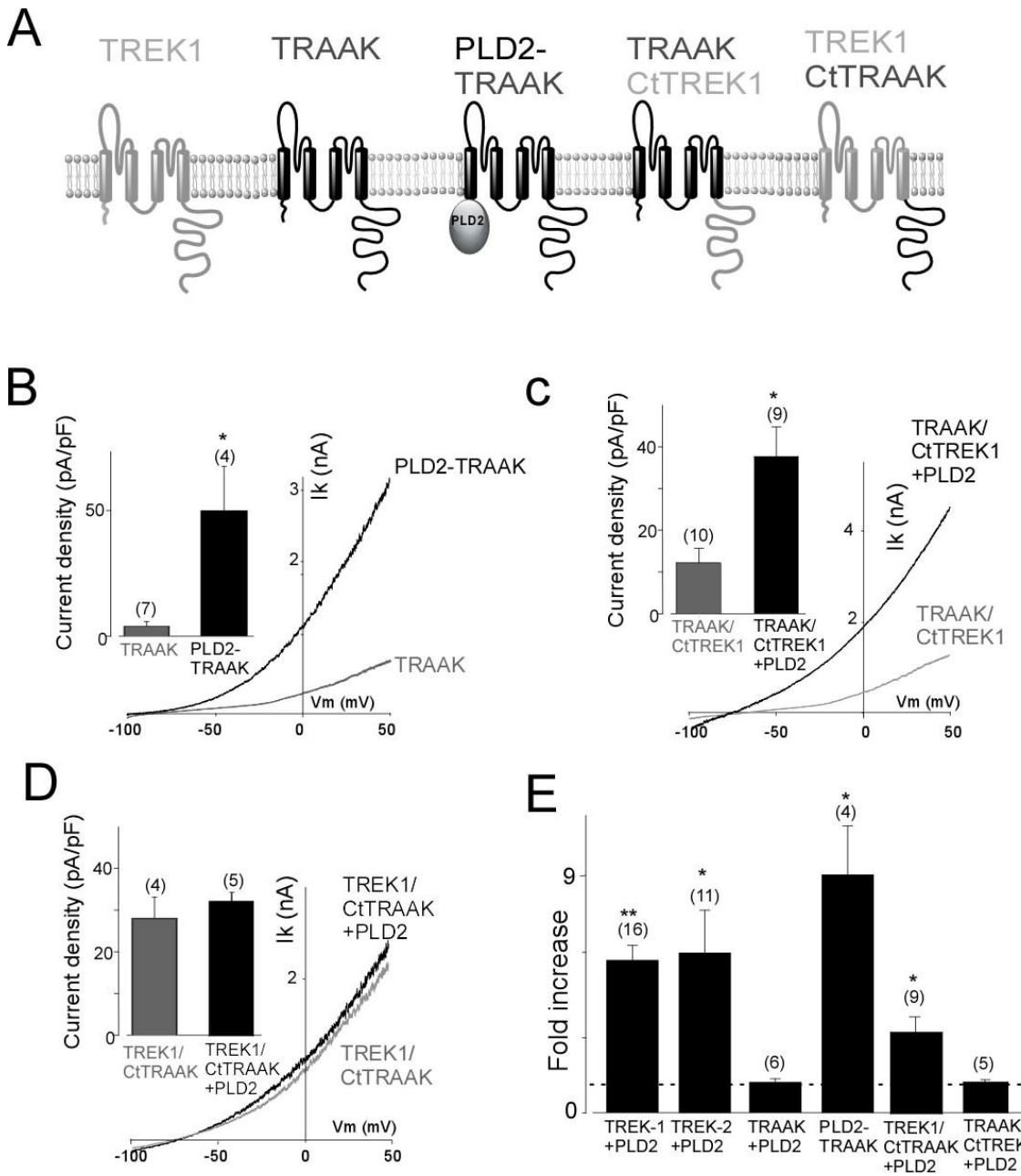

Figure 7.4. Binding of PLD2 to the cytoplasmic tails of TREK1 and TREK2 enables specific regulation (A) Schematic representing the different constructs used. (B) N-terminal fusion of PLD2 to TRAAK potentiates TRAAK current. Inset, comparison of TRAAK and PLD2-TRAAK current densities. (C-D) The specificity of PLD2 regulation of TREK1 is mediated by the cytoplasmic tail of TREK1. (C) PLD2 co-expression potentiates current from a chimeric TRAAK/Ct-TREK1 channel containing the core region of TRAAK fused to the cytoplasmic Ctd of TREK1. Inset, TRAAK/Ct-TREK1 current densities in the presence or absence of co-expressed PLD2. (D) PLD2 co-expression does not alter current from a chimeric TREK1/Ct-TRAAK channel containing the core region of TREK1 fused to the cytoplasmic Ctd of TRAAK. Inset, TREK1/Ct-TRAAK current densities in the presence or absence of co-expressed PLD2. (E) Summary of the fold increase of current for TREK1, TREK2, TRAAK, PLD2-TRAAK, TRAAK/CtTREK1 and TREK1/CtTRAAK induced by PLD2 co-expression (or fusion in the case of PLD2-TRAAK). Student's *t* tests (**P* < 0.05, ***P* < 0.001) show the difference between PLD2 potentiation of TREK1 and TREK2, PLD2-TRAAK, TRAAK/CtTREK1 or TREK1/CtTRAAK. The numbers of cells tested are indicated in parentheses**.**

We next investigated to which part of the channel PLD2 binds. We hypothesized that this interaction may take place in the Ctd because this is the major part of TREK channels that is accessible to the cytosol and this domain is highly conserved between TREK1 and 2 [37], [10]. To test this hypothesis, we designed chimeras between TRAAK and TREK1 to see if we could transfer PLD2 sensitivity to TRAAK. The Ctd of TRAAK was replaced by the corresponding Ctd of TREK1 to form TRAAK/Ct-TREK1 and the Ctd of TREK1 was replaced by the corresponding Ctd of TRAAK to form TREK1/Ct-TRAAK (Fig. 7.4A). Unlike wild type TRAAK, TRAAK/Ct-TREK1 was sensitive to PLD2 (Fig. 7.4C; current densities were 12 ± 3 pA/pF and 36 ± 7 pA/pF for TRAAK/Ct-TREK1 and TRAAK/CtTREK1 + PLD2, respectively; P<0.05). However, TREK1/Ct-TRAAK was not sensitive to PLD2 co-expression (Fig. 7.4D; current densities were 26 ± 4 pA/pF and 29 ± 2 pA/pF for TREK1/Ct-TRAAK and TREK1/Ct-TRAAK + PLD2 respectively, P>0.8). These results indicate that the specificity of PLD2 depends on the TREK1 Ctd, because the Ctd specifically binds to PLD2 (Fig. 7.5).

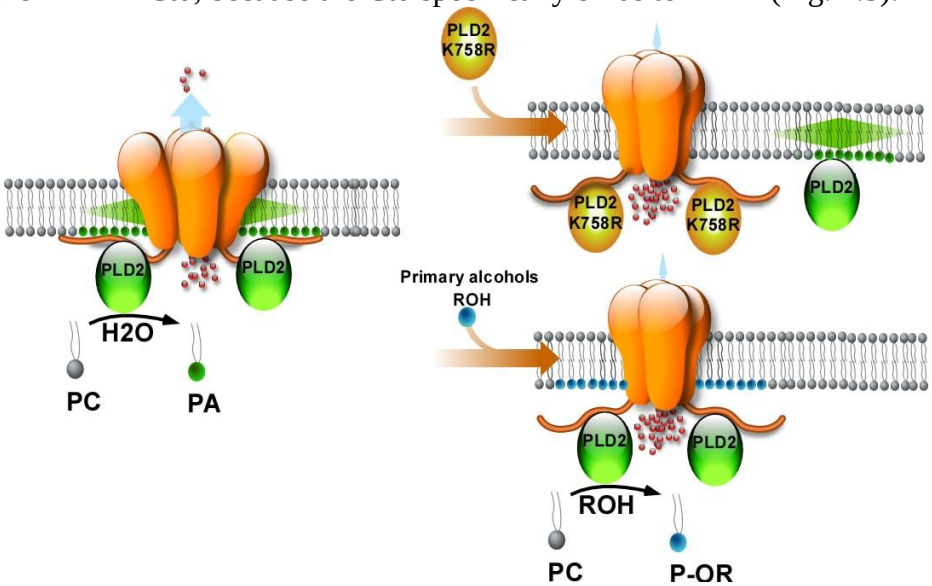

Figure 7.5. Model of channel regulation by PLD2. PLD2 is associated with TREK1 and creates a microdomain rich in PA (gradient of PA is represented by a green arrow) that activates the channel at rest. PLD2-K758R displaces the endogenous PLD2 which leads to a reduction in the local PA concentration near the channel and therefore, reduces TREK channel activity. Alternatively, primary alcohols (ROH) compete with water in the catalytic site of PLD2 which also leads to a reduction of the local PA concentration near the channel and causes a decrease in TREK channel activity.

PA targets native TREK1 channels though physical coupling with endogenous PLD2 in hippocampal neurons

TREK channels are natively expressed in the hippocampus where they contribute to the response to $GABA_B$ receptor activation and are inhibited by protracted primary alcohol application (Fig. 7.1B). Accordingly, we wondered if hippocampal TREK1 channels are regulated by endogenous PLD2 and if this can explain their alcohol sensitivity. To investigate this regulation in the native hippocampal TREK1 channels, we co-expressed the catalytically inactive mutant of PLD2, PLD2-K758R, along with the TREK1-PCS[20].

In cultured hippocampal neurons transfected with the TREK1-PCS, alternating illumination between 380 nm and 500 nm modulated the resting membrane potential by 4.3 ± 0.9 mV (Fig. 7.6A). Co-expression of PLD2-K758R decreased this voltage change significantly (Fig. 7.6B, E; 1.3 ± 0.2 mV; $P<0.01$). Consistent with this, in voltage clamp at a holding potential of -20 mV, TREK1-PCS transfected neurons had photocurrents of 20 ± 4 pA (Fig. 7.6C) and co-expression of PLD2-K758R reduced the photocurrents to 4.8 ± 1.7 pA (Fig. 7.6D, F; $P<0.01$) as was observed for protracted EtOH application (Fig. 7.1B). These results show that in hippocampal neurons native TREK1 and PLD2 co-assemble and that this co-assembly leads to a tonic increase in TREK1 activity.

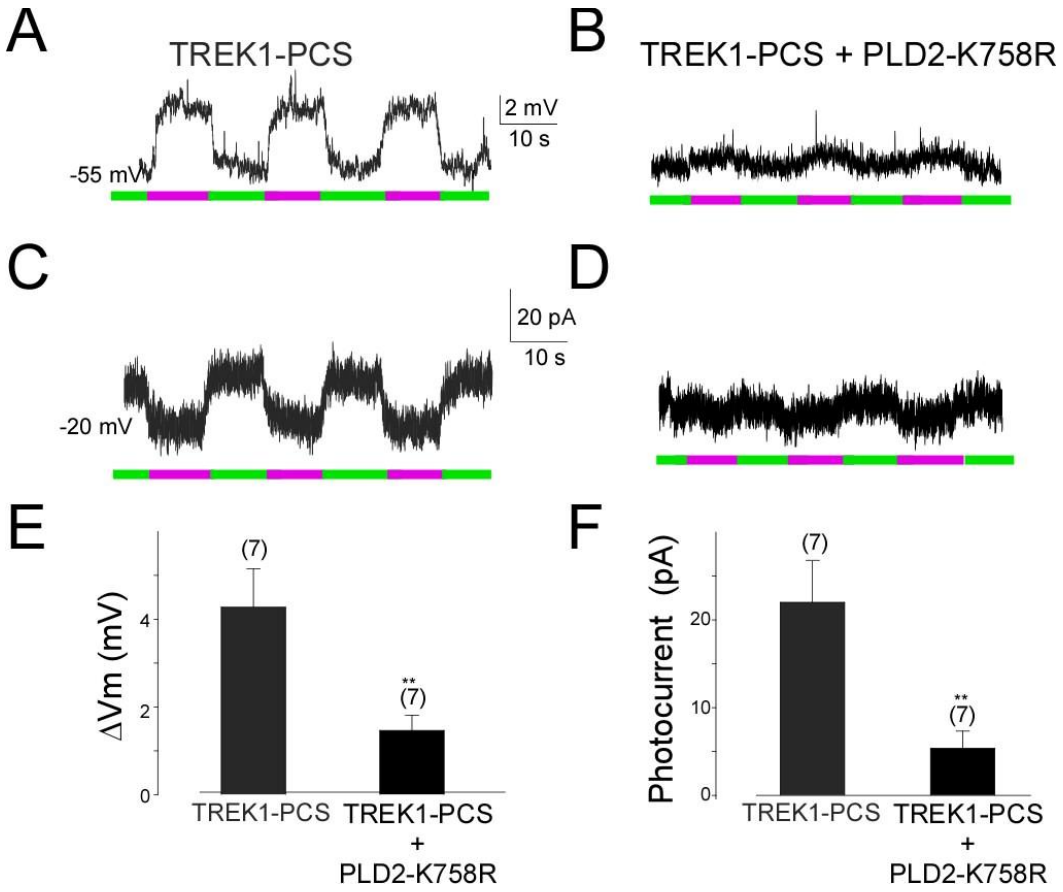

Figure 7.6. PLD2-K758R decreases endogenous TREK1 current in hippocampal neurons. (A) Representative current clamp recording from cultured hippocampal neurons expressing TREK1-PCS shows light modulation of membrane potential. 380 nm light (magenta) leads to channel blockade and depolarization whereas 500 nm light (green) unblocks the channels to induce a hyperpolarization. (B) Same as in (A) for neurons co-expressing TREK1-PCS and PLD2-K758R. (C) Representative whole-cell voltage clamp recording from hippocampal neurons expressing TREK1-PCS. (D) Same as in (C for neurons expressing TREK1-PCS and PLD2-K758R. (E) Average resting membrane potential modulation induced by alternating illumination of neurons with 500 nm and 380 nm. (F) Average photocurrent induced by alternating illumination of neurons with 500 nm and 380 nm. Student's *t* tests (**$P < 0.01$) show the difference between TREK1-PCS and TREK1-PCS co-expressed with PLD2-K758R. The numbers of cells tested are indicated in parentheses.

Discussion:

We report a novel mechanism for the specific regulation of ion channels by an enzyme that generates signaling lipids. We found that the K_{2P} potassium channels TREK1 and TREK2 are potentiated by the phospholipase PLD2, which produces the charged signaling phospholipid PA from phosphatidylcholine. Surprisingly, PLD2 was unable to regulate the related TRAAK channel despite the fact that TRAAK responds to PA in a similar manner to TREK1 and TREK2. Furthermore, we found that PLD1, which catalyzes the same reaction as PLD2, has no effect on TREK1 or TREK2, indicating that this regulation is specific to the subtype of enzyme and not based on a bulk effect on plasma membrane composition.

We found that the specific regulation that we observed by only one of the PLDs of two of the three PA-sensitive K2P channels could be explained by selective co-localization. First, TREK1 and TREK2 directly interact with PLD2, but TRAAK does not, explaining the selective activation of the TREKs by PLD2. Second, PLD1 does not interact with TREK1, explaining its lack of effect. Third, fusion of the PLD2 to TRAAK renders TRAAK responsive to PLD2. Finally, replacement of the TRAAK Ctd with that of TREK1 endowed TRAAK with sensitivity to PLD2, whereas replacement of the TREK1 Ctd with that of TRAAK eliminated the sensitivity of TREK1 to PLD2. These results suggest that PLD2 specificity is due to the direct interaction of PLD2 with either TREK1 or TREK2 *via* the Ctd of the channel. We propose that by complexing directly with TREK1 or TREK2, PLD2 is able to alter the local concentration of PA in a microdomain around the channel in order to stimulate channel activity (Fig. 7.5). This mechanism is consistent with a short half-life of PA in the plasma membrane[5]. In our model, the regulation of TREK channels by PLD2 is specific not because of the enzymatic product, but because the protein-protein interaction between enzyme and channel allows the channel to be directly coupled to the enzymatic production of PA in a way that is independent of the bulk concentration of PA. Independent pools of phospholipids that govern distinct functions in microdomains have been proposed before [38 39]. Our work provides an illustration of such a case and a mechanism by which it can result in specific regulation of a subset of K_{2P} potassium channels.

In addition to regulation by PLD2, we demonstrated that protracted, but not acute, application of primary alcohols inhibits TREK1 and TREK2. We provide evidence that this effect is mediated by PLD2 rather than direct interaction between alcohols and the channel, in contrast to what has been shown for GIRK channels[40]. When exposed to primary alcohols such as ethanol or butan-1-ol, PLD2 catalyzes the production of the biologically inactive phospholipids PEtOH or P-1-BtOH rather than PA. Consistent with the hypothesis that regulation of TREK by alcohols is mediated by removal of tonic stimulation by PLD2, PLD2 is insensitive to secondary alcohols, which were also unable to regulate TREK1 or TREK2. We confirmed this mechanism by showing that primary alcohols also prevent the potentiation effect of PLD2 and that a catalytically inactive mutant of PLD2 is unable to potentiate TREK1 and renders TREK1 insensitive to protracted alcohol treatment. This may be a general mechanism by which ethanol can induce long term physiological changes by changing the phospholipid composition of the membrane.

Given the previously demonstrated crosstalk between the $GABA_B$ receptor, GIRK and TREK and the established role of $GABA_B$ receptors in treatment of alcohol addiction, we wanted to address the possibility that regulation of TREK1 by PLD2, which mediates the effects of ethanol in heterologous systems, occurs natively in mammalian neurons. We tested this in

hippocampal neurons using the TREK1-PCS technique[41]. We found that displacement of the native, wild-type PLD2 by the catalytically inactive mutant PLD2-K578R decreased the endogenous TREK1 depolarization or current by 4 fold as it was observed for protracted ethanol application. Based on this measurement we concluded that, at rest, more than 75% of the hippocampal TREK1 current is associated with potentiation of TREK1 by PA. This result indicates that the regulation of TREK1 by PLD2 occurs natively in neurons of the hippocampus and may be important for mediating some of the effects of protracted ethanol consumption and its reversal by $GABA_B$ receptors[42].

In conclusion, association of specific isoforms of an enzyme that generates signaling lipids with select ion channel subtypes can confer specific regulation of those channels. We conjecture that this specificity is due to the high local concentration of the active lipid product near its site of action on the channel, resulting in strong regulation of the bound channel, while channels that do not interact with the enzyme are not regulated because the bulk concentration of that lipid does not reach levels that are high enough to act at a distance.

Methods:

Molecular Biology and Gene Expression

HEK293T cells were transiently co-transfected using Lipofectamine 2000 (Invitrogen) with a total of 1.6 μg of DNA total per 18 mm diameter cover slip. For co-expression of TREK1, TREK2, or TRAAK with PLD2, PLD1, or PLD2-K758R cells were transfected with a ratio of 1:4. For co-expression of TREK1 and TREK1-PCS a ratio of 1:3 or 1:5 was used. All channel DNA was used in the pIRES2eGFP vector. TREK1-PCS was previously made by PCR and introduced into the pIRES2eGFP expression vector (19). PLD variants were used in the pCGN vector. Chimeras between TREK1 (DDBJ/EMBL/GenBank accession No. U73488) and TRAAK (DDBJ/EMBL/GenBank accession No.NM_008431) were generated by PCR. The Ctd of TRAAK was replaced by the corresponding Ctd of TREK1 (starting at Gly 293) to form TRAAK/Ct-TREK1 and the cytoplasm Ctd of TREK1 was replaced by the corresponding Ctd of TRAAK (starting at Gly 255) to form TREK1/Ct-TRAAK. The tandem between PLD2 and TRAAK was made by PCR, The PLD2 was fused to the N-terminus of TRAAK. Hippocampal neurons were transfected at 9 DIV using the calcium phosphate method. Each 12 mm coverslip received 1 μg of TREK1-PCS DNA and 1 μg of PLD2-K758R DNA or empty vector.

Cell Culture

HEK293 cells were maintained in DMEM with 5% FBS on poly-L-lysine-coated glass coverslips. Dissociated hippocampal neurons were obtained from postnatal rats (P0-1) and plated at 75,000 cells/coverslip on poly-L-lysine-coated glass coverslips (12 mM). Neurons were maintained in media containing MEM supplemented with 5% fetal bovine serum, B27 (Invitrogen), and GlutaMAX (Invitrogen).

Electrophysiology

HEK293 cell electrophysiology was performed 24-72 h after transfection in solution containing (in mM): 145 NaCl, 4 KCl, 1 $MgCl_2$, 2 $CaCl_2$ and 10 HEPES. Glass pipettes of resistance between 3 and 6 MΩ were filled with intracellular solution containing (in mM): 140 KCl, 10 Hepes, 5 EGTA, 3 $MgCl_2$, pH 7.4. Cells were voltage clamped using an Axopatch 200A (Molecular Devices) amplifier in the whole cell mode. Currents were elicited by voltage-ramps (from -100 to 50 mV, 1s in duration) and the current density was calculated at 0 mV. For alcohol experiment, cells were incubated at least one hour before recording. For inside out patch experiments, the internal solution contained (in mM): 155 KCl, 5 EGTA and 10 HEPES and the external solution contained (in mM) 140 KCl, 10 Hepes, 5 EGTA, 3 $MgCl_2$, pH 7.4. To confirm the PA-sensitivity of the TREK channel subfamily, 5μM PA was applied directly to the patches.

Hippocampal neuron whole cell patch clamp electrophysiology was performed 3-6 days after transfection (DIV 12-15 for cultured neurons). For voltage and current clamp experiments in cultured neurons, extracellular solution contained (in mM): 138 NaCl, 1.5 KCl, 1.2 $MgCl_2$, 2.5 $CaCl_2$, 10 glucose, 5 Hepes, 0.002 TTX, pH 7.4. Intracellular solution contained (in mM): 140

K-Gluconate, 10 NaCl, 5 EGTA, 2 $MgCl_2$, 1 CaCl2, 10 Hepes, 2 MgATP, 0.3 Na_2GTP, pH 7.2. Only cells with a resting potential <-45 mV were analyzed.

Optogenetics and electrophysiology

We expressed an engineered TREK1 subunit that renders native TREK1 subject to block by a light-controlled switch [32]. This engineered "photoswitchable conditional subunit", or TREK1-PCS, contains two modifications. The first modification is the introduction of a cysteine attachment site (S121C) near the external mouth of the pore for the covalent attachment of a photoswitchable tethered blocker (PTB). This PTB is called MAQ (Maleimide Azobenzene Quaternary ammonium) [20], [32]. In response to 380 nm light, the tethered MAQ isomerizes from a stable *trans* configuration to a metastable *cis* configuration and allows the quaternary ammonium moiety to block the channel pore. Block is removed by illumination at 500 nm, which isomerizes MAQ back to the *trans* configuration. The second modification is a deletion in the TREK1 C terminal domain that retains TREK1-PCS homomultimeric channels inside the cell. When the TREK1-PCS is expressed in a cell that natively expresses wild-type (WT) TREK1, heteromeric TREK1-PCS/WT channels co-assemble, reach the cell surface and are subject to photo-block. For photoswitching experiments, illumination was controlled using a Polychrome V monochromator (TILL Photonics) through a 20x objective. pClamp software was used for both data acquisition and control of illumination. To conjugate MAQ, cells were incubated in 20-40 μM MAQ for 40 minutes in the dark at room temperature in standard extracellular cell buffer for either HEK293 cells or hippocampal neurons. Cells were washed thoroughly with extracellular buffer before beginning experiments.

Immunocytochemistry

Transfected cells on coverslips were fixed with PBS containing 4% paraformaldehyde (15 min at 21–22°C), then permeabilized with PBS and 0.1% Triton X-100 (PBST) and blocked for 1 h with 5% horse serum (HS) in PBST. Primary and secondary antibodies were diluted in PBST and 5% HS and incubated for 1 h at 21–22°C. Three 5-min washes with PBST were carried out between each incubation step and at the end of the procedure. Coverslips were mounted in Dako® Fluorescent Mounting medium (Dako Corporation, Carpinteria, CA, USA). The following antibodies were used: rabbit anti-TREK1 polyclonal antibodies [43] rat monoclonal antibody 3F10 against hemagglutinin (HA) epitope (Roche Diagnostics), goat anti-rabbit IgGs conjugated to Alexa Fluor® 488 (Molecular Probes Europe BV, Leiden, The Netherlands), donkey anti-rat IgGs conjugated to Alexa Fluor® 594 (Molecular Probes Europe BV, Leiden, The Netherlands). Microscopy analysis and data acquisition were carried out with an Axioplan 2 Imaging Microscope (Carl Zeiss, Le Pecq, France).

Immunoprecipitation and Western blot analysis

HEK293T cells were homogenized in PBS containing saponin (0.5% w/v), Triton X-100 (0.5% w/v) and protease inhibitors (Roche Diagnostics, Basel, Switzerland). Lysates were clarified by centrifugation at 20,000*g* for 30 min. Anti-TREK1 antibodies were immobilized on protein A-Sepharose 4B fast flow columns (Sigma, Saint Louis, MO, USA). Immunoprecipitated proteins

were separated on 10% SDS polyacrylamide gel and blotted onto nitrocellulose membranes (Hybond-C extra, Amersham Biosciences, Freiburg, Germany). Detection was carried out using rat monoclonal antibody 3F10 against hemagglutinin (HA) (Roche Diagnostics).

References:

1 Foster, D. A. & Xu, L. Phospholipase D in cell proliferation and cancer. *Mol Cancer Res* **1**, 789-800 (2003).

2 Jenkins, G. M. & Frohman, M. A. Phospholipase D: a lipid centric review. *Cell Mol Life Sci* **62**, 2305-2316, doi:10.1007/s00018-005-5195-z (2005).

3 Oude Weernink, P. A., Lopez de Jesus, M. & Schmidt, M. Phospholipase D signaling: orchestration by PIP2 and small GTPases. *Naunyn Schmiedebergs Arch Pharmacol* **374**, 399-411, doi:10.1007/s00210-007-0131-4 (2007).

4 Nanjundan, M. & Possmayer, F. Pulmonary phosphatidic acid phosphatase and lipid phosphate phosphohydrolase. *Am J Physiol Lung Cell Mol Physiol* **284**, L1-23, doi:10.1152/ajplung.00029.2002 284/1/L1 [pii] (2003).

5 Cazzolli, R., Shemon, A. N., Fang, M. Q. & Hughes, W. E. Phospholipid signalling through phospholipase D and phosphatidic acid. *IUBMB Life* **58**, 457-461, doi:N30X3718WQ68X283 [pii] 10.1080/15216540600871142 (2006).

6 Yang, S. F., Freer, S. & Benson, A. A. Transphosphatidylation by phospholipase D. *J Biol Chem* **242**, 477-484 (1967).

7 Steed, P. M., Clark, K. L., Boyar, W. C. & Lasala, D. J. Characterization of human PLD2 and the analysis of PLD isoform splice variants. *FASEB J* **12**, 1309-1317 (1998).

8 Lesage, F. *et al.* TWIK-1, a ubiquitous human weakly inward rectifying K+ channel with a novel structure. *Embo J* **15**, 1004-1011 (1996).

9 Fink, M. *et al.* A neuronal two P domain K+ channel stimulated by arachidonic acid and polyunsaturated fatty acids. *Embo J* **17**, 3297-3308 (1998).

10 Sandoz, G. *et al.* Mtap2 is a constituent of the protein network that regulates twik-related K+ channel expression and trafficking. *J Neurosci* **28**, 8545-8552 (2008).

11 Lopes, C. M. *et al.* PIP2 hydrolysis underlies agonist-induced inhibition and regulates voltage gating of two-pore domain K+ channels. *J Physiol* **564**, 117-129, doi:jphysiol.2004.081935 [pii] 10.1113/jphysiol.2004.081935 (2005).

12 Honore, E., Maingret, F., Lazdunski, M. & Patel, A. J. An intracellular proton sensor commands lipid- and mechano-gating of the K(+) channel TREK-1. *EMBO J* **21**, 2968-2976, doi:10.1093/emboj/cdf288 (2002).

13 Sandoz, G., Bell, S. C. & Isacoff, E. Y. Optical probing of a dynamic membrane interaction that regulates the TREK1 channel. *Proc Natl Acad Sci U S A* **108**, 2605-2610, doi:10.1073/pnas.1015788108 (2011).

14 Sandoz, G., Douguet, D., Chatelain, F., Lazdunski, M. & Lesage, F. Extracellular acidification exerts opposite actions on TREK1 and TREK2 potassium channels via a single conserved histidine residue. *Proc Natl Acad Sci U S A* **106**, 14628-14633, doi:0906267106 [pii]10.1073/pnas.0906267106 (2009).

15 Cohen, A., Ben-Abu, Y., Hen, S. & Zilberberg, N. A Novel Mechanism for Human K2P2.1 Channel Gating: FACILITATION OF C-TYPE GATING BY PROTONATION OF EXTRACELLULAR HISTIDINE RESIDUES. *J Biol Chem* **283**, 19448-19455 (2008).

16 Noel, J., Sandoz, G. & Lesage, F. Molecular regulations governing TREK and TRAAK channel functions. *Channels (Austin)* **5**, doi:16469 [pii] (2011).

17 Heurteaux, C. *et al.* TREK-1, a K+ channel involved in neuroprotection and general anesthesia. *Embo J* **23**, 2684-2695 (2004).

18 Noel, J. *et al.* The mechano-activated K+ channels TRAAK and TREK-1 control both warm and cold perception. *EMBO J* **28**, 1308-1318, doi:emboj200957 [pii]10.1038/emboj.2009.57 (2009).

19 Heurteaux, C. *et al.* Deletion of the background potassium channel TREK-1 results in a depression-resistant phenotype. *Nat Neurosci* **9**, 1134-1141 (2006).

20 Sandoz, G., Levitz, J., Kramer, R. H. & Isacoff, E. Y. Optical Control of Endogenous Proteins with a Photoswitchable Conditional Subunit Reveals a Role for TREK1 in GABA(B) Signaling. *Neuron* **74**, 1005-1014, doi:S0896-6273(12)00423-0 [pii]10.1016/j.neuron.2012.04.026 (2012).

21 Welch, E. J., Jones, B. W. & Scott, J. D. Networking with AKAPs: context-dependent regulation of anchored enzymes. *Mol Interv* **10**, 86-97, doi:10/2/86 [pii] 10.1124/mi.10.2.6 (2010).

22 Bockaert, J., Perroy, J., Becamel, C., Marin, P. & Fagni, L. GPCR interacting proteins (GIPs) in the nervous system: Roles in physiology and pathologies. *Annu Rev Pharmacol Toxicol* **50**, 89-109, doi:10.1146/annurev.pharmtox.010909.105705 (2010).

23 Sandoz, G. & Lesage, F. Protein complex analysis of native brain potassium channels by proteomics. *Methods Mol Biol* **491**, 113-123, doi:10.1007/978-1-59745-526-8_9 (2008).
24 Sandoz, G. *et al.* AKAP150, a switch to convert mechano-, pH- and arachidonic acid-sensitive TREK K(+) channels into open leak channels. *Embo J* **25**, 5864-5872 (2006).
25 Deng, P. Y. *et al.* GABA(B) receptor activation inhibits neuronal excitability and spatial learning in the entorhinal cortex by activating TREK-2 K+ channels. *Neuron* **63**, 230-243, doi:10.1016/j.neuron.2009.06.022 (2009).
26 Honore, E. The neuronal background K2P channels: focus on TREK1. *Nat Rev Neurosci* **8**, 251-261, doi:nrn2117 [pii]10.1038/nrn2117 (2007).
27 Selvy, P. E., Lavieri, R. R., Lindsley, C. W. & Brown, H. A. Phospholipase D: enzymology, functionality, and chemical modulation. *Chem Rev* **111**, 6064-6119, doi:10.1021/cr200296t (2011).
28 Kominkova, V., Magova, M., Mojzisova, A., Malekova, E. & Ondrias, K. Effect of ethanol on tracheal potassium channels reconstituted into bilayer lipid membranes. *Physiol Res* **50**, 507-511 (2001).
29 Brodie, M. S., Scholz, A., Weiger, T. M. & Dopico, A. M. Ethanol interactions with calcium-dependent potassium channels. *Alcohol Clin Exp Res* **31**, 1625-1632, doi:ACER469 [pii] 10.1111/j.1530-0277.2007.00469.x (2007).
30 Grissmer, S. *et al.* Pharmacological characterization of five cloned voltage-gated K+ channels, types Kv1.1, 1.2, 1.3, 1.5, and 3.1, stably expressed in mammalian cell lines. *Mol Pharmacol* **45**, 1227-1234 (1994).
31 Kobayashi, T. *et al.* Ethanol opens G-protein-activated inwardly rectifying K+ channels. *Nat Neurosci* **2**, 1091-1097, doi:10.1038/16019 (1999).
32 Banghart, M., Borges, K., Isacoff, E., Trauner, D. & Kramer, R. H. Light-activated ion channels for remote control of neuronal firing. *Nat Neurosci* **7**, 1381-1386 (2004).
33 Su, W. *et al.* 5-Fluoro-2-indolyl des-chlorohalopemide (FIPI), a phospholipase D pharmacological inhibitor that alters cell spreading and inhibits chemotaxis. *Mol Pharmacol* **75**, 437-446, doi:mol.108.053298 [pii] 10.1124/mol.108.053298 (2009).
34 Sung, T. C., Altshuller, Y. M., Morris, A. J. & Frohman, M. A. Molecular analysis of mammalian phospholipase D2. *J Biol Chem* **274**, 494-502 (1999).
35 Sung, T. C. *et al.* Mutagenesis of phospholipase D defines a superfamily including a trans-Golgi viral protein required for poxvirus pathogenicity. *EMBO J* **16**, 4519-4530, doi:10.1093/emboj/16.15.4519 (1997).
36 Czirjak, G., Toth, Z. E. & Enyedi, P. The two-pore domain K+ channel, TRESK, is activated by the cytoplasmic calcium signal through calcineurin. *J Biol Chem* **279**, 18550-18558, doi:10.1074/jbc.M312229200M312229200 [pii] (2004).
37 Lesage, F. & Lazdunski, M. Molecular and functional properties of two-pore-domain potassium channels. *Am J Physiol Renal Physiol* **279**, F793-801 (2000).
38 Simonsen, A., Wurmser, A. E., Emr, S. D. & Stenmark, H. The role of phosphoinositides in membrane transport. *Curr Opin Cell Biol* **13**, 485-492, doi:S0955-0674(00)00240-4 [pii] (2001).
39 Janmey, P. A. & Lindberg, U. Cytoskeletal regulation: rich in lipids. *Nat Rev Mol Cell Biol* **5**, 658-666, doi:10.1038/nrm1434 (2004).
40 Aryal, P., Dvir, H., Choe, S. & Slesinger, P. A. A discrete alcohol pocket involved in GIRK channel activation. *Nat Neurosci* **12**, 988-995, doi:nn.2358 [pii]10.1038/nn.2358 (2009).
41 Sandoz, G. & Levitz, J. Optogenetic techniques for the study of native potassium channels. *Front Mol Neurosci* **6**, 6, doi:10.3389/fnmol.2013.00006 (2013).
42 Boden, J. M. & Fergusson, D. M. Alcohol and depression. *Addiction* **106**, 906-914, doi:10.1111/j.1360-0443.2010.03351.x (2011).
43 Maingret, F. *et al.* TREK-1 is a heat-activated background K(+) channel. *EMBO J* **19**, 2483-2491, doi:10.1093/emboj/19.11.2483 (2000).

Supplementary Figures:

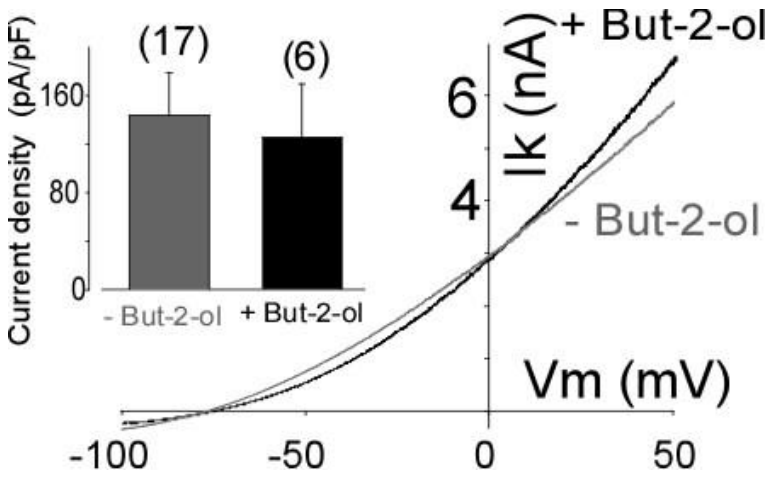

Figure S7.1. Secondary alcohols fail to abolish TREK1 current potentiation by PLD2. Representative traces showing the lack of an effect of protracted butan-2-ol on cells expressing TREK1 and PLD2. Inset, TREK1 current densities before and after protracted butan-2-ol application are shown. The numbers of cells tested are indicated in parentheses.

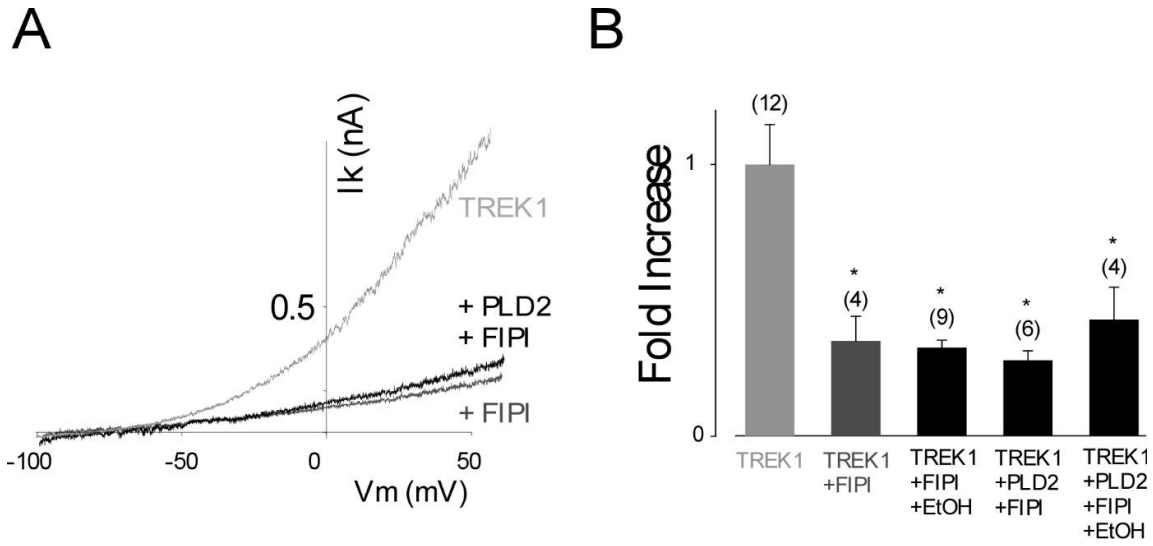

Figure S7.2: TREK1 is inhibited by protracted FIPI application to similar levels with or without PLD2 coexpression. (A) Protracted FIPI application decreases TREK1 current to similar levels with (dark gray) or without (light gray) coexpression of PLD2. (B) TREK1 current densities before and after protracted (>1 hrs) FIPI application are shown. Note that the current amplitude after FIPI application is the same with or without PLD2 coexpression. Current density was 15 ± 5 pA/pF, P>0.6 for TREK1 + FIPI vs. TREK1 + PLD2 + FIPI . (**P* < 0.05) shows the difference between TREK1 and TREK1 + FIPI or TREK1 + PLD2 + FIPI.

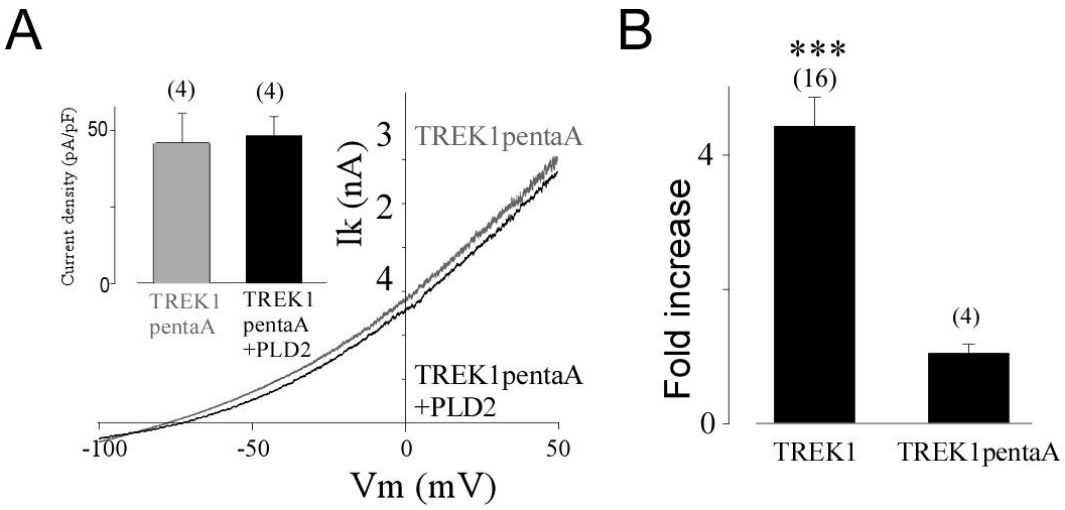

Figure S7.3. PLD2 co-expression does not alter TREK1pentaA current. (A) Effect of PLD2 over-expression on TREK1-pentaA current. Inset, TREK1-pentaA current densities in the presence or absence of co-expression of PLD2. (B) Bar graph showing the normalized TREK1 and TREK1-pentaA current increase induced by PLD2 co-expression. Current densities were 46 ± 9 pA/pF and 48 ± 6 pA/pF for TREK1pentaA and TREK1pentaA + PLD2; P>0.8). Student's *t* tests (****P* < 0.001) show the difference between TREK1 potentiation by PLD2 and TREK1-pentaA potentiation by PLD2. The numbers of cells tested are indicated in parentheses.

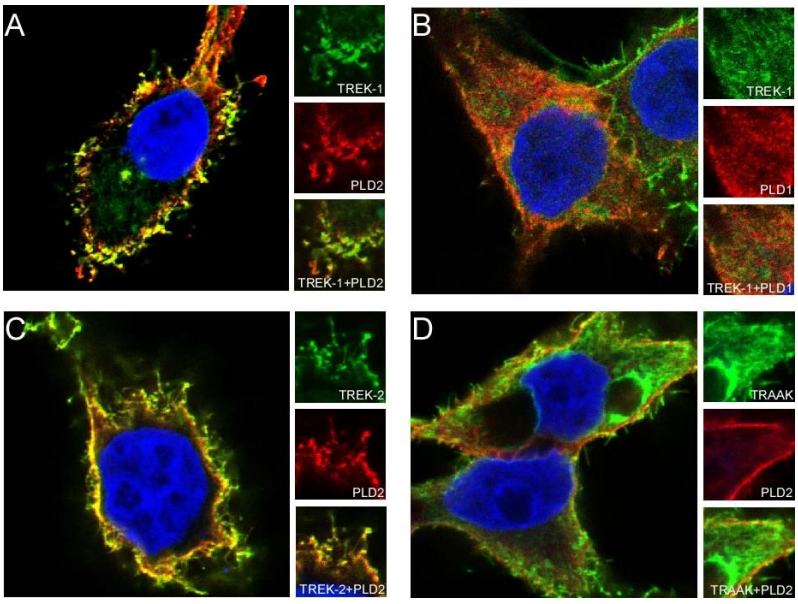

Figure S7.4. PLD2, but not PLD1, colocalize with TREK1 and TREK2 but not TRAAK. (A) Colocalization of TREK1 (green) and PLD2 (red) in permeabilized, antibody-stained HEK293T cells. The nucleus is DAPI-stained and shown in blue. Overlapping green and red labelling is shown in yellow. (B) Same as in (A) with PLD1. (C) Colocalization of TREK2 (green) and PLD2 (red) in permeabilized, antibody-stained HEK293T cells. (D) Same as in (C) for TRAAK.

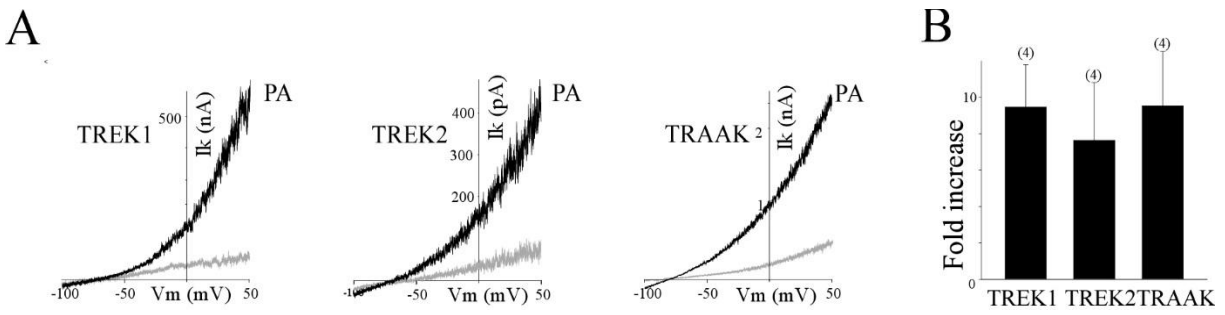

Figure S7.5. The TREK channel subfamily is stimulated by PA. (A) Application of 5µM PA increases current in inside-out patches containing TREK1, TREK2 or TRAAK. (B) Bar graph showing the average effect of PA (5µM) on TREK1, TREK2 and TRAAK. The numbers of cells tested are indicated in parentheses.

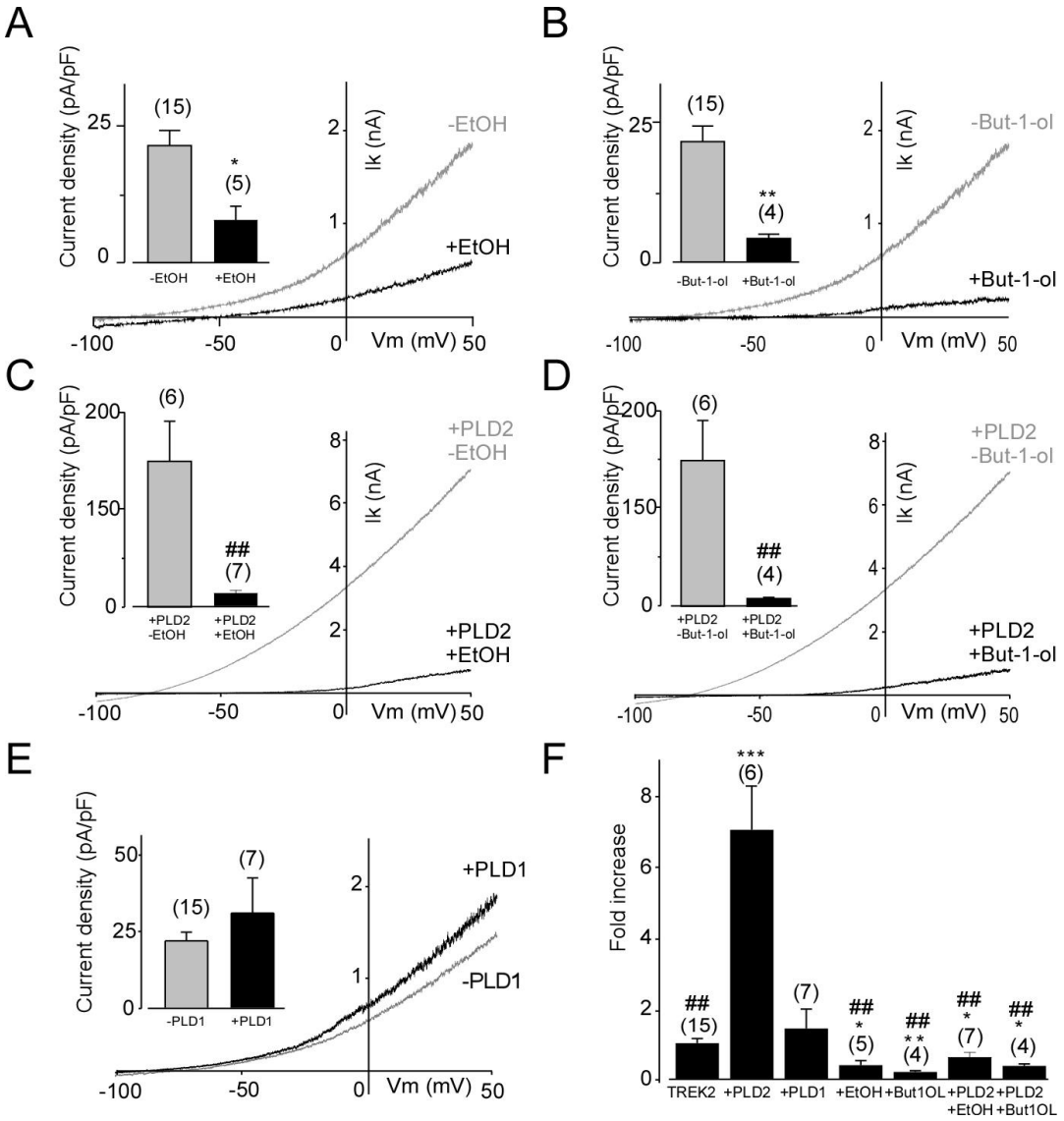

Figure S7.6. **TREK2 is inhibited by protracted primary alcohol application through its specific regulation by PLD2** (A, B) Protracted ethanol (A) or butan-1-ol (B) application inhibits TREK2 current. Inset, TREK2 current densities before and after protracted primary alcohol application. Current densities were 23 ± 3 pA/pF for TREK2 alone and 8 ± 1 for TREK2 + ethanol, 5 ± 1 for TREK2 + butan-1-ol). (C, D) Protracted ethanol (C) or butan-1-ol (D) application inhibits TREK2 current in the presence of PLD2. (E) Unlike PLD2, PLD1 does not regulate TREK2 current. Inset, TREK2 current densities in the presence or absence of co-expressed PLD1. (F) Normalized amplitude of TREK2 current in the presence of either PLD2 or PLD1 and before or after alcohol application in the absence or presence of PLD. Current densities were 144 ± 29 pA/pF for TREK2 + PLD2, 12 ± 3 pA/pF for TREK2 + PLD2 + ethanol, and 9 ± 1 pA/pF for TREK2 + PLD2 + butan-1-ol). Student's *t* tests (**P* < 0.05, ***P* < 0.01) show the difference between TREK2 alone and the other conditions. Student's *t* tests (#*P* < 0.05, ## P< 0.01) show the difference between TREK2 with PLD2 and TREK2 coexpressed with PLD2 after ethanol, butan-1-ol or butan-2-ol treatment. The numbers of cells tested are indicated in parentheses.

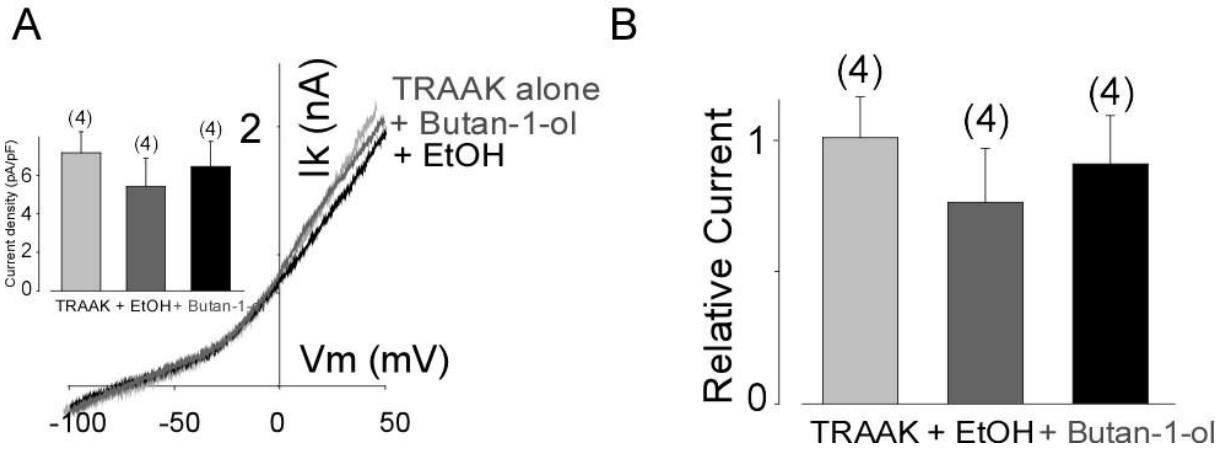

Figure S7.7. **TRAAK is not inhibited by protracted primary alcohol application. (**A) Protracted ethanol or butan-1-ol application does not inhibit TRAAK current. Inset, TRAAK current densities before and after primary alcohol application. (B) Normalized amplitude of TRAAK current in the presence or absence of protracted alcohol application. The numbers of cells tested are indicated in parentheses. Current densities were 7 ± 1 pA/pF for TRAAK alone, 5 ± 1 pA/pF for TRAAK + ethanol, and 6 ± 1 for TRAAK + butan-1-ol; P>0.3 for TRAAK alone vs. TRAAK + ethanol and P>0.5 for TRAAK alone vs. TRAAK + butan-1-ol.

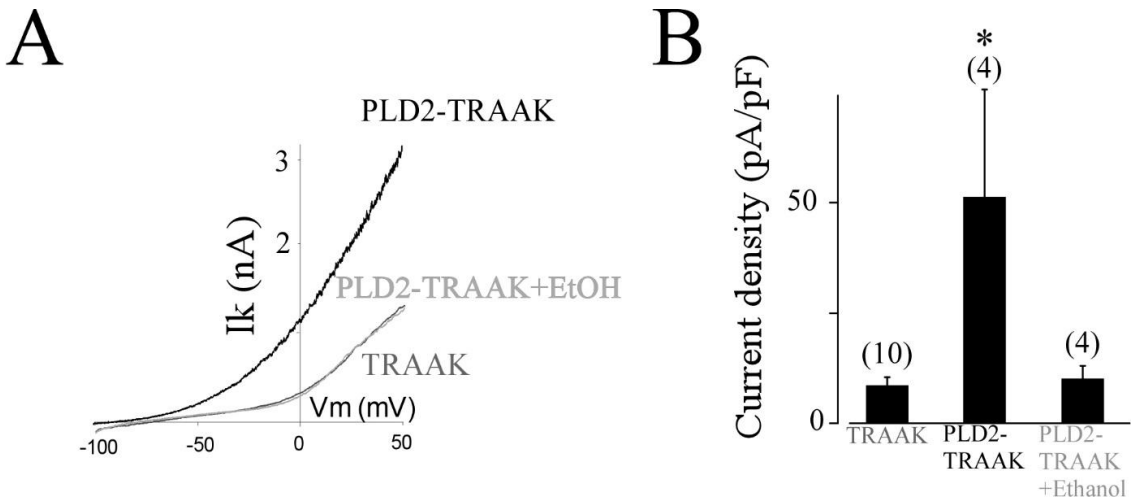

Figure S7.8. PLD2-mediated potentiation by fusion to TRAAK is reversed by ethanol treatment. (A) Ethanol abolishes the TRAAK current potentiation by PLD2 fusion. (B) Current density of TRAAK current in the presence of PLD2 after protracted ethanol application. Current densities were 10 ± 3 pA/pF for TRAAK alone and 14 ± 4 pA/pF for PLD2-TRAAK + ethanol; P>0.4). Student's *t* tests (**P* < 0.05)

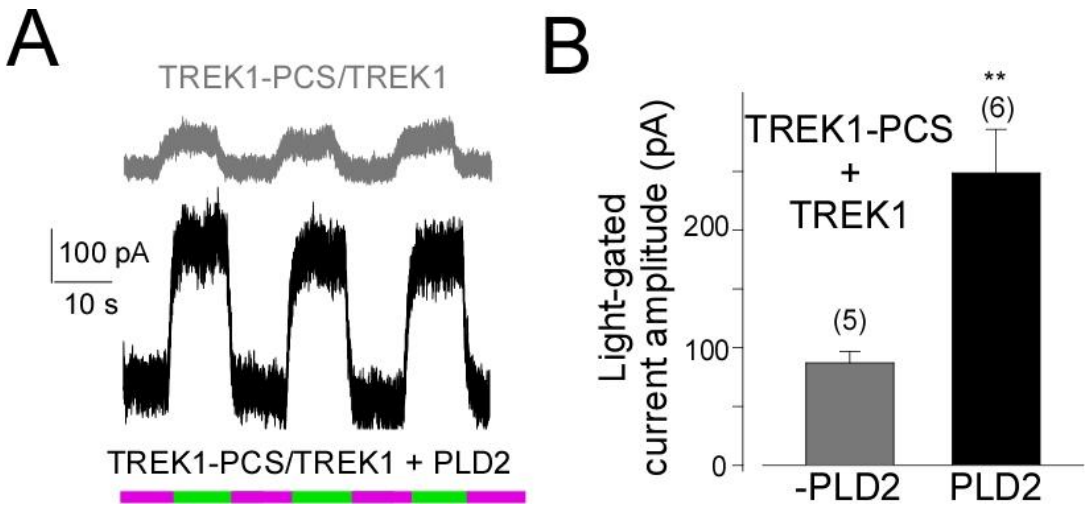

Figure S7.9. **Heteromeric channels formed by TREK1-PCS and TREK1-WT retain normal regulation by PLD2.** (a) PLD2 overexpression potentiates the light-gated current of the TREK1-PCS/WT heteromer. Alternating illumination at 500 nm (green) and 380 nm (magenta) reversibly blocks and unblocks, respectively, the constant outward current, both with or without PLD2 overexpression. (b) Summary of light-gated TREK1 current amplitudes with or without PLD2 overexpression. Student's *t* tests (**$P < 0.01$) show the difference between TREK1-PCS/TREK1 and TREK1-PCS/TREK1 + PLD2. The numbers of cells tested are indicated in parentheses.